

Classical and Hybrid Modeling of Gene Regulatory Networks

I n a u g u r a l d i s s e r t a t i o n

zur

Erlangung des akademischen Grades eines

Doktors der Naturwissenschaften

der

Mathematisch-Naturwissenschaftlichen Fakultät

der

Ernst-Moritz-Arndt-Universität Greifswald

vorgelegt von
Stefan Zeiser
geboren am 02.05.1970
in Herbolzheim

Konstanz, 30.06.2009

Dekan:

. . . . . .

1. Gutachter:

. . . . . .

2. Gutachter:

. . . . . .

Tag der Promotion:

. . . . . .

Abstract

We present classical and hybrid modeling approaches for genetic regulatory networks focusing on promoter analysis for negatively and positively autoregulated networks. The main aim of this thesis is to introduce an alternative mathematical approach to model gene regulatory networks based on piecewise deterministic Markov processes (PDMP).
During somitogenesis, a process describing the early segmentation in vertebrates, molecular oscillators play a crucial role as part of a segmentation clock. In mice, these oscillators are called Hes1 and Hes7 and are commonly modeled by a system of two delay differential equations including a Hill function, which describes gene repression by their own gene products. The Hill coefficient, which is a measure of nonlinearity of the binding processes in the promoter, is assumed to be equal to two, based on the fact that Hes1 and Hes7 form dimers. However, by standard arguments applied to binding analysis, we show that a higher Hill coefficient is reasonable. This leads to results different from those in literature which requires a more sophisticated model. For the Hes7 oscillator we present a system of ordinary differential equations including a Michaelis-Menten term describing a nonlinear degradation of the proteins by the ubiquitin pathway.
As demonstrated by the Hes1 and Hes7 oscillator, promoter behavior can have strong influence on the dynamical behavior of genetic networks. Since purely deterministic systems cannot reveal phenomenons caused by the inherent random fluctuations, we propose a novel approach based on PDMPs. Such models allow to model binding processes of transcription factors to binding sites in a promoter as random processes, where all other processes like synthesis, degradation or dimerization of the gene products are modeled in deterministic manner. We present and discuss a simulation algorithm for PDMPs and apply it to three types of genetic networks: an unregulated gene, a toggle switch, and a positively autoregulated network. The different regulation characteristics are analyzed and compared by numerical means. Furthermore, we determine analytical solutions of the stationary distributions of one negatively, and three positively autoregulated networks. Based on these results, we analyze attenuation of noise in a negative feedback loop, and the question of graded or binary response in autocatalytic networks.

Zusammenfassung

Die vorliegende Arbeit behandelt klassische und hybride Modellierungsmethoden für genregulatorische Netzwerke mit Schwerpunkt auf der Analyse von Promotoren von negativen und positiven autoregulativen Netzwerken. Hauptziel ist die Einführung eines alternativen mathematischen Ansatzes basierend auf stückweise deterministischen Markov Prozessen (PDMP).
Die Somitogenese bezeichnet einen biologischen Prozess, der die frühe Segmentierung von Wirbeltieren beschreibt. Während dieses Prozesses spielen molekulare Oszillatoren als Teil einer Segementationsuhr eine wichtige Rolle. In Mäusen sind dies die beiden Gene Hes1 und Hes7. In der Literatur werden diese üblicherweise mit Hilfe eines zweidimensionalen Delay-Differentialgleichungssystem modelliert. Die Inhibition der Genexpression durch das eigene Genprodukt wird dabei durch eine Hillfunktion beschrieben. Für den Hillkoeffizienten, welcher ein Maß für die Nichtlinearität der Bindung der Proteine an die Bindestellen ist, wird dabei gewöhnlich ein Wert gleich zwei angenommen. Hierbei beruft man sich auf die Tatsache, dass Hes1 und Hes7 als Dimere an die Bindungsstellen im Promotor binden. Anhand eines Standardmodels für die Bindunganalyse zeigen wir jedoch, dass ein höherer Wert realistischer ist. Dies führt jedoch zu Ergebnissen, die sich von denen aus der Lieratur unterscheiden. Diese Diskrepanz erfordert eine feinere Modellierung der negativen Feedbacks. Für den Hes7 Oszillator wird ein System von gewöhnlichen Differentialgleichungen vorgeschlagen, welches ein Michaelis-Menten Term beinhaltet, der den nichtlinearen Abbau des Hes7 Proteins durch den Ubiquitin-Signalweg beschreibt.
Wie die Untersuchungen des Hes1 und Hes7 Oszillators zeigen, kann sich die Promotoraktivität stark auf das dynamische Verhalten eines genregulatorischen Netzwerkes auswirken. Da deterministische Systeme keine Phänomene aufzeigen können, die durch die innewohnenden zufälligen Fluktuationen entstehen, schlagen wir einen neuen Modellierungsansatz vor, der auf PDMPs basiert. Solche Modelle ermöglichen, die Bindung von Transkriptionsfaktoren an die Bindungsstellen im Promotor als zufälligen Prozess zu beschreiben, wohingegen alle anderen Prozesse wie Synthese und Abbau der Genprodukte, oder Dimerization der Proteine als deterministische Prozesse beschrieben werden. Wir präsentieren und diskutieren einen Simulationsalgorithmus, und wenden diesen auf drei verschiedene Netzwerktypen an: ein induzierbares Gen, ein Toggleswitch und ein positiv autoreguliertes Netzwerk. Mittels numerischer Methoden werden die verschiedenen Regulationscharakteristiken analysiert und verglichen. Des Weiteren bestimmen wir die analytischen Lösungen der stationären Verteilungen eines negativ und dreier positiv autoregulierten Netzwerke. Anhand dieser Ergebnisse untersuchen wir die Reduktion von Fluktuationen in einem negativen Feedback, und die Frage einer graduellen oder binären Antwort in autokatalytischen Netzwerken.

"What is Life?"

Erwin Schrödinger[1]

[1] *What is Life? The Physical Aspects of the Living Cell*, Cambridge University Press, 1948

“Life is what happens to you while you’re busy making other plans.”

John Lennon[2]

[2]from *Beatiful Boy* in free adaption of Henry Miller

Contents

Introduction **1**

1 Classical Modeling **11**
1.1 Modeling the Hes1 Oscillator 11
1.1.1 Introduction 11
1.1.2 Analysis of the Hes1 Promoter 15
1.1.3 The Goodwin Model 21
1.1.4 Hopf Bifurcation in the Goodwin Model 22
1.1.5 Numerical Simulations 27
1.1.6 Discussion 31
1.2 Number of binding sites of the Hes7 oscillator 33
1.2.1 Introduction 33
1.2.2 Methods 34
1.2.3 Results 37
1.3 Oscillations of Hes7 42
1.3.1 Introduction 42
1.3.2 Ubiquitination of Hes7 44
1.3.3 Hes7 Oscillator 46
1.3.4 Numerical Simulations 47
1.3.5 Conclusion 51

2 Hybrid Modeling **53**
2.1 Simulation of Genetic Networks 53
2.1.1 Introduction 53
2.1.2 Deterministic versus Stochastic Approach 56
2.1.3 Piecewise Deterministic Markov Process 61
2.1.4 Algorithm for simulation of PDMPs 63
2.1.5 Applications 65
2.1.6 Discussion 87
2.2 Hybrid Modeling of Noise Reduction 91
2.2.1 Introduction 91

2.2.2 1-dimensional PDMP with two discrete states 93
2.2.3 Stationary distributions 97
2.2.4 Stability Analysis 101
2.2.5 Conclusions 108
2.3 Autocatalytic Genetic Networks 111
2.3.1 Introduction 111
2.3.2 PDMP-Models 114
2.3.3 Autocatalytic Genetic Networks 117
2.3.4 Stationary Distributions 121
2.3.5 Discussions and Conclusions 142
2.3.6 Appendix: Proofs of the Theorems 145

Conclusions **153**

Acknowledgements **171**

Introduction

"Every model is wrong, but some models are useful"
G.E.P. Box, 1979

Gene expression denotes the processes of transcribing and translating the information stored in the genome of an organism into mRNA and protein, respectively. A great number of proteins are transcription factors which regulate the expression of their own or other genes. Hence, genes can interact with other genes by their gene products constituting complex genetic networks. Such regulatory networks control a huge number of cellular processes from the cell cycle up to the development of an organism. Due to the mutual cross-linkage of individual genes, genetic networks exhibit complex dynamical behavior. Biological knowledge alone would not be sufficient to understand such complex interactions. Capturing some of the characteristics of the genetic network while neglecting others results in a simplified description of the original network. A mathematical replication of such a simplified network results in a mathematical model of the genetic network, which can be analyzed theoretically or numerically in order to understand the core mechanism and to make predictions. The importance of mathematics in the field of theoretical biology is reflected in the foundation of systems biology. An interdisciplinary study field with focus on the systematic study of complex interactions in biological systems. Mathematical models of genetic networks are the content of the present thesis. We focus on the dynamical behavior of small genetic networks where analytical results are feasible.
The basics of gene expression was already proposed by Francis Crick in the late 50's. Five years after he and James Watson have revealed the double α-helix structure the desoxyribonucliase acid (DNA), [118] a molecule consisting of two long polymers and carrying the genomic information, he formulated the *central dogma of genetics*, [21], [22]. It states, loosely speaking, that the information flow from DNA to active proteins is essentially a one-way street. Besides replication, where

DNA is copied to DNA, the DNA is transcribed to mRNA which is translated to protein. DNA is the library carrying all the information needed by a cell or organism to stay alive. It is stored in a four letter code. The main function of the mRNA is to carry the information stored in a gene to a ribosome. More precisely, after the DNA is transcribed by RNA polymerase into mRNA, it is decoded by a ribosome, which translates the sequence of nucleotides into a sequence of amino acids, building up the protein. Proteins themselves are the entities generating the functionality of a living cell. They are involved in almost all biological processes. The transformation of the information coded in a gene into protein is denoted as gene expression. However, depending on the context, sometimes transcription of mRNA alone is denoted as gene expression.

The central dogma describes a highly complex process in a very succinct way. There are post-transcriptional as well as post-translational modification steps. For example, a gene is not transcribed one-to-one into mRNA. Especially in eukaryotes pre-mRNA is modified by removing the introns and joining the exons. Furthermore, the target gene product is not always a protein. Developments in recent years have revealed that not all RNA molecules are translated into protein but have functionality on their own. For example, such non-coding RNAs are involved in transcription as well as in translation, [120], [25], [77].

Nowadays, sequencing of an arbitrary genome (which is a much better word than the German "entschlüsseln") is more or less a question of money and interest. However, one is still far away from understanding the function of most of the genes. This can easily be perceived by looking at a complex genetic network. The action of one molecular player may have influences on many other components. To understand the dynamics of such a system, mathematical modeling can be very helpful. However, to lead such an approach to success, one has to know the entities, the molecular components, the way they interact with each other, i.e. the chemical reactions, and how strong the interactions are, i.e. the reactions rates. Knowing these ingredients, mathematics can help to understand the dynamics of a biological system in the small and in the large as well.

Typically, chemical reactions are modeled on either of three different scales. The most accurate description of biomolecular reactions is the microscopic view. Here, collisions occur among atoms and molecules. The state space of the system contains the number of the molecular entities, their positions, and momenta. The dynamics of the system is inherently stochastic. However, since the state space is huge, even if all the information would be available, which is certainly not the case, it would be impossible to analyze the system behavior theoretically as well as numerically.

By ignoring the individual interactions of atoms and/or molecules and looking only on the effects of a large collection of reactive entities, we approach the macroscopic scale of chemical reactions. Assuming that the reactants occur in

high numbers, such that the change in the numbers of the reactants, caused by a single firing reaction, is small percentaged to the total numbers of reactants, it is often reasonable to suppose that the change in the respective concentrations can be approximated as continuous and that statistical fluctuations average out. Hence the state space of the system are concentrations instead of molecule numbers and the temporal evolution is described in a deterministic manner using ordinary differential equations.
The mesoscopic view is a description which lies between these two views. The state space consists of the numbers of the reactants but does not keep track of their individual properties like position or momentum. The dynamics follow stochastic laws giving the probability to find a certain number of the reactants at a certain instant of time. Most commonly, such a system is described by a time continuous Markov process with finite state space.
The most precise approach to model chemical reactions is the microscopic one. Besides the huge complexity of such a representation, the number of most of the active molecules is unknown for nearly all regulatory networks. Thus, right now one is far away from a precise quantitative model. To circumvent this one uses one of the two other approaches, namely the macroscopic or the mesoscopic view. Since these two approaches are also quantitative one achieves a deeper insight in the structure and dynamic of a biochemical system even if the precise numbers of actors are unknown.
The difference between the two approaches is not the mathematical tool like ordinary differential equations (ODEs) or partial differential equations (PDEs). Indeed, in both approaches one uses ODEs as well as PDEs. It is the state space in which the biochemical system evolves. For example, if we consider one type of molecule, the temporal evolution of its concentration can be described by one ordinary differential equation in the macroscopic view. However, in the mesoscopic setting we have to consider a system of ODEs, one equation for each number of molecule describing the temporal evolution of the corresponding probability distribution. Thus, even for very simple systems, analytical solutions are unfeasible. As a consequence, the macroscopic view has become the most popular approach.
As stated above, the process from a gene to its product is highly complex and takes place in many intermediate biochemical reactions. A chemical reaction is described by stating the reactants and the products. To specify the kinetics of the reaction, in both the macroscopic and the mesoscopic view, a proportionality constant is needed additionally, which is called the reaction rate constant. We assume that all biochemical reactions can be split into a sequence of elementary reaction channels listed in the reaction scheme (1).
R_1 denotes a zero-order reaction in which the reaction rate is independent of any reactants. The star denotes reactants which are present in constant amounts or outside the considered reaction system and thus does not need to be specified

explicitly.

$$\begin{array}{lccl} R_1\text{:} & * & \longrightarrow & S_i\,, \\ R_2\text{:} & S_i & \longrightarrow & \emptyset\,, \\ R_3\text{:} & S_i & \longrightarrow & S_j\,, \\ R_4\text{:} & S_i + S_i & \longrightarrow & S_j\,, \\ R_5\text{:} & S_i + S_j & \longrightarrow & S_l\,. \end{array} \tag{1}$$

R_2 and R_3 denote first-order or unimolecular reactions. In this case the reaction rate depends linearly on the concentration of the reactants. R_2 describes degradation or decay of the reactant S_i where the symbol $\emptyset$ denotes the products of decomposition which have no influence on the further reactions. R_3 denotes a reaction where a reactant S_i is converted into a product S_j. R_4 and R_5 denote second-order or bimolecular reactions. The reaction channel R_4 describes a bimolecular reaction where two reactants of the same molecular species i react, forming a novel product molecule S_j. R_5 describes a bimolecular reaction consisting of two distinct reactants S_i and S_j forming a novel product molecule S_l. For example, formation of a dimer, i.e. a protein complex consisting of two proteins of equal or different types, is described by reaction channel R_4 in the case of a homodimer, or by R_5 in the case of a heterodimer. Then, a reaction describing the binding of a dimer to a binding site in the regulatory region of a gene, can be split into a reaction of type R_4 or R_5, and into a reaction of type R_5 describing the binding of the dimer to the promoter of the gene.

Throughout this work we assume that the considered biochemical processes obey a kind of Markovian law. That means, it is assumed that the cell is relatively homogeneous and well stirred. For many applications this is approximately fulfilled if more non-reactive than reactive collisions between the individual reactants occur. Then we may suppose that the particular reaction can be described by rate laws, in the deterministic setting, or by Markov processes as it is done mostly in the stochastic setting.

The first application of stochastic approaches to chemical kinetics seems to be the works of Kramers [67] and Delbrück [24] in 1940. However, since analytical treatments are highly complicated or not feasible at all, stochastic approaches were not very popular and received only less attention in the biomolecular community. This changed as computing powers increased. The breakthrough happened in the mid-70's of the last century when Gillespie published two papers describing an algorithm for solving stochastic equations numerically by simulating individuals trajectories, [33], [34]. Gillespie's algorithm can be easily executed in any kind of programming language possessing a pseudo random generator. There are also several software packages including executable realizations [83], [95], [63], [71]. Further support for using stochastic methods derived from experimental research. More and more experiments revealed that transcription and translation in

single cells vary even in isogenetic cell populations, [78], [4], [28], [90]. One possible reason is that in single cells the template for transcription, the DNA, is present only in one or two copies. Due to such small numbers transcription proceeds rather stochastic than deterministic, [52], [16], [88], [91], [111], [19]. In this case, stochastic models are more appropriate.
However, if the stochastic systems become large, simulations become computationally very expensive. To circumvent this problem much work was done to speed up stochastic simulations. To name only a few, the 'next reaction' method of Gibson and Bruck, [31], the 'τ-leap' method of Gillespie [35] and improvements, [32], or the algorithm of Puchalka and Kierzek, [59] which is a combination of the next reaction and the τ-leap method. Besides these more efficient and approximative algorithms hybrid models, too are proposed for modeling gene regulatory networks [79], [47], [62].

In the present thesis we use a classical approach based on ordinary differential equations to model negative feedback loops which underlie the ultradian clocks Hes1 and Hes7. Furthermore, we present a novel approach for hybrid modeling of genetic networks based on piecewise deterministic Markov processes (PDMP). Such an approach can be considered as a bridge between the mesoscopic and the macroscopic view.
In mice the genes Hes1 and Hes7 exhibit cyclic expressions with a period of about 2 hours. Due to this high frequency compared to circadian clocks they are sometimes termed ultradian clocks. Both proteins belong to the basic helix-loop-helix family of transcription factors, [110], [13], and are target genes of the Delta-Notch pathway, a highly conserved pathway consisting of two transmembrane proteins which plays important roles in many organisms, [94], [64], [5]. For example, during neurogenesis in the fruit fly Drosophila it causes a phenomenon called lateral inhibition which is responsible for a proper relation in cell fate decisions between neuron and epidermal cells, [105], [42], [48], [41]. In higher organisms the Delta-Notch pathway is responsible for the synchronization of a kind of expression wave during somitogenesis, a process describing the early segmentation of vertebrates. More precisely, somitogenesis describes the formation of segmented tissue blocks, the somites, which differentiate into skeletal muscle, vertebrae, and dermis. This process takes place in the presomitic mesoderm (PSM), a U-shaped tissue located bilateral to the neural tube. During somitogenesis, the cells express Hes1 and Hes7 periodically with a particular phase shift which results in a kind of expression wave starting at the caudal end, and runs along the anteroposterior axis. At the time when the wave reaches the rostral end two novel somites are separated from the PSM. Afterwards the wave starts again. This oscillatory behavior of Hes1 and Hes7 is generated by a negative feedback loop. Both proteins bind as dimers to the regulatory regions of their own encoding genes, thereby repressing

further transcription [110], [13].
Modeling genetic networks by means of PDMPs is a hybrid approach in the sense that the state space consists of a discrete and a continuous set, where reactions including low reactants numbers are modeled in a stochastic way, and reactions with high reactants numbers are modeled in a deterministic manner. Coupling the stochastic and deterministic state variables in an appropriate way leads to a special class of processes which posses the Markov property. They were introduced by Davis in a more general setting in 1984, [23]. More precisely, the state space of a PDMP is given as the product of a finite set M and a subset of $\mathbb{R}^d$, $d \geq 1$. It can be thought of as split into different branches labeled by elements of the finite set M. The motion of a piecewise deterministic Markov process is determined by three local characteristics: a vector field v, a transition rate function λ, and a transition measure Q. Starting at an initial point the process evolves deterministically, driven by the vector field v up to the first jump time. Then a new branch is chosen according to the transition measure Q. After this the process restarts in the new branch and moves deterministically until the next jump time is reached.
Except for the DNA we assume that the molecular entities in a genetic network occur in such high numbers that a deterministic description by ordinary differential equations is appropriate. Then the states of the genes are described by the discrete elements of the set M, whereas the amount of the gene products are given as concentrations described by continuous variables. Hence processes like production, degradation or dimerization of the gene products take place in a deterministic manner following mass action law and depend only on the present states of the corresponding genes. On the other hand, the time when a gene state is altered, as well as the new adopted state of the gene is random. In proceeding this way, we can focus on the promoter as the only source of randomness during gene expression. In particular, this is an appropriate approach to model deactivation and activation of a particular gene, where activation is often followed by burst like events of mRNA and protein synthesis, [52], [28], [88]. The effect of the resulting variations in the expression levels in single cells is, at least in eukaryotes, in general stronger than synthesis and degradation of the respective gene products, [16].
As far as we know, PDMPs were not used to model gene regulatory networks up to now. However, such a hybrid approach is not entirely new. To some extent similar models already exist in literature. Hybrid processes possessing discrete as well as continuous state variables were proposed using the chemical Langevin equation, like in [98], or ordinary differential equations, like we do. One such approach was proposed by Haseltine and Rawlings, [47]. They partitioned the reaction system into subsets of 'fast' and 'slow' reactions similar to the work of Rao and Arkin, [89]. Then, they modeled the slow reactions as discrete events whereas the fast reactions were approximated by the chemical Langevine equation. The partition

proposed by Haseltine and Rawlings is static and based on the propensity function of the individual reaction channels. A more accurate partitioning was done by Griffith and coworkers, [79]. They proposed a dynamical partitioning algorithm which classifies each reaction as a discrete event by default, and classifies a reaction as fast if it is beyond a relative threshold which is updated dynamically. In [73], ordinary differential equations describing the temporal evolution of the concentration of the gene products are coupled by a random variable describing the activity of the promoter of the particular gene. Provided that the distribution posses a density, it can be described by a system of partial differential equations. Then the system of partial differential equations was approximated by a system of ordinary differential equations and solved numerically to obtain the density of the respective system.

The thesis is organized as follows. The first chapter deals with classical models for the Hes1 and Hes7 oscillators. In the first section we propose a standard approach to model binding of the Hes1 dimers to the binding sites in the promoter of its own encoding gene. Based on few data from binding analysis we build response functions which are fitted by Hill functions to obtain estimates for the Hill coefficient. Furthermore we use Goodwin models to describe the underlying negative feedback loop. In contrast to delay differential equations, in a Goodwin model a time delay is caused by modeling intermediate steps of transcription and translation by single ordinary differential equations. In the second section we estimate the Hill coefficient for the Hes7 oscillator by fitting a Hill function to the corresponding response function. Further, we analyze the dynamical behavior of the Hes7 oscillator numerically by using a system of delay differential equations from literature. In the third section we propose a more sophisticated model for the Hes7 oscillator. We describe degradation of the Hes7 protein by the ubiquitin pathway by a Michaelis-Menten term. Including this nonlinear term in a Goodwin model for the Hes7 oscillator results in a more appropriate model, by which the experimental findings from literature can be brought into agreement to our estimate of the Hill coefficient.
The second chapter deals with hybrid modeling of gene regulatory networks based on PDMPs. In the first section we present and discuss an algorithm for simulation of genetic networks modeled by PDMPs. We show that simulation of a PDMP is nearly as straightforward as executing the standard Gillespie algorithm for simulations of time-continuous, state-discrete Markov processes. We apply the simulation algorithm to three standard genetic modules, namely an inducible gene with constant amounts of inducer, an autocatalytic genetic network, and the so-called toggle switch build up of two genes, where each gene represses expression of the other gene. We calculate the empirical distributions and perform sensitivity anal-

ysis by numerical means. In the second section we analyze attenuation of noise resulting from promoter transitions by a negative feedback loop. By means of the adjoint generator of the PDMP, we present a closed analytical formula for the stationary distribution of a negative feedback loop. The first two central moments are calculated and noise reduction is measured in terms of the coefficient of variation. In the third section we determine the stationary distributions for three different types of autocatalytic networks. We call them a pure autocatalytic network, an autocatalytic network with positive basal transcription rate, and an autocatalytic network with positive basal activation rate. We perform extinction analysis for the pure autocatalytic network, and analyze the response of the three networks to different time lengths and inducer amounts by numerical means.

The thesis is composed of six publications listed on page 175. They are sorted thematically and presented in a uniform LaTeX style. Each section correlates with one publication. Besides minor linguistic changes the contents of the sections are identical to the particular publications. Hence, they can, for the most part, be read independently of one another.
My contributions to these papers are the following. Of all six publications I am the main as well as the corresponding author, and I built the final manuscript of each paper. Furthermore,

- The publication *Modeling the Hes1 Oscillator*, [129] is presented in the first section of the first chapter. I thought of the biological model, and carried out the simulations as well as the calculations.

- The publication *Number of active transcription factor binding sites is essential for the Hes7 oscillator*, [128] is presented in the second section of the first chapter. I came up with the mathematical and the biological model, and performed the calculations as well as the simulations.

- The publication *Oscillations of Hes7 caused by negative autoregulation and ubiquitination*, [130] is presented in the third section of the first chapter. I figured out the biological and the mathematical model. Furthermore I performed the calculations as well as the simulations.

- For the publication *Simulation of Genetic Networks Modeled by Piecewise Deterministic Markov Processes*, [127] is presented in the first section of the second chapter. I thought of the mathematical and the biological models, and performed the calculations as well as the simulations.

- The publication *Hybrid Modeling of Noise Reduction by a Negatively Autoregulated System*, [126] is presented in the second section of the second

chapter. I figured out the mathematical and the biological model, and carried out the calculations as well as the simulations.

- The publication *Autocatalytic Genetic Networks Modeled by Piecewise Deterministic Markov Processes*, [125] is presented in the third section of the second chapter. I thought of the mathematical and the biological models, and performed the simulations and the calculations of the stationary distributions.

Chapter 1

Classical Modeling

1.1 Modeling the Hes1 Oscillator

The present section contains the results published in [129].
Somitogenesis describes the segmentation of vertebrate embryonic bodies which is thought to be induced by ultradian clocks, i.e. clocks with relatively short cycles compared to circadian clocks. One candidate for such a clock is the bHLH factor Hes1 forming dimers which repress the transcription of its own encoding gene. Most models for such small autoregulative networks are based on delay equations where a Hill function represents the regulation of transcription.
The aim of the present section is to estimate the Hill coefficient in the switch of an Hes1 oscillator and to suggest a more detailed model of the autoregulative network.
The promoter of *Hes1* consists of 3 to 4 binding sites for Hes1 dimers. Using the sparse data from literature we find, in contrast to other statements in literature, that there is not much evidence for synergistic binding in the regulatory region of *Hes1*, and that the Hill coefficient is about three.
As a model for the negative feedback loop we use a Goodwin system and find sustained oscillations for systems with a large enough number of linear differential equations. By a suitable variation of the number of equations we provide a rational lower bound for the Hill coefficient for such a system. Our results suggest that there exist additional nonlinear processes outside of the regulatory region of *Hes1*.

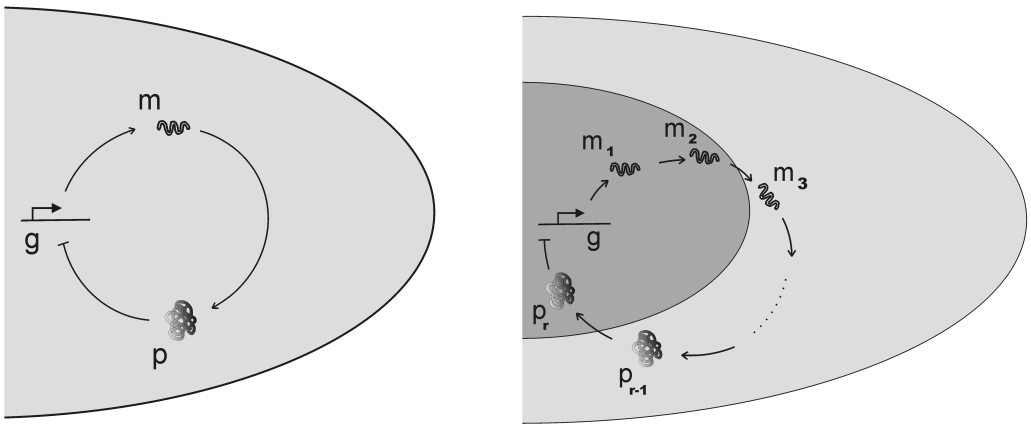
1.1.1 Introduction

Hes oscillators play an important role during somitogenesis, a process in vertebrates embryonic development. In a temporally and spatially highly coordinated way a pair of somites buds off from the anterior end of vertebrates presomitic

mesoderm (PSM). One assumes that this periodic process is regulated by biological clocks with relatively short cycles, so-called ultradian clocks. For a review see [87]. Important components of such clocks are cycling genes, i.e. the expression of which turns on and off in a periodic fashion. An important cyclic gene during somitogenesis of mouse is the bHLH factor Hes1. Cells located in different regions of the PSM express *Hes1* with different phases generating wave-like expression patterns [57]. These gene expression waves sweep with a period of two hours from the posterior to the anterior end of the PSM. When it reaches the anterior end, two somites are separated bilaterally of the neural tube. Hirata et al. showed in [51] that the *Hes1* mRNA and the Hes1 protein oscillate with period approximately equal to 120 min. Here, the molecular oscillator consists of two components where the gene transcription is downregulated by its own gene product, [51], [110]. Because bHLH factors typically form dimers, in mathematical models for Hes1 oscillators the Hill coefficient is often assumed to be equal to two if there is no indication for substantial further regulatory mechanisms that are able to influence the Hill coefficient.

In spite of the fact that the core regulatory network consists of two components only (see Fig. 1.1 (a)), it is not straight forward to derive a suitable mathematical model. The simplest, deterministic model consists of two equations: one for the temporal changes of the density of mRNA m and one for that of the protein p. However, a gene regulation network consisting of two components shows oscillation only when there is both, autocatalytic production *and* negative feedback. Negative feedback alone cannot create cycling gene expression (which can be easily seen from the theory of dynamical systems, e.g. by the Bendixon's negative criterion, see [44]).

In fact, this model is a very strong simplification of the biological reality. Even if – in principle – a gene is down-regulated by its own product independently of all other processes in the cell, the way from mRNA to the regulation of the gene usually requires many steps (see Fig. 1.1(b)). A multitude of concentrations needs to be described; e.g., transcription yields pre-mRNA, m_1, which is spliced into mRNA, m_2, that is transported into the cytoplasm, translated into protein p_1, which perhaps also needs further interactions with other proteins before it finally reaches its active state p_{r-1} and is transported into the nucleus p_r where it is able to interact with the promotor region of the gene. Most of these processes are not known in detail. However, other examples show that quite often first order kinetics represent the essential properties of this pathway in a satisfying manner. We want to emphasise that there may be important nonlinear features hidden in this part of the regulatory pathway. So one of the main themes of the present article is the question whether the experimental facts force us to conclude that in this unknown part of the pathway there are further essential regulatory mechanisms



(a) (b)

Figure 1.1: A negative feedback loop during gene expression described on different levels of granularity: (a) A gene g is transcribed into mRNA which is translated into a protein. Then the protein represses the transcription of its own coding gene (indicated by a $\dashv$). (b) Feedback loop describing intermediate modification processes like transcription, splicing, transport and translation (see text). Many of such processes can be well described by first-order kinetic equations.

or whether the known mechanisms and experimental facts suffice to produce the desired oscillations. We base our model on the following 4 biological facts: There are sustained oscillations with a period of 120 minutes, the half-lives of *Hes1* mRNA and Hes1 protein are about 20 min, Hes1 forms dimers, and Hes1 possesses four binding sites in its regulatory region.

Up to now, there are two approaches to derive models for the Hes1 oscillator. The first one, a system of three ordinary differential equations, was provided by Hirata et al. in [51]. They introduced a third component nonlinearly coupled to the protein and achieved sustained oscillations with a period of 120 min. Here, the Hill coefficient could be chosen equal to two. However, the additional component is rather speculative.

Another approach was taken by Monk in [80]. There, the duration of synthesis of the mRNA and protein are modeled by time delays in the differential equations. Modeling by means of delay equations has the big advantage that not all processes have to be specified explicitly and that their effects on the dynamics can be lumped together into the delay. Monk showed that such a system can generate periodic solutions where the period is determined by the delay of transcription and translation. Using an overall delay equal to 18.5 min and a Hill coefficient equal to 5 he achieved sustained oscillations with period equal to 120 min. Monk assumes that the *Hes1* promoter is a likely source for the discrepancy in the Hill coefficient and

that modification and transport processes may also contribute to this effect.

Both models are not satisfying in either introducing a further key player that is rather speculative or in choosing a Hill coefficient much higher than the expected one. In the present section we address the difficulty to set up a model that meets the minimal requirements by two approaches: investigating the effect of multiple binding sites in the *Hes1* promoter and modeling the transcriptional and translational processes in more detail. The starting point for the analysis of multiple binding sites in the *Hes1* promotor region are experiments of Takebayashi et al. in [110]. They revealed that *Hes1* transcription is repressed by its own gene product. Carrying out a binding analysis they showed that the Hes1 protein binds to four regions in the *Hes1* promoter. Furthermore, by transcriptional analysis of mutated Hes1 promoters they showed that the repression is strongly affected by disrupting one or more binding sites. This analysis and mutation experiments allow to draw relevant conclusion for modeling this regulatory mechanism.

For modeling the binding process of Hes1-dimers to the regulatory region of *Hes1* we use a standard model for ligand binding from mathematical chemistry. It seems reasonable to assume that dimerisation, and association and dissociation of dimers to and from binding sites are in equilibrium. As a model for the *Hes1*-switch we use response functions which give the averaged frequency and duration of occupancy of one of the transcription factor binding sites. To follow the usual approach we approximate a response function by Hill functions. On the basis of the only few data from [110] we find that there are no or only small synergistic effects in the regulatory region of *Hes1*. Such a small synergistic effect would result in a moderate increase of the Hill coefficient. On the basis of the sparse data we estimate that a Hill coefficient as high as 3 could be possible.

Autoregulative genetic networks can also be described by a model which is sometimes referred to as the Goodwin system. It was introduced by Goodwin [38] in 1963 and was analysed by many authors, see for instance [113], [43], [2], [75]. But, as far as we know, its use for ultradian clocks is new. Its rationale is that transcriptional and translational delays are caused by many consecutive mechanisms. For instance, capping, splicing, elongating, transcription, transport in the cytoplasm, transport to the ribosome, translation, and transport of the mature protein from the cytoplasm back into the nucleus play certainly a role. Correspondingly, we describe each of these phenomena by a single differential equation. As a first approach and due to the lack of experimental data we want to keep the model as simple as possible. Thus we use first-order kinetics only. Such processes are often well described by linear equations, for instance in the case of mammalian LT-α and β-globin, [7]. By increasing the number of linear equations successively the Hill coefficient can be decreased to biologically meaningful magnitudes. However, for a realistic number of equations in a Goodwin system there is still a dis-

crepancy in the value of the Hill coefficient required to obtain sustained oscillations and to the one estimated by response functions. Thus, it seems that there are also intermediate steps in the feedback loop which follow nonlinear kinetics.

1.1.2 Analysis of the Hes1 Promoter

Takebayashi et al. showed in [110] that the Hes1 protein negatively regulates its own promoter activity. By binding analysis of the Hes1 protein to the *Hes1* promoter they found that Hes1 binds to three so-called N-boxes in the promoter region. Furthermore, they found weak binding to a N-box downstream of the transcription initiation site and to a region around position -10, which did not conform to a typical N-box. The role of the N-boxes in transcription repression was confirmed by transcriptional analysis of the *Hes1* promoter. For this they used a constant amount of Hes1 vectors and CAT plasmids containing either the wild-type or mutated Hes1 promoter. Mutations in the N-box sequences in the promoter region lead to a decrease in the repression activity of Hes1 protein. Wild-type

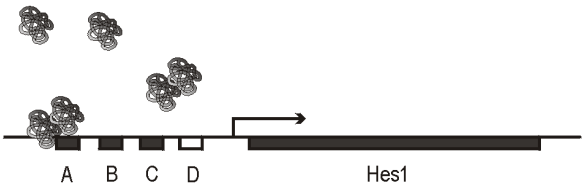


Figure 1.2: The *Hes1* regulatory system. Hes1 dimers bind to four binding sites upstream of the transcriptional initiation site (indicated by an arrow). Beside the three N-boxes, indicated by the filled out rectangles A, B, and C, there is also a weak binding to a region around position -10, indicated by the unfilled rectangle D.

promoters exhibited a 30- to 40-fold repression by Hes1 proteins. A deletion, caused by mutation of the N-box sequences, of one of the three N-boxes yields a 14-fold repression and a deletion of two N-box resulted in a seven-fold repression. Furthermore, deletions of all three promoter N-boxes resulted in a two-fold repression by Hes1 protein. A possible explanation for this weak transcription repression could be the region around position 10 upstream of the transcription initiation site. As assumed by Takebashi et al. each dimer binds to one N-box thus each bounded Hes1 dimer increases repression nearly two-fold. Takebashi et al. suggest that this would imply a synergistic binding. However, our analysis shows

that the available data suggests no or only weak synergy among different binding sites.

We propose a simple model for the regulatory mechanism of *Hes1*. More details and reviews can be found in [102], [116], [6], [115], [103], [123], [17] and [82]. For the sake of completeness we will start with the easiest case when there is only one transcription factor binding site in the promoter region, showing the well known fact that in this case the Hill coefficient is equal to two.

Promoter with a single binding site. We assume that the dimers are formed in solution rather than on the DNA. In this case dimerisation and binding of a dimer to a binding site can be described by

$$\begin{aligned} 2X &\overset{k_d}{\underset{k_{-d}}{\rightleftharpoons}} X_2\,, \\ X_2 + B_0 &\overset{k_1}{\underset{k_{-1}}{\rightleftharpoons}} B_1, \end{aligned}$$

where k_i and k_{-i} denote the respective association and dissociation constants, and X, X_2, B_0, and B_1 denote a monomer, a free dimer, a free binding site and a bound dimer binding site complex, respectively.

These processes are described by four differential equations, two for the dimerisation and two for the binding of the dimer to the transcription factor binding sites in the promoter. For simplicity, we assume that these biochemical reactions are in equilibrium. In that case, differential equations are reduced to two simple algebraic equations:

$$K_d = \frac{k_d}{k_{-d}} = \frac{[X_2]}{[X]^2},\ K_{eq} = \frac{k_1}{k_{-1}} = \frac{[B_1]}{[B_0][X_2]}, \tag{1.1}$$

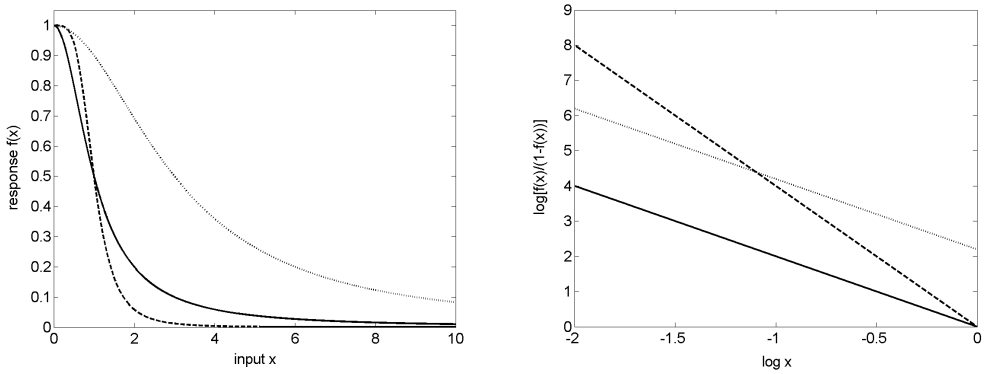
where K_d and K_{eq} denote the equilibrium constants of dimerisation and promoter binding, respectively, and $[X]$, $[X_2]$, $[B_0]$, and $[B_1]$ the concentrations or numbers of the respective reaction components.

Response Functions, Hill Functions and Hill Plots. The effect of a dimer X_2 on the transcription of a gene is described by a response function $f([X])$. It varies between zero and one and gives the average relative occupancy of the promoter by a transcription factor. Consider one binding site, and let B_0 denote the state where the promoter is not occupied and B_1 the state where it is occupied. Then, an inhibitory response function has the following form:

$$f([X]) = \frac{[B_0]}{[B_0] + [B_1]}.$$

Rearranging and inserting equation (1.1) into the response function gives

$$f([X]) = \frac{1}{1 + K_{eq}K_d[X]^2}. \tag{1.2}$$



(a) (b)

Figure 1.3: (a) Inhibitory Hill-type functions with Hill coefficient and Hill constant equal to two and one (solid), four and one (dashed), and two and three (dotted), respectively. (b) Hill plot of the respective Hill-type functions.

Using the normalised input $x = \sqrt{K_{eq}K_d}[X]$, equation (1.2) takes the simpler form $f(x) = 1/(1 + x^2)$. This is a Hill-type function with Hill constant one and Hill coefficient two.
In general, most inhibitory response functions can be well approximated by so called Hill-type functions of the form

$$f(x) = \frac{H^h}{H^h + x^h}, \tag{1.3}$$

where $h \geq 1$ and $H > 0$ are called the Hill coefficient and the Hill constant, respectively. The Hill constant is the input signal, which gives 50% response, and the Hill coefficient is related to the slope of the function, see Figure 1.3 (a). As an example, Figure 1.3 (a) displays three different Hill functions. Two functions have Hill constant one and Hill coefficient equal to two (solid) and four (dashed). The third function has Hill constant equal to three and Hill coefficient equal to two. To approximate an arbitrary response function by a Hill-type function one constructs the so called Hill plot where $\log\left(f(x)/(1 - f(x))\right)$ is plotted versus $\log x$. Then the negative slope of the regression line is used as an estimate of the Hill coefficient. For example, the Hill plots of the above Hill functions are shown in Figure 1.3 (b). In the following, we will determine the Hill coefficient several times by fitting a linear function to the central part of the Hill plot.
Multisite regulatory systems. Calculating the response function of a promoter with more than two binding sites is more complex. One has to consider each possible way how dimers can bind to the different binding sites. We will show below that this will lead to a higher Hill coefficient. To describe also the situations occuring

in the mutation experiments of [110], we need the response function for the case of one, two, three and four binding sites. However, in all cases the arguments are parallel such that we restrict ourselves to the case of three binding sites and merely state the result for the other cases.
Again, let us assume that dimerisation takes place in solution only, rather than on the DNA. Then, there are six possible reaction paths for sequential binding of dimers to one of the three binding sites. In a sloppy but intuitive way the reaction paths read

$$\begin{array}{lllllll}
X_2 + B_{000} & \underset{k_{-1}}{\overset{k_1}{\rightleftharpoons}} & X_2 + B_{100} & \underset{k_{-2}}{\overset{k_2}{\rightleftharpoons}} & X_2 + B_{110} & \underset{k_{-3}}{\overset{k_3}{\rightleftharpoons}} & B_{111} \\
X_2 + B_{000} & \underset{k_{-1}}{\overset{k_1}{\rightleftharpoons}} & X_2 + B_{100} & \underset{k_{-4}}{\overset{k_4}{\rightleftharpoons}} & X_2 + B_{101} & \underset{k_{-5}}{\overset{k_5}{\rightleftharpoons}} & B_{111} \\
X_2 + B_{000} & \underset{k_{-6}}{\overset{k_6}{\rightleftharpoons}} & X_2 + B_{010} & \underset{k_{-7}}{\overset{k_7}{\rightleftharpoons}} & X_2 + B_{110} & \underset{k_{-3}}{\overset{k_3}{\rightleftharpoons}} & B_{111} \\
X_2 + B_{000} & \underset{k_{-6}}{\overset{k_6}{\rightleftharpoons}} & X_2 + B_{010} & \underset{k_{-8}}{\overset{k_8}{\rightleftharpoons}} & X_2 + B_{011} & \underset{k_{-9}}{\overset{k_9}{\rightleftharpoons}} & B_{111} \\
X_2 + B_{000} & \underset{k_{-10}}{\overset{k_{10}}{\rightleftharpoons}} & X_2 + B_{001} & \underset{k_{-11}}{\overset{k_{11}}{\rightleftharpoons}} & X_2 + B_{101} & \underset{k_{-5}}{\overset{k_5}{\rightleftharpoons}} & B_{111} \\
X_2 + B_{000} & \underset{k_{-10}}{\overset{k_{10}}{\rightleftharpoons}} & X_2 + B_{001} & \underset{k_{-12}}{\overset{k_{12}}{\rightleftharpoons}} & X_2 + B_{011} & \underset{k_{-9}}{\overset{k_9}{\rightleftharpoons}} & B_{111}
\end{array} \tag{1.4}$$

Again, X_2 denotes a Hes1 dimer, and B_{ijk} denotes the state of the three binding sites in the regulatory region, where 0 and 1 indicate whether a specific binding site is unoccupied or occupied, respectively. As in the case of one binding site, we assume that all bindings of an Hes1-dimer to an N-box are in equilibrium. This leads to 18 algebraic equations, three for each reaction path. For example, the three equations for the first reaction path in system (1.4) are of the form

$$K_{000/100} = \frac{[B_{100}]}{[X_2][B_{000}]},\ K_{100/110} = \frac{[B_{110}]}{[X_2][B_{100}]},\ K_{110/111} = \frac{[B_{111}]}{[X_2][B_{110}]},$$

where $K_{ijk/i'j'k'}$ denote the respective equilibrium constants. Let us first consider the case that binding is independent and that all equilibrium constants are equal, i.e $K_{eq} = K_{ijk/i'j'k'}$ (we will drop this assumption below). We assume that the occupation of any binding site prohibits transcription. This yields the general response function

$$f([X]) = \frac{[B_{000}]}{[B_{000}] + [B_{100}] + [B_{010}] + [B_{001}] + [B_{110}] + [B_{101}] + [B_{011}] + [B_{111}]}.$$

Inserting the algebraic relations from the equilibrium conditions we obtain after rearrangement the response function

$$f([X]) = \frac{1}{1 + 3K_{eq}K_d[X]^2 + 3K_{eq}^2K_d^2[X]^4 + K_{eq}^3K_d^3[X]^6}.$$

With the normalised variable $x = \sqrt{K_{eq}K_d}[X]$ one gets

$$f(x) = \frac{1}{1 + 3x^2 + 3x^4 + x^6}.$$

This leads to a Hill coefficient of about 2.4 (Hill plot not shown).
For synergistic binding, as suggested in [110], the equilibrium constants $K_{ijk/i'j'k'}$ for the binding of a second or third dimer are increased by dimers which are already bounded to one or two binding sites. We assume that the binding of a dimer to an arbitrary operator increases the equilibrium constant for a second dimer by a factor $\kappa \geq 1$, and that these two bounded dimers increase the binding constant of the third dimer by a constant $\delta \geq 1$. Furthermore, we assume that the order of binding of dimers to an N-box does not influence these constants. Then the equilibrium constants for the first reaction path of system (1.4) becomes

$$K_{eq} = K_{000/100},\ K_{100/110} = \kappa K_{eq},\ K_{110/111} = \delta K_{eq},$$

which results in

$$f(x) = \frac{1}{1 + 3x^2 + 3\kappa x^4 + \delta x^6}. \tag{1.5}$$

Response functions are a model-based approach to analyze the data below. Fitting these functions does not only enable us to estimate the Hill coefficient but it also helps to derive biologically interesting information about synergistic effects in the promotor region.
Estimating the Hill Coefficient for the Hes1 Regulatory System. As stated above, the regulatory region of *Hes1* has at least three strong binding and one weak binding site, i.e. the three N-boxes and the region around position -10. We use the data of the experiment described above, where some of the N-boxes are deactivated by mutations, such that one, two, three or all four of them are active. The data yield that a binding of a dimer to the region around position -10 causes a two-fold. If additionally, the first N-Box is active, a seven-fold repression can be observed. In the situation were the second and third N-box are active we obtain a 14- and 30-fold repression, respectively. To estimate the Hill function for the Hes1 promoter activity from these data one has to calculate the response function for a promoter with one, two, three and four binding sites. This computation parallels the arguments above, and we find the result given in Table 1.1.
By means of the very few data one can estimate the Hill coefficient only roughly. If we assume that the equilibrium constants are not effected by the mutations, nearly the same input x should lead in the respective response functions to a 2, 7, 14 and 30-fold repression. We obtain the following equation system

No of active binding sites	Response function	fold repression (experimental)
1	$f_1(x) = 1/(1+x^2)$	2
2	$f_2(x) = 1/(1+2x^2+\kappa x^4)$	7
3	$f_3(x) = 1/(1+3x^2+3\kappa x^4+\delta x^6)$	14
4	$f_4(x) = 1/(1+4x^2+6\kappa x^4+\delta x^6+\epsilon x^8)$	30

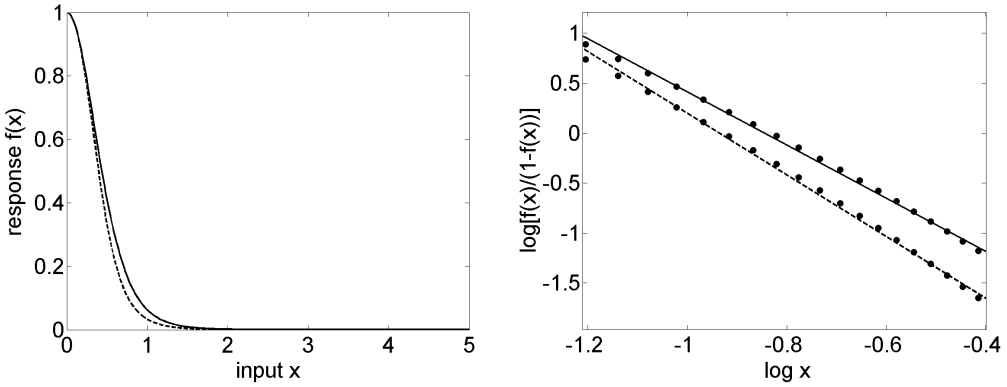
Table 1.1: Given one, two, three or four active binding sites, the response functions and the repression (determined experimentally in [110]) are stated. For a cooperative binding, the parameters should satisfy the restriction $1 \leq \kappa \leq \delta \leq \epsilon$.

$$\begin{aligned} \frac{1}{1+x_1^2} &= \frac{1}{2}, \\ \frac{1}{1+2x_2^2+\kappa x_2^4} &= \frac{1}{7}, \\ \frac{1}{1+3x_3^2+3\kappa x_3^4+\delta x_3^6} &= \frac{1}{14}, \\ \frac{1}{1+4x^2+6\kappa x_4^4+4\delta x_4^6+\epsilon x_4^8} &= \frac{1}{30}. \end{aligned} \tag{1.6}$$

If always the same amount of Hes1-dimers were present in the transcriptional analysis of the *Hes1* promoter, one would obtain $x_1 = x_2 = x_3 = x_4$. This leads to the meaningless result $\delta = -2$. However, since *Hes1* vectors were used instead of Hes1 proteins, a constant amount of the first will not always result in a constant amount in the latter. We do not solve the System (1.6) under this condition, but find parameter sets κ, δ, ϵ which lead to values x_1, x_2, x_3, x_4 as close as possible to each other.

For independent binding, i.e. $\kappa = \delta = \epsilon = 1$, solving system (1.6) leads to $x_1 = 1$, $x_2 = 1.28$, $x_3 = 1.19$, and $x_4 = 1.16$. Thus, the densities x_i differ only moderately. This indicates that the assumption $\kappa = \delta = \epsilon = 1$ is compatible with the data. I.e., there is no evidence for a stronger synergistic effect.

We also minimise $\sum_{i=2}^{4}(x_i - 1)^2$ among all solutions of (1.6) corresponding to affinity constants within the two restriction sets $1 \leq \kappa \leq \delta \leq \varepsilon$ and $\kappa, \delta, \varepsilon \geq 1$. By scanning in discrete steps the minimum under the latter restriction is $x_1 = 1$, $x_2 = 1.06$, $x_3 = 1$, $x_4 = 1.02$ obtained at $\kappa = 3, \delta = \varepsilon = 1$. Optimising under the restriction $1 \leq \kappa \leq \delta \leq \epsilon$ leads to $x_1 = 1$, $x_2 = 1.11$, $x_3 = 1.02$, and $x_4 = 0.998$ for $\kappa = \delta = \epsilon = 2.3$. The resulting response functions are almost indistinguishable (graphs not shown) so we choose the response function with $\kappa = \delta = \epsilon = 2.3$ for further analysis. Since transcription factors can increase the



(a) (b)

Figure 1.4: (a) Inhibitory response functions $f(x) = 1/(1 + 4x^2 + 6\kappa x^4 + 4\delta x^6 + \epsilon x^8)$ for independent binding, i.e. $\kappa = \delta = \epsilon = 1$, (solid) and for weak synergistic binding with $\kappa = \delta = \epsilon = 2.3$ (dashed). (b) Hill plots of the respective response functions.

affinity 10 fold or higher (for instance see [53]) we interpret this as weak binding. Such a quite small increase in the affinity of the binding sites is reflected by a moderate increase of the Hill coefficient. Actually, the response functions for the cases $\kappa = \delta = \epsilon = 1$ and $\kappa = \delta = \epsilon = 2.3$ are very close, see Figure 1.4 (a).

Since we now know the response function for the different assumptions (synergistic binding present or not), we may use these functions in order to estimate the Hill coefficient by Hill plots. For a totally independent binding the Hill coefficient is about 2.7 and for the weak synergistically binding it is about 3.1, see Figure 1.4 (b), showing the values of the transformed functions and the corresponding regression lines.

Thus, on the basis of the Hill plot done according to the very few data we suggest an independent binding and an Hill coefficient between 2.7 and 3.1.

1.1.3 The Goodwin Model

The Hes1 oscillator is one of the simplest example of a regulated pathway. It consists of a sequence of reactions where the product of the last reaction regulates the first reaction.

The first who considered such a system of coupled ordinary differential equations as a mathematical model of a biochemical oscillator based on negative feedback was Goodwin in 1963, see [38] and [39]. In the context of Hes1 it can be written

in the following form,

$$\begin{array}{rcccccc}
\dot{m}_1 & = & kf_{H,h}(p_s) & - & b_1 m_1 & - & a_1 m_1 \\
\dot{m}_2 & = & a_1 m_1 & - & b_2 m_2 & - & a_2 m_2 \\
 & \vdots & & & & & \\
\dot{m}_{r-1} & = & a_{r-2} m_{r-2} & - & b_{r-1} m_{r-1} & - & a_{r-1} m_{r-1} \\
\dot{m}_r & = & a_{r-1} m_{r-1} & - & b_r m_r & & \\
\dot{p}_1 & = & c m_r & - & d_1 p_1 & - & e_1 p_1 \\
\dot{p}_2 & = & e_1 p_1 & - & d_2 p_2 & - & e_2 p_2 \\
 & \vdots & & & & & \\
\dot{p}_{s-1} & = & e_{s-2} p_{s-2} & - & d_{s-1} p_{s-1} & - & e_{s-1} p_{s-1} \\
\dot{p}_s & = & e_{s-1} p_{s-1} & - & d_s p_s & &
\end{array} \tag{1.7}$$

where $\dot{m}_i$ and $\dot{p}_i$ indicate the temporal change of the ith mRNA and protein, respectively. To describe the repression of mRNA synthesis by Hes1 proteins we use a Hill function of the form

$$f_{H,h}(p_s) = \frac{H^h}{H^h + p_s^h}, \tag{1.8}$$

where $H > 0$ and $h \geq 1$ indicate the Hill constant and the Hill coefficient, respectively.

One way to give the system (1.7) a meaning in the present context is as follows: The first equation could be interpreted as the temporal change of pre-mRNA in the nucleus and equations 2 to r could describe the temporal evolution of modified and transported mRNA. The parameters b_i, $1 \leq i \leq r$, would denote the degradation rates of the respective mRNA types then. The constants k and a_i, $1 \leq i \leq r-1$, would then be the synthesis rates of pre-mRNA, and the modification or transport rates, respectively. Similarly, p_1 would describe the temporal changes of the protein which is translated from the mRNA m_r where the constant c would denote the synthesis rate. The equations for p_2 to p_s would describe post-translational modifications and transport of the protein from the cytoplasm into the nucleus. The constants e_j, $1 \leq j \leq s-1$, would denote the transport or modification rates and d_j, $1 \leq j \leq s$, would denote the decay rates of the modified or transported protein types.

1.1.4 Hopf Bifurcation in the Goodwin Model

For a special case of the Goodwin system (1.7) analytical results are available. In order to keep this section self-contained, we report here briefly the corresponding results of Tyson and Othmer, [113]. Making some simplifications, they showed

by local stability analysis that a Hopf bifurcation can occur which results in a sustained periodic oscillation around the steady state.
For convenience, the variables m_i, p_j are renamed to x_i, $1 \leq i \leq n = r + s$. The assumption $\alpha = a_1 + b_1 = a_2 + b_2 = \cdots = d_{s-1} + e_{s-1} = d_s$ allows for further simplification. Under that assumption, the Goodwin system (1.7) can be rewritten in the following form:

$$\begin{aligned} \dot{x}_1 &= k f_{H,h}(x_n) - \alpha x_1, \\ \dot{x}_i &= \beta_{i-1} x_{i-1} - \alpha x_i, \ 2 \leq i \leq n. \end{aligned} \tag{1.9}$$

Note that this assumption does *not* correspond to system (1.7) with constant rates over all species and compartments. Nevertheless, via the linear chain trick [76], this model corresponds to a delay differential equations model with Γ-distributed delays. Such a model was used e.g. by [92] in a similar context.
The steady state $\hat{\mathbf{x}} = (\hat{x}_1, \ldots, \hat{x}_n)$ of (1.9) is obtained by an easy calculation as

$$k f_{H,h}(\hat{x}_n) = \alpha \hat{x}_1 = \frac{\alpha^2}{\beta_1} \hat{x}_2 = \cdots = \frac{\alpha^n}{\beta_1 \cdots \beta_{n-1}} \hat{x}_n. \tag{1.10}$$

By introducing new parameters $\rho = (k\beta_1 \cdots \beta_{n-1})^{1/n}$ and $\gamma = \frac{\alpha}{\rho}$ the steady state equation (1.10) can be written in the simple form

$$\gamma^n \hat{x}_n^{h+1} = 1 - \gamma^n \hat{x}_n \tag{1.11}$$

which has always a unique positive solution $\hat{x}_n > 0$. For stability analysis near the steady state one has to compute the Jacobian matrix J consisting of the partial derivatives of the right hand sides in system (1.9):

$$J = \begin{pmatrix} -\alpha & 0 & \cdots & 0 & -k\theta^n \\ \beta & -\alpha & \cdots & 0 & 0 \\ \vdots & \vdots & \ddots & \vdots & \vdots \\ 0 & 0 & \cdots & \beta & -\alpha \end{pmatrix},$$

where $\theta^n = h\hat{x}_n^{h-1}\,(1+\hat{x}_n^h)^{-2}$. Solving the characteristic equation $\det(J - \lambda \mathrm{I}) = 0$ leads to

$$(-1)^n(\alpha + \lambda)^n - (-1)^{n+1}\theta^n k\beta_1 \cdots \beta_{n-1} = 0.$$

With the notations defined above this can be simplified to $(\alpha + \lambda)^n + \theta^n \rho^n = 0$ and has solutions

$$\lambda_l = \cos\Big(\frac{2l+1}{n}\pi\Big)\theta\rho - \mathrm{i}\sin\Big(\frac{2l+1}{n}\pi\Big)\theta\rho - \alpha,$$

for $l = 0, 1, \ldots, n-1$. Hopf bifurcation with sustained oscillations occurs when a pair of complex eigenvalues crosses the imaginary axis from left to right as α

decreases. Thus a necessary condition is that the real part of λ has to be zero. This is first possible for $l = 0$. Furthermore, for the steady state becoming unstable one must have

$$\theta > \gamma \left(\cos \frac{\pi}{n}\right)^{-1}.$$

Therefore $\theta^n = h\gamma^n(1 - \gamma^n \hat{x}_n) > \gamma^n \cos(\frac{\pi}{n})^{-n}$. This gives us a lower bound of the Hill coefficient for which oscillation is possible:

$$h > \frac{1}{1 - \gamma^n \hat{x}_n} \left(\cos \frac{\pi}{n}\right)^{-n}.$$

For the lowest number of equations, $n = 3$, where oscillation is possible at all one obtains $h > 8$, since $0 < \gamma^n \hat{x}_n < 1$. This was found first by Griffith [43]. However, this value is too high to match the values developed in the previous section. By increasing the number of equations the Hill coefficient can be decreased: for $n = 4$ one obtains $h > 4$. Such a system can be interpreted as pure transport model between 2 compartments, e.g. after transcription the mRNA is transported into the cytoplasm where the protein is translated and afterwards transported into the nucleus. Thus even in the case of a pure transport system a more realistic value for the Hill coefficient is possible. Other constraints for h are listed in Table 1.2.

$n =$	5	7	9	11	13	15	17	34
$h >$	2.88	2.07	1.75	1.57	1.47	1.39	1.34	1.16

Table 1.2: Lower bounds for the Hill coefficient for the occurrence of oscillations in the Goodwin system with different numbers of equations.

Using Hopf's Theorem, see e.g. [69], it is possible to compute the parameter α for which sustained oscillations with period equal to 120 min are obtainable. At the bifurcation point there exists a periodic solution with period

$$\triangle_T = \frac{2\pi}{\Im(\lambda)}. \tag{1.12}$$

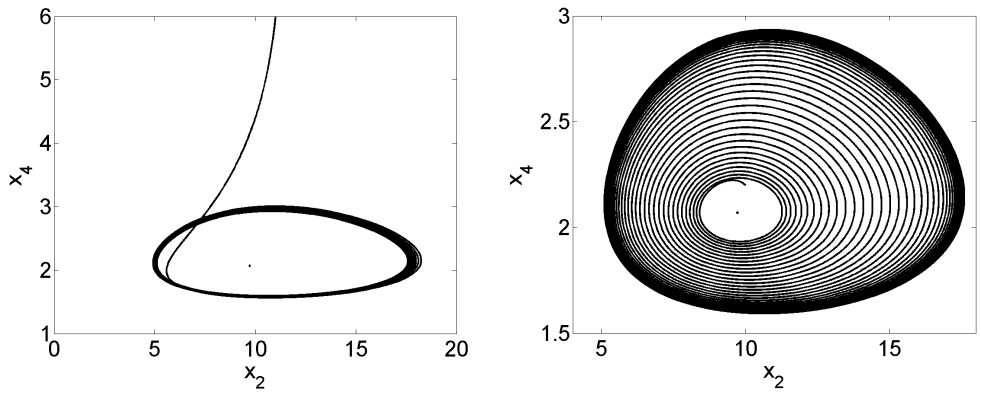
Solving $\Re(\lambda) = 0$ one gets $\theta\rho = \alpha / \cos(\frac{\pi}{n})$ by which $\Im(\lambda)$ can be expressed in terms of α and n:

$$\Im(\lambda) = \sin(\frac{\pi}{n})\theta\rho = \alpha \tan(\frac{\pi}{n}).$$

Thus, in the homogeneous Goodwin model (1.9) with n equations, the period is mainly determined by the decay and the modification rates. For periodic solutions with period equal to 120 min one gets

$$\alpha = \frac{\pi}{\tan(\frac{\pi}{n}) 60 \text{ min}}.$$

In particular, this gives an upper bound for the decay rates of the mRNA and the protein for which sustained oscillations are possible at all. For instance, in a system with 4 or 7 equations one obtains $\alpha = 0.052$ min^{-1} and $\alpha = 0.108$ min^{-1}, respectively. In [51], the decay rates of the *Hes1* mRNA and the Hes1 protein were experimentally determined as 0.028 min^{-1} and 0.031 min^{-1}, respectively. Since both rates are smaller than $\alpha = 0.052$ min^{-1}, oscillations are possible even in the pure transport model of the Hes1 oscillator. We demonstrate this using the parameters $n = 4$, $h = 4.5$, $k = 30$, and the *Hes1* mRNA decay rate $b = 0.028$ min^{-1}. Thus, $\beta_i = \alpha - b = 0.024$ min^{-1} for $1 \leq i \leq n$. The steady state is calculated from equation (1.11): $\hat{\mathbf{x}} = (21.08, 9.73, 4.49, 2.07)$. As shown by Figure (1.5) $\hat{\mathbf{x}}$ becomes unstable and the generic trajectory approaches a limit cycle.



(a) (b)

Figure 1.5: Undamped oscillations of the x_i correspond to the evolution towards a limit orbit around the steady state $(\hat{x}_1, \hat{x}_2, \hat{x}_3, \hat{x}_4) = (21.089.734.492.07)$ in the phase space. For two different initial conditions the system evolution is plotted in the x_2–x_4–plane: (a) $(x_1(0), x_2(0), x_3(0), x_4(0)) = (20, 11, 1, 6)$; (b) $(x_1(0), x_2(0), x_3(0), x_4(0)) = (20, 10, 5, 2.2)$.

Starting nearby $\hat{\mathbf{x}}$ produces very small fluctuations around the steady state. From other initial conditions the curves surround the unstable steady state and evolve towards the limit cycle, independent from whether the system starts outside, 1.5 (a) or within 1.5 (b) the attractive orbit.

A Rough Delay Estimate

A disadvantage in the Goodwin approach is the fact that the intermediate states of the transport process are only loosely related to physical transport in the cell, like

the transport within the cytosol, but also take care for other processes like splicing etc. Thus it is not straight forward to choose the number of states n and to interpret the single components. Furthermore, an experimental investigation does not seem possible at the moment. However, the basic effect of these transport processes is a delay that leads to the oscillation. Delays may be more simple to address resp. manipulate by experiments. Therefore, we want to know how to connect the parameters and the effective delay in the Goodwin model. In particular, we will show that the oscillation period depends on the overall delay mainly, like for a delay differential equation.

We investigate the fate of one mRNA particle produced. The delay corresponds to the time until the protein molecules prooduced by this mRNA particle return to the cell nucleus of the cell and influences the production term. The relevant part of the pathway consists of linear terms only. More precisely, the system gets the following form:

$$\begin{pmatrix} \dot{x}_1(t) \\ \dot{x}_2(t) \\ \vdots \\ \dot{x}_n(t) \end{pmatrix} = \begin{pmatrix} -\alpha & 0 & \cdots & 0 & 0 \\ \beta_1 & -\alpha & \cdots & 0 & 0 \\ \vdots & \vdots & \ddots & \vdots & \vdots \\ 0 & 0 & \cdots & \beta_{n-1} & -\alpha \end{pmatrix} \begin{pmatrix} x_1(t) \\ x_2(t) \\ \vdots \\ x_n(t) \end{pmatrix}. \tag{1.13}$$

The system (1.13) is analytical solvable and for the particular initial conditions

$$(x_1(0), \ldots, x_n(0)) = (C, 0, \ldots, 0),$$

where $C > 0$, the solution reads

$$x_i(t) = C \frac{1}{(i-1)!} \prod_{j=0}^{i-1} \beta_j \mathrm{e}^{-t\alpha} t^{i-1},\ 1 \leq i \leq n. \tag{1.14}$$

As overall delay $\triangle_D$ we define the time from the maximal expression value of the first molecular species x_1, to the maximal expression value of the last molecular species x_n. For system (1.13) with the specific initial condition it equals the time where the concentration x_n is maximal. We obtain

$$\triangle_D = \frac{n-1}{\alpha}, \tag{1.15}$$

i.e., similar to the oscillation period, the delay is the inverse of the modification rate plus the half-life rate times the number of equations minus one. Inserting equation (1.15) into (1.12) one obtains the following functional dependency of the oscillation period on the overall delay:

$$\triangle_T = \frac{2\pi}{(n-1)\tan(\frac{\pi}{n})}\ \triangle_D\ . \tag{1.16}$$

Thus, for a fixed number of equations n, the oscillation period near the bifurcation point is proportional to the overall delay. This shows that as in the case of a delay system the oscillation period in a Goodwin system is mainly determined by the overall delay. But in contrast to a delay system, where the delay and the half-lives are independent of each other, [80], equation (1.15) shows that in a Goodwin model both the half-lives of the mRNA and of the protein influence the delay. This is an interesting fact, because it may has strong implications on the modeling of Hes oscillators in mutants where the half-lives of the mRNA or protein are de- or increased.

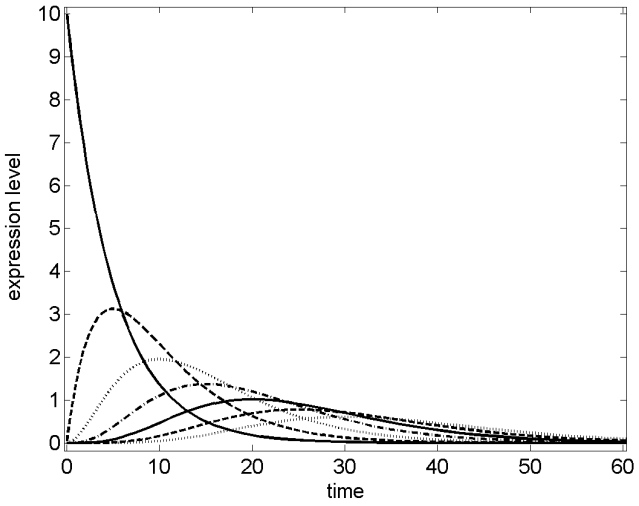


Figure 1.6: Effect of additional linear equations in (1.13): expression level decreases and expression maxima are shifted to higher times.

We have simulated the system (1.13) with $\alpha = 0.2,\ \beta_i = 0.17$ and initial values $(x_1(0), \ldots, x_7(0)) = (10, 0, 0, 0, 0, 0, 0)$ resulting in a delay equal to 30 min. The result in Figure 1.6 shows that the maximal expression values of consecutive reactants decrease and that they are shifted towards larger times. Furthermore, the unimodal expression curves become more spread, i.e. the variance in the delay of the expression of subsequent molecular species increases.

1.1.5 Numerical Simulations

In the following we weaken the parameter constraints of the last two sections to get a more realistic model for the Hes1 oscillator. For the decay rates of the different types of mRNAs and proteins we use the values determined in [51], i.e. $b_i = 0.028$ and $d_j = 0.031$ for all $1 \leq i \leq r$ and $1 \leq j \leq s$, respectively.

Furthermore, because there are no more data, we assume that the modification rates of the different types of mRNA and protein are all equal, i.e. $a_i = a$ for all $1 \leq i \leq r$ and $e_j = e$ for all $1 \leq j \leq s$. Specifically, we consider the following system of differential equations:

$$\begin{array}{rcccccc}
\dot{m}_1 & = & kf_{H,h}(p_s) & - & bm_1 & - & am_1 \\
\dot{m}_2 & = & am_1 & - & bm_2 & - & am_2 \\
 & \vdots & & & & & \\
\dot{m}_{r-1} & = & am_{r-2} & - & bm_{r-1} & - & am_{r-1} \\
\dot{m}_r & = & am_{r-1} & - & bm_r & & \\
\dot{p}_1 & = & cm_r & - & dp_1 & - & ep_1 \\
\dot{p}_2 & = & ep_1 & - & dp_2 & - & ep_2 \\
 & \vdots & & & & & \\
\dot{p}_{s-1} & = & ep_{s-2} & - & dp_{s-1} & - & ep_{s-1} \\
\dot{p}_s & = & ep_{s-1} & - & dp_s & &
\end{array} \tag{1.17}$$

Although such a system is still a strong simplification, analytical analysis becomes nearly hopeless. Thus, we simulate system (1.17) by adjusting the parameters from the previous sections. For fixed b and d we varied the other variables and searched for a set of parameters for which undamped oscillations with a oscillation period of about 120 min can be observed.

r	s	a	e	c	H	k	h	$\triangle_T$	$\triangle_m$	$\triangle_p$
2	2	0.05	0.09	0.2	10	30	6.2	122	18	23
5	2	0.25	0.1	0.18	20	30	4.5	120	25	19
38	2	1.9	1.4	0.1	15	130	4.3	125	34	20

Table 1.3: Parameter values for the Goodwin system (1.7) for which sustained oscillations were obtained. Additionally, for each simulation the values of $\triangle_T$, $\triangle_m$ and $\triangle_p$, i.e. of the oscillation period, the transcriptional and translational delay, respectively, are displayed.

To investigate the effects of different numbers of equations on the Hill coefficient in the Hes1 oscillator we consider 3 systems with 4, 7 and 40 equations. The used parameter sets are given by Table 1.3. The meaning of the parameters is given in the text beneath equation system (1.7).

The 4–equations system: We started with a system consisting of four equations, i.e. using $r = s = 2$. As mentioned above, such a system can be interpreted as a pure transport system. The synthesis of mRNA in the nucleus is described by the first equation. Then the mRNA is transported into the cytoplasm and translated into protein, specified by the second and third equation, respectively. After that,

the protein is transported in the nucleus, given by the fourth equation. There it represses the transcription of its encoding gene.
For the homogeneous Goodwin model (1.9) oscillations are possible for a Hill coefficient somewhat greater than 4, see Figure 1.5. In contrast to this, we found for this more realistic model, under the restrictions imposed by the decay rates and an oscillation period of about 120 min, sustained oscillations only for a Hill coefficient above 6, see Figure 1.7 (a). For the parameter set listed in Table 1.3 the system oscillated with period $\triangle_T$=122.7. Table 1.3 displays also estimates for the transcriptional and translational delays, $\triangle_m$ and $\triangle_p$, respectively. Another reason for the necessity of such a high Hill coefficient is the equation of the formation of the mature mRNA m_2. There, m_2 is only degraded so that the total modification rate of the mature mRNA $\alpha_2 = b_2 = 0.028$ differs quite strongly from the total modification rate of the pre-mRNA m_1, $\alpha_1 = a_1 + b_1 = 0.078$. We see that even a slight change in the mathematical model can yield quite different predictions of the dynamics of the pathway.

The 7–equations system: Increasing the number of equations, $r = 5, s = 2$, corresponds to describing the negative feedback loop on a finer level. The system could be interpreted in the following way: The synthesis of pre-mRNA in the nucleus is described by the first equation. In the next steps, the pre-mRNA is transported by diffusion from the DNA to the spliceosom and becomes spliced, given by equations two and three. After that, the spliced mRNA is transported into the cytoplasm, equation four, and then, by diffusion, to the ribosome, equation five, where it accumulates. The mature mRNA is then translated into protein, described by equation six, which is transported in the nucleus, equation seven, where it represses the transcription after the Hes1 protein amount has exceed a certain threshold.
To achieve sustained oscillations with period equal to 120 min in an 7–equations system we have, according to equation (1.15), to increase the parameter values of a and e, see Table 1.3. We find undamped oscillations for a Hill coefficient equal to 4.5, see Figure 1.7 (b) where the time evolution of the fifth and seventh component are displayed. Again, if one would use the simplified Goodwin system where all modification rates are equal one could achieve sustained oscillations for a Hill coefficient equal to 3.3.
The 40–equations system: An additional lowering of the Hill coefficient becomes very difficult, indicating that the Hill coefficient may converge to some limit value greater than four. For a system consisting of 40 equations, $r = 38, s = 2$, we could lower the Hill coefficient only by 0.2: for a Hill coefficient equal to 4.3 we achieved undamped oscillations with oscillation period about 125 min, see Figure 1.7 (c).
Using such a high number of equations means, that the autoregulative network is

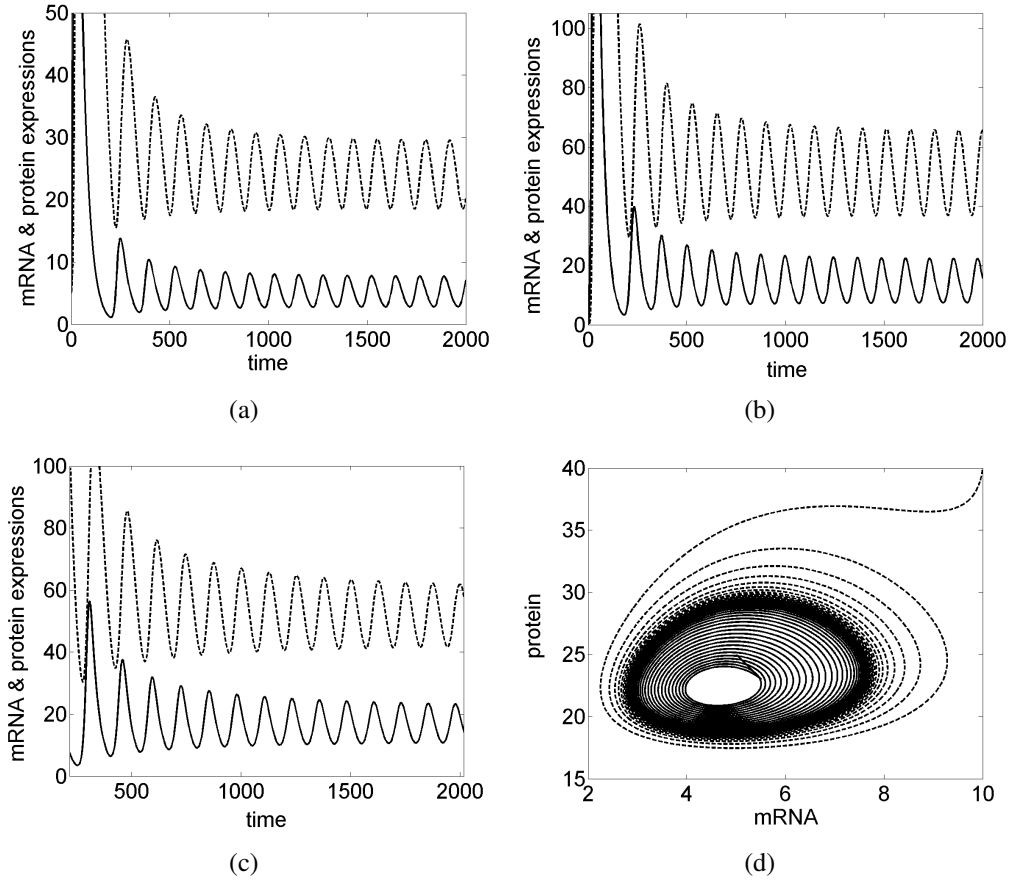


Figure 1.7: Time evolution of mature mRNA and protein in the 4, 7, and 34 equations systems. (a) 4 eqns system: m_2 solid, p_2 dashed (b) 7 eqns system: m_5 solid, p_2 dashed (c) 40 eqns system: m_{38} solid, p_2 dashed (d) Limit cycle behavior of the 4 eqns model in the (m_2, p_2) plane.

modeled on a very fine level. This comprehends that single intermediate steps like elongation of transcription and translation would be considered.

As in the simplified model of the previous sections the systems above show only weak dependence on initial conditions. For example, corresponding to the sustained oscillations in Figure 1.7 (a) the $(m_2, p_2)-$curve evolves towards a limit cycle in the $(m_2, p_2)-$phase plane which is demonstrated in Figure 1.7 (d). There, the level of mature protein, p_2, is plotted as a function of mature mRNA, m_2, for four different initial conditions: $(m_1, m_2, p_1, p_2) = (5, 10, 4, 40)$ and $(5, 5, 4, 25)$.

1.1.6 Discussion

In our experience the strongest challenge in modeling papers addressing Hes1 oscillators is the uncertainty about the value of the Hill coefficient. We estimated the Hill coefficient of the switch in the Hes1 oscillator using response functions derived from a model for ligand binding. On the basis of experimental data from binding analysis we assumed that the regulatory region of *Hes1* consists of four binding sites. Using the results from transcriptional analysis we suggest that there is no or only a small synergistic binding of Hes1 dimers to these four binding sites and that the Hill coefficient ranges between 2.7 and 3.1. Of course, an estimate based on dose-response data, if it existed, would be much more accurate. Our analysis shows that the Hill coefficient is crucial for understanding periodic oscillations. Thus, further experimental analysis of the *Hes1* promoter is of great importance.

To model the time delay arising from transcription and translation more explicitly, we used the Goodwin system. Under the assumptions that transcription and translation are well described by first-order kinetics we use linear differential equations to describe the temporal change of the intermediate steps between mRNA synthesis and mature protein. For analytical analysis we made several simplifications. We showed that the oscillation period of a Goodwin system depends mainly on the transcriptional and translational delay. In the case of a delay differential equations model this was demonstrated by Monk, [80]. Differently from Monks model, the overall delay in a Goodwin model depends also on the decay rates of the mRNA and the protein. This feature is important for the prediction of the dynamics of the pathway in mutants with altered decay rates.

By simulations, we studied a more realistic variant of the Goodwin model. We achieved sustained oscillations with period of about 120 min for different Hill coefficients by increasing the number of linear equations. For a pure transport model consisting of four equations oscillation is possible only for a Hill coefficient equal to 6.2.

A more realistic value for the Hill coefficient is obtained for a system consisting of seven equations. Here, sustained oscillations are obtained for a Hill coefficient equal to 4.5. Such a system is well interpretable assuming that splicing and transport of mRNA and protein can be regarded as linear processes.

For a smaller Hill coefficient, it becomes more and more difficult to achieve sustained oscillations. For instance, for a system consisting of 40 coupled differential equations still a Hill coefficient of at least 4.3 is required for this goal. Using such a big system means to model the genetic network on a very fine level which makes it very difficult to verify the system by biological experiments: It is very unlikely to obtain biological data for all the parameters. Furthermore, we shown that the modification rates should be in the same magnitude. Otherwise the Hill coefficient

would increase again. In the case of the 40–equations system this means that all modification processes have a very low variability implying that they are highly coordinated by intracellular mechanisms which is unlikely too.
We want to note here that there is a large gap between the critical Hill coefficients of the homogeneous Goodwin model (1.9), which is very similar to the delay differential equation models from literature, and the realistic Goodwin model (1.17) used in our simulations.
On the basis of our findings, we suggest as a realistic value for the Hill coefficient a value equal to 4.5 or higher. Comparing it to the value estimated by response functions there is still a gap of about 1.5. Such a discrepancy indicates that besides the linear processes there must be further, nonlinear mechanisms, which increase the complexity of such an autoregulative network.
A possible explanation for this could be additional nonlinear processes. Similar to the *Per* gene in *Drosophila* [26], Ström et al. showed in [109] that Hes1 is also phosphorylated. Usually, phosphorylation is modeled as a nonlinear process, see for instance [37]. Any additional nonlinearity in the feedback loop could lead to a smaller Hill coefficient more compatible with our model for the transcription of *Hes1*. It should not be too difficult to build this into our model.
Finally, we want to remark that these models do not apply to the Hes1 oscillator only. Although this was not the focus of the present work, the derivations and parameters can be easily adapted to similar situations like the Hes7 oscillator in mouse, or the Her1 and Her7 oscillators in zebrafish.

1.2 Number of active transcription factor binding sites is essential for the Hes7 oscillator

The current section presents the results published in [128].
It is commonly accepted that embryonic segmentation of vertebrates is regulated by a segmentation clock, which is induced by the cycling genes Hes1 and Hes7. Their products form dimers that bind to the regulatory regions and thereby repress the transcription of their own encoding genes. An increase of the half-life of Hes7 protein causes irregular somite formation. This was shown in recent experiments by Hirata et al. In the same work, numerical simulations from a delay differential equations model, originally invented by Lewis, gave additional support. For a longer half-life of the Hes7 protein, these simulations exhibited strongly damped oscillations with, after few periods, severely attenuated the amplitudes. In these simulations, the Hill coefficient, a crucial model parameter, was set to 2 indicating that Hes7 has only one binding site in its promoter. On the other hand, Bessho et al. established three regulatory elements in the promoter region.
We show that – with the same half life – the delay system is highly sensitive to changes in the Hill coefficient. A small increase changes the qualitative behaviour of the solutions drastically. There is sustained oscillation and hence the model can no longer explain the disruption of the segmentation clock. On the other hand, the Hill coefficient is correlated with the number of active binding sites, and with the way in which dimers bind to them. In this section, we adopt response functions in order to estimate Hill coefficients for a variable number of active binding sites. It turns out that three active transcription factor binding sites increase the Hill coefficient by at least 20% as compared to one single active site.
Our findings lead to the following crucial dichotomy: either Hirata's model is correct for the Hes7 oscillator, in which case at most two binding sites are active in its promoter region; or at least three binding sites are active, in which case Hirata's delay system does not explain the experimental results. Recent experiments by Chen et al. seem to support the former hypothesis, but the discussion is still open.

1.2.1 Introduction

In mouse embryos, a pair of somites is separated from the anterior end of the presomitic mesoderm every two hours [87]. This process is assumed to be induced by the bHLH factors Hes1 and Hes7 [84], [11], which also oscillate with a period of about two hours. Their oscillation is caused by a negative feedback loop in which the proteins repress the transcription of their corresponding genes [12], [13], [51], [55]. Hirata et al. [50] showed that the Hes7 protein has a half-life of about 22 minutes. To demonstrate that this is crucial for oscillation, they used

mouse mutants with a longer Hes7-half-life of about 30 minutes, but with normal repressor activity. In mice with a smaller protein decay rate, somite segmentation became irregular, and Hes7 expression did not show cyclic behaviour. Lewis [72] used delay differential equations to model the mechanism for the homologous zebrafish Her1 and Her7 oscillators. Delay equations allow intermediate synthesis steps such as transport, elongation and splicing to be subsumed in the delays. Thus, only two equations are needed, one for the mRNA and one for the protein, in contrast to compartment models where at least three equations are needed. Repression of Her7 transcription by Her7 is represented by an inhibitory Hill function. The latter is of sigmoid form and decreases from one to zero. The modulus of steepest descent is called the Hill coefficient. As shown in Section 1.1, it correlates with the number of and the cooperativity between transcription factor binding sites. Hirata et al. chose a Hill coefficient of 2, corresponding to a promoter with one single binding site for Hes7 dimers. On the other hand, Bessho et al. [12] showed that Hes7 has one N box and two E boxes as regulatory elements in the promoter region. By transcription analysis they demonstrated that transcription can be repressed by both N box- and E box-containing promoters. Thus, as in Hes1, there are at least three binding sites in the regulatory region of Hes7 to which Hes7 dimers could bind. In the present section, we show that three active transcription-factor binding sites cause an increase of the Hill coefficient, and that such an increase results in a completely different behaviour of the delay system, which does no longer reflects the observations made by Hirata et al., [50].

1.2.2 Methods

Model of the Hes7 switch

To compute the Hill coefficient in the Hes7 oscillator we use a similar model as in Section 1.1, which mimics the chemical reactions model for ligand binding in [96], [97]. In this approach, the transcriptional activity of the Hes7 promoter and its dependence on the concentration of Hes7 is represented by a response function. For convenience, we will approximate the response functions by Hill-type functions later. We assume that a single bound dimer represses the transcription of Hes7 completely. Then the response function is the long-term relative frequency of occupation of one of the binding sites in dependence on the protein concentration. If $[X]$ denotes the Hes7 concentration, the response is given by the ratio of the concentrations $[P_U]$ and $[P_T]$ of the unoccupied and total promoter configurations:

$$f([X]) = \frac{[P_U]}{[P_T]}$$

To express $[P_U]$ and $[P_T]$ in terms of [X], let ijk denote a generic promoter configuration. For example, $i = 1$ indicates that the first binding site is occupied and $i = 0$ that it is not; $ijk = 010$ is the configuration where only the second site is occupied. There are six possible reaction channels through which three dimers can bind successively to the three sites (Fig. 1.8).

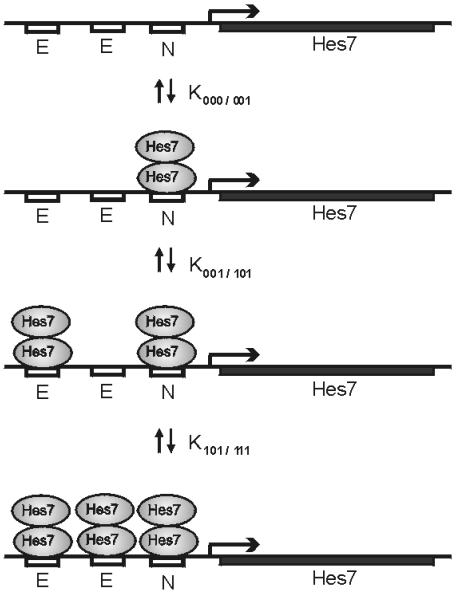


Figure 1.8: Schematic representation of Hes7-dimer binding in the regulatory region of Hes7. Binding sites are indicated by three rectangles. E and N denote an E- or an N-box binding site, respectively. We assume that association and dissociation are in equilibrium. K denotes the respective equilibrium constants. 0 or 1 indicates whether the respective binding sites are occupied or not.

We assume that binding of dimers to any promoter configuration is in equilibrium. Let $K_{ijk/hlm}$ be the equilibrium constant for the reaction that changes the promoter configuration from ijk to hlm. Let $[X_2]$ and $[P_{ijk}]$ denote the concentrations of free Hes7 dimers and promoter configurations, respectively. Then we obtain the three equations

$$K_{000/001} = \frac{[P_{001}]}{[X_2][P_{000}]}, K_{001/101} = \frac{[P_{101}]}{[X_2][P_{001}]}, K_{101/111} = \frac{[P_{111}]}{[X_2][P_{101}]}.$$

We will assume that dimerization is in equilibrium as well. The equilibrium con-

stant of this reaction is $K_d = [X_2]/[X]^2$. For the configuration 000, where no dimer is bound to any of the three binding sites, the equilibrium constants for binding of a dimer to one of the three binding sites are equal, and we may set $K_{eq} = K_{000/hlm}$ for all h, l, m. Under these simplifying assumptions, the response function has the form

$$f([X]) = \frac{1}{1 + 3K_{eq}K_d[X]^2 + 3\gamma K_{eq}^2 K_d^2 [X]^4 + \delta K_{eq}^3 K_d^3 [X]^6}$$

see [96]. The constants γ and δ represent the change in affinity to a dimer of the second and third binding sites. We assume that bound dimers increase the affinity of the remaining unoccupied binding sites, hence $\gamma, \delta \geq 1$. In terms of the normalized variable $x = \sqrt{K_{eq}K_d}[X]$ the response function reads

$$f(x) = \frac{1}{1 + 3x^2 + 3\gamma x^4 + \delta x^6}. \tag{1.18}$$

The steepness of (1.18) is determined by means of a Hill plot. For this purpose, $\log(f_h(x)/(1 - f_h(x)))$ is plotted against $\log(x)$ for $0.1 \leq f_h(x) \leq 0.9$. The absolute slope of the regression line for the Hill plot yields a reliable estimate of the Hill coefficient. Then, in the above range, response functions of the form (1.18) are well approximated by Hill-type functions

$$f_h(x) = \frac{1}{1 + (x/H)^h} \tag{1.19}$$

with the Hill coefficient h and Hill constant H.

Model of the Hes7 oscillator

The temporal course of *Hes7* mRNA and Hes7 protein concentrations was modeled by delay differential equations. The system reads

$$\begin{aligned} \frac{\mathrm{d}p(t)}{\mathrm{d}t} &= am(t - T_p) - bp(t), \\ \frac{\mathrm{d}p(t)}{\mathrm{d}t} &= kf_h\big(p(t - T_m)\big) - cm(t). \end{aligned} \tag{1.20}$$

where $p(t)$ and $m(t)$ denote the amounts of *Hes7* mRNA and Hes7 proteins at time t. The Hill-type function f_h in (1.19) describes the negative feedback of Hes7 protein on *Hes7* mRNA synthesis. The entries k and a are the basal transcription rate in the absence of inhibitory proteins, and the rate constant of translation, respectively. Finally, the protein and mRNA decay rates are denoted by b and c. The latter are inversely proportional to the respective protein and mRNA half-lives τ_p and τ_m. More precisely, we have $b = \ln 2/\tau_p$ and $c = \ln 2/\tau_m$.

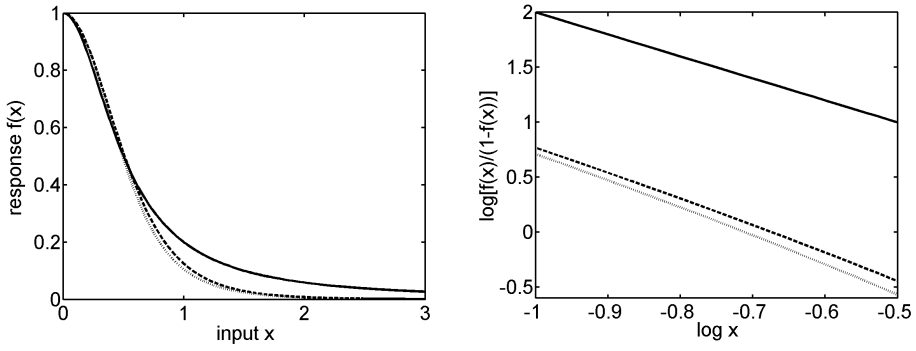
Numerical Simulations

We carried out numerical simulations for the delay system (1.20) with the different Hill coefficients resulting from the calculations for different binding scenarios sketched above. For numerical integration of the delay system, we used the DDE solver of the software package MATLAB. All parameters except the Hill coefficient were taken from [50]: in particular, the experimentally determined protein half-lives of $\tau_p = 20$ min or $\tau_p = 30$ min were used as input. The overall delay $T_m + T_p = 37$ min was split into $T_m = 30$min and $T_p = 7$ min ([55] do not specify T_m and T_p), which has no influence on the dynamics [80]. The remaining parameters were taken from the original zebrafish model [72]: *Hes7* mRNA half-life $\tau_m = 3$ min, protein synthesis rate $a = 4.5$ molecules per mRNA molecule per min, basal transcription rate $k = 4.5$ mRNA molecules per min, and a Hill constant $H = 40$ protein molecules per cell. The Hill coefficient was varied from 2.0 (the value used in [50]) to 2.4 and 2.6. The latter values were obtained by mathematical analysis of the model for the regulatory region of *Hes7*. Details are reported in the results section.

1.2.3 Results

Estimation of the Hill Coefficient

We calculated the Hill coefficient of the response function (1.18) for two scenarios.
(A) The equilibrium constant K_{eq} of the unoccupied binding sites is not changed by a bound dimer, so $\gamma = \delta = 1$. The dimers bind non-synergistically or independently to any one of the three binding sites.
(B) A bound dimer changes the equilibrium constant of one of the remaining free binding sites, so the binding is synergistic or (positively) cooperative. Therefore, at least one of the parameters γ or δ is greater than one.
For the case $\gamma = \delta = 1$ (A), the response function (1.18) is plotted as a dashed line in Fig. 1.9(a). If Hes7 has only one transcription factor binding site, as assumed by Hirata et al. [50], the response function is a Hill function with a Hill coefficient $h = 2$. For a Hill constant of $H = 1$ it is plotted as a solid line. Fig. 1.9(a) shows that an increase in the number of binding sites yields a steeper curve and thus results in increasing strength of the switch. To quantify this, the corresponding Hill plots were constructed (Fig. 1.9(b)). For a Hill function with a coefficient of $h = 2$ the Hill plot is a straight line with a slope of -2. The Hill plot of the response function (1.18) with $\gamma = \delta = 1$ is plotted as a dashed line. The slope of the fitted regression line gives a Hill coefficient of about 2.4.



(a) (b)

Figure 1.9: (a) Response functions for a promoter with two (solid line) and three (dashed and dotted lines) binding sites. (b) Hill plots of the three response functions: $\log(f_h(x)/(1-f_h(x)))$ is plotted versus $\log(x)$.

In (B), we assumed synergistic binding of the dimers. As an example, we consider the case where the affinity of the second binding site to Hes7 dimers is increased by 50%, and the affinity of the third binding site is uninfluenced, i.e. $\gamma = 1.5$, $\delta = 1$ (dotted line in Fig 1.9(a)). The plot shows that a small increase in the affinity of the second binding site results in a small increase of the strength of the switch. Regression of the Hill plot gives a Hill coefficient equal to 2.6 (Fig. 1.9(b) dotted line). Thus, an increase in the number of binding sites or in the affinity of a binding site results in an increase of the Hill coefficient. This effect becomes stronger if the affinity of one of the binding sites is increased by a bound dimer.

Numerical Analysis of the Delay System

We simulated the delay system (1.20) for the different Hill coefficients calculated above. Figures 1.10(a) and 1.10(b) display the simulation results for the parameters used in [55]: for a protein half-life of $\tau_p = 20$ min and a Hill coefficient of $h = 2$, the system shows undamped oscillations with a period of about 120 min (Fig. 1.10(a)). For a greater protein half-life of 30 min, oscillation is strongly damped and the amplitude becomes vanishingly small after four to five cycles (Fig. 1.10(b)). This might explain the results found by Hirata and colleagues [50]. There it was shown that cyclic expression of *Hes7* fails for mouse mutants with a longer Hes7 protein half-life. However, the delay system exhibits a completely different behaviour if the Hill coefficient is increased. For a Hill coefficient equal to 2.4, the damping of the oscillations is much more restrained: After 1700 minutes, during which time more than 14 somites are formed, the oscillation amplitude is greater than after 3 oscillations in the system with a Hill coefficient equal

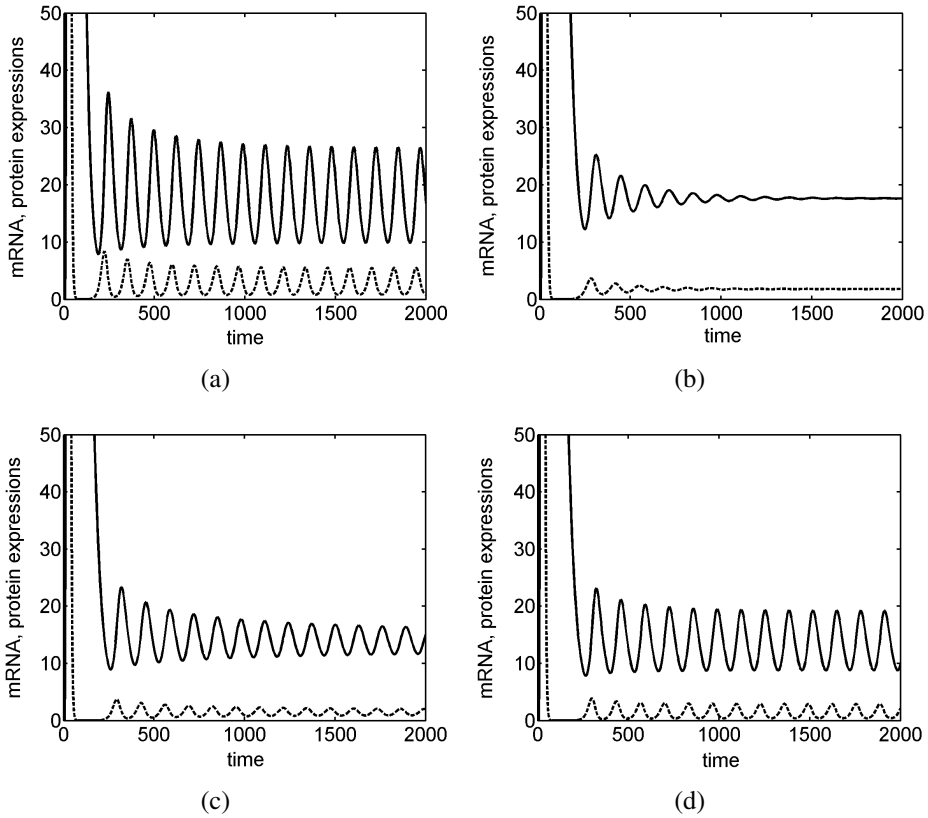


Figure 1.10: Numerical simulation of the Hes7 autoregulatory network for different values for the protein half-life and the Hill coefficient h. The expression curves of the mRNA and the protein are given by the dashed and the solid curves, respectively. For better representation, the protein expression curves were scaled by 0.05. (a)$\tau_p = 20$ min, $h = 2$. (b) $\tau_p = 30$ min, $h = 2$. (c) $\tau_p = 30$ min, $h = 2.4$. (d) $\tau_p = 30$ min, $h = 2.6$.

to 2 (Fig. 1.10(c)). This effect becomes even stronger when the Hill coefficient is increased further. A Hill coefficient equal to 2.6 leads to a sustained oscillation (Fig. 1.10(d)).

Discussion and Conclusions

We used response functions to model the binding of Hes7 dimers to the regulatory region of *Hes7*. Because no experimental data from transcriptional analysis of *Hes7* were available, we assumed that one bound Hes7 dimer can repress transcription of *Hes7* completely. We showed that both an increase in the number of binding sites and positive cooperativity increase the value of the Hill coefficient.

Taking into account that *Hes7* has three potential transcription factor binding sites [12], our model suggested an increase of the Hill coefficient of at least 20% compared to a promoter with only one binding site. In the case of independent binding of Hes7 dimers to one of the three binding sites, the Hill coefficient increased from 2 to 2.4. In the case of positive cooperativity, an increase of 50% in the affinity constant of one binding site resulted in a further increase of the Hill coefficient to a value of approximately 2.6.
Numerical analysis of the delay differential equation system proposed by Hirata et al., [50] revealed that oscillations of the *Hes7* autoregulatory network depend predominantly on the strength of the switch. For a longer half-life of the Hes7 protein, a 20% increase in the Hill coefficient changed the behaviour of the delay system drastically: oscillations become highly damped, and for a Hill coefficient of 2 become insignificant after 5 oscillations. In contrast, a Hill coefficient equal to 2.4 leads only to a weak dampening of the oscillations. After 14 oscillations the system still showed significant amplitudes.
There are two conceivable explanations for these phenomena. On the one hand, if the delay system proposed by Hirata and colleagues [50] describes the *Hes7* oscillator correctly, their results and our findings suggest a Hill coefficient less than 2.4. If this is the case, there should be no more than two active binding sites in the *Hes7* promoter. Recent *ex vivo* experiments by Chen et al. [55] support this interpretation. Nevertheless, the following questions are not answered yet:

- There are several potential transcription factor binding sites in the Hes7 promoter [12], so why are no more than two of them active?
- Our numerical analysis of the delay system demonstrates that the model is highly sensitive to changes in the Hill coefficient. Is this inherent in the Hes7 oscillator or is it just an artefact of the model?

Therefore, it might be helpful to carry out *in vivo* experiments that reveal the underlying mechanisms in the promoter region in more detail. To allow for a more precise estimation of the Hill coefficient, more data will definitely have to be collected.
On the other hand, if further experiments support a higher value of the Hill coefficient, our results show that the proposed delay system cannot explain irregular somite formation in terms of a longer Hes7 half-life. One possible reason might be that the model is too simple. There might be other mechanisms, hidden in the delay of such a system, that could be influenced by a longer Hes7 protein half-life and explain the effects found by Hirata and colleagues [50]. In this case, a more sophisticated model should be developed.
Let us finally stress once more that further experimental data on the processes in the Hes7 feedback network are required to decide finally on one of the alterna-

tives. For instance, a dose-response curve might be recorded from transcriptional analysis of the Hes7 promoter with various Hes7 dimer concentrations. Then (see the subsection *Model of the Hes7 switch* in Section 1.2.2) an estimate for the Hill coefficient could be obtained from the Hill plot.

1.3 Oscillations of Hes7 caused by negative autoregulation and ubiquitination

Loss of Hes7 function leads to irregular somite formation demonstrating that Hes7 is a crucial component of the segmentation clock during somitogenesis. Experiments revealed that not only the repressor functionality but also the half-life of the protein is crucial for oscillatory expression of Hes7 and regular somite formation. Numerical integration of a delay equation system supported this finding. However, in Section 1.2 it was shown that the number of binding sites is also decisive for damped or undamped oscillations. It was shown that for more than one binding site the Hill coefficient increases. This leads to a completely different behavior. The oscillations are undamped and thus the mathematical model can no longer explain the results observed in the experiments.
In this section we propose a more sophisticated model for the Hes7 oscillator. Since Hes7 is degraded by the ubiquitin-proteasome pathway we include Michaelis-Menten kinetics for the ubiquitination of Hes7. We identify the Michaelis-Menten constant as an additional model parameter for oscillatory behavior. By increasing the Michaelis-Menten constant we found damped oscillations even if the Hill coefficient is increased.

1.3.1 Introduction

Segmentation of vertebrate embryonic bodies is induced by the ultradian clocks Hes1 and Hes7. These form homo-dimers which repress the transcription of their own encoding genes, see Figure 1.11. Thus, forming a negative feedback causes cyclic expressions of the respective mRNA and protein. Loss of repressor function of Hes7 results in abnormal somite formation [13]. Beside the repressor activity the half-life of the Hes7 protein is crucial for normal somite formation, too [50]. Mice with mutant Hes7 proteins in which a particular lysine residue is replaced by arginine have longer Hes7 half-lives, and exhibit irregular somite formation and damped *Hes7* mRNA and Hes7 protein oscillations. This was supported also by a mathematical model. Using delay equations for the temporal development of the *Hes7* mRNA and the Hes7 protein it was shown that for a half-life of about 30 min the simulations exhibited strongly damped oscillations after few periods. The regulation of transcription by the Hes7 protein is represented by a Hill function with a Hill coefficient equal to two indicating that Hes7 has only one transcription factor binding site to which Hes7 dimers can bind.
On the other hand, [13] revealed that there are three N-boxes in the promoter of *Hes7* to which Hes7 can bind. In Section 1.2 it was demonstrated that, if all three transcription factor binding sites are active, this would lead to a Hill coefficient

≥ 2.4 and that the delay system used by Hirata et al. is highly sensitive to changes in the Hill coefficient. An increase of 20% of the Hill coefficient leads to fairly weakly damped oscillations and an increase of 30% of the Hill coefficient results in completely undamped oscillations. Thus for a Hill coefficient higher than 2.4 the model can no longer explain the disruption of the segmentation clock.

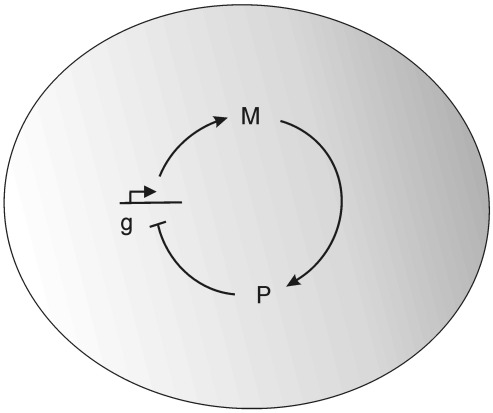


Figure 1.11: Schematic representation of gene regulation induced by a negative feedback: gene g is transcribed into mRNA M which is translated into protein P. By binding to the promoter of the gene g the protein P represses further transcription of g.

In the present section we propose a model which can explain the experimental results found in [50] for both scenarios: for a Hill coefficient equal to two and a Hill coefficient greater than 2.4. The model consists of five coupled differential equations. Two equations describe the time evolution of the *Hes7* mRNA and the Hes7 protein located in the nucleus, and another two equations describe the temporal development of the respective cytoplasmic *Hes7* mRNA and Hes7 protein. Thereby, cytoplasmic mRNA and protein can migrate into and out of the nucleus, obeying linear kinetics. Finally, one equation describes the temporal course of the ubiquitinated Hes7 protein. We will assume that ubiquitination of Hes7 is well described by a Michaelis-Menten term and that only ubiquitinated Hes7 protein can be degraded by the proteasome, see Figure 1.12 for a schematic representation.
Because of the lack of information from biological experiments we do not know if the lysine-to-arginine point mutation has influence either on the affinity of Hes7 to ubiquitin, or on the ability of the proteasome to cleave Hes7, or on both. A possible explanation for this can be that the point mutation leads to a conformation change of the Hes7 protein which causes a decrease of the affinity of Hes7 to ubiquitin, or to a protein configuration and protein conformation which is harder

for the proteasome to cut it down. Furthermore, we assume that the decrease in the affinity of Hes7 to ubiquitin has influence on the association only but not on the dissociation of Hes7 and ubiquitin. As a consequence, the association constant or the decay constant or both of them would be decreased.
Using a Hill coefficient equal to two and a half-life of the Hes7 protein equal to 20 min we will show that such as system exhibits sustained oscillations with a period of about 120 min. Furthermore, we will show that a decrease of the association constant leads to an increase of the Michaelis-Menten constant which has only weak influence on the half-life. Then, keeping the Hill coefficient fixed and increasing the half-life, results in damped oscillations, but increasing also the Hill coefficient will lead again to sustained oscillations. Now, if we increase both the Hill coefficient and the Michaelis-Menten constant the system shows damped oscillations even for a Hill coefficient equal to 2.6. Thus, in the case of a greater Hill coefficient an enlargement of the half-life alone is not sufficient to obtain damped oscillations. An increase of the Michaelis-Menten constant is also necessary, identifying it as an additional crucial model parameter in the Hes7 oscillator.

1.3.2 Ubiquitination of Hes7

In order to demonstrate the importance of the instability for sustained oscillations of Hes7, [50] manipulated the half-life of Hes7 in mouse mutants. By introducing a single lysine-to-arginine point mutation at each lysine residue of Hes7 they created several mutants with normal repressor activity of Hes7 but with different half-lives. Dependent on the particular lysine residue, the half-life was increased as well as decreased. The effect of the half-life on the segmentation clock was studied by analyzing a mouse mutant with a half-life of Hes7 of about 30 min.
The increase of the half-life, caused by replacement of lysine with arginine, may have different origins. However, since the half-life of Hes7 can do both increase as well decrease, we assume that it does not originate from the possible number of lysine to which ubiquitin can bind to. Thus, since no further information is available, we assume that it is caused by a decrease of the affinity of Hes7 to ubiquitin or by a reduced degradability by the proteasome or that both processes may contribute to this effect. Both may be caused by a conformation and/or configuration change of Hes7. In the following, we investigate the effect of a decrease of the affinity of Hes7 to ubiquitin. We assume that this influences only the association of Hes7 and ubiquitin but not the dissociation of the Hes7-ubiquitin complex.
Hes7 is degraded by the ubiquitin-proteasome pathway, [11]. Ubiquitin is a relatively small protein which marks target proteins for degradation through a three-step enzymatic cascade [86]. It is activated by an enzyme E1 and transferred to a ubiquitin-conjugating enzyme E2. In a last step it is bound to lysine residues of a

target protein by a ubiquitin-protein ligase E3. Ubiquitin itself has several lysines by which it can be further conjugated by another ubiquitin to form a polyubiquitin chain, [20]. The polyubiquitinated target protein is then recognized and degraded by the 26S proteasome into short peptides.
Whereas there is only one E1 enzyme in eukaryotic cells, multiple E2 and E3 enzymes direct selective protein degradation, [20]. Since the selection of target proteins is done by particular E2 and E3 enzymes we assume that ubiquitination is limited by the second or third enzymatic step and that it follows Michaelis-Menten kinetics.
If we pool the three enzymatic steps in to one enzymatic reaction, ubiquitination can be displayed by the following reaction scheme:

$$P + E \underset{\gamma_{-1}}{\overset{\gamma_1}{\rightleftharpoons}} \overline{PE} \overset{\gamma_2}{\rightarrow} P^U + E\,. \tag{1.21}$$

Here P and P^U denote the unubiquitinated and ubiquitinated Hes7 protein, respectively. The free ubiquitination catalyzing enzyme is denoted by E and $\overline{PE}$ denotes the complex formed by binding of E to P. In the reaction scheme we have assumed further that reassociation of P^U and E is negligible.
Based on the principle of mass action the reaction scheme (1.21) can be translated into a set of ordinary differential equations:

$$\begin{aligned} \dot{P} &= \gamma_{-1}\overline{PE} - \gamma_1 PE \\ \dot{\overline{PE}} &= \gamma_1 PE - (\gamma_{-1} + \gamma_2)\overline{PE} \\ \dot{P}^U &= \gamma_2 \overline{PE} \end{aligned}$$

Assuming that the total amount of the enzyme E is constant yields a conservation of mass equation for the total amount of catalyzing enzymes $E^{\text{tot}} = E + \overline{PE}$. Furthermore, assuming that the amount of E is small compared to the amount of P_C we can conclude that the temporal change of $\overline{PE}$ becomes zero, i.e. $0 = \gamma_1 PE - (\gamma_{-1} + \gamma_2)\overline{PE}$. This pseudo steady state assumption leads to the following algebraic equation

$$K = \frac{PE}{\overline{PE}} = \frac{\gamma_{-1} + \gamma_2}{\gamma_1}, \tag{1.22}$$

where K is called the Michaelis-Menten constant. Rearranging the conservation of mass equation for E and inserting it into the equation above gives $K = P(E^{\text{tot}} - \overline{PE})/\overline{PE}$. Solving this for $\overline{PE}$ and including it in the term for $\dot{P}^U$ we arrive at the nonlinear term describing the synthesis of the ubiquitinated Hes7 protein

$$\dot{P^U} = \frac{\gamma_2 E^{\text{tot}} P}{K + P} = \frac{VP}{K + P}, \tag{1.23}$$

where V is the maximal velocity at which product formation $\overline{PE}$ can take place. Thus, based on the assumption that the decrease of the affinity of Hes7 to ubiquitin effects only the association constant γ_1, equation (1.22) shows that this results in a larger Michaelis-Menten constant in the synthesis term of the ubiquitinated Hes7 protein.

1.3.3 Hes7 Oscillator

To model the dynamic behavior of *Hes7* mRNA and Hes7 protein we consider two types of *Hes7* mRNA and three types of Hes7 protein. Pre-mRNA M_N is transcribed in the nucleus and transported into the cytoplasm. There, the cytoplasmic mRNA M_C accumulates and a part of it is degraded. The remaining mRNA is translated into cytoplasmic protein P_C. A part of the cytoplasmic protein migrates into the nucleus. There, the nuclear protein P_N represses transcription of M_N or migrates back into the cytoplasm. The remaining fraction of cytoplasmic protein becomes ubiquitinated, P^U, which is degraded by the proteasome, (see Figure 1.12 for a schematic representation).

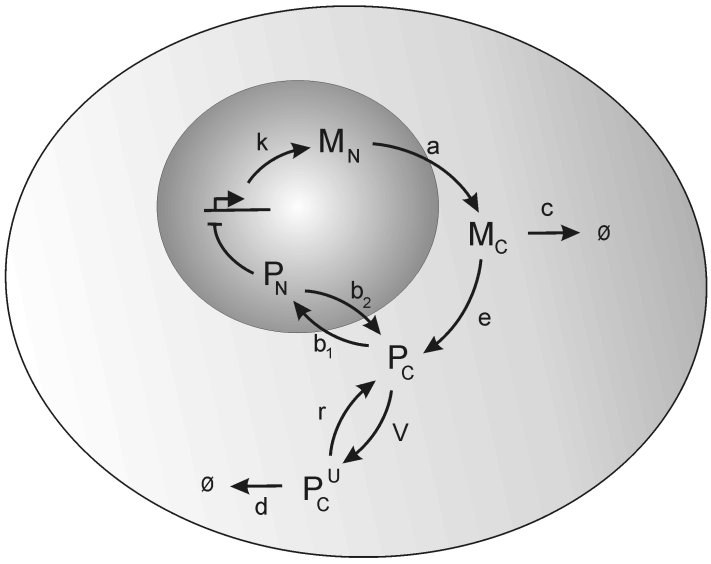


Figure 1.12: Model of the Hes7 oscillator including ubiquitination of Hes7. It is assumed that only the cytoplasmic mRNA and the ubiquitinated protein become degraded, denoted by the symbol $\emptyset$. For a more detailed description see the corresponding text.

Then the dynamic is governed by

$$\begin{aligned}
\dot{M}_N &= kf(P_N) - aM_N \\
\dot{M}_C &= aM_N - cM_C \\
\dot{P}_C &= eM_C + rP_C^U + b_2P_N - b_1P_C - \frac{VP_C}{K+P_C} \\
\dot{P}_C^U &= \frac{VP_C}{K+P_C} - dP_c^U - rP_c^U \\
\dot{P}_N &= b_1P_C - b_2P_N.
\end{aligned} \tag{1.24}$$

In the above equations, the parameter k denotes the basal rate of transcription in absence of P_N; a represents the constant rate of mRNA transport from the nucleus into the cytoplasm while c and d denote the degradation rate constants of mRNA and protein, respectively. In the Michaelis-Menten term V denotes the maximum velocity of ubiquitination and K represents the Michaelis constant. Thereby, deubiquitination is assumed to obey linear kinetics with rate constant r. Transport of cytoplasmic protein, P_C, into the nucleus and transport of protein located in the nucleus back into the cytoplasm is assume to take place with constant rate of b_1 and b_2, respectively. Furthermore, f_h denotes a Hill function with Hill coefficient h. It is defined by

$$f_h(P_N) = \frac{1}{1+P_N^h}$$

and describes the repression of transcription of M_N by the protein P_N. For Hes7 it is assumed that h is equal or greater to two which arises from the fact that Hes7 forms dimer.

1.3.4 Numerical Simulations

Since theoretical analysis of system (1.24) is not tractable we solved the ODE system by numerical integration. Using $h = 2,\ c = 0.231$, and $d = 0.035$ from [50], we found sustained oscillations with oscillation period of about 123 min for the following values of the remaining parameters: $a = 0.02$, $b_1 = 0.2$, $b_2 = 0.18$, $k = 10$, $V = 6$, $K = 0.1$, $r = 0.2$, $e = 0.2$. The time evolution of M_N, M_C, P_C^U, and P_N are given in Figure 1.13. It also contains the temporal change of the total amount of protein concentration $P^{\text{tot}} = P_N + P_C^U + P_C$.
To show that system (1.24) can mimic the results found in [50] for a Hill coefficient equal to two we varied the decay rate d of the ubiquitinated Hes7 protein P_C^U and kept the other parameters fixed. Figure 1.14 (a) shows once more the temporal change of M_C and P_N for the parameter set used for Figure 1.13. Now, if one uses a decay rate equal to 0.023 instead of 0.035 (which corresponds to a half-life of 30 instead of 20 min) the systems shows damped oscillations, Figure 1.14 (b). This

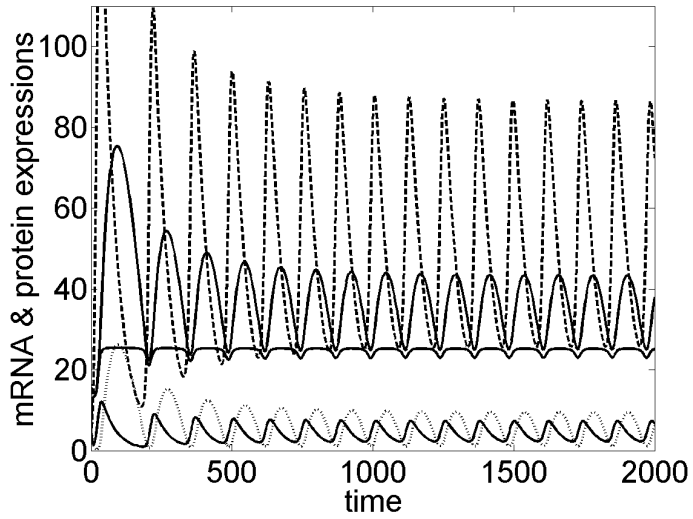


Figure 1.13: Sustained oscillations in the Hes7 model including degradation of Hes7 protein by the ubiquitin-proteasome pathway. The temporal change of the ubiquitinated protein P_C^U shows a kind of floating line with small oscillations around a expression level of about 25 (solid line). Thus, the total amount of Hes7 protein (also represented as a solid line) oscillates above this floating line. The remaining curves display the time evolution of M_N (dashed), M_C (solid), and P_N (dotted). The time course of the cytoplasmic protein P_C is not shown because it is very close to the one of P_N.

is in accordance with experimental findings as well as with numerical simulation of the delay system in [50]. However, increasing the Hill coefficient to a value of 2.6, as suggested on the basis of three binding sites, see Section 1.2, the system shows sustained oscillations, Figure 1.14 (c). Thus, as it was shown for the delay system in Section 1.2, the ODE system exhibits the same behavior if only the decay rate is changed. Thus, a change of the decay rate alone cannot explain the experimental finding in the case of a greater Hill coefficient. On the other hand, mutation of a lysine residue in Hes7 suggests that the affinity of Hes7 to ubiquitin may change dramatically. This would be reflected in the association constant and as we have shown above, this leads to an increase of the Michaelis-Menten constant. Indeed, scaling up the Michaelis-Menten constant by factor three results in strongly damped oscillations, see Figure 1.14 (d).

To exclude the possibility that the damped oscillations for the parameter set used for Figure 1.14 (d) do not originate from an increased half-life $\tau_{1/2}$ of Hes7, caused by an increase of the Michaelis-Menten constant K, we analyze the dependency

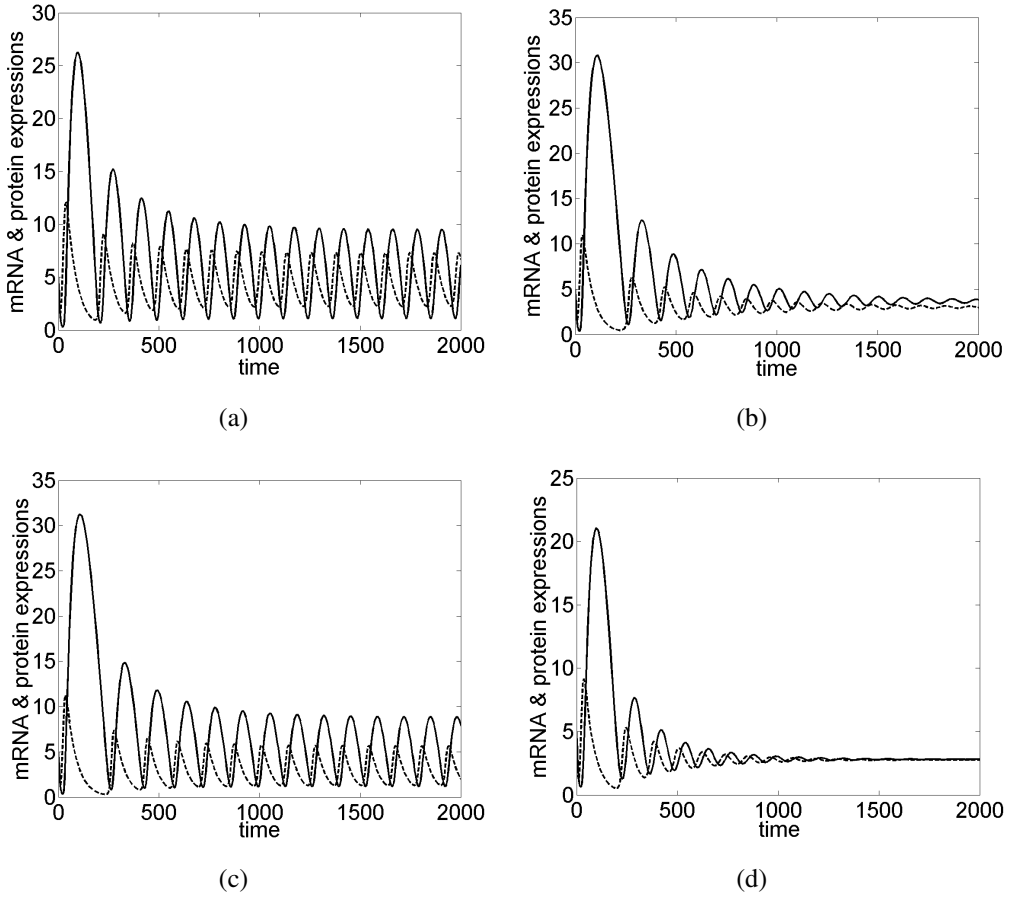


Figure 1.14: Temporal changes of the cytoplasmic mRNA M_C (dashed) and the protein located in the nucleus P_N (solid) for different values of the Hill coefficient h, rate constant of protein degradation d, and Michaelis-Menten constant K. (a) $h = 2$, $d = 0.035$, $K = 0.1$; (b) $h = 2$, $d = 0.023$, $K = 0.1$; (c) $h = 2.6$, $d = 0.023$, $K = 0.1$; (c) $h = 2.6$, $d = 0.023$, $K = 0.3$.

of $\tau_{1/2}$ on K by numerical methods. We extract from the general system (1.24) a small subsystem describing the decay of P_C from the ubiquitination process to its final degradation by the proteasome. The system reads

$$\begin{aligned} \dot{P}_C &= rP_C^U - \frac{VP_C}{K + P_C} \\ \dot{P}_C^U &= \frac{VP_C}{K + P_C} - dP_c^U - rP_c^U \end{aligned} \tag{1.25}$$

where the parameters have the same meaning as in system (1.24). Their values are the same as those used for generating the expression curves in Figure 1.13. As initial values we use the mean expression value of P_C^U and P_C. Reading it off from Figure 1.13 we use $P_C^U(0) = 25$ and $P_C(0) = 5$. Of course, since the mean value of P_C is 50 times greater than the Michaelis-Menten constant K, we expect only a small influence of $\tau_{1/2}$ on K.
Figure 1.15 displays the temporal changes of $P_C^U,\ P_C$ and of the total cytoplasmic protein amount, $P_C^{\text{tot}} = P_C^U + P_C$.

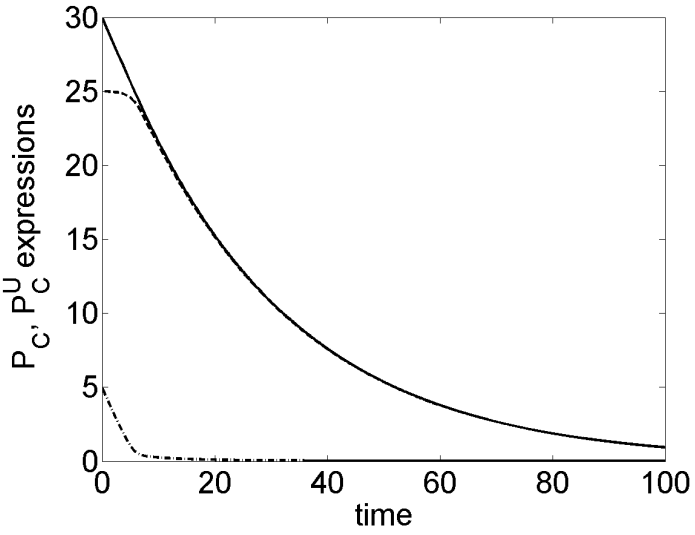
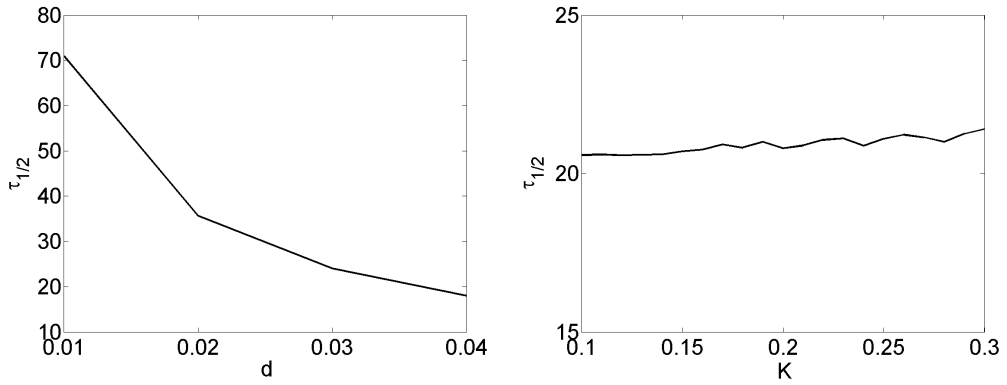


Figure 1.15: Time evolution of P_C (dot-dashed), P_C^U (dashed) and the total amount of cytoplasmic protein $P_C^{\text{tot}} = P_C^U + P_C$ (solid) in the small regulatory network considering only the cytoplasmic and the ubiquitinated protein. The curves are obtained by numerical integration of subsystem (1.25).

It shows that the total amount of cytoplasmic Hes7 decays exponentially. After few minutes, this is also true for P_C^U which is then hard to distinguish from P_C^{tot}. The offset of P_C^U to the right is caused by the presence of P_C which becomes very small after some minutes. Furthermore, Figure 1.15 shows that the half-life of the total amount of the cytoplasmic protein P_C^{tot} in the small subsystem agrees very good with the half-life determined by experiments in [50]. This can also be gather from Figure 1.16 (a). It shows the strong dependency of the half-life on the decay rate d. However, the half-life shows only a very weak dependency on the Michaelis-Menten constant K, Figure 1.16 (b). A threefold increase of K from 0.1 to 0.3 causes an increase of the half-life of about one minute only.



(a) (b)

Figure 1.16: Dependency of the half-life $\tau_{1/2}$ on (a) the rate constant of protein degradation d, and on (b) the Michaelis-Menten constant K.

1.3.5 Conclusion

To address the problem that the delay system in [50] can no longer explain the experimental findings of damped oscillations in the case of a Hill coefficient greater than 2.4 we propose a novel model for the Hes7 oscillator. Beside transport of *Hes7* mRNA and Hes7 protein out and into the nucleus we also consider ubiquitination of Hes7. By numerical integration of the resulting ODE system of 5 equations we find for a Hill coefficient equal to two and a half-life of 20 min sustained oscillations with oscillation period of about 120 min. Furthermore, increasing the half-life to 30 min leads to damped oscillations. However, a simultaneous increase of the Hill coefficient to 2.6 results again in sustained oscillations. Thus, for the fixed particular Michaelis-Menten constant the system behaves very similar to the delay system proposed in [50]. Assuming that a decrease of the affinity of Hes7 to ubiquitin, caused by the lysine-to-arginine point mutation in the Hes7 protein, affects mainly the binding rate constant we show that this leads to an increase of the Michaelis-Menten constant. Thus, we increase the Michaelis-Menten constant while keeping the other parameter values fixed. In this case we find that the system exhibits strongly damped oscillations.

To demonstrate that this does not stem not from a further increase of the half-life induced by the increased Michaelis-Menten constant, we consider a subsystem consisting of the un- and ubiquitinated Hes7 protein. Numerical analysis shows that a change in the Michaelis-Menten constant has just a little influence on the half-life. Hence the increase of the half-life is caused mainly by the activity of the proteasome.

Furthermore, the results suggest that ubiquitination of Hes7 is likely to explain the effect of sustained oscillations if only the Hill coefficient and the half-life are increased. Moreover, we identify the Michaelis-Menten constant in the ubiquitination term as a novel crucial parameter in the Hes7 oscillator.
Since there are no further data available up to now, our model is theoretical but based on reasonable assumptions. Moreover, since the Michaelis-Menten constant is a measurable quantity, a change of its amount should be verifiable by future experiments.

Chapter 2

Hybrid Modeling

2.1 Simulation of Genetic Networks Modeled by Piecewise Deterministic Markov Processes

The present section describes the results published in [127].
We propose piecewise deterministic Markov processes as an alternative approach to model gene regulatory networks. A hybrid simulation algorithm is presented and discussed, and several standard regulatory modules are analyzed by numerical means. We show that despite of the partial simplification of the mesoscopic nature of regulatory networks such processes are suitable to reveal the intrinsic noise effects due to the low copy numbers of genes.

2.1.1 Introduction

This section is concerned with modeling the dynamics of gene expression regulated by different modules. Gene expression is often modeled as a deterministic process by means of ordinary differential equations. When the abundance of reactants is large deterministic models are powerful tools to understand the dynamical behavior of such systems. However, in the last decade more and more experiments revealed that transcription and translation in single cells vary even in isogenetic cell populations, [78], [4], [28]. In single cells the template for transcription, the DNA, is present only in one or two copies. Due to such small numbers transcription proceeds rather stochastic than deterministic, [52], [16], [88]. In this case, stochastic models are more appropriate. Often a time-continuous Markov process with discrete state space is used as a choice of matter. Since most systems are analytically not tractable, the only way to analyze such processes is to simulate individuals trajectories, [33], [34]. However, if the system contains many reactions, or if some of the reactants are present in large numbers, simulation be-

comes computationally expensive. Beside efficient and approximative algorithms which can reduce computation costs, [31], [32], also hybrid models are proposed for modeling gene regulatory networks [79], [47], [62].
We propose an alternative hybrid approach which is to some extent similar to models already existing in literature. The model we present is a special class of stochastic processes for modeling genetic networks. We show that coupling the stochastic and deterministic parts in an appropriate way leads to processes possessing the Markov property. Such processes were introduced by Davis in 1984, [23]. They are called piecewise deterministic Markov processes, PDMP for short. Here, we use them to simulate standard genetic circuits such as inducible promoters, positive feedbacks and toggle switches. Provided that most of the molecular entities in a genetic network occur in such high numbers that a deterministic description is appropriate they will be modeled by ordinary differential equations. We have to remark that in general it is difficult to give a precise line of separation when this criterion is fulfilled.
On the other hand, the DNA is always present in very low numbers such that activation and deactivation of the particular gene followed by pulses of mRNA synthesis will lead to variations in the expression levels of single cells. At least in eukaryotes this effect is in general stronger than synthesis and degradation of the respective gene products, [16]. In the present section we focus only on the promoter as a source of the inherent randomness in gene expression, and restrict ourselves to model only transitions between different promoter states in a stochastic manner. Processes like transcription, translation, degradation and dimerization are supposed to be given by deterministic equations. We will show that provided such an approach is appropriate it is useful to model stochasticity in gene expression in eukaryotic cells caused by random transitions of the promoter.
As already mentioned, if the number of reactions is large or if some of the molecular species appear in great numbers numerical computations become very time consuming. Hence in networks with many reactions or with reactants occurring in high numbers the stochastic simulation algorithm becomes inefficient. On the other hand, small numbers of some of the members of a genetic network makes an approximation by a purely deterministic approach often inaccurate. To solve this dilemma much work was done to speed up stochastic simulations in the last few years. To name only a few, the 'next reaction' method of Gibson and Bruck, [31], the 'τ-leap' method of Gillespie [35] and improvements, [32], or the algorithm of Puchalka and Kierzek, [59] which is a combination of the next reaction and the τ-leap method. Beside discrete state processes also hybrid processes were proposed possessing discrete as well as continuous state variables. In such approaches mostly the chemical Langevin equation, like in [98], or ordinary differential equations, like we do, are proposed to model the time evolution of the continuous state variable. We will shortly discuss the works which are most

closely related to our approach. One such approach was proposed by Haseltine and Rawlings, [47]. Similar to Rao and Arkin, [89], they partitioned the reaction system into subsets of 'fast' and 'slow' reactions. Then, they modeled the slow reactions as discrete events whereas the fast reactions were approximated by the chemical Langevine equation. Furthermore, they proposed an approximation of the Langevine equation by ordinary differential equations which can be justified by taking the thermodynamic limit. To illustrate the accuracy and the potential speedup of their algorithm they performed simulations of a model for crystallization and viral infection.
The partition proposed by Haseltine and Rawlings is static and based on the propensity function of the individual reaction channels. A more accurate partitioning was done by Griffith and coworkers, [79]. They proposed a dynamical partitioning algorithm which classifies each reaction as a discrete event by default, and classifies a reaction as fast if it is beyond a relative threshold which is updated dynamically. When a reaction channel is classified as fast it is modeled as a deterministic ordinary differential equation. Their approach was applied to a model of a HIV-1 transaction network introduced by Weinberger et al., [119].
In the two approaches above the reacting particles are partitioned into two regimes depending on the speed of the reaction channels to which they are involved. As already indicated, in our approach the partition of the reacting molecular population is done due to high and low state numbers of the individual species. Since we are only interested in fluctuations of gene expression levels arising from promoter transitions we model only the states of the promoter as discrete entities. All other processes are modeled as continuous process. Such an approach can be justified by the thermodynamic limit when the numbers of the gene products are large compared to the numbers of the gene copies. However we have to note that even when the thermodynamic limit is fulfilled the deterministic approach can fail, see [99].
A similar ansatz was done in [73]. There ordinary differential equations describing the temporal evolution of the concentration of the gene products are coupled by a random variable describing the activity of the promoter of the particular gene. Provided that the distribution posses a density it can be described by a system of partial differential equations. Then the system of partial differential equations was approximated by a system of ordinary differential equations and solved numerically to obtain the density of the respective system. Summarizing, in the situation described in the beginning partitioning the system into deterministic and stochastic components seems natural to us.
We start with an example of an inducible gene discussing the difference between a deterministic and a stochastic approach. The stochastic approach is analyzed by numerical means. In the second section we give a formal definition of a PDMP, following the construction of Davis in [23]. In the third section we present and discuss an algorithm. We will show that simulation of a PDMP is nearly as

straightforward as executing the standard Gillespie algorithm for simulations of time continuous, state-discrete Markov processes, [33], [34]. In the next section we apply it to three standard genetic modules, namely an inducible gene with constant amounts of inducer, an autocatalytic genetic network, and the so-called toggle switch build up of two genes where each gene represses expression of the other gene. The empirical distributions are calculated and sensitivity analysis is done numerically. In the last section the results are summarized and discussed.

2.1.2 Deterministic versus Stochastic Approach

Consider transcription of a gene g for which external inducers are present in constant amounts in the observed time interval or activation takes place independently of any external stimulus. Hence we assume that g is activated and deactivated with constant rates κ_1 and κ_{-1}. Let g_0 and g_1 denote the inactive and active state of g. In a simplified manner this can be described by four equations and three reactants displayed in reaction scheme (2.1) below. If the gene is active, mRNA m is transcribed with rate constant α and is degraded with rate constant γ. In the other case, when the gene is inactive, only degradation takes place. The degradation products are denoted by the symbol $\emptyset$.

$$\begin{array}{lcl} g_0 & \xrightarrow{\kappa_1} & g_1\,, \\ g_1 & \xrightarrow{\kappa_{-1}} & g_0\,, \\ g_1 & \xrightarrow{\alpha} & g_1 + m\,, \\ m & \xrightarrow{\gamma} & \emptyset\,. \end{array} \tag{2.1}$$

In a deterministic approach one would write down two equations. One describing transcription and degradation, if the gene is active, and the other describes degradation of the mRNA in the case the gene is inactive. In the former case the evolution is given by

$$\dot{x} = \alpha - \gamma x, \tag{2.2}$$

where in the latter case the temporal development is determined by

$$\dot{x} = -\gamma x. \tag{2.3}$$

In the active state concentration of the mRNA converge towards $\frac{\alpha}{\gamma}$, and towards zero in the inactive state. However, there exists no autonomous pure deterministic system by which one could couple these two equations describing the whole process consisting of transition of the gene from the inactive to the active state and back, and transcription and degradation of the mRNA.
In a stochastic approach typically time-continuous Markov processes with discrete state space are used to describe the above system of mRNA transcription. Since the two states of the gene are mutually exclusive the motion of the process can be

described in a two dimensional state space. One component describes the state of the gene, and the second component denotes the number of mRNA. Then, changes in the number of reactants can be described by the following two dimensional stoichiometric vectors: $v_1 = (1, 0), v_2 = (-1, 0), v_3 = (0, 1)$, and $v_4 = (0, -1)$. The probability that a R_μ reaction takes place in an infinitesimal time interval is given by so called propensity functions, [33]. For a reaction R_μ the propensity function a_μ is defined as the product of a combinatorial function h_μ, which denotes the number of possible combinations of R_μ molecules, times the associated stochastic reaction rate constant c_μ giving the average probability that in an infinitesimal time interval a particular R_μ reaction will occur. The state of the system at a given instant t is given by a two dimensional vector $X_t = x = (i, m)$. Then, the evolution of the distribution of X_t is given by the chemical master equation

$$\frac{\partial}{\partial t}P(x,t) = \sum_{\mu=1}^{4} \big(a_\mu(x - v_\mu)P(x - v_\mu, t) - a_\mu(x)P(x,t)\big). \tag{2.4}$$

For instance, for the reaction scheme (2.1) the propensity functions are given by $a_1(x) = \kappa_1|i - 1|$, $a_2(x) = \kappa_{-1}i$, $a_3(x) = \alpha i$, and $a_4(x) = \gamma m$.
In general, solving equation (2.4) is complicated and often not feasible. For this reason, one has to make approximations or has to integrate equation (2.4) numerically.

Parameter set	κ_1	κ_{-1}	α	γ
(1)	0.01	0.01	1	0.06
(2)	0.01	0.01	1	0.005
(3)	0.01	0.03	1	0.025
(4)	0.03	0.01	1	0.025

Table 2.1: Parameter sets used for simulation of mRNA transcription. The parameters are given in units s^{-1}

An alternative approach is stochastic simulation. The simulation algorithm is often referred as Stochastic Simulation Algorithm (SSA) or Gillespie's algorithm [33],[34]. Gillespie's exact algorithm is based on the reaction density function $P(\tau, \mu)$ defined as

$$P(\tau,\mu)d\tau \quad = \quad \text{probability that given the state } x \text{ at time } t, \text{ the next reaction in } V \text{ will occur in the differential time interval } (t+\tau, t+\tau+d\tau), \text{ and will be an } R_\mu \text{ reaction}$$

In [33] it was shown that

$$P(\tau,\mu)d\tau = a_\mu \mathrm{e}^{-\tau a_0}\mathrm{d}\tau \tag{2.5}$$

where $a_0 = \sum_\nu a_\nu$. The probabilities of the next reaction and the next jumping time are given by the marginal distributions of (2.5). If R denotes the random variable indicating the next reaction, then R possesses the discrete distribution

$$\mathbb{P}(R = R_\mu) = a_\mu / a_0. \tag{2.6}$$

Further, the probability that this reaction will fire in the infinitesimal time interval $\mathrm{d}t$ after t time units is given by

$$\mathbb{P}(t \leq \tau \leq t + \mathrm{d}t) = a_0 \mathrm{e}^{-t a_0} \mathrm{d}t. \tag{2.7}$$

Moreover, R and τ are independent which leads to Gillespie's direct algorithm, see Algorithm 1 or [33].

Algorithm 1 Stochastic Simulation Algorithm (SSA)

set $T \Leftarrow 0$, $x \Leftarrow (i, m)$;
repeat
  calculate $a_\mu = h_\mu c_\mu$;
  choose τ according to (2.7);
  choose μ according to (2.6);
  set $T = T + \tau,\ x = x + v_\mu$;
until $T \geq T_{end}$

We have simulated reaction system (2.1) by Algorithm 1 for four different parameter sets listed in Table 2.1. Each simulation ran 1000 time units and was repeated 5000 times with initial state $x = (1, 0)$. The empirical distributions of the process at time $t = 1000$ are displayed in Figure 2.1.

Parameter set	$\mathbb{E}(M_t)$	$\mathbb{V}(M_t)$	$< M_t >$	$\sigma^2(M_t)$
(1)	8.33	60.42	7.97	60.44
(2)	100	2100	98.65	2089.8
(3)	10	125.39	9.3	121.54
(4)	30	145.39	29.63	146.54

Table 2.2: Distribution parameters for the state discrete Markov process. The empirical distribution parameters, denoted by $< M_t >$ and $\sigma^2(M_t)$, were obtained by simulating the SSA.

Since the system is small, beside numerical analysis it is possible to calculate the first two moments and the stationary distribution by means of generating functions. Let M_t denote the random variable giving the number of mRNA at a given

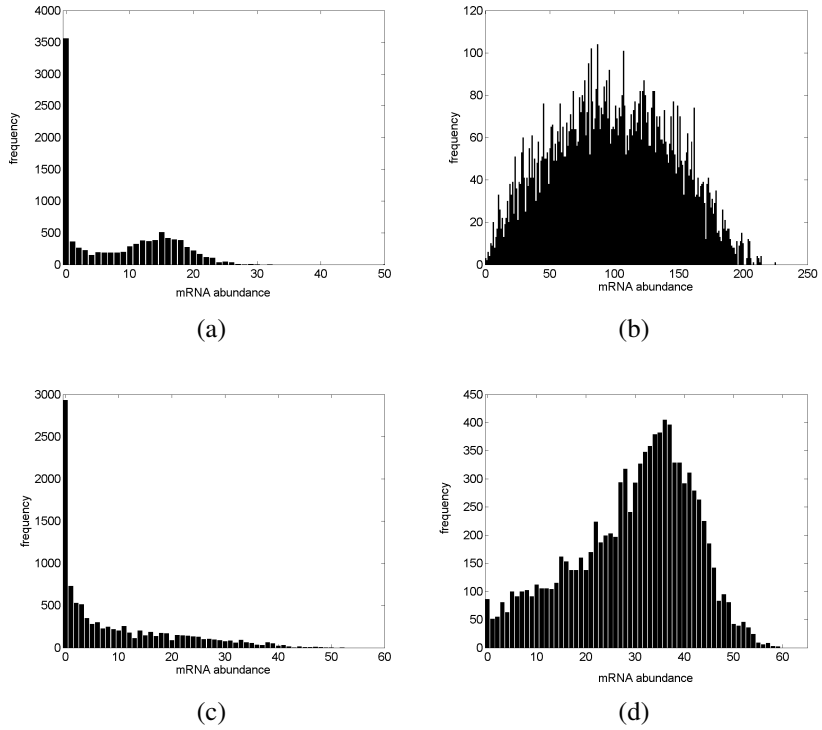


Figure 2.1: Empirical distributions of mRNAs in the discrete Markov process obtained by numerical simulations using the SSA. The respective parameter sets are listed in Table 2.1 .

instant t. In [85] it was shown that the stationary expectation of the numbers of mRNA molecules is given by

$$\mathbb{E}(M_t) = \frac{\alpha}{\gamma} \frac{\kappa_1}{\kappa_1 + \kappa_{-1}}. \tag{2.8}$$

For the variance it was shown that it holds

$$\mathbb{V}(M_t) = \frac{\alpha}{\gamma} \frac{\kappa_1}{\kappa_1 + \kappa_{-1}} + \frac{\alpha^2 \kappa_1 \kappa_{-1}}{\gamma(\kappa_1 + \kappa_{-1})^2(\gamma + \kappa_1 + \kappa_{-1})}. \tag{2.9}$$

The obtained theoretical and empirical values of the mean and the variance for the parameter values in Table 2.1 are given in Table 2.2. The good agreement indicates that for the chosen time length the process has already approached its stationary distribution.
To measure the dependency of the expectation and the variance on the individual parameters we consider the relative variation of gene expression. As a measure we use the coefficient of variation c_v also called the noise of the system defined as

the ratio of the standard deviation to the mean. From equations (2.2.3) and (2.2.3) we obtain the formula

$$c_v = \sqrt{\frac{\gamma}{\alpha}\frac{\kappa_1 + \kappa_{-1}}{\kappa_1} + \frac{\gamma\kappa_{-1}}{\kappa_1(\gamma + \kappa_1 + \kappa_{-1})}}. \tag{2.10}$$

Consequently, c_v will converge towards infinity as κ_1 tends to zero. On the other hand, it will converge towards $(\gamma/\alpha)^{1/2}$ as κ_1 tends to infinity, see Figure 2.2(a). This is intuitively clear since when κ_1 becomes smaller the gene will stay longer in its inactive state. Hence most of the gene product will be degraded such that

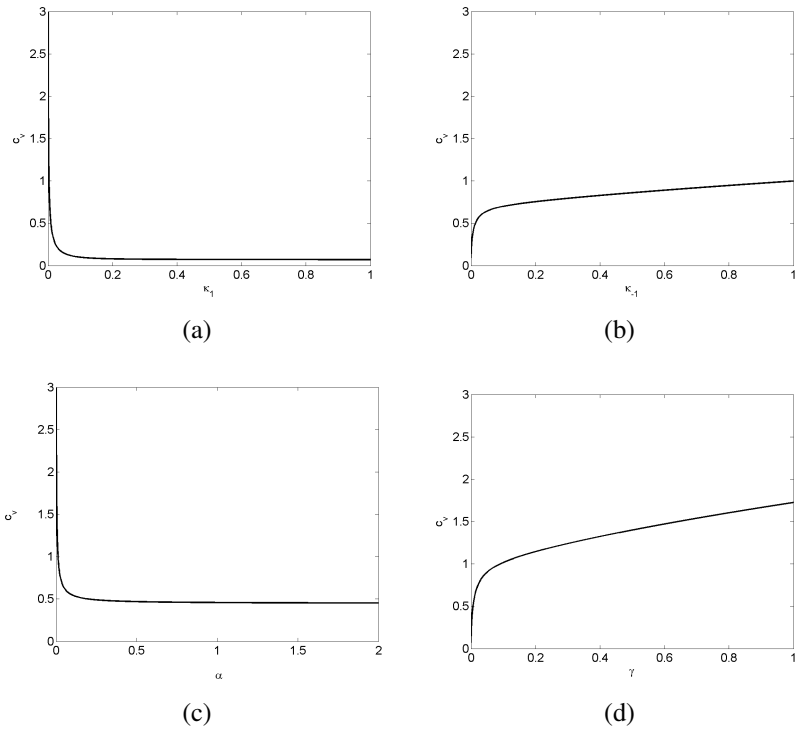


Figure 2.2: The coefficient of variation c_v of the discrete state Markov process as a function of (a) κ_1, (b) κ_{-1}, (c) α, and (d) γ.

the expected number of the gene product will tend faster towards zero than the standard deviation. In the other case when κ_1 increases the gene will stay longer in its active state. Thus the number of of the gene product will tend towards its expected value α/γ whereas the standard deviation will tend to $(\alpha/\gamma)^{1/2}$.
As expected, c_v behaves subject to κ_{-1} the other way round. If κ_{-1} gets smaller, c_v converges towards $(\gamma/\alpha)^{1/2}$, and if it increases c_v converges to infinity, see Figure 2.2(b).

For the synthesis rate we receive from equation (2.10) that c_v depends hyperbolic an α. Thus, c_v tends to infinity if α tends to zero, and it tends to the square root of the second term in the root of equation (2.10), if α tends to infinity. See the graph in Figure 2.2(c) for a functional dependency. Again, the reason for this is that the second power of the mean converges faster to zero than the variance, and it converges in the same order as the variance as α tends to infinity.
The opposite behavior is observed for the parameter γ, see Figure 2.2(d). If γ decreases, c_v tends to zero, and it tends to infinity, if γ increases. The reason for this is that the second power of the mean increases faster than the standard deviation as γ tends to zero. On the other hand, the second power of the mean converges faster to zero than the standard deviation as γ tends to infinity.

2.1.3 Piecewise Deterministic Markov Process

In the previous section we have mentioned that gene transcription which is independent of external stimuli cannot be described by a pure autonomous deterministic system. Beside a pure stochastic model one could couple these two ordinary differential equations by a stochastic variable indicating in which state the gene is. We will show that this can be done in a mathematical rigorous way leading us to so called piecewise deterministic Markov processes, PDMP for short.
PDMP were introduced by Davis in [23]. They can be thought of as a mixture of a deterministic and a stochastic approach. As an example consider the reaction system (2.1) describing transcription of mRNA m from a particular gene g. Assuming that m is present in large enough numbers we can suppose that a deterministic description of synthesis and degradation of the mRNA is appropriate. However, since there is only one copy of the gene g, a deterministic description of transitions from its active to its inactive state and back would fail. Beside a pure stochastic model another quite natural approach is to couple the two ordinary differential equations (2.2) and (2.3) by transitions between the two states of the gene g in a Poisson like fashion. For the considered example, the state space would consists of two elements g_0 and g_1 indicating the states of the gene g. The state space of the deterministic part of the process, describing the concentration of the mRNA m for the two states g_0 and g_1 would be the positive real line. Then, between two random jumps from g_0 to g_1 and backwards, the temporal evolution of the mRNA would proceed deterministically given by the ordinary differential equations (2.2) and (2.3). Here, the only randomness is contained in the jump times. For a more general system, for instance when the gene g possesses more than one binding site, there would be additional randomness in the way transition takes place at given random jump times.
PDMP constitute a subclass of Markov processes, by which events described above can be modeled in a general way. Up to random jump times the process

moves deterministically. At the jump times the process transits randomly to a new state. For the definition of a PDMP we follow the construction given by Davis in [23]. We need four components: the state space of the process; vector fields describing the deterministic evolutions of the continuous part of the process; distributions of the jump times; and the distributions of the discrete states after a jump has happened.
Let M be a finite set. The state space of a PDMP is given by

$$S = \{(i, z) : \ i \in M, \ z \in \mathbb{R}^n\}.$$

For each $t \in \mathbb{R}_+$ the PDMP $X_t : \ \Omega \to S$ can be written as $X_t = (\theta_t, \xi_t)$. We call the subspace $\{i\} \times \mathbb{R}^n$ a branch or an arm of the process. For each $i \in M$ let

$$v^{(i)} : \ \mathbb{R}^n \to \mathbb{R}^n$$

be a vector field defined by an ordinary differential equation $\dot{z} = v^{(i)}(z)$. In general, it is assumed that for each $i \in M$ $v^{(i)}$ is globally Lipschitz. Here, we consider only differential equations with bounded right hand sides. Thus, the process is well defined for all $t \geq 0$. In particular, there is a unique integral curve which solves

$$\frac{\mathrm{d}}{\mathrm{d}t}\phi_i(t, z) = \ v^{(i)}\left(\phi_i(t, z)\right)$$

subject to $\phi_i(0, z) = z$ for all $z \in \mathbb{R}^n$. ϕ is called the integral curve of the vector field $v^{(i)}$.
Jumps of the PDMP from one branch to another are governed by a transition rate function

$$\lambda : \ S \to [0, \infty)$$

and a transition kernel

$$P : S \times \mathcal{B}(S) \to [0, 1],$$

where $\mathcal{B}(S)$ denotes the Borel sets of S. The function λ is a measure for the jump intensity of the process. It is assumed that the map $u \to \lambda\left(i, \phi^{(i)(u,z)}\right)$ is measurable for $u \geq 0$. The transition kernel gives the distribution of the process at the instant when a jump has occurred. That means that $P(x, B)$ is the probability that the process jumps into set B if at the jump time the process is in state x.
With these ingredients we can construct the PDMP $(X_t)_{t\geq 0}$ as follows. Let $x_0 = (i_0, z_0)$ be the initial state of X_t. The distribution function of the holding times in the particular branches is defined as

$$F(i, z, t) = 1 - \exp\left(-\int_0^t \lambda(i_0, \phi_{i_0}(u, z_0))\mathrm{d}u\right).$$

Then, the first jump time is given by a random variable τ_1 which is distributed according to

$$\mathbb{P}(\tau_1 \leq t) = F(i_0, z_0, t). \tag{2.11}$$

After that, an S-valued random variable (I_1, Z_1) is independently chosen having distribution

$$P\left(\left(i_0, \phi_{i_0}(\tau_1, z_0)\right), \cdot\right). \tag{2.12}$$

In this way, the process X_t is defined up to the first jump time, and is given by

$$X_t = (\theta_t, \xi_t) = \begin{cases} (i_0, \phi^{(i_0)}(t, z_0)), & t \in [0, \tau_1), \\ (I_1, Z_1), & t = \tau_1. \end{cases}$$

Starting from X_{τ_1} the sojourn time $\tau_2 - \tau_1$ in the branch $\{i_1\} \times \mathbb{R}^n$ is distributed according to (2.11) and the post-jump location is obtained from (2.12) in a similar way. Proceeding in this way we obtain a piecewise deterministic trajectory with random jump times $\tau_1, \tau_2, \ldots$. It can be shown that the so constructed stochastic process possesses the Markov property, [23]. From the above construction we derive easily a general rule how to simulate individual trajectories.

2.1.4 Algorithm for simulation of PDMPs

Simulating the temporal evolution of the process is accomplished as follows. Starting at an initial state (i_0, z_0) the process remains in the branch $\{i_0\} \times \mathbb{R}^n$ until it reaches the first jump time τ_1. Up to τ_1 it moves deterministically along a vector field $v^{(i_0)}$. To obtain τ_1 from the survival function $S(t)$ we have to integrate the rate function λ along the integral curve ϕ_{i_0} determined by the initial concentration z_0 and the vector field $v^{(i_0)}$. At the jump time τ_1 the process jumps to another branch keeping its concentration value z_{τ_1}. The post-jump state is chosen according to the transition measure $P\left(\left(i_0, \phi_{i_0}(\tau_1, z_0)\right), \cdot\right)$. From the new state the process starts afresh again. Realizations of the PDMP can be thought of as an execution of Algorithm 2. Hence simulation of a PDMP is straightforward and

Algorithm 2 Hybrid stochastic Algorithm (HSA)

set $T \Leftarrow 0,\ \theta_0 \Leftarrow i,\ \xi_0 \Leftarrow x$;
repeat
  select τ with $P(\tau \leq t) = F(t)$;
  set $\theta_t = i$, $\xi_t = \phi^{(i)}(t - T, z)$ for $t \in [T, T + \tau)$;
  select $\theta_{T+\tau}$ according to $P\left(\left(i_0, \phi_{i_0}(\tau_1, z_0)\right), \cdot\right)$;
  set $T = T + \tau$;
until true

nearly as simple as to simulate a finite-state Markov process by the SSA. However there are some pitfalls one has to pay attention to. We will discuss these in the following.
If transitions between different branches occur with a constant rate κ, the inverse of the distribution function F exists in closed analytical form and the jumping time is given by

$$\tau = \frac{1}{\kappa} \log(\frac{1}{u})$$

where $u \in [0, 1]$ is a realization of a uniform random variable. In this case simulating by the HSA is very similar to simulating by the SSA. But in general the PDMP is not constant between two jump times as it is the case for a discrete state Markov process. If F is obtainable in a closed analytic form, τ can be easily received from the pseudo inverse of F

$$\tau = \sup\{t \geq 0 : \ F(t) \leq u\}.$$

If F is not given analytically one has to find this inverse numerically. This is the case for nearly all nonlinear systems. One example is the autocatalytic network including dimerization of the gene product below. In this case the integral equation

$$\int_0^\tau \lambda(i_0, \phi_{i_0}(t, z_0))\mathrm{d}t = \log(\frac{1}{u})$$

has to be solved numerically. This can be done by solving the coupled differential equations system

$$\begin{aligned} \frac{\mathrm{d}}{\mathrm{d}t}\phi_i(t, z) &= v^{(i)}\left(\phi_i(t, z)\right), \\ \frac{\mathrm{d}}{\mathrm{d}t}F(i, z, t) &= \lambda\left(i, \phi(i, t, x)\right) F(i, x, t), \end{aligned}$$

up to the time instance with $F(i, z, t) = u$.
Further, in contrast to a discrete-space Markov process, the sojourn time τ of a PDMP may become infinity, i.e. τ can have a mixed distribution obeying

$$\mathbb{P}(\tau = \infty) = c > 0, \ \text{ and } \ \lim_{t\to\infty} \mathbb{P}(\tau < t) \to 1 - c.$$

As we will show below, this is the case for an autocatalytic network even when the concentration is not equal to zero. This circumstance can be easily handled by distinction of cases in the step of Algorithm 2 where the jumping times are selected.

2.1.5 Applications

We consider three standard regulatory modules. At first we analyze transcription and translation for an inducible promoter. As a second example we analyze gene expression in an autocatalytic network assuming that gene expression can only take place when an inducer is bound to the regulatory region of the particular gene. The third module is a synthetic circuit called toggle switch. It consists of two repressors each one suppresses transcription of the encoding gene of the other repressor.

Transcription and Translation of an Inducible Gene

In the following we will consider an extension of the model for mRNA transcription given by (2.1) from the section *Deterministic versus Stochastic Approach*. Thereby, we will also take translation of mRNA into protein into account. Essentially, we add to system (2.1) the following two reaction channels describing translation and degradation of the protein p:

$$\begin{array}{rcl} m & \xrightarrow{\beta} & m+p\,, \\ p & \xrightarrow{\delta} & \emptyset\,. \end{array} \tag{2.13}$$

The parameters β and δ denote the translation and degradation rate, respectively. The remaining parameters and equations are taken from system (2.1). Assuming that the mRNA and the protein occur in a high enough amount we can chose the state space

$$S = \{(i, y, z) :\ i \in \{0, 1\},\ y, z \in \mathbb{R}\}.$$

Here and in the following, y and z indicate the concentration of mRNA and protein. Again 0 and 1 denote the two different states the gene g can adopt. The PDMP is denoted by $(X_t)_{t\in\mathbb{R}^+}$ and takes values in S. By writing $X_t = (\theta_t, \xi_t)$, θ_t indicates the discrete state of the gene at time t and ξ_t denotes the two-dimensional vector of concentrations. The vector fields in the two branches are given by

$$v^{(0)}(y, z) = \begin{pmatrix} -\gamma y \\ \beta y - \delta z \end{pmatrix} \text{ and } v^{(1)}(y, z) = \begin{pmatrix} \alpha - \gamma y \\ \beta y - \gamma z \end{pmatrix}.$$

Since we have assumed that transition between the two promoter states happens independently of any other reactants, the transition functions are constant in the individual branches:

$$\lambda(0, y, z) = \kappa_1 \text{ and } \lambda(1, y, z) = \kappa_{-1}.$$

In this case the holding times are, as for a discrete-state Markov process, expo-

nentially distributed. The survival function is given by

$$F(i,t) = \begin{cases} \mathrm{e}^{-\kappa_1 t}, & i = 0 \\ \\ \mathrm{e}^{-\kappa_{-1} t}, & i = 1. \end{cases}$$

Since the process possesses two branches only and concentrations of the gene products are unaffected by a discrete jump, the transition kernel is trivial and the process is specified. Observe that outside of the jump times the process could also be described by ordinary differential equations of the form

$$\begin{aligned} \dot{\xi}_1(t) &= \alpha\theta_t - \gamma\xi_1(t), \\ \dot{\xi}_2(t) &= \beta\xi_1(t) - \delta\xi_2(t). \end{aligned}$$

Interpreting θ_t as an random telegraph signal one obtains the following formulas for the first two moments by taking the Fourier transforms of the respective autocorrelation functions, [88]:

$$\mathbb{E}(\xi_1) = \frac{\alpha}{\gamma}\frac{\kappa_1}{\kappa_1 + \kappa_{-1}} \tag{2.14}$$

and

$$\mathbb{V}(\xi_1) = \frac{\alpha^2\kappa_1\kappa_{-1}}{\gamma(\kappa_1 + \kappa_{-1})^2(\gamma + \kappa_1 + \kappa_{-1})}. \tag{2.15}$$

Comparing these two formulas with the one for the discrete Markov process given by equations (2.2.3) and (2.2.3) shows that the expectation coincides for the discrete-state and the piecewise deterministic Markov processes. Thus, con-

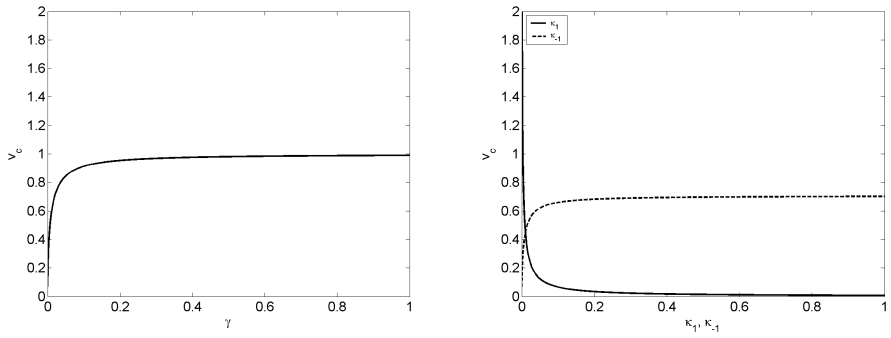
Parameter set	$\mathbb{E}(\xi_1)$	$\mathbb{V}(\xi_1)$	$< \xi_1 >$	$\sigma^2(\xi_1)$
(1)	8.33	52.08	8.51	52.18
(2)	100	2000	98.75	2080
(3)	10	115.39	10.02	116.16
(4)	30	115.39	30.11	114.34

Table 2.3: Theoretical and empirical distribution parameters of the mRNA. The empirical distribution parameters were obtained by 1000 simulations of the HSA.

cerning the first moment there is no loss of information by using PDMP instead of discrete-state Markov processes. On the other hand, the variance of the gene product in the PDMP is always less than the one in the discrete Markov process provided that the expectation is positive. Furthermore, from (2.14) and (2.15) we obtain the coefficient of variation

$$c_v = \sqrt{\frac{\gamma\kappa_{-1}}{\kappa_1(\gamma + \kappa_1 + \kappa_{-1})}}. \tag{2.16}$$

Hence, compared to the discrete state Markov process the relative variation of the mRNA for a PDMP does not depend on the synthesis rate α. Furthermore, although the graphs of c_v as a function of γ and κ_{-1} have the same shapes as the one for the discrete-state Markov processes, their asymptotic behavior is different. If γ tends to infinity, the coefficient of variation tends to its asymptotic

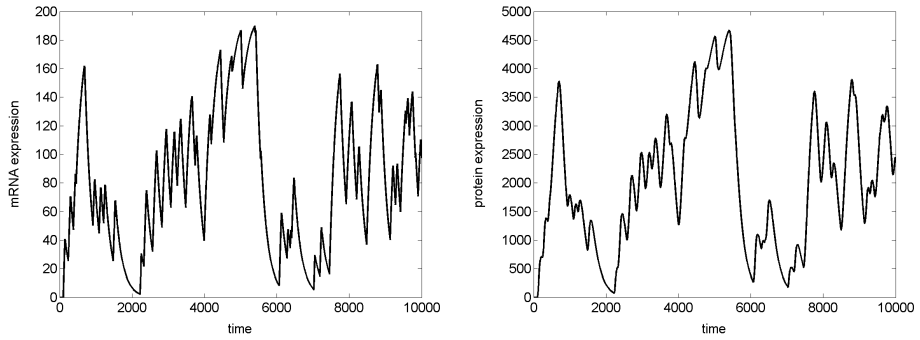


(a) (b)

Figure 2.3: The coefficient of variation c_v of the mRNA as a function of (a) γ, and (b) κ_1 and κ_{-1} for the PDMP.

value $(\kappa_{-1}/\kappa_1)^{1/2}$ instead to infinity as for the discrete-state Markov process. If γ decreases, c_v tends to zero like for the discrete state Markov process, see Figure 2.3(a). If κ_{-1} increases, the coefficient of variation tends to its asymptotic value $(\gamma/\kappa_1)^{1/2}$. Note, that in this case c_v tends to infinity for the discrete-state Markov process. If κ_{-1} tends to zero, c_v converges to zero too, see Figure 2.3(b), whereas it converges to $(\gamma/\alpha)^{1/2}$ for the discrete-state Markov process. Similar results are observed for κ_1. As for the discrete state Markov process, a hyperbolic dependency of c_v on κ_1 is received from formula (2.16). It increases rapidly if κ_1 tends to zero, and converges towards zero if κ_1 is increased, see Figure 2.3(b). For the discrete Markov process we received in the latter case that it converges towards the asymptotic value equal to $(\gamma/\alpha)^{1/2}$. Hence, the main difference in modeling of noise of mRNA transcription by a PDMP compared to a discrete state Markov process arises in the dependency on the parameters α, γ, and κ_{-1}. The noise in a PDMP does not depend on the synthesis rate, and it is bounded by a upper bound if γ or κ_{-1} converge to infinity.

We have simulated the PDMP of transcription and translation given by the reaction schemes (2.1) and (2.13) according to Algorithm 2. Figure 2.4 displays typical expression curves for the mRNA and the protein. The process starts in the active state with zero amount of mRNA and protein. Up to the first jump time it stays in the active state and moves exponentially fast to the amount given by the



(a) (b)

Figure 2.4: Simulated time course of (a) mRNA and (b) protein concentrations using the parameters $\kappa_1 = 0.01,\ \kappa_{-1} = 0.01,\ \alpha = 1,\ \gamma = 0.005,\ \beta = 0.5,\ \delta = 0.02$ with initial point $(\theta_0, \xi_1, \xi_2) = (0, 0, 0)$.

quotient of the transcription and the degradation rate. At the jump time the gene transits to the inactive state and the mRNA decays in an exponential manner, see Figure 2.4(a). At the next jump time the gene switches back in the active state

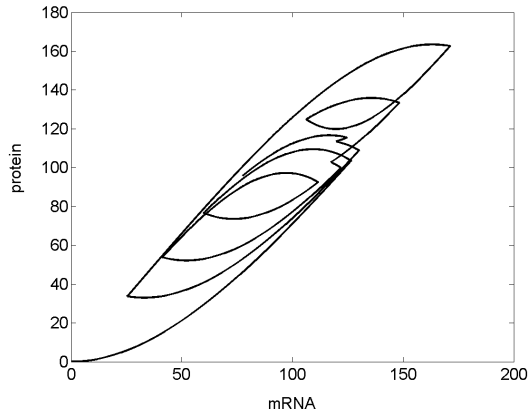


Figure 2.5: Phase diagram of the time evolution of the mRNA and the protein for a simulation length of 2000 time units. Here, the protein expression curve was scaled to the size of mRNA expression levels.

and mRNA production starts again. The protein follows the time evolution of the mRNA with more smooth changes between the active and the inactive branches, see Figure 2.4(b) and Figure 2.5. To compare the distributions of the discrete-state Markov process with the one of the PDMP we have simulated the process using Algorithm 2 for the same four parameter configurations as we have done it for

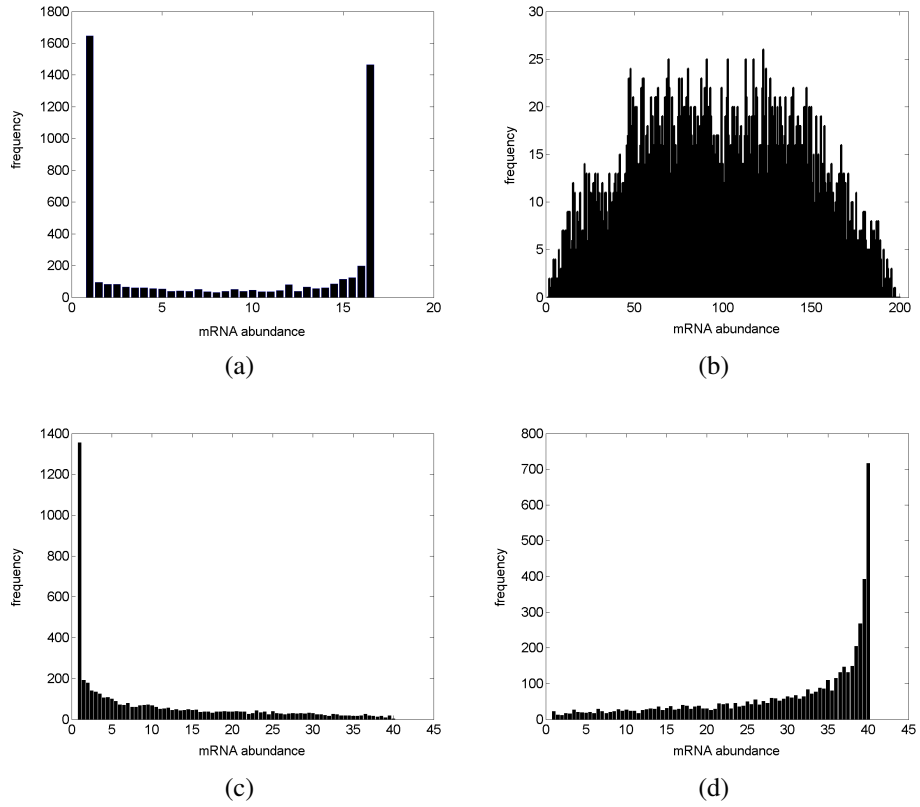


Figure 2.6: Empirical distributions of mRNAs for the PDMP obtained by numerical simulations using Algorithm 2. The histograms (a)-(d) correspond to the parameter sets (1)-(4) from Table 2.1. Each simulation runs for a time period equal to 1000 time units and starts at $(\theta_0, \xi_1(0)) = (0, 0.1)$.

the Gillespie algorithm, see Table 2.1. For the rates of translation and degradation of the protein we have chosen $\beta = 0.5$ and $\delta = 0.02$ for each parameter set (a)-(d). The empirical distributions for the four different parameter arrangements are displayed in Figure 2.6 and Figure 2.7. As in the discrete case, the distributions are calculated from 5000 simulations by running each simulation 1000 time units. The theoretical and empirical first two moments of the mRNA are listed in Table 2.3. A comparison of the theoretical and empirical values of the mRNA shows that they are in good agreement indicating that the PDMP has already approached its stationary distribution. Comparing the individual distributions in Figure 2.1 and Figure 2.6 shows that the distribution of the discrete-state Markov process is very diffuse on the right part of its range whereas the right border of the distribution of the PDMP is very sharp. The reason for this is easy to see. For a PDMP there exists an upper bound for the amount of mRNA and protein whereas for the

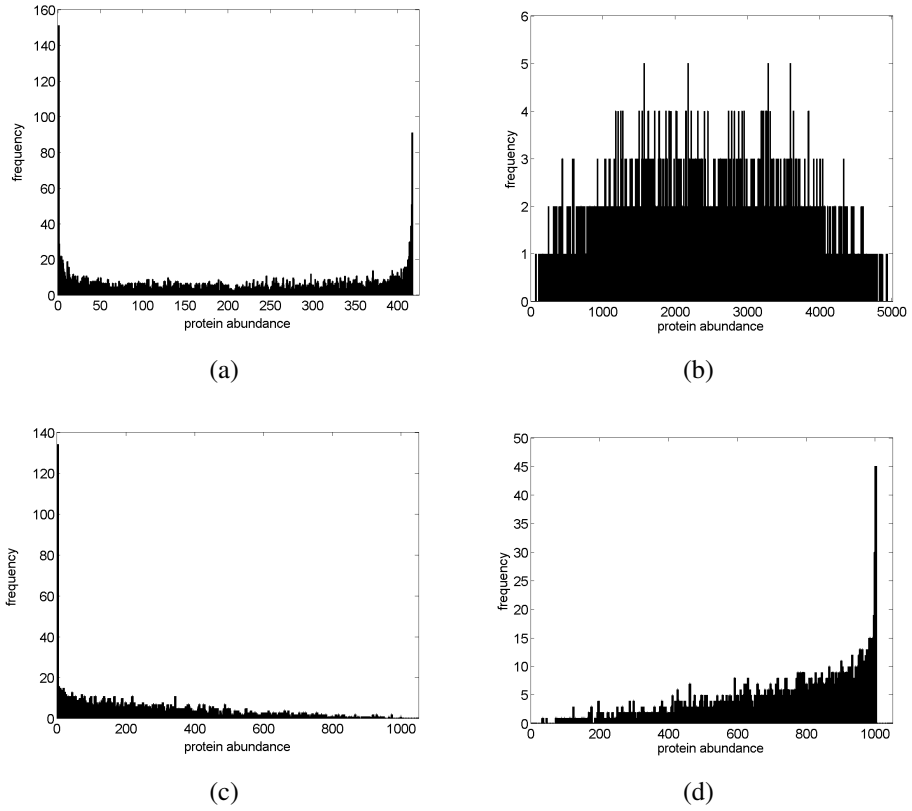


Figure 2.7: Empirical distributions of proteins for the PDMP obtained by numerical simulations using Algorithm 2. The parameters of the translation process are $\beta = 0.5$ and $\delta = 0.02$. The remaining parameters and the initial points are the same as for Figure 2.6.

discrete Markov process no such threshold exists. However, beside the behavior at the right border the expression patterns for the discrete-state and the piecewise deterministic Markov processes have the same shape. Comparing the empirical distributions for the mRNA of the PDMP with the density function of a Beta distribution shows a good agreement for all parameter sets. Indeed, up to a scaling of the x-axis the stationary distribution of the PDMP is given by a Beta distribution, see the supplementary information of [88].
A comparison of Figure 2.6 and Figure 2.7 shows that if the parameter of synthesis and degradation for the mRNA and the protein are of the same order the shape of the two distributions are very similar. The protein shows the same behavior as the mRNA. However, one would expect that the protein occurs in high amount even if the amount of the mRNA is less which is not the case for the given parameter set, compare Figure 2.6(c) and Figure 2.7(c). Since the half life of the protein is in

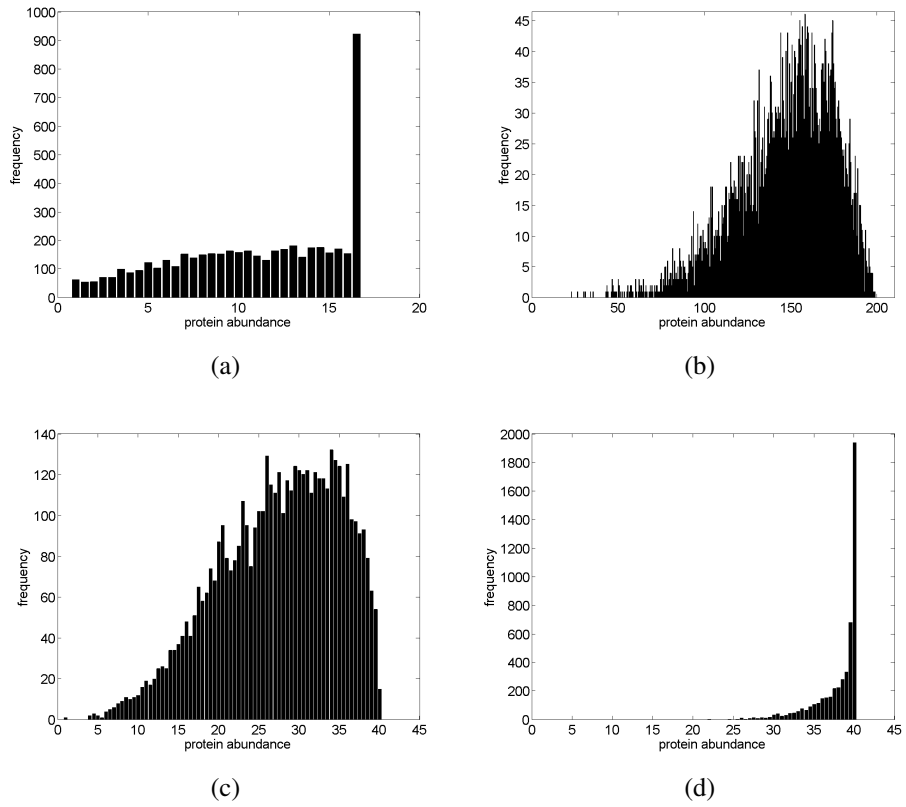


Figure 2.8: Empirical distributions of proteins for the PDMP using the same parameters as for Figure 2.6 and Figure 2.7 except for δ. The values of the protein decay rate are (a) $\delta = 0.006$, (b) $\delta = 0.0005$, (c) $\delta = 0.0025$, (d) $\delta = 0.0025$.

general much bigger than the half life of the mRNA we have calculated each distribution for the four parameter configurations once again but now with a protein decay rate always ten times smaller than the mRNA decay rates. The empirical distributions are displayed in Figure 2.8. Now, the empirical distributions are always unimodal where the mode is located at high expression levels independent of the shape of the mRNA distributions.

To measure the difference in the speed of the hybrid simulation algorithm and the classical SSA we have run several simulations each for a time length of 10000 time units, and measured the cpu time. The parameters are $\kappa_1 = \kappa_{-1} = 0.01$, $\alpha = 3$, and $\gamma = 0.09$. The comparison yield that the hybrid simulation algorithm needs around 4.92 seconds of cpu time on average, whereas the SSA needs around 90.62 seconds of cpu time on average. Hence, for the simplest system the hybrid algorithm consumes only around 5% of the computing time of the classical SSA. In [15] a random telegraph process was used to model response of an engineered

GAL1 promoter of the yeast *S. cerevisiae*. In [88] such a process was used to model mRNA variations and propagation of mRNA variations to variations in protein levels in mammalian cells. The typical distribution of the mRNA and the protein they had found had the shape as the one in Figure 2.6(c) and Figure 2.7(c). Furthermore, they could fit model parameters to the experimental distributions.

Autocatalysis

In the present section we consider an autoregulative network. In such networks genes are activated or deactivated by binding of its own gene products to binding sites in its regulatory region. Proteins that can regulate transcription of other or its own gene are called transcription factors. Whereas a negative feedback loop can stabilize gene expression, [9], or can cause oscillatory behavior [46], a positive feedback can lead to multimodal expression patterns [8], [54]. Here, we explore the influence of dimer formation in an autocatalytic network. Suppose that the ptotein can activate transcription of its own encoding gene. Thus, the activation rate depends on the concentration of the protein, and is given by the product of the association rate constant and the concentration of the transcription factor. In the case that there is no gene product or any other external stimulus present, no synthesis will take place. For simplicity, we ignore intermediate synthesis and modification steps such that we can describe the synthesis process by only one equation. Furthermore, we assume that there is only one binding site in the promoter of g to which the protein p can bind to. Such an autocatalytic network can be described by the following four reaction channels:

$$\begin{array}{rcl} g_0 + p & \xrightarrow{\kappa_1} & g_1\,, \\ g_1 & \xrightarrow{\kappa_{-1}} & g_0 + p\,, \\ g_1 & \xrightarrow{\alpha} & g_1 + p\,, \\ p & \xrightarrow{\gamma} & \emptyset\,, \end{array} \tag{2.17}$$

Let g_0 and g_1 denote the unoccupied and the occupied state of the promoter. Since p acts as an enhancer, g_0 and g_1 denote as in the example of an inducible gene the inactive and the active state of the gene, respectively. The protein is synthesized at an overall rate α and degraded with rate γ. In contrast to the previous example, switching on of the promoter of the gene g depends now on the concentration z of the gene product p. Dissociation of p from the promoter still takes place at constant rate κ_{-1}. Then, the transition rate function for the two branches are given by

$$\lambda(0, z) = \kappa_1 z \;\text{ and }\; \lambda(1, z) = \kappa_{-1}.$$

As in the previous example, on the two branches the dynamics are determined by

$$\dot{z}(t) = -\gamma z,$$

if the gene is deactivated, and

$$\dot{z}(t) = \alpha - \gamma z,$$

if it is active. Thus, the process will tend to α/γ as long as the promoter is turned on, and will tend to zero when the promoter has turned off. In contrast to the inducible gene with constant inducer amounts, the holding time in the off-branch depends now on the concentration z of the gene product:

$$F(0,z,t) \;=\; 1 - \exp\left(-\int_0^t \kappa_1 z(u)\mathrm{d}u\right) = 1 - \exp\left(-\frac{\kappa_1 z_0}{\gamma}(1-\mathrm{e}^{-\gamma t})\right).$$

In the previous example, in which the switching from the off-branch to the on-branch is independent of the concentration of the gene product, the probability that the process stays for an arbitrary long time in the off-branch tends to zero. However, when the switching rate depends on the concentration z this remains no longer true, since

$$\lim_{t\to\infty} F(0,z,t) = 1 - \exp\left(-\frac{\kappa_1 z_0}{\gamma}\right) < 1. \tag{2.18}$$

Thus, with a positive probability the process remains in the off branch even if the amount of protein is still positive. The concentration of the gene product tends to zero and will not activate further synthesis. From equation (2.18) we gain that the probability that the process will not jump back to the activated state depends directly on the decay and the activation rate constants, and indirectly on the synthesis and the deactivation rate by the concentration of the transcription factor z_0. The probability increases if the degradation rate becomes larger, and it decreases if the switching rate κ_1 increases. Since the probability depends also on z_0, i.e., the amount of the protein at the time when the process has jumped to the off-branch, the probability of dying out decreases if the synthesis rate α increases. On the other hand, it increases for larger values of the deactivation rate. Since, if κ_{-1} increases, the process will stay on average in the activated state for shorter time intervals which leads to smaller values of z_0. Thus, as one would expect, the probability that gene expression sustains in an autocatalytic network increases for greater synthesis and activation rates, and for smaller degradation and deactivation rates.

The effects on the time course of the protein are shown in Figure 2.9(a) and 2.9(b), displaying two typical trajectories. The individual trajectories are simulated for a time length equal to 1000 time units. If the process is in the on-branch, it tends to the stationary value α/γ. When the promoter turns off it tends to zero which

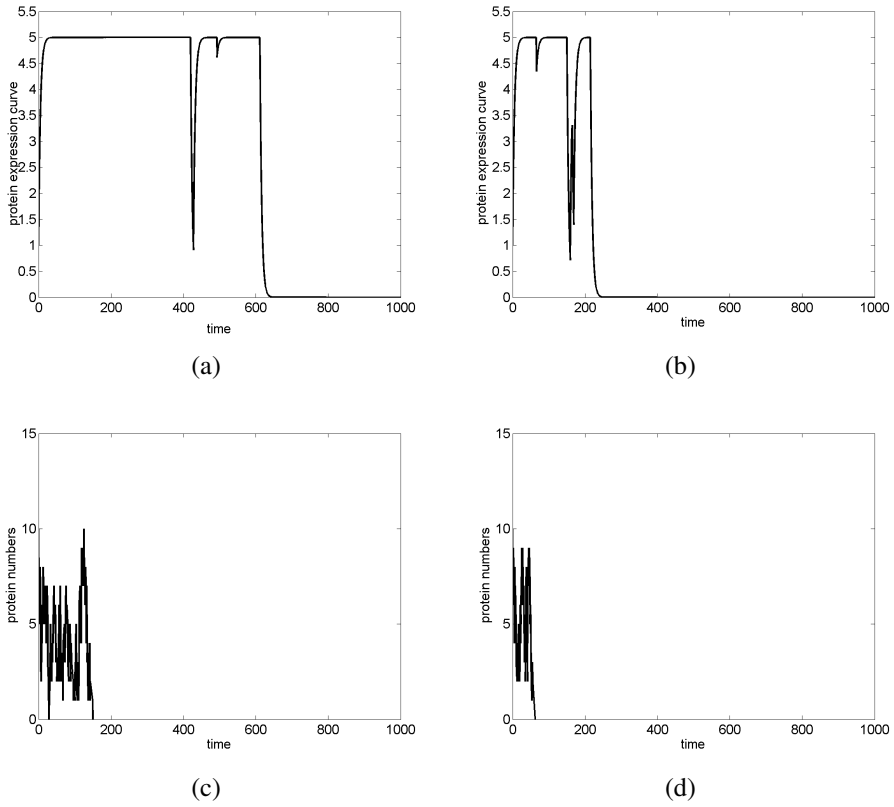


Figure 2.9: Typical sample paths of a piecewise deterministic and a discrete state Markov process. (a) and (b): Temporal evolution of the concentration of protein in two simulations of the autocatalytic network modeled by a PDMP. The parameters are $\kappa_1 = 0.02, \kappa_{-1} = 0.02, \alpha = 1$ and $\gamma = 0.2$. The process starts in the on branch with initial protein concentration equal to 1. (c) and (d): Time course of the numbers of protein in two simulations of the autocatalytic network modeled by a discrete state Markov process. The parameters and the time length are the same as for the PDMP. The process starts in the activated state with initial protein numbers equal to 10.

leads to strong variations in the amount of protein. Within a time interval of 1000 time units it always will jump to the off-branch and remains there.
We have seen that although the protein concentration is not zero the gene remains in its off state. To show that this is not an artefact of the PDMP we have simulated the positive feedback loop as a discrete-state Markov process, too. We have used the same parameter set and the same simulation period as for the PDMP. Figures 2.9(c) and 2.9(d) show two typical time courses of the numbers of the proteins in an autocatalytic network. As expected, the time courses of the protein numbers

of the discrete Markov process show more fluctuations than the time courses of the protein concentrations of a PDMP. However, like the PDMP process dies out within a period of 200 time units.
We want to compare the speed of the two algorithms for the autocatalytic system, too. The parameters are chosen in such a way that the process does not die out in a time range of 10000 time units. The values are $\kappa_1 = \kappa_{-1} = 0.02$, $\alpha = 2$, and $\gamma = 0.02$. Now, the difference of the speed is much greater than for the inducible promoter. For 10000 time units the classical SSA takes 161.67 seconds of cpu time, whereas the PDMP needs only 2.83 seconds on average.
To measure the sensitivity of the system's behavior to parameter changes, we use again the coefficient of variation. The dependency of the autocatalytic network on the individual parameters is shown in Figure 2.10. There, c_v is evaluated at discrete values of the individual parameters listed in Table 2.4. For κ_1 the distribution

κ_1	0.001	0.005	0.01	0.02	0.03	0.05
κ_{-1}	0.001	0.005	0.01	0.02	0.03	0.05
α	0.01	0.25	0.5	1	1.5	2
γ	0.001	0.01	0.05	0.1	0.15	0.2
κ_1	0.075	0.1	0.15	0.2	0.25	0.3
κ_{-1}	0.075	0.1	0.15	0.2	0.25	0.3
α	2.5	3	3.5	4	5	8
γ	0.25	0.3	0.4	0.7	1	2

Table 2.4: Parameter values used for sensitivity analysis.

is unimodal up to a value equal to 0.03 with peak at zero expression levels. The high values of c_v and its fluctuations results from a smaller mean compared to the standard deviation, Figure 2.10(a). From $\kappa_1 = 0.05$ more and more cells exhibit the maximal expression level. The peak at zero gets smaller, and the mode at high expression levels increases: the distributions become bimodal. The increase in the mean results in a decrease of c_v. From a value equal to 0.25 most of the cells exhibit maximal expression levels, and if κ_1 is greater than 0.3 the distribution is more or less unimodal with a peak located at the maximal expression level.
The inverse behavior is observed for κ_{-1}. For $\kappa_{-1} = 0.001$ the distribution is bimodal with two equally high peaks, one located at zero and the other at the maximal expression level. For increasing κ_{-1} the peak at the maximal expression levels gets smaller, and from a value of κ_{-1} equal to 0.02 all cells exhibit zero expression levels. This is reflected in an increasing value of c_v since the mean tends faster to zero than the standard deviation, see Figure 2.10(b). The fluctuations of c_v shows that this measure can be very sensitive if the mean tends to zero.
If the synthesis rate α is small, the distribution is unimodal with peak at zero. This

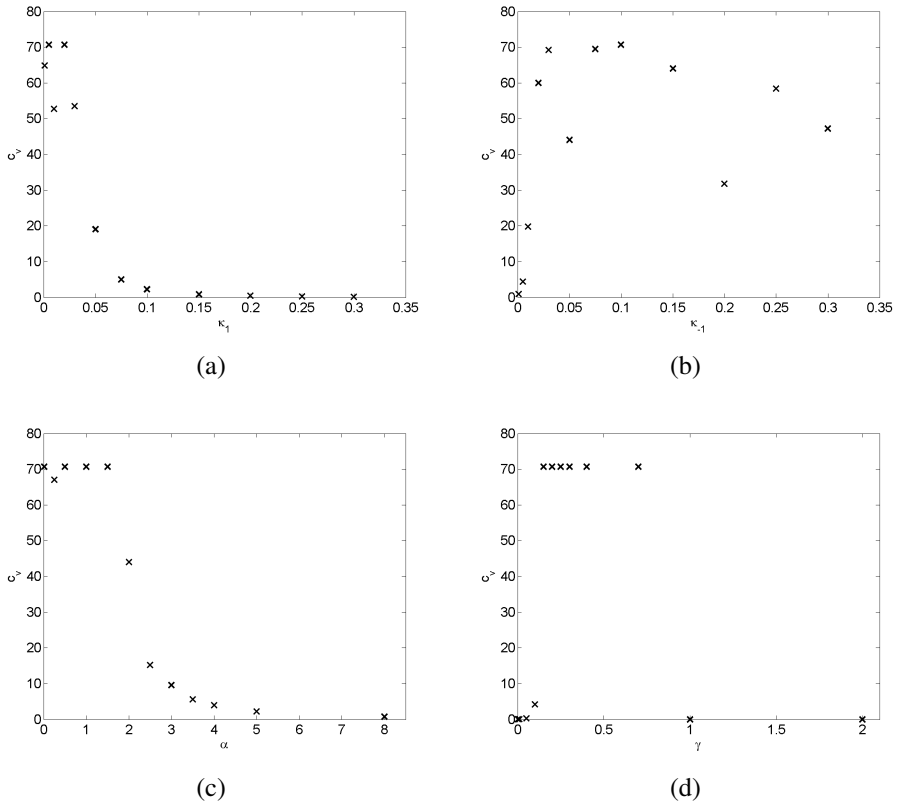


Figure 2.10: The coefficient of variation, c_v as a function on the individual parameters of the autocatalytic system. The functional dependency is calculated for the parameter configuration $\kappa_1 = \kappa_{-1} = 0.02$, $\alpha = 1$, $\gamma = 0.2$ by varying one parameter according to the values listed in Table 2.4 and keeping the remaining parameters fixed.

is reflected in a high value of c_v, Figure 2.10(c). Around $\alpha = 2.5$ the distribution becomes bimodal with one peak at zero and the other at the maximal expression level. If α increases further, the mode at the maximal expression level gets higher and higher which is reflected in a decreasing value of c_v. However, for $\alpha = 7$ still half of the population exhibits no expressions.
The opposite is observed for the degradation rate γ. For $\gamma = 0.001$ the whole population is in the maximal expression level. At $\gamma = 0.01$ the mode at the maximal expression level gets broader, and at $\gamma = 0.05$ the distribution is bimodal with an additional peak at zero. This is reflected in small values of c_v, Figure 2.10(d). At $\gamma = 0.15$ more or less all cells exhibit zero expression levels, which results in high values of c_v. For a value of γ higher than 0.7 the fluctuations are zero, i.e. all cells have zero expression levels, resulting in a c_v equal to zero. Hence, for each pa-

rameter there are two ranges where the distribution is unimodal, one with mode at low expression levels and one with mode at high expression levels, and one range where the distribution is bimodal. In each cases the two ranges with an unimodal distribution are separated by the region where the distribution is bimodal.
The situation displayed in Figure 2.9 changes if one includes dimerization of the gene product p. Let us suppose that activation of the gene g happens only when a dimer p_2 is bound to the promoter. Such a system can be described by adding to reaction system (2.17) two reactions describing reversible dimerization of the transcription factor p

$$p + p \underset{\varepsilon_{-1}}{\overset{\varepsilon_1}{\rightleftharpoons}} p_2 \,,$$

and by replacing the activation and deactivation of the gene g by the reversible reaction channels

$$g_0 + p_2 \underset{\kappa_{-1}}{\overset{\kappa_1}{\rightleftharpoons}} g_1 \,.$$

Now, the process shows a different behavior, see Figure 2.11. The time the process stays in the off-branch is shorter leading to less variation in the protein amount, Figure 2.11(a). Furthermore, the concentration tends to its stationary value and does not peter out, at least not in the observed time interval. A similar behavior is observed for the dimer p_2. With small variations it tends to its stationary value, Figure 2.11(b).
This behavior is consistent with the behavior of the corresponding discrete-state Markov process. Modeling all reaction steps as discrete events results in time courses of the numbers of monomers and dimers as shown in Figure 2.11(c) and Figure 2.11(d). As for the PDMP both the monomers and the dimers converge to their stationary values. Hence, dimerization in a positive feedback loop can reduce strong fluctuations. This is similar to the findings in [19] where it was shown that in a negative feedback loop dimerization taking place in solution is superior in noise attenuation to dimerization taking place on the DNA strand. Moreover, our findings suggest that an additional role of dimerization in a positive feedback could be to effect sustained expressions and reduce the probability of petering out.
To compare the speed of the two algorithms we have run both algorithms 10000 time units. Both processes starts in the on branch with initial amounts of proteins and dimers equal to one. Compared to the monomer case where the waiting times are given in closed analytical forms now the hybrid algorithm takes longer. On average it takes 24.79 seconds of cpu time. However, it is still 23-fold faster than the SSA which takes 565.55 seconds of cpu time on average.
The dependency of a positive feedback loop including dimerization under parameter variation was analyzed by means of the coefficient of variation. Since the

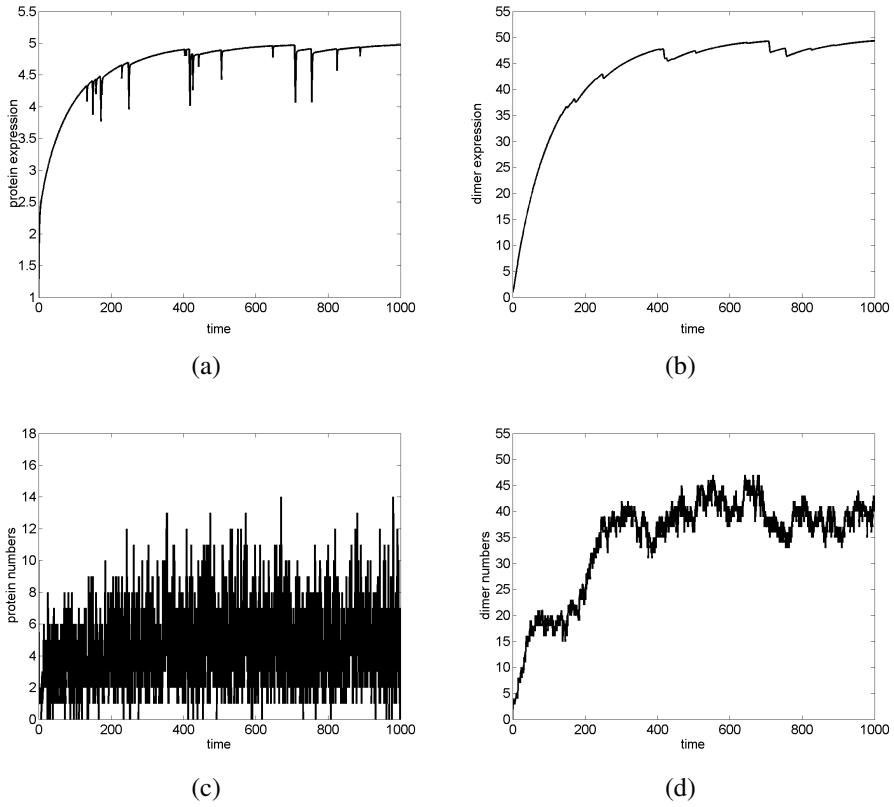


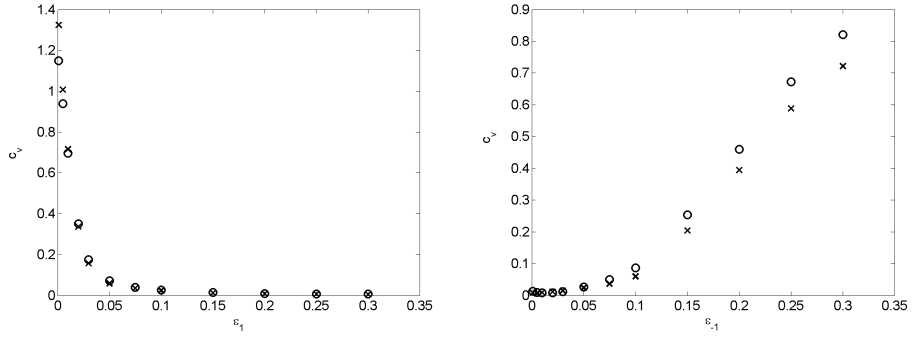
Figure 2.11: Time course of the concentration of (a) monomers and (b) dimers in an autocatalytic circuit. The parameters of dimerization are $\varepsilon_1 = 0.1$ and $\varepsilon_{-1} = 0.05$. The remaining parameters are the same as for Figure 2.9. The process starts in the on branch with initial concentrations of proteins and dimers equal to 1. Time course of the numbers of (c) monomers and (d) dimers in an autocatalytic network modeled by a discrete space Markov process. The parameters are taken the same as those used for the PDMP. The process starts in the off branch with initial protein numbers equal to 10 and with zero dimers.

functional dependency of c_v on the activation and the deactivation rate as well as on the synthesis and degradation rate is quite similar as in the monomer case, only the dependency on the forward and backward rates of dimerization are displayed, Figure 2.12. The analysis was done taking the same values as in Figure 2.9 and Figure 2.11 by varying one particular parameter. The coefficient of variation was evaluated at the discrete values of ε_1 and ε_{-1} listed in Table 2.5. For the analysis of the dependency of c_v on the remaining parameters the same values were taken as listed in Table 2.4.
For small values of ε_1 dimerization of the transcription factor takes place with

$\varepsilon_1,\ \varepsilon_{-1}$	0.001	0.005	0.01	0.02	0.03	0.05
$\varepsilon_1,\ \varepsilon_{-1}$	0.075	0.1	0.15	0.2	0.25	0.3

Table 2.5: Parameter values used for sensitivity analysis in the autocatalytic network based on dimers.

small rates. Thus, the system is similar to an autocatalytic network including only monomers. In this case the distribution is unimodal with mode located at zero resulting in a high value of c_v, Figure 2.12(a). If ε_1 increases the distribution becomes bimodal. A further increase results in a unimodal distribution with mode



(a) (b)

Figure 2.12: Dependency of c_v on the (a) forward and (b) backward rate of dimerization. The c_v of monomers and dimers are denoted by a cross and a circle, respectively.

located at the maximal expression level yielding to a decrease in c_v. The contrary behavior is observed for the backward rate ε_{-1}. For small ε_{-1} dimerization is stable such that all cells are in their maximal expression level reflected in very small values of c_v, Figure 2.12(b). If ε_{-1} increases the maximal expression level of the dimers decreases whereas the distribution remains unimodal up to $\varepsilon_{-1} = 0.1$. For higher values than 0.1 the distribution becomes unimodal resulting in increasing values of c_v.

As already mentioned the qualitative dependency of c_v on the remaining parameters is similar to the system based on monomers. However, if the positive feedback loop is built-on dimers the system is more stable as it was already observed in the situation of Figure 2.11. This means that the cells reach their maximal expression levels at smaller or higher values of the particular parameters. For example, in the presence of dimers the distribution of the concentration of the monomers and dimers is at $\alpha = 1$ already unimodal with mode around the maximal expression

level. For comparison, in the case when the feedback loop is based on monomers the distribution is at $\alpha = 7$ still bimodal with one peak at zero expression levels. A similar behavior is observed for κ_1. At $\kappa_1 = 0.01$ the distribution of the autocatalytic module based on dimers is unimodal with mode around the maximal expression level. In case of monomers it is still bimodal at $\kappa_1 = 0.05$. On the other hand, the situation is reversed for κ_{-1} and γ. If the feedback loop is based on monomers, all cells are in the lowest expression stage whereas in the case of dimers there are cells exhibiting non-zero expression levels even at $\kappa_{-1} = 0.3$.

In the autocatalytic network based on monomers all cells exhibit zero expression levels from a decay rate equal to 0.15. If the regulation is based on dimers all cells are in the maximal expression level already for a value of γ equal to 0.3.

It is a known fact that positive feedback can create bistability, [74]. Based on our analysis it should be possible to generate or destroy bistability by varying one of above parameters in the appropriate direction. Furthermore it should be possible to give parameter ranges where the system is in a low or high state of gene expression. Testing our finding by biological experiments is difficult since the respective literature is rare. A first step in this direction was done in a recently published paper, [1]. The observed behavior of their engineered positive feedback loop was in line with the prediction of their deterministic mathematical model. By increasing the synthesis rate they could show that the system remains in the activated state even for transient stimulus which is in accordance to our findings on the dependency of c_v on the production rate α.

Toggle Switch

As an example for a PDMP with more than two discrete states we consider a simple model for a toggle switch. For alternative stochastic approaches and a more detailed analysis see [3], [112]. A toggle switch is a regulatory module consisting of two core components where each gene product represses the synthesis of the other component. A synthetic toggle switch was first analyzed both theoretically and experimentally by Gardner et al., [30]. The module consists of two constitutive promoters fused with two repressors, and was implemented on plasmids in *Escherichia coli*. Each repressor inhibits transcription by the promoter of the opposite construct, see Figure 2.13 for a schematic representation. In [66] a synthetic toggle switch could also be implemented in mammalian cells. A further synthetic circuit, the repressilator, composed of three mutually repressing promoters was studied in [29]. Whereas the latter shows oscillatory behavior, the toggle switch can exhibit bistable expressions.

The circuit can be described by six reactants and eight reaction channels, summarized in the following reaction scheme:

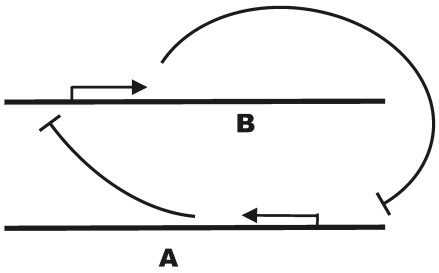


Figure 2.13: Diagram of a toggle switch. Synthesis of the genes A and B is mutually repressed by each other.

$$\begin{array}{llll} A_0 + b & \xrightarrow{\kappa_1} & A_1\,, & B_0 + a \xrightarrow{\mu_1} B_1\,, \\ A_1 & \xrightarrow{\kappa_{-1}} & A_0 + b\,, & B_1 \xrightarrow{\mu_1} B_0 + a\,, \\ A_0 & \xrightarrow{\alpha} & A_0 + a\,, & B_0 \xrightarrow{\beta} B_0 + b\,, \\ a & \xrightarrow{\gamma} & \emptyset\,, & b \xrightarrow{\delta} \emptyset\,. \end{array}$$

A_i and B_j denote the two fused gene constructs, and a and b the respective gene products. The indices i and j indicate whether the gene is occupied or not. The two promoters in the toggle switch can adopt one of the following four configurations:

$$M = \{A_0B_0,\ A_1B_0,\ A_0B_1,\ A_1B_1\}.$$

Assuming that at a given instant t only one protein dissociates or associates from or to a binding site only eight transitions are possible, see Figure 2.14. In the following we will also denote by a and b the concentration of the respective gene products. The construction of the PDMP is explained by focusing on the state A_0B_1. The state space is given by $S = \{(i, z) :\ i \in M,\ z = (a, b) \in \mathbb{R}^2\}$ and the vector field in state $i = A_0B_1$ reads

$$v^{(i)}(z) = \begin{pmatrix} \alpha - \gamma a \\ -\delta b \end{pmatrix}.$$

The holding times in $i = A_0B_1$ are governed by the rate function

$$\lambda(A_0B_1, z) = \kappa_1 b + \mu_{-1}.$$

Last we have to specify the state to which the process jumps to after a jump has occurred. The post-jump state i posses the discrete distribution

$$P\left((i, z), \cdot\right) = \frac{\kappa_1 b}{\lambda(A_0B_1, z)}\delta_{(A_1B_1,z)} + \frac{\mu_{-1}}{\lambda(A_0B_1, z)}\delta_{(A_0B_0,z)}$$

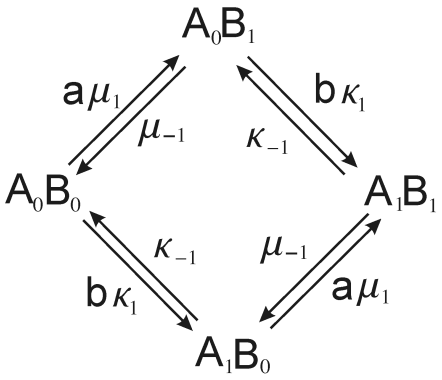
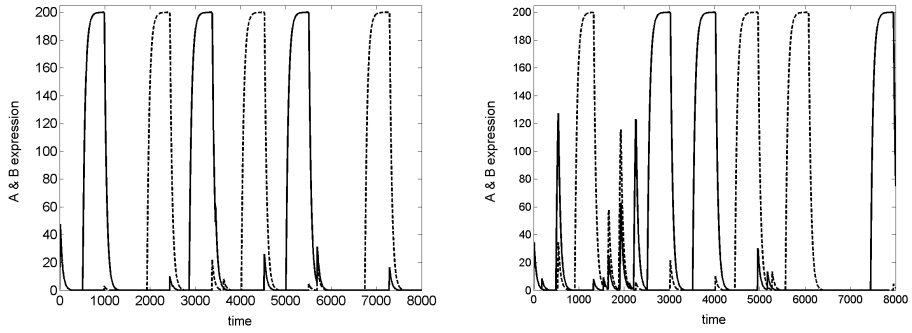


Figure 2.14: Possible transitions between different branches in the toggle switch.

where δ_x denotes the Dirac measure concentrated at point $x \in S$. In other words, the process jumps with probability $\kappa_1 b/(\kappa_1 b + \mu_{-1})$ into A_1B_1, and into A_0B_0 otherwise. Individual trajectories were simulated by executing Algorithm 2.
One can easily show that a deterministic model of a toggle switch, where each promoter possesses only one binding site and where the gene products are present as monomers, possesses only one stationary point, [30]. On the other hand one



(a) (b)

Figure 2.15: Temporal evolution of the gene product concentrations a (solid) and b (dashed) for the parameter set $\kappa_1 = 0.002, \kappa_{-1} = 0.001, \mu_1 = 0.002, \mu_{-1} = 0.001, \alpha = 4, \beta = 4, \gamma = 0.02, \delta = 0.02$.

would expect that the system switches between the minimal and the maximal concentration of the two gene products. For a stochastic model this is indeed the case. Figure 2.15 displays two typical expression curves of the construct A (solid line)

and construct B (dashed line). In contrast to a deterministic model of the toggle switch, a stochastic model possesses three states which it will visit in turns: high amounts of a and low amounts of b and vice versa, and states with low amounts of a and b. States with positive amounts of a or b are interrupted by states where both genes are suppressed, see Figure 2.15. The resulting empirical distributions of the two genes would be a bimodal graph with one peak around zero and the other around the maximal expression level of A and B. However, we gather from Figure 2.15 that the time the process stays in one of these three states is short. It is in the order of $10^2 - 10^3$ time units. Thus, the system rather flips from one state to another which is not the behavior one would expect from a bistable system. Furthermore, one would demand that the time the process stays in the off-state A_1B_1 would be very short compared to the sojourn times in the states A_0B_1 and A_1B_0. For the given system we have not found a parameter set leading to such a behavior which will be shown in the following analysis of the systems behavior dependent on parameter changes.

To analyze the dependency of the systems behavior on the individual parameters we measure the average time the process stays in one of the four states. The average time is calculated by running the simulation 5000 time units. As an example, the dependency on the association parameter κ_1 is displayed in Figure 2.16. In accordance with the expression curves in Figure 2.15 the system stays very short in state A_0B_0, Figure 2.16(a), and for relatively long time periods in state A_1B_1, Figure 2.16(d). In the states A_1B_0 and A_0B_1 the process stays about one third of the time it remains in state A_1B_1, Figure 2.16(b) and (c). As one would expect, the average time spend in states A_0B_0 and A_0B_1 decreases as κ_1 increases, Figure 2.16(a) and Figure 2.16(c), respectively. On the other hand, the sojourn time in states A_1B_0 and A_1B_1 increase as κ_1 increase, see Figure 2.16(b) and Figure 2.16(d).

The average sojourn time in state A_0B_0 shows very weak dependency on the parameter κ_{-1}. It varies between 4.6 and 4.9 time units. As one would expect, the sojourn time in states A_1B_0 and A_1B_1 decreases as κ_{-1} increases. In state A_1B_0 it decreases from 220 time units to 70 time units. In state A_1B_1 the average sojourn time decreases from 1100 time units to 300 time units. If κ_{-1} increases, the average sojourn time in state A_0B_1 increases from 40 time units to 110. A further increase will lead to a decrease of the sojourn time to 80 time units.

For increasing production rate α the average sojourn time in the states A_0B_0 and A_1B_0 decreases. Whereas it varies between 5 and 7 time units for state A_0B_0, it decreases from 180 to 130 time units for state A_1B_0. The sojourn time in state A_0B_1 increases from 110 to 127 time units as α increases. For state A_1B_1 a consistent tendency could not be observed. The sojourn time varies between 554 and 562 time units.

The opposite behavior is observed for the degradation rate γ. The sojourn time

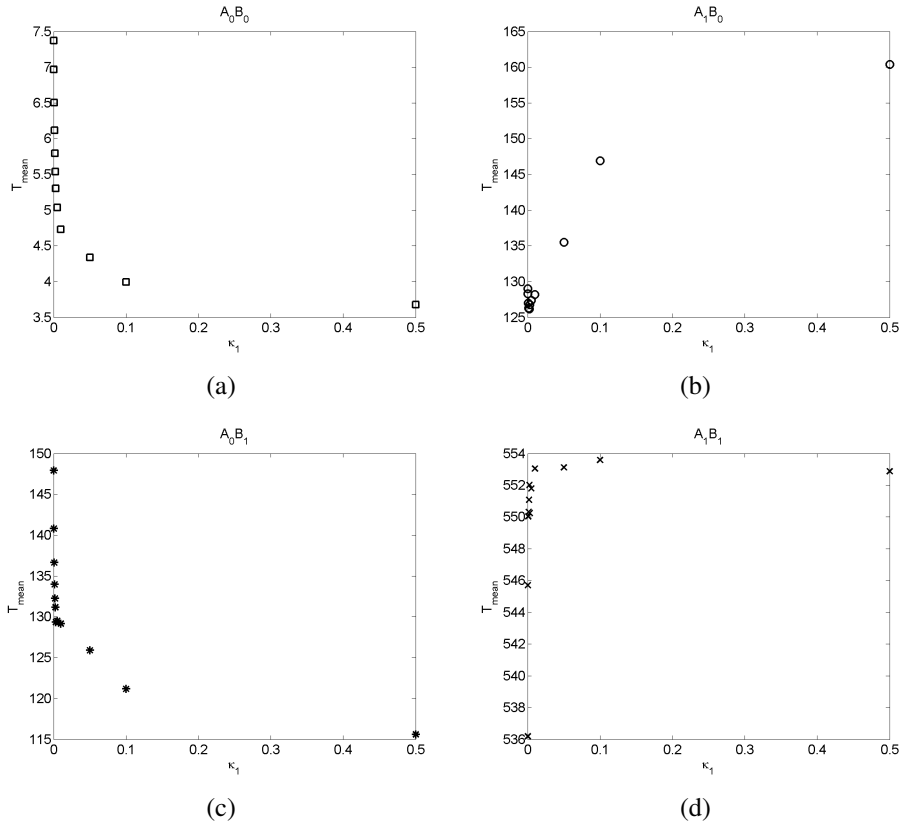


Figure 2.16: Dependency of the averaged time on κ_1 for which the system remains in one of the four states (a) A_0B_0, (b) A_1B_0, (c) A_0B_1, and (d) A_1B_1.

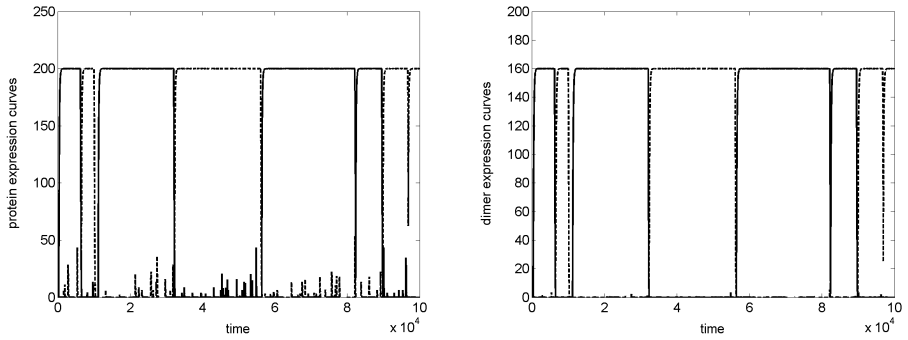
in states A_0B_0 and A_1B_0 increases for increasing γ. As for κ_1, κ_{-1}, and α the change of the average sojourn time in state A_0B_0 is small, whereas it increases from nearly 0 to 150 time units in state A_1B_0. For state A_0B_1 the average sojourn time decreases from 190 to about 135 time units as γ increases. As for the synthesis rate, the sojourn time in state A_1B_1 shows only weak dependency on the degradation rate γ. It varies between 552 and 559 time units.

Since the gene products used in [30] form multimers we include the following reversible reactions describing dimerization of the two proteins a and b:

$$a + a \underset{\varepsilon_{-1}}{\overset{\varepsilon_1}{\rightleftharpoons}} a_2\,, \quad b + b \underset{\nu_{-1}}{\overset{\nu_1}{\rightleftharpoons}} b_2\,,$$

Typical expression curves for the concentrations of the proteins a and b are displayed in Figure 2.17. Now, the system shows the desired behavior. Indeed the system still visits all four states but now the sojourn times in state A_0B_0 and A_1B_1 are very short compared to the ones in state A_1B_0 and A_0B_1. In the main, the sys-

tem toggles only between two expression levels. A state with high concentration



(a) (b)

Figure 2.17: Temporal evolution of the protein (a) and dimer (b) concentrations in the toggle switch including dimerization of both gene products. The solid lines in (a) and (b) represent the expression curves of a and a_2, respectively, and the dashed lines display the time courses of b and b_2. The parameters describing promoter switching, synthesis and degradation are the same as for Figure 2.15. The parameters for dimerization are $\epsilon_1 = 0.0002, \epsilon_{-1} = 0.05, \nu_1 = 0.0002$, and $\nu_{-1} = 0.05$.

of a and low concentration of b, and vice versa. The time the system exhibits one of the two expression levels is in the order of 10^4 time units, Figure 2.17.
This can also be seen by looking at the average times the process stays in one of the four states $A_0B_0, \ldots, A_1B_1$. Figure 2.18 displays the average sojourn time for different values of κ_1. The times are calculated for the same parameter values as for Figure 2.15 and Figure 2.17 by varying the values of κ_1. Figure 2.18 shows that the sojourn times in states A_0B_0 and A_1B_1 for the toggle switch including dimers decreases compared to the toggle switch with monomers, see Figure 2.16 and 2.18. On the other hand, the time the process remains in one of the two states A_1B_0 and A_0B_1 increases if the toggle switch is based on dimers which is in accordance with Figure2.17. The qualitative dependency of the sojourn time on κ_1 is quite similar to the case where the toggle switch operates by monomers only. For instance, the sojourn time increases in state A_1B_0 and decreases in state A_0B_1 as κ_1 increases, see Figure 2.18(b) and Figure 2.18(c). However, the times the process remains in state A_1B_0 or A_0B_1 are not much greater than the times it remains in state A_1B_1. The reason for this is that the remaining times in state A_1B_0 or A_0B_1 are often interrupted by short times the process stays in the state A_0B_0, see Figure 2.17(a). Thus, the time the process stays in a state with high levels of a or b can be quite different from the sojourn times in states A_0B_1 or

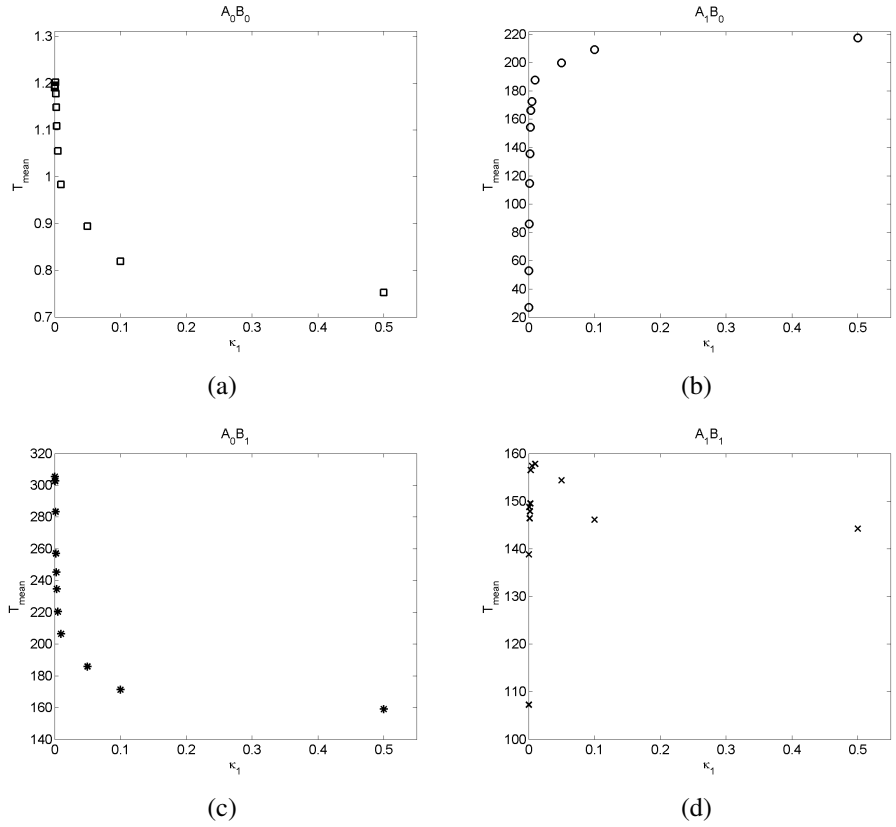


Figure 2.18: Average sojourn times of the toggle switch containing dimers in the four promoter configurations (a) A_0B_0, (b) A_1B_0, (c) A_0B_1, and (d) A_1B_1.

A_1B_0, respectively. Hence for a more detailed quantitative analysis one should use a more sophisticated measure.

More insight concerning the amount of time the process exhibits a particular expression level is gained by looking at individual expression curves. Figure 2.19 shows typical expression levels for low and high values of the parameters α and κ_1. If α is half of the value of β, the process stays almost always in the state with high expression levels of b and low expression levels of a, Figure 2.19(a). On the other hand, if α is twofold of the value of β, the process exhibits high expression levels of a and low expression of b, Figure 2.19(b). Hence, if the production rate of one of the two repressors is at least twice as high as the one of the other repressor the system is monostable. This is also predicted by the deterministic model and could be observed by experiments done by Gardner and colleagues in [30]. By altering the ribosome binding sites they could change the synthesis rate of one of the repressor and found that the system posses only one stable state.

From the parameter dependency displayed in Figure 2.18 we would expect the

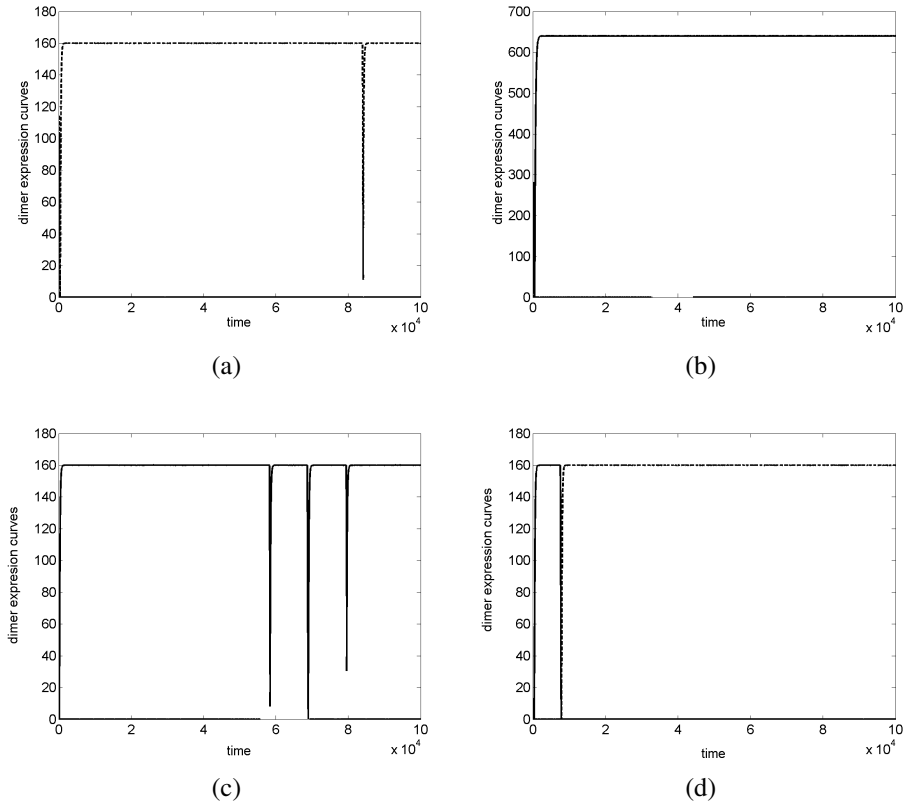


Figure 2.19: Expression curves of the toggle switch including dimerization for different values of the synthesis and the association rates α and κ_1, respectively. Dimers of the gene products of the genes A and B are given as a solid and dashed line, respectively. (a) $\alpha = 2$, (b) $\alpha = 8$, (c) $\kappa_1 = 0.0005$, (d) $\kappa_1 = 0.005$.

same behavior in case of changing the association rate κ_1. For $\kappa_1 = 0.0005$ the system exhibits high expression levels of a and low expression levels of b, Figure 2.19(c). On the other hand, if the value of κ_1 is doubled compared to the value in Figure 2.17 the system is nearly always in the state with high expression levels of b and low expression levels of a, Figure 2.19(d). The opposite behavior is observed for the dissociation rate κ_{-1}. Decreasing κ_{-1} leads to high expression levels of b and low expression levels of a and conversely for increasing κ_{-1}. However, as far as we know there are no experiments which have tested these settings.

2.1.6 Discussion

We proposed piecewise deterministic Markov processes to model gene regulatory networks. PDMP comprise inherent stochasticity to reveal important sources of

random effects caused by the small numbers of reactants. We focused on intrinsic randomness during gene expression caused by transitions of a gene between different promoter states. Beside promoter bindings we have modeled all other processes as a deterministic process. We presented a simulation algorithm and discussed it by means of several regulatory networks.

The simplest system of gene expression is an inducible gene with constant amount of inducer in time, i.e. for which the transitions of the promoter between its active and inactive states take place with constant rates. We have analyzed the stationary distribution of such a system by numerical means and compared it with the one of the corresponding discrete-state Markov process. Taking the same parameter values for both models shows that both models exhibit the same qualitative behavior. The profiles for four different parameter combinations have always the same shape. However, whereas the distribution of the PDMP has a clearly defined range (between zero and the ratio of the transcription to the degradation rate) the distribution of the discrete-state Markov process is more diffused especially at the right border of the distribution. This is reflected by the expectation and the variance of the two model systems. Using results from literature we show that the expectation of a PDMP coincides with the one of a discrete state-space Markov process. On the other hand, the variance of a hybrid Markov process is always less than the one of a discrete-state Markov process. The variance of the latter is equal to the variance of the former plus the value of the expectation. To measure the dependency of the system's variation on the parameters we have chosen the coefficient of variation defined as the ratio of the standard deviation to the mean. By means of the closed formula for the mean and the variance this can be done analytically. Whereas the coefficient of variation for the discrete state Markov process depends on the synthesis rate α, the one for the PDMP does not, i.e., is constant. However, since c_v for the discrete process converges rapidly towards its asymptotic value as α increases, this difference becomes noticeable only for small production rates. Furthermore, c_v for the discrete state process increases to infinity as the decay or the deactivation rates γ and κ_{-1}, respectively, tend to infinity whereas the coefficient of variation for the PDMP is bounded. For small values of γ and κ_{-1} the two measures are in the same range. Moreover, we have shown that the distributions of the mRNA and the protein could be bimodal in principle. However, choosing for the decay rate of the protein realistic values revealed that the distribution of the protein will always be unimodal independent of the shape of the distribution of the mRNA.

For a positive feedback loop consisting of a transcription factor present in form of a monomer and a gene with one binding site in its regulatory region to which the transcription factor can bind to we could determine a simple formula giving the probability that gene expression will peter out. In contrast to a discrete-state Markov process this takes place even when the protein concentration is positive.

However, simulations of the corresponding discrete process have shown that this behavior is in accordance with the discrete model. The probability depends directly on the degradation and the association rate, and, indirectly through the concentration of the protein, on the production and the dissociation rate. For a fixed time interval this can lead to unimodal or bimodal distributions. Thus in contrast to a deterministic model the hybrid model exhibits bimodal distributions even in the absence of cooperativity. Numerical analysis of the dependency of the coefficient of variation on the individual parameters confirmed this finding. For a fixed time interval there are always two parameter ranges where the distribution is unimodal separated by a parameter region where the distribution is bimodal.
To investigate the role of dimerization in such an autocatalytic network we additionally modeled a network in which the transcription factors can form dimers. Now, taking the same parameter set the behavior changes. For the same time length of simulation the protein concentration does not vanish anymore. It converges towards its steady state showing smaller fluctuations. The same behavior was observed for a positive feedback loop modeled by a discrete state process. Thus, in a pure autocatalytic circuit dimerization can stabilize gene expression, and keeps expression running. Nevertheless, the system still can show bimodal expression profiles in agreement with the deterministic model. This was found by analyzing the dependency of the coefficient of variation on the individual parameters. The qualitative behavior is the same as in the monomer case. However there is a shift in the parameter range when the individual distribution shapes appear, i.e., uni- or bimodality occur at higher or lower parameter values compared to the monomer case.
Our predictions concerning the system behavior in respect to the production rate is in agreement with recent experimental findings, [1]. It will be interesting if our predictions about the remaining parameters will be in agreement with future experiments about autocatalytic networks.
As a further gene circuit we have modeled a toggle switch. In a model in which both genes have one binding site and the gene product is present as monomer the system switches between a state in which one of the gene is present at maximal expression level while the other is present at lowest expression level, and a state in which both genes are suppressed. Such a behavior cannot be understood from a deterministic model which possesses only one steady state. However, in the case of monomers the system remains only for a short time in one of these states. Furthermore, one would expect that the system transits only between two states – high expression levels of the one gene and low expression levels of the other gene, and vice versa. Such a behavior could not be observed for this system. In a further model we have analyzed the effects of dimers in a toggle switch. If the proteins form dimers, the module shows a more switch-like behavior. In large time intervals the system just toggles back and forth between the two states where

one gene is highly and the other is lowly expressed. Now, the time in which both genes are suppressed is very short compared to the time the system exhibits high expression levels of one of the two genes. Hence, dimerization stabilizes the switch by preventing it from flipping from one state to the other. Such a behavior is in accordance with the deterministic model in which two stable states exists, if the Hill coefficient for both genes is greater than one, [30].
To compare the computation time of the classical SSA with the hybrid algorithm we have measured the cpu time of both algorithms for the inducible promoter system, and the positive feedback loop with and without dimerization of the transcription factors. When the holding times are given by a analytical formula, i.e. in the case of the inducible promoter system and the autocatalytic network including only monomers, the hybrid algorithm needs only 5 or less than 2%, respectively, of the computing time of the SSA. For the autocatalytic network including dimers the cpu cost of the hybrid algorithm is less than 5% of the one of the SSA. It could be expected that this effect will be enforced for more complex system including more reaction channels or species which are present in higher numbers. However, a universal comparison can not be drawn since the speed of the hybrid approach depends on the stiffness of the particular differential equations.
Concluding, PDMP are adapted for modeling biological processes with different ranges in numbers of reactants. They help to reduce computational costs in large networks by modeling reactions with large numbers of active molecules by replacing discrete by continuous models. However, they capture enough stochasticity in particular to reflect the intrinsic noise in gene expression. Moreover, in doing so PDMP can help to understand the sources of random effects caused by low numbers by ignoring the low randomness caused by reactions including large numbers of reactants.

2.2 Hybrid Modeling of Noise Reduction by a Negatively Autoregulated System

The current section reproduces the results from [126].
We analyze the reduction of intrinsic noise caused by transition of a promoter between its active and inactive state in a negatively regulated genetic network, i.e. transcription of the gene is inhibited by its own gene product. To measure the noise attenuation we compare its behavior to an inducible gene for which activation and deactivation of the gene take place at constant rates.
As a model we choose a hybrid approach in which some of the reaction channels are modeled as discrete events, and other reactions are modeled as continuous processes. Such a model is appropriate for investigations of noise caused by low reactant numbers. By focusing on intrinsic noise originating from the switching behavior of the regulatory system of a particular gene we model only the transition between two different promoter states as a discrete event.
We show that the stationary distributions of the unregulated and the autoregulated system are given as a solution of two coupled ordinary differential equations. Beside the distribution densities also the first two central moments are derived in closed analytical forms. We give conditions on the parameters when one or the other system shows lower fluctuations.

2.2.1 Introduction

Genes can regulate their expression by inhibiting or enhancing transcription by its own gene products. Such autoregulative modules can lead to different expression profiles. Positive feedback loops can lead to hysteresis and bistability, or can create and maintain cellular decision, [8], [58], [107]. On the other hand, negative feedback loops can reduce noise in gene expression but can also destabilize expression levels leading to oscillations, [9], [46], [51], [113]. Here we consider regulation of noise by an autoregulative network composed of a negative feedback loop.
Single cell experiments have shown that expression patterns in individual cells can differ strongly even in isogenic cell populations. Such noisy gene expression takes place on the transcriptional as well as on the translational level, [88], [28]. These experiments indicate that gene expression on the level of single cells takes place in a rather random than deterministic way. One distinguishes between two sources of noise which affect gene expression: intrinsic and extrinsic. Inherent stochasticity in synthesis of mRNA and protein defines intrinsic noise whereas other cellular variations contribute to extrinsic noise, [28]. One cause for intrinsic noise are the small numbers of large molecules, in particular the DNA [78].

A possible way how cells could reduce noise is by using negative feedback loops which was discussed in the classical work of Savageau, [100]. In [9] an unregulated and an autoregulated construct of a repressor and a green fluorescent protein, implemented in *Escherichia coli*, was used to analyze stability in gene networks. Noise was measured in form of the coefficient of variation. It was shown that noise in the regulated network was reduced compared to the unregulated system. This was confirmed by a simple theoretical model adding disturbance to the steady state solution of an ordinary differential equation. However, in both the experiment as well as in the theoretical model it is difficult to determine the nature of noise.
Here, we focus on reduction of intrinsic noise by negative feedback loops. More precisely, we consider fluctuations in gene expression levels originating from the transitions of a promoter between its active and inactive state which we will call in the following *promoter noise*. As a model we choose so called piecewise deterministic Markov processes (PDMP) introduced by Davis in [23] in a much more general setting. PDMP are hybrid stochastic processes in the sense that the state space is a product space of a discrete times a continuous set, and that they can move deterministically as well as randomly. Between two random jumps, where the jump time as well as the post jump state are random, the process moves deterministically determined by ordinary differential equations. At a jump time the

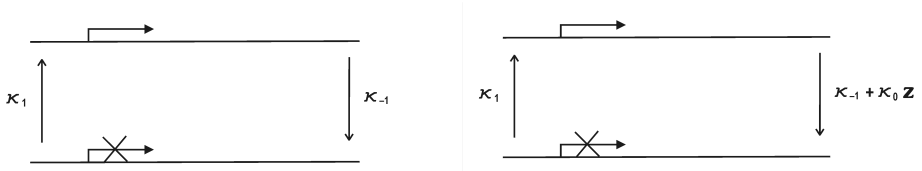


Figure 2.20: Transition schemes of an unregulated and a regulated gene. Arrows to the right indicate the initiation site of transcription. The deactivated gene is displayed by a crossed arrow. (a) In an unregulated gene the promoter switches between its active and inactive state with constant rates κ_1 and κ_{-1}. (b) If the gene is regulated by its own gene product the rate of transition from its active to its inactive state is increased by a rate constant κ_0 times the concentration of the gene product z.

process chooses another discrete state according to some discrete probability distribution.
We study two models of an unregulated and an auto-regulated genetic network where the autoregulation is realized by a negative feedback loop. The first one is a simple model for an inducible gene without negative feedback. It is assumed that

external inducers are present in constant amounts. Hence the promoter switches between its active and inactive state with constant rates, see Figure 2.20 (a).
The second one is a simplified model for a negative feedback loop. Transitions of the promoter from its inactive to its active state are still to be assumed to happen with constant rates. Furthermore, in the absence of any gene products the promoter is turned off with constant rate. However, now turning off depends additionally on the amount of the gene product. In the presence of gene products the transition rate is increased by a rate constant times the amount of the gene product, see Figure 2.20 (b). In both models it is assumed that the promoter of the particular gene is only present in one of two states: on or off. Furthermore it is assumed that the gene product is present in high enough amount such that processes like synthesis and degradation can be described by ordinary differential equations. For simplicity we ignore all intermediate steps during synthesis of the gene product. Hence, the temporal evolution of the concentration of the product can be described by one equation only.

2.2.2 1-dimensional PDMP with two discrete states

To define a PDMP we follow the construction in [23]. Let $M = \{0, 1\}$ and $X_t = (\theta_t, \xi_t),\ t \geq 0$, be a family of random variables taking values in the state space

$$S = \{(i, z) :\ i \in M,\ z \in \mathbb{R}_+\}.$$

The state space consists of two branches: $\{0\} \times \mathbb{R}_+$, the gene is off, and $\{1\} \times \mathbb{R}_+$, the gene is on. The random variable θ_t takes values in M and signifies the particular branch in which the process stays at time t. The random variable ξ_t describes the deterministic dynamic of the process in the particular branch, i.e. the temporal evolution of the concentration of the product. X_t is completely determined by the following objects: two velocity functions $v^{(i)}$ and a transition rate function λ. The velocity functions

$$v^{(i)} :\ \mathbb{R} \to \mathbb{R},\ i \in M$$

determine the deterministic movement of the process on a particular branch. Integration of $v^{(i)}$ leads to the corresponding (phase) flows $\phi_i,\ i \in M$. The time how long the process stays in one of the two branches is governed by the measurable rate function

$$\lambda :\ S \to \mathbb{R}_+. \tag{2.19}$$

With these ingredients the process X_t can be constructed in the following way. Define a survival function $R :\ \mathbb{R}_+ \to \mathbb{R}_+$ by

$$R(t) = \exp\left(-\int_0^t \lambda\big(i, \phi_i(u, z_0)\big)\mathrm{du} \right).$$

The distribution of the holding time of the process in the initial state $x_0 = (i_0, z_0)$ is given by $F(t) = 1 - R(t)$, i.e. the first jump time τ_1 is distributed according to

$$\mathbb{P}(\tau_1 \leq t) = F(t).$$

At time τ_1 the process jumps to the branch $\{j\} \times \mathbb{R}_+$ with $j = i + 1 \mod 1$. Then, for given initial values $\theta_0 = i_0,\ \xi_0 = z_0$ the process $(X_t)_{t\geq 0}$ is defined up to the first jump time,

$$X_t = (\theta_t, \xi_t) = \begin{cases} (i_0, \phi_{i_0}(t, z_0)), & t < \tau_1, \\ (j, \phi_i(\tau_1, z_0)), & t = \tau_1. \end{cases}$$

Let $z_1 = \phi_i(\tau_1, z_0)$. Then, the process starts afresh again at (j, z_1).
Using these ingredients simulation of the PDMP is straightforward. At time $t = 0$ the process starts in an initial value z_0 in one of the two branches $\{i_0\} \times \mathbb{R}$, $i_0 \in \{0, 1\}$. It moves deterministically by following the flow $\phi_{i_0}(t, z_0)$ up to the first jump time τ_1 which is selected according to the distribution function F(t). Then at time τ_1 it jumps to the other branch, select the second holding time τ_2, and moves deterministically until it reaches the jumping time $\tau_1 + \tau_2$. After that it starts afresh again until the time has reached the simulation length. For more details see Section 2.1.

PDMP for an unregulated promoter

Suppose that a gene g is turned on and off with constant rates κ_1 and κ_{-1}, respectively. Such a system can be described by the following four elementary reaction channels:

$$\begin{array}{rcl} g_0 & \xrightarrow{\kappa_1} & g_1\,, \\ g_1 & \xrightarrow{\kappa_{-1}} & g_0\,, \\ g_1 & \xrightarrow{\alpha} & g_1 + p\,, \\ p & \xrightarrow{\gamma} & \emptyset\,. \end{array} \tag{2.20}$$

States of activation and deactivation of g are denoted by g_1 and g_0, respectively. As long as the gene stays in the active state the gene product p is synthesized at constant rate α. The product is degraded at rate constant γ where the decay products are indicated by the symbol $\emptyset$. In the following we will denote with $i \in M$ both the state of the gene and the branch in the state space. Thus, if the gene g is deactivated the process is located in the off-branch, and vice versa.
Let z denote the concentration of p and let i indicate the branch of the process. Since transition between the two promoter states happens independently the transition rate function (2.19) is constant for each branch. Thus, the transition function is given by

$$\lambda(0, z) = \kappa_1 \ \text{ and } \ \lambda(1, z) = \kappa_{-1}.$$

Hence, the holding times on both arms are exponentially distributed,

$$F(t) = \begin{cases} \mathrm{e}^{-\kappa_1 t}, & \text{if} \quad X_t \in \{0\} \times \mathbb{R}, \\ \mathrm{e}^{-\kappa_{-1} t}, & \text{if} \quad X_t \in \{1\} \times \mathbb{R}. \end{cases}$$

Between two exponentially distributed jump times $\tau_i, \tau_{i+1},\ i \geq 0$, the process moves deterministically determined by

$$\dot{z}(t) = -\gamma z, \ \text{ if } \theta_t = 0$$

and

$$\dot{z}(t) = \alpha - \gamma z, \ \text{ if } \theta_t = 1.$$

The temporal evolution of the protein concentration between two jump times is given by

$$z(t) = z_i \mathrm{e}^{-\gamma(t-\tau_i)}, \quad t \in [\tau_i, \tau_{i+1}), \tag{2.21}$$

if $\theta_t = 0$. If $\theta_t = 1$ it evolves according to

$$z(t) = \frac{\alpha}{\gamma} + \left(z_i - \frac{\alpha}{\gamma} \right) \mathrm{e}^{-\gamma(t-\tau_i)}, \quad t \in [\tau_i, \tau_{i+1}) \tag{2.22}$$

where $z_i = \xi_{\tau_i}$.

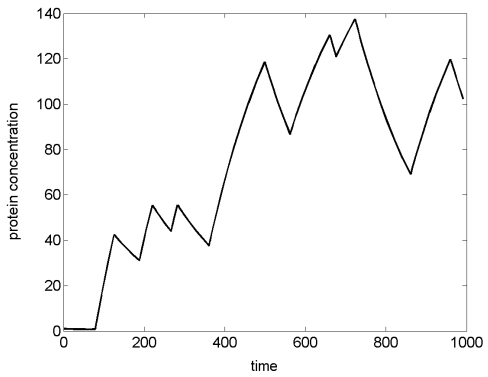


Figure 2.21: Time evolution of the protein concentration for the unregulated promoter for a time length of 1000 time units with initial values $\theta_0 = 0$, and $z_0 = 1$. The parameters are $\kappa_1 = 0.01, \kappa_{-1} = 0.01,\ \alpha = 1,\ \gamma = 0.005$.

Thus, if the process starts in a fixed but arbitrary point, and if t is large enough, the protein concentration will evolve between 0 and α/γ, see Figure 2.21 which shows a typical expression curve of an unregulated promoter.

PDMP for a negative feedback loop

In contrast to the unregulated network we suppose now that deactivation of a gene g depends on the concentration of its gene product p. In such a case the gene product is termed a transcription factor. Such an autoregulatory module is obtained by adding to reaction scheme (2.20) a reaction channel describing the binding of a transcription factor p to its own promoter, and thereby suppressing further synthesis. The resulting reaction scheme reads

$$\begin{array}{rcl} g_0 & \xrightarrow{\kappa_1} & g_1\,, \\ g_1 & \xrightarrow{\kappa_{-1}} & g_0\,, \\ g_1 + p & \xrightarrow{\kappa_0} & g_0\,, \\ g_1 & \xrightarrow{\alpha} & g_1 + p\,, \\ p & \xrightarrow{\gamma} & \emptyset\,. \end{array} \tag{2.23}$$

Again, the gene product is synthesized at rate α and degraded at rate constant γ. In contrast to the previous system, switching off of the promoter can take place with constant rates κ_{-1}, but depends also on the concentration of the protein p. However, activation of the promoter still takes place with constant rate κ_1. The transition function is given by

$$\lambda(0,z) = \kappa_1 \;\text{ and }\; \lambda(1,z) = \kappa_{-1} + \kappa_0 z.$$

This implies that the distributions of the holding times in the active state are no longer exponentially distributed. To determine the holding times we also have to take into account the flow in the branch $\{0\} \times \mathbb{R}$. The flows are the same as for the unregulated system given by equations (2.21) and (2.22).

As in the case of the unregulated system the holding time in the inactive state is exponentially distributed. However, the survival function for the active state reads

$$\begin{aligned} R(t) &= \exp\left(-\int_0^t (\kappa_0 + \kappa_{-1} z(u))\mathrm{d}u\right) \\ &= \exp\left(-\kappa_{-1} t - \frac{\kappa_0}{\gamma}\Big(\alpha t - \Big(\frac{\alpha}{\gamma} - z_0\Big)\left(1 - \mathrm{e}^{-\gamma t}\right)\Big)\right). \end{aligned}$$

Thus, the distribution function in a regulated system can differ strongly from the one of an unregulated system. This is reflected in the expression curve for a regulated system, see Figure 2.22. Although the velocity and hence the flows in the particular arms are identically the expression curves in the two systems differ considerably.

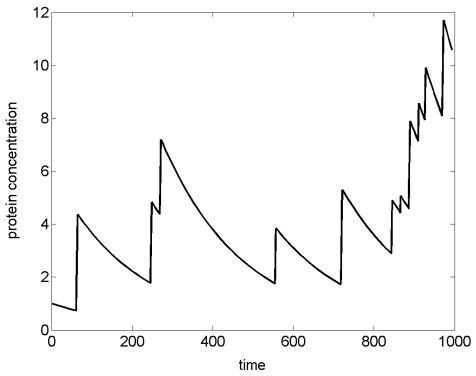


Figure 2.22: Time evolution of the protein concentration for the autoregulated module for a time length of 1000 time units with initial values $\theta_0 = 0$, and $z_0 = 1$. The parameters are $\kappa_1 = 0.01,\ \kappa_{-1} = 0.01,\ \kappa_0 = 0.05,\ \alpha = 1,\ \gamma = 0.005$.

2.2.3 Stationary distributions

In the following we will determine the stationary distributions of the autoregulated and regulated system. Recall the notation ${}_1F_1$, denoting the Confluent Hypergeometric function which is also called Kummer's function, [106]. For the stationary distribution of the autoregulated system we obtain the following result.

Proposition 2.2.1. *Let $X_t = (\theta_t, \xi_t)$ be the PDMP of the regulated network (2.23). The stationary distribution of the gene product ξ_t is given by*

$$\rho(z) = Kz^{p-1}(\alpha - \gamma z)^{r+q-1}\mathrm{e}^{\frac{\gamma}{\alpha}rz}$$

with

$$K = \frac{\gamma^p}{\alpha^{p+r+q-1}}\frac{\Gamma(p+r+q)}{\Gamma(p)\Gamma(r+q)}\frac{1}{{}_1F_1(p, p+r+q, r)}$$

where $p = \kappa_1/\gamma, q = \kappa_{-1}/\gamma,\ r = \alpha\kappa_0/\gamma^2$. The expectation $\mathbb{E}(\xi_t)$ and the variance $\mathbb{V}(\xi_t)$ of the stationary distribution read

$$\mathbb{E}(\xi_t) = \frac{\alpha}{\gamma}\frac{p}{p+r+q}\frac{{}_1F_1(p+1, p+r+q+1, r)}{{}_1F_1(p, p+r+q, r)}$$

and

$$\begin{aligned}\mathbb{V}(\xi_t) \;=\; & \frac{\alpha^2}{\gamma^2}\frac{p}{p+r+q}\left(\frac{p+1}{p+r+q+1}\frac{{}_1F_1(p+2, p+r+q+2, r)}{{}_1F_1(p, p+r+q, r)}\right.\\ & \left.-\frac{p}{p+r+q}\frac{{}_1F_1{}^2(p+1, p+r+q+1, r)}{{}_1F_1{}^2(p, p+r+q, r)}\right).\end{aligned}$$

Setting $\kappa_0 = 0$ we obtain easily the first two moments of the stationary distribution of an unregulated promoter:

Corollary 2.2.2. *Let X_t be the PDMP of the unregulated genetic network (2.20). Then, the stationary distribution of the gene product ξ_t is equal to*

$$\rho(z) = Kz^{p-1}(\alpha - \gamma z)^{q-1}$$

with

$$K = \frac{\gamma^p}{\alpha^{p+q-1}} \frac{\Gamma(p+q)}{\Gamma(p)\Gamma(q)}$$

where $p = \kappa_1/\gamma$, and $q = \kappa_{-1}/\gamma$. Furthermore, the expectation $\mathbb{E}(\xi_t)$ and the variance $\mathbb{V}(\xi_t)$ of the stationary distribution are given by

$$\mathbb{E}(\xi_t) = \frac{\alpha}{\gamma} \frac{p}{p+q},$$

and

$$\mathbb{V}(\xi_t) \quad = \quad \frac{\alpha^2}{\gamma^2} \frac{pq}{(p+q)^2(p+q+1)}.$$

Note that the same result is obtained by modeling the unregulated network using two ordinary differential equations coupled by a random telegraph signal, see [114] and the supporting material to [88].
For an unregulated system, it is also possible to determine the first two central moments of the stationary distribution for the discrete model, [85], [61]. There it was shown that the mean and the variance are given by

$$\mathbb{E}(N_t) = \frac{\alpha}{\gamma} \frac{p}{p+q},$$

and

$$\mathbb{V}(N_t) = \frac{\alpha}{\gamma} \frac{p}{p+q} + \frac{\alpha^2}{\gamma^2} \frac{pq}{(p+q)^2(p+q+1)}$$

where $(N_t)_{t\geq 0}$ denotes the discrete Markov process. Hence, with respect to the mean there is no loss of information when using a hybrid model instead of a discrete model. On the other hand, modeling the production and degradation of the gene product in a deterministic and continuous way instead of a random and discrete way leads to a discrepancy in the variance. The variance of the gene product in the hybrid approach is smaller than the variance in the discrete model, by a value equal to its expectation.
As far as we know there exists no closed analytical formula for the expectation and variance of the stationary distribution for a negatively autoregulated system

modeled by a discrete process. Hence, we cannot compare the two expressions in the same way as for the unregulated system. However, since the two expressions differ for the unregulated system we expect that they will differ for more complex systems too.

Proof (of above Proposition). Let f be a continuous function vanishing at infinity. Then, the (strong) generator is given by

$$\begin{aligned} Gf\,(0,z) &= -\gamma z f_z(0,z) + \kappa_1\big(f(1,z) - f(0,z)\big), \\ Gf\,(1,z) &= (\alpha - \gamma z) f_z(1,z) + (\kappa_{-1} + \kappa_0 z)\big(f(0,z) - f(1,z)\big). \end{aligned}$$

See [23] for the general formula of the generator. In the following let the function ρ be given as $\rho(z) = \rho(0,z) + \rho(1,z)$. A stationary solution is characterized by the condition

$$G^*\rho(i,z) = 0, \quad i \in \{0,1\} \tag{2.24}$$

where G^* denotes the dual operator of G. From

$$\begin{aligned} < Gf, \rho > &= \int_0^\infty (-\gamma z) f_z(0,z)\rho(0,z)\mathrm{d}z \\ &\quad + \int_0^\infty \kappa_1\big(f(1,z) - f(0,z)\big)\rho(0,z)\mathrm{d}z \\ &\quad + \int_0^\infty (\alpha - \gamma z) f_z(1,z)\rho(1,z)\mathrm{d}z \\ &\quad + \int_0^\infty (\kappa_{-1} + \kappa_0 z)(f(0,z) - f(1,z))\rho(1,z))\mathrm{d}z \end{aligned}$$

we reason that $\rho(0,z)$ and $\rho(1,z)$ have to be weakly differentiable. Furthermore, $\rho(1,z)$ has to vanish at $z = 0$. Partial integration together with the stationarity condition (2.24) yield

$$\begin{aligned} \partial_z\big(-\gamma z\rho(0,z)\big) &= -\kappa_1\rho(0,z) + (\kappa_{-1} + \kappa_0 z)\rho(1,z), \\ \partial_z\big((\alpha - \gamma z)\rho(1,z)\big) &= \kappa_1\rho(0,z) - (\kappa_{-1} + \kappa_0 z)\rho(1,z). \end{aligned} \tag{2.25}$$

By adding the first and the second equation, and integration afterwards we find

$$(\alpha - \gamma z)\rho(1,z) - \gamma z\rho(0,z) = C$$

for a constant C. Supposing that $\rho(z)$ has at the borders only singularities of orders less or equal than 1 we receive from $\rho(1,0) = 0$ that $C = 0$. (For a slightly more general discussion, see [81].) Thus

$$\rho(0,z) = \frac{\alpha - \gamma z}{\gamma z}\rho(1,z) \tag{2.26}$$

which is valid for all $z \neq 0$. Since $\rho(0,z), \rho(1,z) \geq 0$, we conclude $z \leq \frac{\alpha}{\gamma}$. Inserting (2.26) in the bottom equation of system (2.25) we receive

$$\rho_z(1,z) = \left(\frac{\gamma - \kappa_{-1} - \kappa_0 z}{\alpha - \gamma z} + \frac{\kappa_1}{\gamma z}\right)\rho(1,z)$$

which is valid for $0 < z < \frac{\alpha}{\gamma}$. Variation of constants yields

$$\rho(1,z) = Kz^{\frac{\kappa_1}{\gamma}}(\alpha - \gamma z)^{\frac{\alpha\kappa_0}{\gamma^2} + \frac{\kappa_{-1}}{\gamma} - 1}\mathrm{e}^{\frac{\kappa_0}{\gamma}z} \tag{2.27}$$

for some $z_0 \in (0, \frac{\alpha}{\gamma})$, and a constant $K > 0$. Inserting into equation (2.26) we obtain

$$\rho(0,z) = K(\gamma z)^{\frac{\kappa_1}{\gamma} - 1}(\alpha - \gamma z)^{\frac{\alpha\kappa_0}{\gamma^2} + \frac{\kappa_{-1}}{\gamma}}\mathrm{e}^{\frac{\kappa_0}{\gamma}(z - z_0)}. \tag{2.28}$$

Summing up equations (2.27) and (2.28) and using the definition of $p,\ q$, and r we obtain for the total density

$$\rho(z) = Kz^{p-1}(\alpha - \gamma z)^{r+q-1}\mathrm{e}^{\frac{\gamma}{\alpha}rz}. \tag{2.29}$$

To ensure that $\rho(z)$ is a density the scaling constant has to be equal to

$$K = \frac{\gamma^p}{\alpha^{p+r+q-1}}\frac{\Gamma(p+r+q)}{\Gamma(p)\Gamma(r+q)}\frac{1}{{}_1F_1(p, p+r+q, r)}. \tag{2.30}$$

From equations (2.29) and (2.30) we obtain for the expectation of ξ

$$\begin{aligned}
\mathbb{E}(\xi) &= \int_0^{\alpha/\gamma} Kz^p(\alpha - \gamma z)^{r+q-1}\mathrm{e}^{\frac{\gamma}{\alpha}rz}\mathrm{d}z \\
&= K\frac{\alpha^{p+r+q}}{\gamma^{p+1}}\frac{\Gamma(p+1)\Gamma(r+q)}{\Gamma(p+r+q+1)}{}_1F_1(p+1, p+r+q+1, r) \\
&= \frac{\alpha}{\gamma}\frac{p}{p+r+q}\frac{{}_1F_1(p+1, p+r+q+1, r)}{{}_1F_1(p, p+r+q, r)}.
\end{aligned}$$

To calculate the variance we need the second moment of ξ which is given by

$$\begin{aligned}\mathbb{E}(\xi^2) &= \int_0^{\alpha/\gamma} K z^{p+1}(\alpha-\gamma z)^{r+q-1}\mathrm{e}^{\frac{\gamma}{\alpha}rz}\mathrm{d}z \\ &= K\frac{\alpha^{p+r+q+1}}{\gamma^{p+2}}\frac{\Gamma(p+2)\Gamma(r+q)}{\Gamma(p+r+q+2)}{}_1F_1(p+2,p+r+q+2,r) \\ &= \frac{\alpha^2}{\gamma^2}\frac{p(p+1)}{(p+r+q)(p+r+q+1)}\frac{{}_1F_1(p+2,p+r+q+2,r)}{{}_1F_1(p,p+r+q,r)}.\end{aligned}$$

□

Equation system (2.25) is often called the system of the one dimensional correlated random walk. Variations of this system were studied by many authors, see [36], [60], [45].

2.2.4 Stability Analysis

In [9] a synthetic autoregulative circuit was constructed composed of a *tet*-repressible promoter and a *tet*R-EGFP fusion protein. The unregulated counterpart was obtained by mutation of *tet*R, thereby inhibiting binding to the promoter. Expression of the autoregulative network was compared with the expression of the unregulated counterpart. Due to the fact that the means in the unregulated and the regulated network can differ considerably the coefficient of variation c_v, defined as the ratio of the standard deviation to the mean, was used as a measure of variability. It was found that the value of c_v of the autoregulative network is smaller compared to the one of the unregulated module, which was reflected in the gene expression profiles. The one of the regulated system exhibits a much narrower distribution than the one of the unregulated gene construct. This could be confirmed by modification of a mathematical model proposed in [121]. Describing gene expression by an ordinary differential equation they add random variables of the same relative range to the steady state value for both the autoregulated and the unregulated system. Their findings are in good agreement with the classical result of Savageau, [100] that negatively autoregulated circuits are superior to unregulated systems in respect of noise attenuation. However, for both the experimental and the theoretical system the kind of noise is difficult to determine. Hence, one cannot specify if the variations in the expression levels are caused by extrinsic or intrinsic effects. Therefore, one cannot decide if the negative feedback loop reduces noise originating from intrinsic or extrinsic impacts, or from both.
Using the hybrid model presented in the previous section it is easy to analyze noise originating from random transitions of the promoter. Due to the design of our models the only randomness occurs by random transitions of the promoter.

Therefore, in the following we will term such fluctuations as *promoter noise*. Following the work of Becskei and Serrano we will use the coefficient of variation as a measure of noise, too. For a PDMP of an unregulated and regulated system described in the previous section the coefficient of variation can be given in a closed analytical form. For the unregulated system it is given by the following simple formula

$$c_v^{unreg} = \sqrt{\frac{\gamma\kappa_{-1}}{\kappa_1(\kappa_1+\kappa_{-1}+\gamma)}}. \tag{2.31}$$

In particular, the coefficient of variation of the unregulated system for the hybrid model is independent of the synthesis rate α. Furthermore, compared to the discrete model, the square of c_v^{unreg} is reduced by the summand $\gamma(\kappa_1+\kappa_{-1})/\alpha\kappa_1$. For a more detailed numerical analysis of the stationary distributions of an unregulated system modeled by a discrete and a hybrid process see Section 2.1.
A more complex formula is obtained for the coefficient of variation of the autoregulated system. It reads

$$c_v^{reg} = \sqrt{\left(\frac{\alpha\gamma\kappa_0+\gamma^2\kappa_{-1}}{\kappa_1(\kappa_1\gamma+\alpha\kappa_0+\gamma\kappa_{-1}+\gamma^2)}+1\right)HG-1}$$

where

$$HG = \frac{{}_1F_1(\frac{\kappa_1}{\gamma}, \frac{\gamma(\kappa_1+\kappa_{-1})+\alpha\kappa_0}{\gamma^2}, \frac{\alpha\kappa_0}{\gamma^2}){}_1F_1(\frac{\kappa_1}{\gamma}+2, \frac{\gamma(\kappa_1+\kappa_{-1})+\alpha\kappa_0}{\gamma^2}+2, \frac{\alpha\kappa_0}{\gamma^2})}{{}_1F_1{}^2(\frac{\kappa_1}{\gamma}+1, \frac{\gamma(\kappa_1+\kappa_{-1})+\alpha\kappa_0}{\gamma^2}+1, \frac{\alpha\kappa_0}{\gamma^2})}.$$

Since the formula of c_v^{reg} is complex and depends on five parameters, a complete analytical investigation of its dependency on the parameters is not practicable. Hence we perform the analysis individually for each single parameter.
At first we investigate the relationship between the turning on and off rates, and the degradation rate. Degradation can be slower or faster than promoter transitions, or can lie in between the turning on and off rates. For a constant negative feedback strength, i.e. for fixed κ_0, and for a fixed synthesis rate α we get eight possible configurations, see Table 2.6. In the literature, the following orders of magnitude for the different rates are stated. Values for the turning on and off rates are reported in the order of 10^{-3}min^{-1}, and 10^{-3} to 10^{-1}min^{-1}, respectively, [70], [101]. A realistic value for the production rate lies in the order of 1 to 10nMmin^{-1}, [108]. Decay rates for proteins were determined to be in the range of 10^{-4} to 10^{-1}min^{-1}, [10]. The chosen parameter values and the resulting values for the coefficients of variation are listed in Table 2.6. Surprisingly, only for the parameter configuration (vi) the coefficient of variation of the regulated system is smaller than the one of the unregulated system. In all other cases c_v^{reg} is greater than c_v^{unreg}.

Parameter set	κ_1 [min^{-1}]	κ_{-1} [min^{-1}]	κ_0 [(nM min)$^{-1}$]	α [nM min^{-1}]	γ [min^{-1}]	c_v^{reg}	c_v^{unreg}
(i)	0.01	0.01	0.05	1	0.005	0.52	0.44
(ii)	0.01	0.01	0.05	1	0.05	1.65	0.85
(iii)	0.03	0.01	0.05	1	0.005	0.29	0.19
(iv)	0.03	0.01	0.05	1	0.02	0.59	0.33
(v)	0.03	0.01	0.05	1	0.05	0.92	0.43
(vi)	0.01	0.03	0.05	1	0.005	0.53	0.58
(vii)	0.01	0.03	0.05	1	0.02	1.08	1
(viii)	0.01	0.03	0.05	1	0.05	1.68	1.29

Table 2.6: Parameter configurations and corresponding values of the coefficients of variation.

In the following we analyze the dependency of the coefficient of variation on the individual parameters in more detail. The dependency of c_v^{reg} and c_v^{unreg} on κ_0 for the parameter configurations (ii), (v), (vi), and (vii) can be seen in the graphs displayed in Figure 2.23. There, c_v^{reg} and c_v^{unreg} are plotted as functions of κ_0. The graph of c_v^{unreg} is a constant dotted line whereas the graph of c_v^{reg} is plotted as a solid line. Except for parameter set (vi) c_v^{reg} increases and converges rapidly towards its asymptotic value for increasing κ_0. For parameter set (vi) c_v^{reg} decreases but converges rapidly for increasing κ_0, too.

The dependency of c_v^{reg} and c_v^{unreg} on the remaining parameters is displayed in Figure 2.24. The graphs are obtained by setting $\kappa_0 = 0.05$ and varying in each case one parameter while the others are chosen to be equal to $(\kappa_1, \kappa_{-1}, \alpha, \gamma) = (0.01, 0.01, 1, 0.005)$.

For κ_1 being the independent variable the graphs of c_v^{reg} and c_v^{unreg} have a hyperbolic shape, see Figure 2.24 (a). Thus, if the turning on rate is low both systems show high variability in their expression levels and exhibit very low variability if the turning on rate is high. For the given parameter set c_v^{reg} is always higher than c_v^{unreg}.

A totally different behavior is obtained for the turning off rate κ_{-1} being the independent variable. The graph of c_v^{reg} is more or less a straight line with a small positive slope. On the other hand, the graph of c_v^{unreg} has a shape of a root, see Figure 2.24 (b). For small values of κ_{-1} the coefficient of variation of the unregulated system stays below the one of the unregulated system. For high values of κ_{-1}, higher than ten fold of the value of κ_1, the coefficient of variation of the unregulated system is greater than the one of the regulated system. This means that only if the unregulated system stays for long times in its activated state noise stabilization in the regulated system is superior to the one of the unregulated sys-

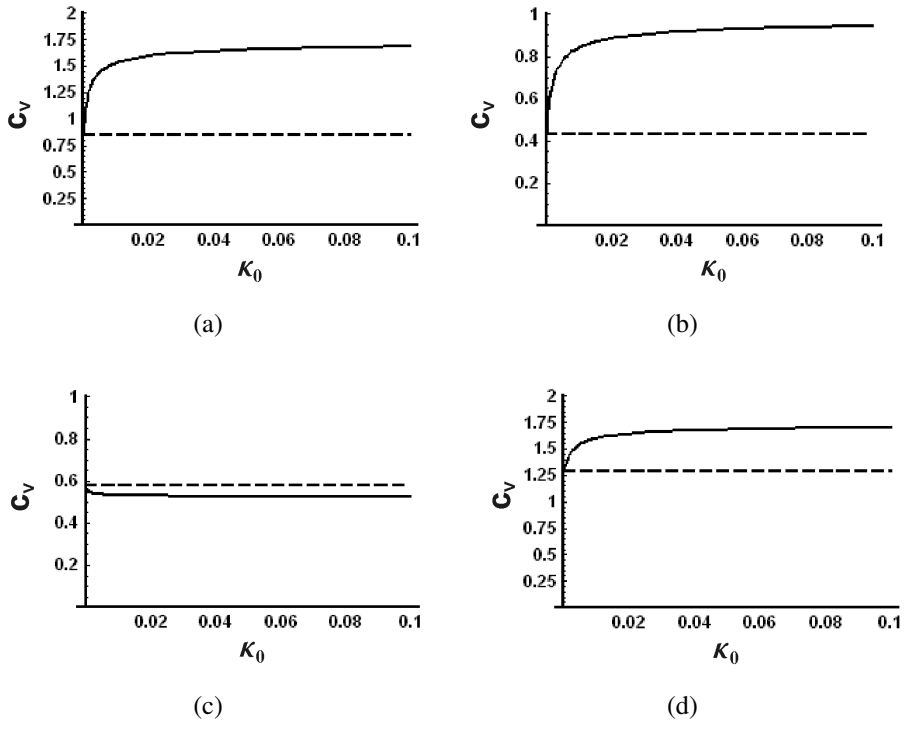


Figure 2.23: Dependency of c_v on the parameter κ_0 for the regulated system (solid) compared with the one of the unregulated system (dashed) for the parameter configurations (ii), (v), (vi), and (viii) from Table 2.6. (a) parameter set (ii), (b) parameter set (v),(c) parameter set (vi), and (d) parameter set (viii).

tem.

Since the coefficient of variation of the unregulated system does not depend on the synthesis rate constant α, see equation (2.31), c_v^{unreg} is constant. For the regulated system c_v^{reg} increases and converges rapidly towards its asymptotic value for increasing α. As for κ_1, c_v^{reg} is always greater than c_v^{unreg}, Figure 2.24 (c).

For increasing γ the coefficient of variation of the unregulated system increases and converges rapidly towards its asymptotic value. In the regulated system, c_v^{reg} increases for increasing γ to a value three fold higher than the one of c_v^{unreg}. A further increase of γ leads to a decrease of c_v^{unreg}, see Figure 2.24 (d). In the range between zero and two, c_v^{reg} is always at least two fold higher than c_v^{unreg}. Only for small values of γ the coefficients of both systems are approximately equal.

The simulated distributions of the unregulated and autoregulated system for the four parameter sets (ii), (v), (vi), and (viii) are shown in Figure 2.25. The histograms in the left column are obtained by simulations of the regulated system. The histograms for the unregulated system are displayed in the right column. The

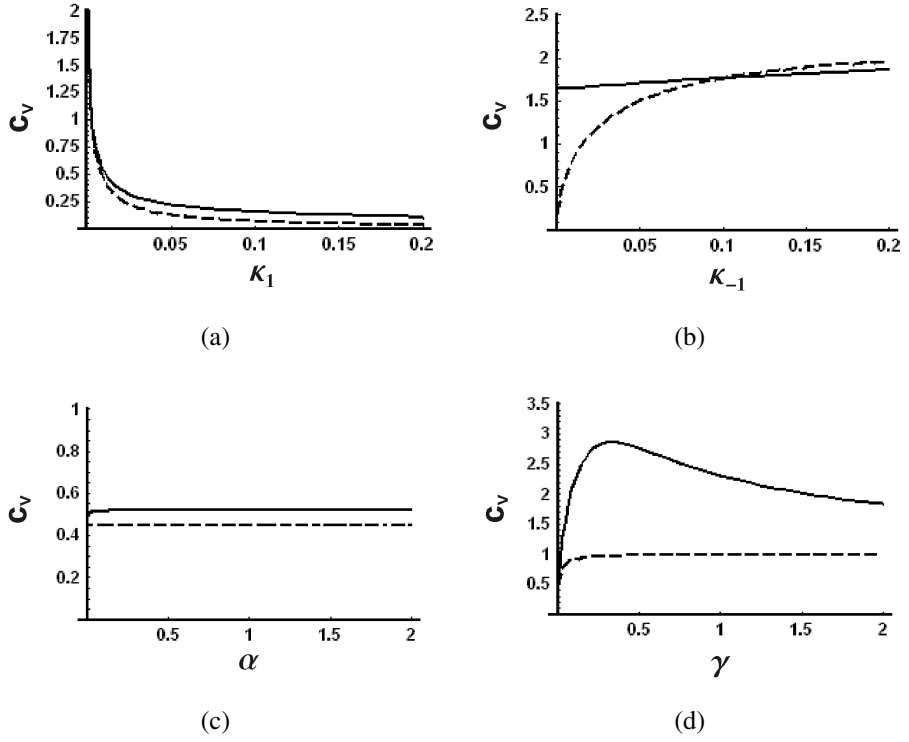


Figure 2.24: Coefficients of variation as functions of the individual parameters in the unregulated (dashed) and autoregulated (solid) systems.

distributions are listed from top to down for increasing number of the corresponding parameter sets.

For the parameter set (ii) the regulated and the unregulated exhibit different expression distributions, see Figure 2.25 (a) and (b). While in the regulated system most cells exhibit no or very low expression, the distribution of the unregulated system is bimodal with peaks at the lowest and highest expression levels. As can be seen from the distributions, the higher coefficient of variation of the regulated system results from a wider distribution range. In the regulated system it is more than four fold wider than in the unregulated system. However, for the given parameter set the coefficient of variation should not be used without hesitation, since for bimodal distributions the coefficient of variation is rather unsuitable as a measure of dispersion. A more adapted measure would be the interquartile range measuring the difference between the third and first quartiles. The interquartile range of the standardized distribution of the unregulated system, IQR^{unreg} is equal to 1.9. For the regulated system we find $IQR^{reg} = 1.26$. Thus, based on the interquartile range the negatively regulated system is superior to the unregulated

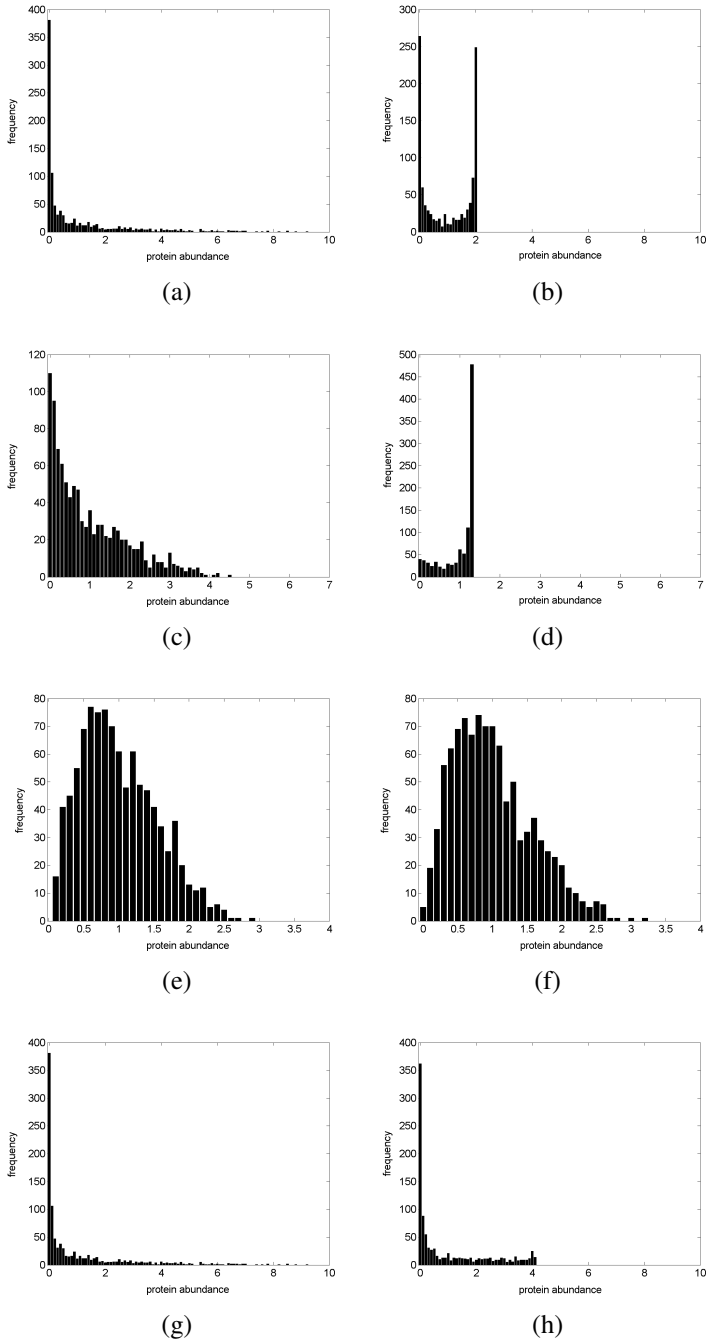


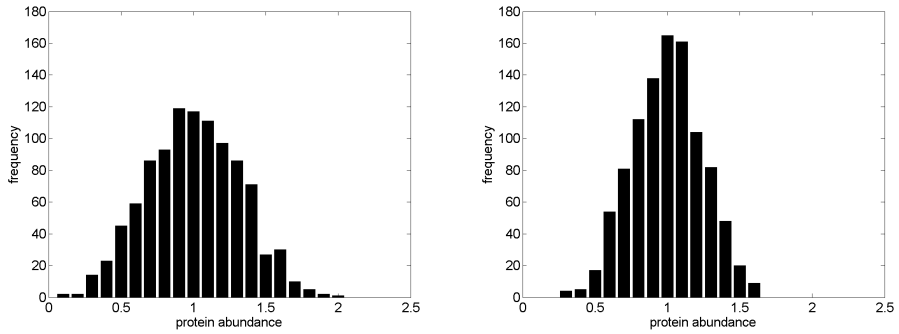
Figure 2.25: Simulated distributions of protein concentrations for the parameter sets (ii), (v), (vi), and (viii) of the regulated (first column) and unregulated network (second column).

system in respect of noise reduction.
The distributions of the two systems for the parameter set (v) show also a different profile. In both systems the distributions are unimodal. However, in the regulated system the peak is centered at low expression levels whereas in the unregulated system most cells are centered at the highest expression level, Figure 2.25 (c) and (d). As for parameter set (ii) the range of distribution of the regulated system is wider than the one of the unregulated system resulting in a higher coefficient of variation. Here, the range of the regulated system is more than two fold wider than in the unregulated system. For parameter set (vi) both systems show a very similar distribution. It is unimodal and skewed to the left, see Figure 2.25 (e) and (f). The peak of the distribution of the regulated system is narrower than the one of the unregulated system. Also, the range of the distribution is a little smaller than the one of the unregulated system resulting in a lower coefficient of variation of the regulated system.
As for parameter set (vi) the distributions for parameter set (viii) are very similar for both systems. Now, there is a sharp peak at the left distribution boundary, see Figure 2.25 (g) and (h). Since the distribution range of the regulated system is nearly twice as wide as the one of the unregulated system the coefficient of variation of the regulated system is higher than the one of the unregulated system.
We have also calculated the coefficients of variations of the empirical distributions listed in Table 2.7. Since the values of the empirical distributions are in very good agreement with the theoretical ones we can suppose that for the given time period the process has already reached its stationary distribution.

Parameter set	(ii)	(v)	(vi)	(viii)
c_v^{reg} (emp.)	1.64	0.95	0.54	1.63
c_v^{unreg} (emp.)	0.85	0.42	0.57	1.3

Table 2.7: Empirical values of the coefficient of variation for the unregulated and the regulated system. The parameter sets are the same as in Table 2.6.

So far we have seen that the classical result of Savageau, [100] does not hold in general for promoter noise modeled by PDMP. To compare our results with the ones of Becskei and Serrano, [9] we choose similar values for the degradation and production rate. In their simulations the degradation rate γ is equal to $6 \times 10^{-4}\text{min}^{-1}$, and the production rate α is in the range of 100nMmin^{-1}. Choosing $\kappa_1 = \kappa_{-1} = 10^{-2}$ min^{-1} and $\kappa_0 = 5 \times 10^{-2}$ nM^{-1} min^{-1} we find qualitatively similar results. The empirical distributions of the unregulated and regulated system are displayed in Figure 2.26. Both distribution are symmetric and unimodal.



(a) (b)

Figure 2.26: Scaled empirical distributions of the (a) unregulated and (b) regulated system using a parameter set similar to the one of [9].

Compared to the distribution of the unregulated system, the distribution of the regulated system is narrower yielding a smaller value for the coefficient of variation. For $\gamma = 10^{-4}$ we find the empirical values $c_v^{unreg} = 0.32$ and $c_v^{reg} = 0.24$. A tenfold increase of the degradation rate leads to $c_v^{unreg} = 0.34$ and $c_v^{reg} = 0.26$. Hence, for a decay rate smaller than 10^{-3} min^{-1} the regulated system is superior to the unregulated system with respect to noise attenuation. However, the situation changes if the decay rate is increased further. As we have seen above, for $\gamma = 5 \times 10^{-3}$ min^{-1} we have found $c_v^{unreg} < c_v^{reg}$, see parameter set (i) in Table 2.6. Thus with respect to promoter noise, we find the same results as Becskei and Serrano for relatively high half lives of the gene product only.

2.2.5 Conclusions

We analyzed promoter noise, defined as fluctuations in gene expression caused by random transitions of the promoter between its active and inactive states. As a model we proposed a hybrid model called piecewise deterministic Markov process (PDMP). The state of such a system is described by a discrete and a continuous variable. Transitions between discrete states, i.e. changes of the value of the discrete variable, take place in a random manner. The temporal evolution of the continuous variable is determined by deterministic rate equations. Hence, the only source of randomness are transitions between discrete states. Since genes are typically present in one or two copies only, we model the individual promoter states as discrete states whereas the remaining reactions are modeled as deterministic processes. Doing so the proposed model is suitable to analyze noise originating from the switching behavior of a promoter of a gene.
We compare an unregulated system with an autoregulated system composed of a

negative feedback loop, i.e. a regulatory network in which the gene product represses its own synthesis. In the unregulated system transitions of the promoter take place in a Poisson like fashion whereas in the autoregulated system the turning off rate consists of a component independent of the gene product and a component dependent on the concentration of the gene product. By varying the dependent rate constant we can vary the strength of autoregulation. Setting the rate equal to zero we obtain the unregulated system. For both system we determine the distribution of the steady state as well as the expectation and the variance in a closed analytical form.
The coefficient of variance is used as a measure of noise which is also determined in a closed formula. For the unregulated system it is given by a very simple formula and independent of the synthesis rate. For the regulated system the formula is more complex. It obtains a fraction consisting of Confluent Hypergeometric functions. Hence, a global analytical analysis of the dependency of c_v on the parameters is difficult. For this reason the analysis is done for the different parameters individually. We compare all possible relations of the degradation rate to the turning on and turning off rates resulting in eight different parameter configurations. For four parameter sets we analyze the dependency of the coefficient of variations on the strength of the negative feedback. Furthermore, we study the dependency on the remaining parameters, i.e. on the synthesis and degradation rate, and on the two transition rates which induce transitions independently of the product concentrations.
In contrast to the results stated in the literature, [100], [9] for the eight chosen parameter configurations we have found only one parameter set for which the regulated system is superior to the unregulated system with respect to noise reduction. For this parameter set, the noise in the regulated system is always lower than the noise in the unregulated system in dependency of the strength of autoregulation. For the other parameter sets, the noise in the regulated network is always higher than in the unregulated system. As the strength of the negative feedback increases, noise increases too, and converges rapidly to an asymptotic value.
When analyzing the dependency of noise on the remaining parameters, the strongest dependency is found for the turning on rate in both systems. A relative strong dependency of the coefficient of variation is found for the turning off rate in the unregulated system whereas a very weak dependency is found in the regulated system. Furthermore, the coefficient of variation of the unregulated system is independent on the synthesis rate. For the regulated system it shows only weak dependency. A similar behavior is found for the dependency of the coefficient of variation on the degradation rate in the unregulated system. It increases for increasing decay rate and converges rapidly towards its asymptotic value. On the other hand, for the regulated system the coefficient of variation increases towards a three fold higher value as in the unregulated system. If the degradation rate is

increased further, the coefficient of variation decreases towards a value two fold higher than the one of the unregulated system.
Moreover, we have simulated both systems and calculated the empirical distributions. The empirical and the theoretical values for the coefficients of variation are in good accordance, indicating that the systems converge relatively fast to their stationary distributions. The normalized distributions show that the difference in the values of the coefficient of variation originates not from the different profiles of the distributions, but from the different ranges. Except for one parameter configuration, the distribution range of the regulated system is always wider than the one of the unregulated system. Furthermore, it shows that the two systems can have different distributions profiles. For instance, in one case the regulated system possesses a unimodal distribution whereas the distribution of the unregulated system is bimodal. In this case the coefficient of variation is rather unsuitable and the interquartile range should be used as a measure of dispersion. On the basis of this measure, the regulated system is superior to the unregulated system in contrast to taking the coefficient of variation as a measure of noise. Nevertheless, it seems that for promoter noise it is rather the exception than the rule that autoregulation reduces such noise by a negative feedback loop.
When using similar parameter values as in [9], we have found similar results. However, this holds only for a parameter region with quite small degradation rates. For systems including gene products with small half lives this does not hold anymore. Up to now we have not found any experimental results which may prove our disprove or findings. Since a complete analysis of the parameter space is difficult even for such small systems, a final answer for promoter noise attenuation modeled by a PDMP is still open.

2.3 Autocatalytic Genetic Networks Modeled by Piecewise Deterministic Markov Processes

The current section presents the results published in [125].
We propose an alternative approach to model autocatalytic networks, called piecewise-deterministic Markov processes. These were originally introduced by Davis in 1984. Such a model allows for random transitions between the active and inactive state of a gene, whereas subsequent transcription and translation processes are modeled in a deterministic manner.
We consider three types of autoregulated networks, each based on a positive feedback loop. It is shown that if the densities of the stationary distributions exist, they are the solutions of a system of equations for a one dimensional correlated random walk. These stationary distributions are determined analytically. Further, the distributions are analyzed for different simulation periods and different initial concentration values by numerical means. We show that, depending on the network structure, beside a binary response also a graded response is observable.

2.3.1 Introduction

Biochemical reaction networks, such as gene regulatory networks, are commonly modeled by a system of ordinary differential equations or by a discrete Markov process in continuous time. The more exact approach is the stochastic one in which the state of the system consists of the numbers of the particular reactants. However, if the numbers of the reactant molecules are large the deterministic approach is mostly sufficiently accurate. It has become the more powerful one, since analysis in the stochastic approach is hard or even impossible.
The situation changes in molecular biology, where many reactants in a cell are present only in two-digit numbers. At least one molecule, the DNA, is present in higher organisms one or two times only. Such small numbers may cause random fluctuations in gene expression levels leading to heterogeneous expression patterns in cell populations, [65], [78]. Single cell experiments revealed noisy gene expression on the transcription as well as on the translation level. Often, transcription of mRNA and translation of protein occur in burst-like events [52], [28], [16], [88]. Thus, modeling gene expression on single cell levels has to consider the intrinsic stochasticity of turning on and off gene expression.
For this purpose, we propose an alternative approach for modeling gene regulatory networks. Combining the pros of the deterministic and the stochastic approach results in a hybrid model. Whenever the population of a certain molecular species is large, a system of ordinary differential equations is chosen to model the temporal evolution of the concentrations of the particular molecular species. In the other

case, when the amount of the reactants is small, the temporal change in the numbers of reactants is modeled like a time-continuous finite-state Markov process. As a model we choose piecewise-deterministic Markov processes, PDMP, introduced by Davis in a much more general setting in 1984, [23]. The state space of a PDMP is given as the product of a finite set M and a subset of $\mathbb{R}^d,\ d \geq 1$. It can be thought of as split into different branches labeled by elements of the finite set M. The motion of a piecewise deterministic Markov process depends on a vector field v, a transition rate function λ, and a transition measure Q. Starting from an initial value, up to the first jump time the process evolves deterministically driven by the vector field v. Then a new branch is chosen according to the transition measure Q. After that the process restarts deterministically in the new branch.
Modeling genetic networks in a hybrid fashion using a mixture of discrete and continuous state variables is not entirely new. Similar approaches were used by several authors. For instance, Edwards et al. used a similar approach to model coupled ultradian oscillators, [27]. Booth et al. proposed an approach using the chemical master equation in combination with chemical rate equations to model genetic networks in prokaryotes, [18]. Griffith et al. applied a dynamical partitioning algorithm between fast and slow reaction channels to model an HIV transaction network, [79].
We consider models for gene expression of various types of positive feedback loops. Such feedback loops are often used by nature as a genetic switch in prokaryotes as well as in eukaryotes [54], [8], [40]. Positive feedbacks can be realized in different ways. In a positive autoregulatory loop [8] or by a toggle switch where two mutual repressors regulate the transcription of each other [30], [66]. Here we focus on autocatalytic networks where the gene product activates transcription of its own encoding gene.
A graded increase in the stimulus of inducer concentration can lead to a graded as well as a binary response in gene expression, even in isogenic cell populations, [14], [68], [56], [117]. However, positive feedback loops typically convert a graded stimulus into an all or none response, [104], [8], [74]. Maamar et al. studied the ComK system in *B. subtillus*, [74]. If the autoregulatory loop of ComK is inactivated, the cells show a graded response on increased inducer amounts. On the other hand, when the positive feedback loop is intact the expression profile becomes bimodal for increasing inducer concentrations. A similar expression behavior was stated by Becskei et al. for the synthetic positive feedback system of rtTA in *Saccharomyces cerevisiae*, [8]. There, a constitutive system was compared to an autocatalytic system. Whereas the constitutive system exhibits a graded response on increasing inducer concentrations, the autocatalytic system shows a binary response. In [74] and [104] also the dependency of the expression profile on the time length was investigated for the comK system and the *araBAD* promoter in *Escherichia coli*, respectively. Both systems start in a unimodal distribution at low

expression levels. As time proceeds the distribution becomes bimodal. We analyze the response of three autocatalytic systems with respect to different inducer concentrations and expression periods. The different inducer concentrations are mimicked by different initial concentrations, whereas the different expression periods are realized by different simulation lengths.

In the present section we consider a PDMP with $|M| = 2$ and $d = 1$. The two elements of M indicate whether the particular gene is turned on or off indicated by 1 and 0, respectively. The elements of $\mathbb{R}$ denote the concentration of the particular gene product. We consider four different promoter types, Model I - IV, displayed in Figure 2.27 (a)-(d). Model I is an unregulated promoter which switches between its active and inactive states with constant transition rates, see Figure 2.27(a). We do not analyze this promoter type. It will be used for the purpose of comparison. For more detailed analysis see [114], the supplemental material to [88], and Section 2.1. It is assumed that gene expression takes place only in the active state indicated by a broken arrow. The inactive state is displayed as a crossed arrow.

In the promoter of Model II the gene product activates its encoding gene by binding to the binding site of the promoter. Hence activation of the gene depends on the amount of the protein, see Figure 2.27(b). In this case expression takes place only in the presence of the particular gene product or in the presence of some external inducer. Switching back from the active to the inactive state proceeds independently of any inducer at a constant rate.

In the promoter of Model III expression takes place in both promoter states. We denote the two states by basic and excited promoter state. In the basic promoter state expression proceeds at a certain small rate, always greater than zero. If a gene product molecule is bound to the promoter, the gene is enhanced and the rate of expression is increased, see Figure 2.27(c). The excited state is pictured by a thick arrow while the basic state is indicated by a thin arrow. As in the case of the previous two promoter types, switching back from the excited to the basic promoter state occurs at a constant rate.

The promoter of Model IV consists of an activated and an inactivated state. As for the first two promoter types, expression can only take place when the promoter is in the activated state. In contrast to the second promoter type, now the promoter can switch from the inactive to the active state with positive probability, even when there is no gene product present. If proteins are present, the rate of transition from the inactive to the active state is increased proportionally to the amount of the gene product, Figure 2.27(d). Thus in contrast to the third promoter type, the chance of expression but not the expression rate is increased, which is indicated by multiple transcription initiation sites.

The section is organized as follows. We start with a formal definition of a PDMP for the present setting, following the construction of Davis [23]. As an introduc-

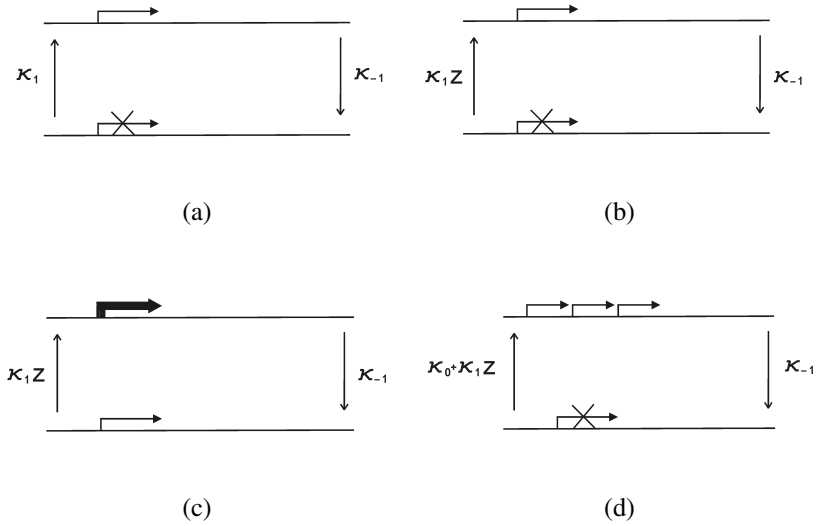


Figure 2.27: Schematic representation of four different promoter types. The transcription initiation site is indicated by a broken arrow. (a) Model I: Independent switching from the deactivated to the activated state and vice versa. (b) Model II: Transitions from the deactivated to the activated state depend on the amount of inducer. (c) Model III: The promoter possesses an excited and a basic state. In the excited state expression takes place with higher production rate indicated by a thick arrow. (d) Model IV: The promoter is in an activated or in a deactivated state. Transitions from the deactivated to the activated state take place with constant basal transition rate but can be increased by the gene products. The increase of the chance of expression is indicated by multiple transcription initiation sites.

tory example we will consider the unregulated promoter type, Model I. We show that if the stationary distribution possesses a density then it is obtained as solution of the equation system of the correlated random walk. For Model II we show that the only stationary distribution is given by the point mass at zero. For Model III and IV we give the explicit formulas of the stationary distributions. Furthermore we analyze the gene expression in each network by numerical means. The empirical distributions are calculated for four different initial concentrations and four different simulation lengths.

2.3.2 PDMP-Models

To give a formal definition of a PDMP for an autocatalytic gene regulatory network, we follow the construction of Davis in [23]. Since we are mainly interested

in analytical results, and to avoid too complex calculations, we consider genes having only one binding site in their promoter to which the gene product can bind. Furthermore, we simplify the temporal evolution of the mature gene product by ignoring intermediate synthesis steps. The two promoter states are denoted by 0 and 1, specifying whether the binding site is vacant or occupied, respectively. For the protein it is assumed that it is present in such high amounts that a change of its concentration can be described in a continuous fashion. Then the temporal evolution of the concentration of the gene product takes place on the positive real line. Hence, the process evolves in the state space S defined as

$$S = \{(i, z) : \ i \in M, \ z \in \mathbb{R}_{\geq 0}\}, \tag{2.32}$$

where $M = \{0, 1\}$. S can be considered as a disjoint union of copies of $\mathbb{R}_{\geq 0}$, labeled by $i \in M$. A copy $\{i\} \times \mathbb{R}_{\geq 0}$ is called an *arm* or a *branch* of the process. The state of the process at time t will be denoted by $X_t = (\theta_t, \xi_t)$. The random variable θ_t takes values in M and signifies the particular branch in which the process stays at time t. The random variable ξ_t describes the deterministic dynamics of the process in the particular branch. The temporal evolution of $(X_t)_{t\geq 0}$ is determined by the dynamics on the particular arms, given by some velocities $v^{(i)}, \ i \in M$, and a transition rate function λ. The dynamics on the particular branches are determined by ordinary linear differential equations, describing the synthesis and degradation of the protein. Hence, if $v^{(i)} : \ \mathbb{R}_{\geq 0} \to \mathbb{R}_{\geq 0}, \ i \in M$ are the velocity functions, the temporal evolution of the protein concentration z is given by

$$\dot{z} = v^{(i)}(z) . \tag{2.33}$$

The sojourn times of the process in the two branches are governed by the measurable rate function

$$\lambda : \ S \to \mathbb{R}_+.$$

More precisely, the probability that the process makes a transition from branch i to branch $j = i + 1 \mod 2$ in the infinitesimal time interval $[t, t + \mathrm{d}t)$ is given by $\lambda(i, z)\mathrm{d}t$, given that it is in branch i and has concentration z at time t. Let κ_1 and κ_{-1} denote the transition rate constants for transitions of the promoter from the activated to the deactivated state and vice versa. We assume that transition from the activated to the deactivated state always happens independently from any other reactants. Thus the transition rate function reads

$$\lambda(1, z) = \kappa_{-1}. \tag{2.34}$$

For the reverse direction we consider three types of transitions: independent, concentration dependent and concentration dependent with basal transition rate constant.

With these ingredients, the PDMP can be constructed in the following way. Suppose that in the beginning the process starts in $x_0 = (i, z_0) \in S$. Let $\phi_i(u, z_0),\ u \geq 0$ denote the unique integral curve belonging to the vector fields $v^{(i)}$, where z_0 denotes the amount of protein product at time $t = 0$. Define a survival function $R:\ \mathbb{R} \to \mathbb{R}_+$ by

$$R(t) = \exp\left(- \int_0^t \lambda\big(i, \phi_i(u, z_0)\big) \mathrm{du} \right).$$

The holding time of the process in the initial state x_0 has distribution function $F(t) = 1 - R(t)$. This means that we choose a random variable τ_1 such that

$$F(t) = \mathbb{P}(\tau_1 \leq t).$$

At time τ_1 the process jumps to the branch $\{j\} \times \mathbb{R}$ with $j = i + 1 \mod 2$, i.e. setting $1 + 1 = 0$.
By means of these notations, the process $(X_t)_{t \geq 0}$ is defined up to the first jump time through

$$X_t = (\theta_t, \xi_t) = \begin{cases} (i, \phi_i(t, z_0)), & t < \tau_1, \\ (j, \phi_i(\tau_1, z_0)), & t = \tau_1. \end{cases} \tag{2.35}$$

After $t = \tau_1$ the process moves deterministically from position X_{τ_1} and remains in that branch up to a similarly defined time τ_2. That means, the holding time $\tau_2 - \tau_1$ is chosen independently of τ_1 and ξ_{τ_1} by $F(t) = \mathbb{P}(\tau_2 - \tau_1 \leq t)$. Proceeding this way, the process is defined between all consecutive jump times $\tau_n,\ n \geq 0$. The resulting process possesses the Markov property and is called a PDMP, [23].
Simulation of the PDMP is straightforward. Starting at time $T = 0$ in an initial value x_0, the first jump time τ_1 is selected according to the survival function $R(t)$. Until the process reaches τ_1, it moves deterministically following the flow ϕ. Then at time τ_1 it jumps to the other branch, selects the second holding time $\tau_2 - \tau_1$, and moves deterministically until it reaches the jumping time τ_2. After that it starts over again. Of course, an autocatalytic network composed of one gene with one binding site is a simple system. However, even for more complex systems simulating a PDMP remains easy, and is as simple as the simulation of a purely discrete system executing Gillespie's algorithm, [33]. In a more complex system, the transition from one branch to another is not deterministic, as it is the case for the networks considered in the present section. Switching from one branch to another is governed by a discrete distribution similar to Gillespie's algorithm. On the other hand, between these jumps the process proceeds deterministically, resulting in lower computation times in general. For a more detailed discussion of the two simulation algorithms see Section 2.1.

We are interested in the temporal evolution of the distribution of the PDMP for an autoregulative network, which is given by the adjoint of the strong generator of the associated transition group. In the finite-state setting, the generator of a Markov process is also called a Q-matrix. The components of this matrix are given as the temporal derivative of the transition probabilities at zero. Hence, the generator describes the evolution of the distribution of the process for small enough time intervals. For processes with uncountable state spaces, the generator is expressed in terms of bounded measurable functions. It is defined by

$$Gf = \lim_{t \searrow 0} \frac{1}{t}\big(Gf - f\big)$$

for all bounded measurable functions $f : S \to \mathbb{R}$ for which the above limit exists. For a PDMP we obtain the explicit formula of the generator by the formula of the extended generator $\bar{G}$ of a PDMP. $\bar{G}$ was characterized by Davis in [23]. From there we obtain in our special case the following simple formula of the generator of the PDMP. For all $f : S \to \mathbb{R}$ in the domain of G it holds that

$$Gf(i,z) = v^{(i)}(z) f_z(i,z) + \lambda(i,z)\big(f(j,z) - f(i,z)\big), \tag{2.36}$$

where f_z denotes the partial derivative with respect to z, and $j = i + 1 \mod 2$.

2.3.3 Autocatalytic Genetic Networks

In the present section we present the different autocatalytic networks. The starting point of our analysis is a result which links up PDMPs for genetic networks with correlated random walks of population dynamics. We start with the simplest genetic network of an inducible promoter. However, this system will serve as a reference model only.

Model I: Inducible promoter

Consider a promoter of an inducible gene, for which it is assumed that the amount of inducers is constant in time. Then the gene g is turned on and off with constant rates κ_1 and κ_{-1}, respectively, see Figure 2.27(a). The activated and deactivated states of the gene are denoted by g_1 and g_0. As long as the gene is activated, gene product is synthesized at rate α. The gene product is degraded at rate constant γ. The individual reaction channels are listed in the following reaction scheme:

$$\begin{array}{rcl} g_0 & \xrightarrow{\kappa_1} & g_1\,, \\ g_1 & \xrightarrow{\kappa_{-1}} & g_0\,, \\ g_1 & \xrightarrow{\alpha} & g_1 + p\,, \\ p & \xrightarrow{\gamma} & \emptyset\,, \end{array} \tag{2.37}$$

where the symbol $\emptyset$ denotes the decay products. The two branches of the process are denoted by 0 and 1, indicating the activation status of the gene g. Let z denote the concentration of p. Then the state space of $(X_t)_{t\geq 0}$ is given by (2.32). Since transitions between the two promoter states happen independently of any other reactants, the transition rate functions are constant:

$$\lambda(0, z) = \kappa_1 \text{ and } \lambda(1, z) = \kappa_{-1}.$$

Therefore the holding times on both arms are exponentially distributed,

$$F(t) = \begin{cases} \mathrm{e}^{-\kappa_1 t}, & \text{if} \quad X_t \in \{0\} \times \mathbb{R}, \\ \mathrm{e}^{-\kappa_{-1} t}, & \text{if} \quad X_t \in \{1\} \times \mathbb{R}. \end{cases} \tag{2.38}$$

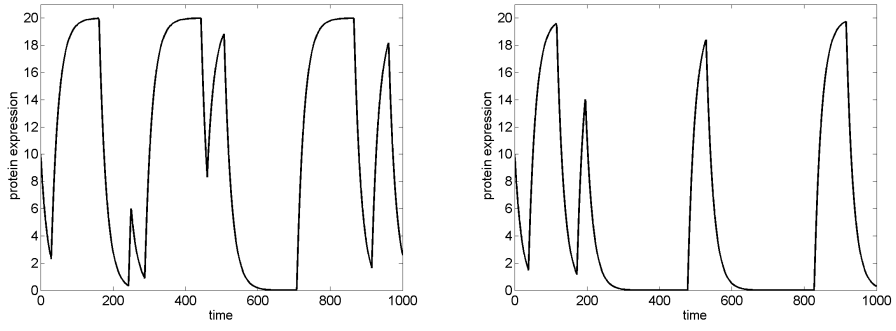
Between two exponentially distributed jump times $\tau_i, \tau_{i+1},\ i \geq 0$, the process moves deterministically according to

$$\dot{z} = -\gamma z, \tag{2.39}$$

if the process is in the off-branch, i.e., $\theta_t = 0$, and

$$\dot{z} = \alpha - \gamma z, \tag{2.40}$$

if it is in the on-branch, i.e., $\theta_t = 1$.
Figure 2.28 displays two typical simulated expression curves. The process starts in the off-branch at $z = 10$. As long as it stays in the off-branch, the concentration



(a) (b)

Figure 2.28: Typical time courses of the protein concentrations $(\xi_t)_{t\geq 0}$ for an inducible gene with an unregulated promoter. The parameters are $\kappa_1 = \kappa_{-1} = 0.01$, $\alpha = 1$, and $\gamma = 0.05$.

decays exponentially fast. At the jump time it transits to the on-branch. There,

protein is synthesized, and its concentration converges to the quotient of the transition rate over the degradation rate. At the next jump time the gene transits back to the inactive state, and the concentration of the protein converges towards zero. Hence, starting with an arbitrary but fixed initial value z_0, the process tends to zero in the off-branch and to α/γ in the on-branch as t tends to infinity. So in the long run the process only takes values between zero and α/γ.
The dimensions of the association and dissociation rates of the system above and the systems below are given in $\text{nM}^{-1}\text{min}^{-1}$ and min^{-1}, and the dimensions of the synthesis and degradation rates are given in $\text{nM}^{-1}\text{min}^{-1}$ and min^{-1}, respectively. For the rates of an inducible gene as well as for the autocatalytic networks discussed below, we have not found any experimentally determined values for a particular organism. Thus, we use the following orders of magnitude for the particular reaction rates, stated in the literature for different systems. Association and dissociation rates are reported in the order of $10^{-3} - 10^{-2}$ $\text{nM}^{-1}\text{min}^{-1}$ and $10^{-3} - 10^{-1}$ min^{-1}, respectively, [70], [122], [101], [124]. Synthesis and decay rates are stated in the order of $1 - 10$ $\text{nM}^{-1}\text{min}^{-1}$, and $10^{-4} - 10^{-1}$ min^{-1}, respectively, [108], [93] ,[10].
The above example is a simple use of modeling genetic networks by PDMPs. Since there are no interactions between the gene and its gene product, activation and deactivation take place in a Poisson manner. In the following we will model the effects of the gene product on gene expression when the protein acts as an activator or enhancer. We consider the three promoter types mentioned in the introduction, Figure 2.27(b)-(d).

Model II: Pure autocatalytic networks

Consider the promoter displayed in Figure 2.27(b). Activation of the promoter depends on the concentration of the protein z, whereas deactivation takes place at constant rates. Proteins which can activate or enhance transcription of their own encoding genes are also called transcription factors. Such a genetic module is the prototype of a positive feedback loop, which we call a *pure autocatalytic network*. The corresponding reaction scheme is obtained by replacing the first two reaction channels in (2.37) by the following two elementary reactions describing the reversible binding of a transcription factor p to the binding site of its encoding gene g:

$$\begin{array}{ccc} g_0 + p & \xrightarrow{\kappa_1} & g_1 \,, \\ g_1 & \xrightarrow{\kappa_{-1}} & g_0 + p \,. \end{array} \tag{2.41}$$

As for the unregulated promoter, the gene product is synthesized at rate α and degraded at rate constant γ. The transition rate function is given by

$$\lambda(0, z) = \kappa_1 z \;\text{ and }\; \lambda(1, z) = \kappa_{-1}, \tag{2.42}$$

and the vector fields in the two branches are determined by the differential equations given in equations (2.39) and (2.40).

Model III: Autocatalysis with positive basal transcription rate

In a pure autocatalytic network, the synthesis of a transcription factor only takes place in the presence of the gene product itself. In the following we assume that synthesis always takes place at least with a small positive transcription rate. The corresponding promoter is depicted in Figure 2.27(c). Such a system may serve as a model for gene expression, where the gene is either in an excited or in a basic production state, but is never completely turned off. We will call it an *autocatalytic network with positive basal transcription rate*. The system is described by the following five reaction channels:

$$\begin{array}{rcl} g_0 + p & \xrightarrow{\kappa_1} & g_1\,, \\ g_1 & \xrightarrow{\kappa_{-1}} & g_0 + p\,, \\ g_0 & \xrightarrow{\alpha_0} & g_0 + p\,, \\ g_1 & \xrightarrow{\alpha_1} & g_1 + p\,, \\ p & \xrightarrow{\gamma} & \emptyset\,. \end{array} \tag{2.43}$$

The basic production state will be denoted by 0. By 1 we will denote the excited or induced state. Transitions between the two states are assumed to proceed in the same way as in the pure autocatalytic network. The more gene product is present, the more likely it is that the gene switches to the excited state. On the other hand, transitions back to the basal state occur independently of any other reactants. Thus the transition rate functions of the two states are given by the equations (2.42). Since synthesis takes place in the basic as well as in the induced state, the vector fields are given by the following two differential equations:

$$\dot{z} = \alpha_0 - \gamma z, \tag{2.44}$$

if $\theta_t = 0$, and

$$\dot{z} = \alpha_1 - \gamma z, \tag{2.45}$$

if $\theta_t = 1$, where $\alpha_1 > \alpha_0 > 0$.

Model IV: Autocatalysis with positive basal activation rate

Another promoter type is obtained by combining the features of an unregulated promoter and a pure autocatalytic network. In such a model, gene activation would be caused by inducers present in a constant amount and by the gene product itself. Hence, compared to an autocatalytic network with positive basal transcription rate, binding of the gene product to the promoter increases the probability

of transcription rather than the expression level. Such a model includes two reaction channels describing activation by the inducer and the gene product, and two reaction channels describing the corresponding deactivations of the gene. For simplicity, we identify the two reactions describing the deactivation of the gene. Hence, we assume that the dissociation of the inducer and the gene product from the promoter takes place with the same dissociation rate. The reaction scheme describing such a system is obtained by replacing the first reaction channel in (2.37) by the following two elementary reactions:

$$\begin{array}{rcl} g_0 & \xrightarrow{\kappa_0} & g_1\,, \\ g_0 + p & \xrightarrow{\kappa_1} & g_1\,. \end{array} \tag{2.46}$$

Thus, even if there is no gene product present, the gene can spontaneously be activated with positive rate κ_0. If there is some gene product present, the rate of activation is increased by κ_1 times the amount of protein p. We will call such a system an *autocatalytic network with positive basal activation rate*. In this case, the transition function is given by

$$\lambda(0,z) = \kappa_0 + \kappa_1 z \;\text{ and }\; \lambda(1,z) = \kappa_{-1}. \tag{2.47}$$

As in the pure autocatalytic network, synthesis takes place only in the active state. Hence, the temporal evolution of the protein concentration is given by the equations (2.39) and (2.40).
The four models together with the characterizing vector fields and transition rates are listed in Table 2.8.

2.3.4 Stationary Distributions

We will start with a result about the dual operators of the strong generators of the PDMPs from the previous section. We determine the respective formulas and the solutions of the corresponding stationary conditions. After that, we will use these results to find the stationary distributions of the respective autocatalytic networks. Furthermore we will investigate the empirical distributions for different simulation lengths and different initial values by numerical means.
We call a PDMP $(X_t)_{t\geq 0}$ an *autocatalytic PDMP* if it is one of the types II to IV.

Theorem 2.3.1. *(1) Let $(X_t)_{t\geq 0}$ be an autocatalytic PDMP with generator G. Then the dual operator G^* is given by*

$$\begin{aligned} G^*\rho(0,z) &= -\frac{\partial}{\partial z}\big(v^{(0)}(z)\rho(0,z)\big) + \lambda(1,z)\rho(1,z) - \lambda(0,z)\rho(0,z), \\ G^*\rho(1,z) &= -\frac{\partial}{\partial z}\big(v^{(1)}(z)\rho(1,z)\big) + \lambda(0,z)\rho(0,z) - \lambda(1,z)\rho(1,z), \end{aligned} \tag{2.48}$$

Model type	$v^{(0)}(z)$	$v^{(1)}(z)$	$\lambda(0,z)$	$\lambda(1,z)$
Model I: inducible gene	$-\gamma z$	$\alpha-\gamma z$	κ_1	κ_{-1}
Model II: pure autocatalytic network	$-\gamma z$	$\alpha-\gamma z$	$\kappa_1 z$	κ_{-1}
Model III: autocatalysis with positive basal transcription rate	$\alpha_0-\gamma z$	$\alpha_1-\gamma z$	$\kappa_1 z$	κ_{-1}
Model IV: autocatalysis with positive basal activation rate	$-\gamma z$	$\alpha-\gamma z$	$\kappa_0+\kappa_1 z$	κ_{-1}

Table 2.8: Summary of the four models together with the characterizing vector fields and transition rates.

for weakly differentiable functions $\rho:\ M\times\mathbb{R}\to[0,\infty)$ *satisfying the boundary conditions*

1. $\rho(0,\frac{\alpha}{\gamma})=\rho(1,0)=0\,,\quad$ *if* $v^{(0)}(z)=-\gamma z,\ v^{(1)}(z)=\alpha-\gamma z$;

2. $\rho(0,\frac{\alpha_1}{\gamma})=\rho(1,\frac{\alpha_0}{\gamma})=0\,,\quad$ *if* $v^{(0)}(z)=\alpha_0-\gamma z,\ v^{(1)}(z)=\alpha_1-\gamma z$;

(2) Let $(X_t)_{t\geq 0}$ *be an autocatalytic PDMP with generator* G*. Then the system of equations* $G^*\rho(i,z)=0,\ i=0,1$ *possesses the following solutions:*

1. *For* $\lambda(0,z)=\kappa_1 z,\ \lambda(1,z)=\kappa_{-1},\ v^{(0)}(z)=-\gamma z,\ v^{(1)}(z)=\alpha-\gamma z$ *and* $z_0\in(0,\frac{\alpha}{\gamma})$ *the unique solution is given by*

$$\begin{aligned}\rho(1,z) &= \rho(1,z_0)\mathrm{e}^{\frac{\kappa_1}{\gamma}(z-z_0)}\left(\frac{\alpha-\gamma z}{\alpha-\gamma z_0}\right)^{\frac{\kappa_{-1}}{\gamma}-1},\\ \rho(0,z) &= \rho(1,z_0)\mathrm{e}^{\frac{\kappa_1}{\gamma}(z-z_0)}\frac{1}{\gamma z}\frac{(\alpha-\gamma z)^{\frac{\kappa_{-1}}{\gamma}}}{(\alpha-\gamma z_0)^{\frac{\kappa_{-1}}{\gamma}-1}}.\end{aligned}\tag{2.49}$$

2. *For* $\lambda(0,z)=\kappa_1 z,\lambda(1,z)=\kappa_{-1},\ v^{(0)}(z)=\alpha_0-\gamma z,\ v^{(1)}(z)=\alpha_1-\gamma z$*, and* $z_0\in(\frac{\alpha_0}{\gamma},\frac{\alpha_1}{\gamma})$ *the unique solution is given by*

$$\begin{aligned}
\rho(1,z) &= \rho(1,z_0)\mathrm{e}^{\frac{\kappa_1}{\gamma}(z-z_0)}\left(\frac{\gamma z-\alpha_0}{\gamma z_0-\alpha_0}\right)^{\frac{\alpha_0\kappa_1}{\gamma^2}}\left(\frac{\gamma z-\alpha_1}{\gamma z_0-\alpha_1}\right)^{\frac{\kappa_{-1}}{\gamma}-1}, \\
\rho(0,z) &= \rho(1,z_0)(\alpha_1-\gamma z)\mathrm{e}^{\frac{\kappa_1}{\gamma}(z-z_0)}\frac{(\gamma z-\alpha_0)^{\frac{\alpha_0\kappa_1}{\gamma^2}-1}}{(\gamma z_0-\alpha_0)^{\frac{\alpha_0\kappa_1}{\gamma^2}}}\left(\frac{\gamma z-\alpha_1}{\gamma z_0-\alpha_1}\right)^{\frac{\kappa_{-1}}{\gamma}-1}.
\end{aligned} \tag{2.50}$$

3. *For* $\lambda(0,z)=\kappa_0+\kappa_1 z,\ \lambda(1,z)=\kappa_{-1},\ v^{(0)}(z)=-\gamma z,\ v^{(1)}(z)=\alpha-\gamma z$, *and* $z_0\in(0,\frac{\alpha}{\gamma})$ *the unique solution is given by*

$$\begin{aligned}
\rho(1,z) &= \rho(1,z_0)\mathrm{e}^{\frac{\kappa_1}{\gamma}(z-z_0)}\left(\frac{\alpha-\gamma z}{\alpha-\gamma z_0}\right)^{\frac{\kappa_{-1}}{\gamma}-1}\left(\frac{z}{z_0}\right)^{\frac{\kappa_0}{\gamma}}, \\
\rho(0,z) &= \rho(1,z_0)\mathrm{e}^{\frac{\kappa_1}{\gamma}(z-z_0)}\frac{(\alpha-\gamma z)^{\frac{\kappa_{-1}}{\gamma}}}{(\alpha-\gamma z_0)^{\frac{\kappa_{-1}}{\gamma}-1}}\frac{(\gamma z)^{\frac{\kappa_0}{\gamma}-1}}{(\gamma z_0)^{\frac{\kappa_0}{\gamma}}}.
\end{aligned} \tag{2.51}$$

Conditions *1.*, *2.* and *3.* from part *(2)* of above theorem correspond to the Models II, III and IV of Table 2.8, respectively.
Quite surprisingly, equation (2.48) of above result connects a PDMP with a correlated random walk and thus establishes a link between genetic networks and population dynamics.
Remark. *The equation system obtained by setting the left hand side of (2.48) equal to zero is often called the system of the one-dimensional correlated random walk. Thus, the stationary density function of an autocatalytic PDMP , provided it exists, is given as a solution of the correlated random walk equations. These equations and variations of them were studied by many authors in different settings, see [36], [60], [49], [45].*
The proof of the theorem above is placed in the appendix at the end of this section.

Model II: Pure autocatalytic networks

We start with the simplest system of a pure autocatalytic network. However it will turn out that this is the trickiest case for which the results of Theorem 2.3.1 are not directly applicable. The dynamics for the on and off branch are given by the two differential equations

$$\dot{z}=\alpha-\gamma z \quad \text{and} \quad \dot{z}=-\gamma z, \tag{2.52}$$

respectively. Thus, between two consecutive jump times the process moves according to

$$z(t) = \begin{cases} \mathrm{e}^{-\gamma(t-\tau_n)} z_n, & \text{if} \quad \theta_t = 0, \\ \frac{\alpha}{\gamma} + (z_n - \frac{\alpha}{\gamma})\mathrm{e}^{-\gamma(t-\tau_n)} & \text{if} \quad \theta_t = 1, \end{cases} \tag{2.53}$$

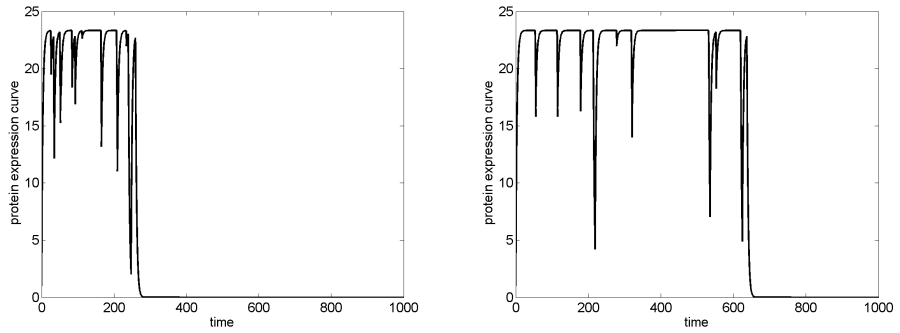
where τ_n and z_n denote the most recent jump time and the product concentration at the jump event. From equation (2.42) we know that switching from the on-branch to the off-branch is independent of the concentration of the gene product. Hence the process stays in the on-branch for an exponentially distributed time, so that the probability that the process stays in the on-branch for an arbitrary long time tends to zero. However, when the switching rate depends on the concentration of the protein this no longer remains true in general. If $\theta_t = 0$, the survivor function reads

$$R(t) \;=\; \exp\left(- \int_{\tau_n}^{\tau_n + t} \kappa_1 z(u) \mathrm{d}u \right) \;= \exp\left(-\frac{\kappa_1 z_n}{\gamma} (1 - \mathrm{e}^{-\gamma(t-\tau_n)}) \right) \tag{2.54}$$

Letting t tend to infinity we find

$$\lim_{t \to \infty} R(t) = \exp\left(-\frac{\kappa_1 z_n}{\gamma} \right) > 0. \tag{2.55}$$

Thus, when the process has transitted to the off-branch it remains there with a positive probability. This means that there will be no further synthesis and that the product concentration tends to zero, which can be observed by simulating the process. Figure 2.29 displays two typical expression curves of a pure autocatalytic process. We use the same values for the turning on and off rate as for the inducible gene from Figure 2.28. The remaining parameters are chosen in such a way that the process becomes extinct in most of the runs within a time interval of 1000 time units. Since the process starts in the on-branch, gene product is produced and the concentration tends towards its maximal expression level of about 23 units. Then the gene is turned off and on several times. If it is turned off the concentration decreases, and if it is turned on the concentration tends to its maximal level again. Compared to Model I, now the period during which the gene is deactivated is very short even if the turning on and off rates are chosen to be equal, see Figure 2.28 and 2.29. However, during a simulation period of 1000 time units the gene is turned off at a random time instant and remains in the off-state. As a result, the concentration vanishes. Thus, the resulting expression profile depends strongly on the simulation period. If one would measure the concentrations after a short period of time, say at 200 time units, most of the expression curves would adopt maximal values. Hence, the distribution will have one peak at maximal expression



(a) (b)

Figure 2.29: Typical time courses of the protein expressions in a pure autocatalytic network. The simulations started in the on branch with initial value $z = 1$ and run 1000 time units. The parameters are $\kappa_1 = 0.02,\ \kappa_{-1} = 0.02,\ \alpha = 7,\ \gamma = 0.3$.

level. If one would increase the measuring time point more and more, the probability that the system is in its off state would constantly increase. For instance, measuring the concentrations between 300 and 600 time units would result in a bimodal expression profile with one peak located at very low and one peak located at maximal expression levels. When increasing the measuring time point to a higher value, e.g. 800 time units, nearly all of the expression curves would be at very low levels. Hence, the distribution would be unimodal again, but now with a peak located around zero. In particular this would imply that the point measure at $(0, 0)$ would be the only stationary distribution. This was already observed in Section 2.1 where a more detailed numerical analysis of the dependency of the limiting probability on the individual parameters was carried out. There, we have noted that it seems that the pure autocatalytic process will always become extinct. In the following we will show that this is indeed the case.
Recall that up to a constant C the solution of the correlated random walk (2.49) is given by

$$\rho(z) = C\mathrm{e}^{\frac{\kappa_1}{\gamma}z}\frac{1}{z}(\alpha - \gamma z)^{\frac{\kappa_{-1}}{\gamma}-1},$$

where $\rho(z) = \rho(0, z) + \rho(1, z)$. Since there is a pole at $z = 0$, $\rho(z)$ cannot be normalized. Hence we cannot use the results of Theorem 2.3.1 to find a stationary distribution. Instead it holds that:

Theorem 2.3.2. *The only invariant probability for the pure autocatalytic PDMP* $(X_t)_{t\geq 0}$ *is* $\delta_{(0,0)}$.

The proof is postponed to the appendix section.

As we have seen in the simulations for Figure 2.29 the expression curves always become extinct within a time interval of 1000 units. However, in the following we will show that for other realistic parameters this will not be the case in general. Especially, we show that the pure autocatalytic process can be far away from being in its stationary distribution. We have simulated the PDMP for different time lengths and different initial concentration values. The simulations were repeated 10,000 times for each time length and each initial concentration value.

Time dependency

The histograms of the simulations for four different simulations periods are shown in Figure 2.30. The mean and the variance of the empirical distributions are listed

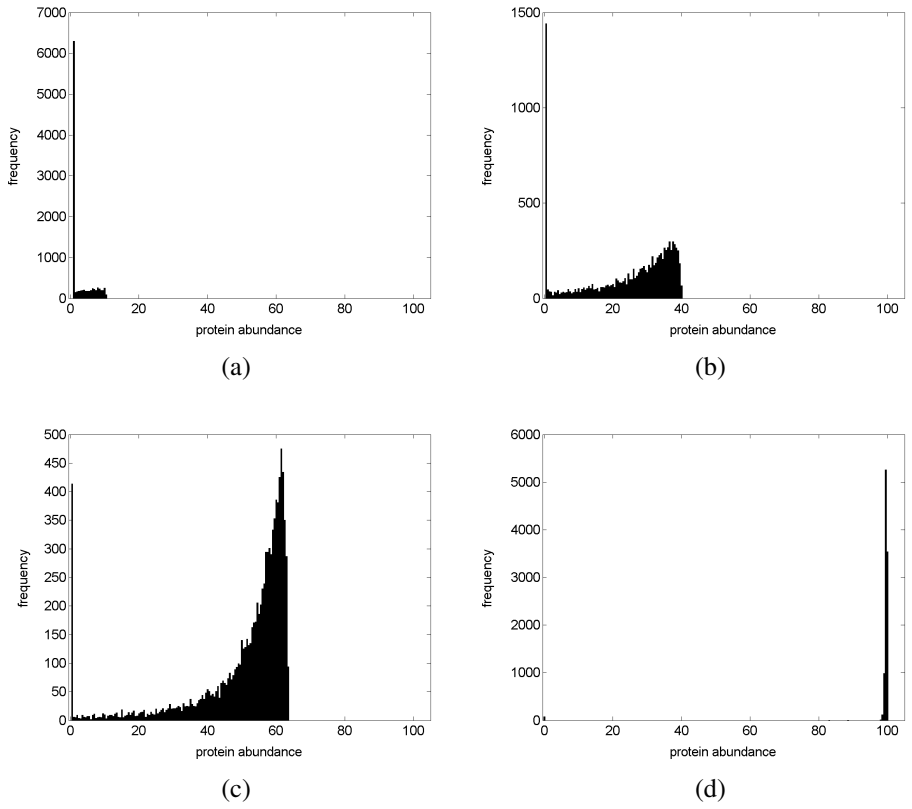


Figure 2.30: Empirical distributions of the protein concentrations of Model II for four different lengths of simulations. The simulations start at $x_0 = (i, z_0) = (0, 1)$ and run for (a) 10, (b) 50, (c) 100, and (d) 1000 time units. The parameters are $\kappa_1 = 0.05,\ \kappa_{-1} = 0.025,\ \alpha = 1$, and $\gamma = 0.01$.

in Table 2.9. A first glance at the distributions and the respective distribution parameters shows that the distribution parameters exhibit a graded behavior whereas

the distribution exhibit a rather binary expression pattern. Running the simulation

time length	10	50	100	1000
$\langle X \rangle$	2.85	24.01	50.24	98.84
$\sigma^2(X)$	8.93	174.42	238.54	74.94

Table 2.9: Empirical distribution parameters for four different simulation lengths of the pure autocatalytic process.

with a time period equal to 10 time units results in a distribution displayed in Figure 2.30(a). More than 60% of the cells show no expression. The remaining cells have expressed the gene product with concentrations varying between 0 and around 10. An increase of the time period to 50 time units leads to an increase in the number of cells exhibiting gene expression, and in an increase of the maximal expression level. The maximal expression level is increased from 10 to a value near to 40. Furthermore, the distribution becomes more bimodal. One mode is centered around zero and the other one is centered around an expression level of about 35, Figure 2.30(b). When increasing the simulation period to 100 time units, the distribution is still bimodal. One peak is at zero and the other is around 60 concentration levels. However, now most of the cells show expression of the gene product, Figure 2.30(c). When increasing the simulation period further, the bimodal expression pattern nearly disappears. Now the distribution becomes nearly unimodal. More or less all cells have approached a maximal expression level of about 100. Only some few cells show no exressions, Figure 2.30(d). This binary behavior cannot be observed by looking only at the means of the respective distributions. The mean increases gradually for an increasing time length, see Table 2.9.
A similar time dependency was shown for the positive feedback loop of comK during the development of competence in *Bacillus subtilis* and the *araBAD* promoter in *Escherichia coli*. Both systems start in an unimodal distribution at low expression levels. At increasing observation periods the distribution becomes bimodal, [74], [104].

Initial concentration dependency

The empirical distributions for four different initial concentration values are displayed in Figure 2.31. Each simulation runs over 500 time units and was repeated $10,000$ times. The empirical distribution parameters are listed in Table 2.10. Again, a comparison of the first two central moments and the histograms exhibit a different behavior. Whereas the average increases gradually for increasing initial protein concentrations, the distribution shows a binary behavior. If the

initial concentration	0.005	0.05	0.5	5
$\langle X \rangle$	2.52	20.82	89.8	98.92
$\sigma^2(X)$	238.21	1581,7	745.95	0.08

Table 2.10: Empirical distribution parameters for four different initial concentrations of the pure autocatalytic process.

initial amount is below a certain threshold, more or less all cells stay in the inactive state. For example, for an initial concentration equal to 0.005 only a small subpopulation is activated and exhibits expression at maximal expression level, see Figure 2.31(a). An increase of the initial concentration to 0.05 leads to a more

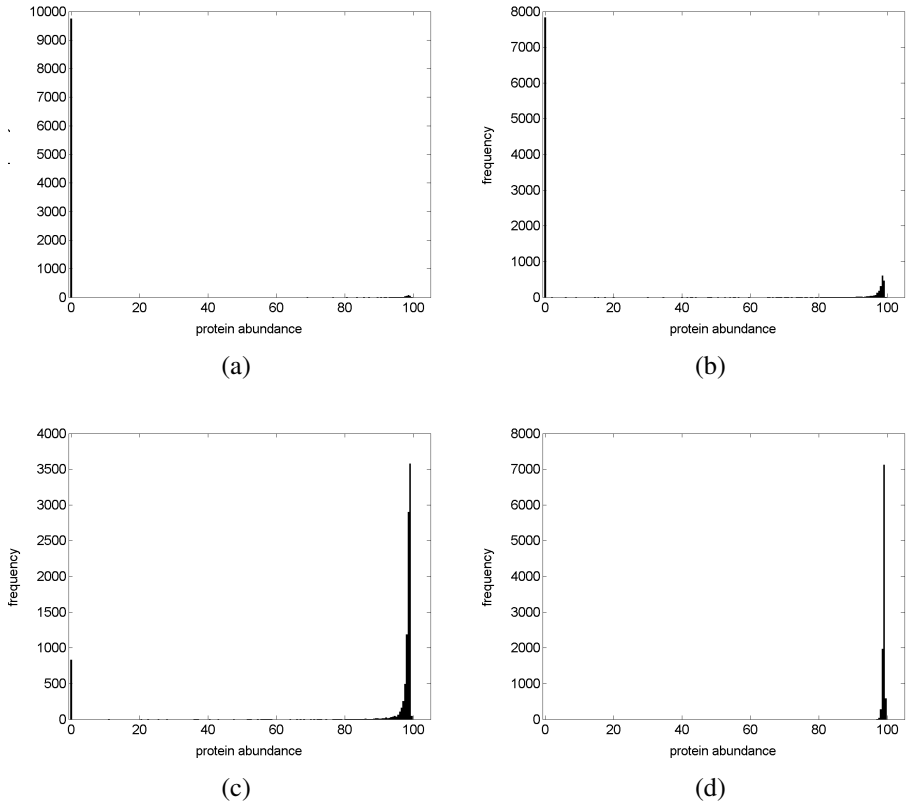


Figure 2.31: Empirical distributions of the protein concentrations of Model II for four different initial concentrations. The simulations start in the off-branch with initial product concentration equal to (a) 0.005, (b) 0.05, (c) 0.5, and (d) 5. The parameters are the same as the one used in Figure 2.30.

bimodal distribution. Most of the cells still show no expression whereas about

20% of the cells exhibit maximal expression levels. In contrast to the distributions of different time lengths, now no cells show intermediate expression levels. The cells are either turned off or have approached their maximal expression level around 100, see Figure 2.31(b). If the initial concentration is increased to 0.5 the population is still partitioned into two subpopulations whereas the size of the subpopulation with maximal expression level increases, see 2.31(c). By increasing the initial stimulus beyond a certain threshold leads to a unimodal distribution, Figure 2.31(d). For an initial concentration equal to 5, all cells are activated and exhibit highest expression levels which is reflected in a very small variance, see Table 2.10.
A similar expression behavior was stated for the ComK system in *B. subtillus* and for the synthetic autocatalytic system of rtTA in *Saccharomyces cerevisiae*. If the positive feedback loop of ComK is deactivated the cells respond in a graded fashion on increased inducer amounts. On the other hand, if the positive feedback loop is intact the expression profile becomes bimodal for increasing inducer concentrations, [74]. In *S. cerevisiae* a constitutive system was compared to an autocatalytic system. Whereas the constitutive system exhibits a graded response on increasing inducer concentrations, the autocatalytic system responds in a binary way, [8].
Below we will see that for the same simulation length of 1000 time units Model III and IV are more or less always in their stationary distributions. However, as we have seen above for a given time length the pure autocatalytic network can reach or can be far away from its stationary distribution, see Figure 2.29, and Figures 2.30 and 2.31. Before we consider Model III and IV, we examine the extinction of the pure autocatalytic network in more detail.

Extinction Analysis

We consider the two cases when the process starts in the on and off-branch. For both cases we calculate the expected time of the first jump, and the expected change in concentration until the time of the first jump. Furthermore, we compute the expected time of the second jump and the expected concentration at the second jump time, conditioned on that the process starts in the off branch and that the first jump occurs in finite time. The results are listed in the following proposition.

Proposition 2.3.1. *Let $X_t = (\theta_t, \xi_t)$ denote the pure autocatalytic network, and $\tau_n, n \geq 1$ the respective jump times.*

1. *For $\theta_0 = 1$ and $\xi_0 = z_0$ it holds that:*

   (a) *The expected time of the first jump is*

$$\mathbb{E}\big(\tau_1 \big| X_0 = (1, z_0)\big) = \frac{1}{\kappa_{-1}}.$$

(b) *The expected change in concentration during the first jump occurs is*

$$\mathbb{E}\big(\xi_{\tau_1} - \xi_0 \big| X_0 = (1, z_0)\big) = \big(\frac{\alpha}{\gamma} - z_0\big)\frac{\gamma}{\gamma + \kappa_{-1}}.$$

2. *For $\theta_0 = 0$ and $\xi_0 = z_0$ it holds that:*

(a) *The expected time of the first jump is*

$$\mathbb{E}\big(\tau_1 \big| X_0 = (0, z_0)\big) = \infty.$$

(b) *The expected change in concentration between $t = 0$ and the first jump is*

$$\mathbb{E}\big(\xi_{\tau_1} - \xi_0 \big| X_0 = (0, z_0)\big) = \frac{\gamma}{\kappa_1}\big(\mathrm{e}^{-\frac{\kappa_1 z_0}{\gamma}} - 1\big)$$

(c) *The expected time of the first jump conditioned on that the process has a jump in finite time reads*

$$\mathbb{E}\big(\tau_1 \big| X_0 = (0, z_0), \tau_1 < \infty\big) = \frac{\kappa_1 z_0}{\gamma^2}\frac{\exp(-\frac{\kappa_1 z_0}{\gamma})}{1 - \exp(-\frac{\kappa_1 z_0}{\gamma})} I(\kappa_1, \gamma, z_0),$$

where $I(\kappa_1, \gamma, z_0) := -\int_0^1 \ln(t)\exp(\frac{\kappa_1 z_0}{\gamma}t)\mathrm{d}t$.

(d) *The expected change in protein concentration until the first jump has occurred, conditioned on that the first jump time is finite is given by*

$$\begin{aligned}\mathbb{E}\big(\xi_{\tau_1} - \xi_0 \big| X_0 = (0, z_0), \tau_1 < \infty\big) &= \frac{1}{\kappa_1}\big(\gamma + \kappa_1 z_0 - \gamma\exp(\frac{\kappa_1 z_0}{\gamma})\big) \\ &\quad \times \frac{\exp(-\frac{\kappa_1 z_0}{\gamma})}{1 - \exp(-\frac{\kappa_1 z_0}{\gamma})}.\end{aligned}$$

(e) *The expected time of the second jump conditioned on that the first jump time is finite is given by*

$$\begin{aligned}\mathbb{E}\left(\tau_2 | X_0 = (0, z_0), \tau_1 < \infty\right) &= \mathbb{E}\left(\tau_2 | X_{\tau_1} = (1, z_0 e^{-\tau_1}), \tau_1 < \infty\right) \\ &\quad + \mathbb{E}(\tau_1 | X_0 = (0, z_0), \tau_1 < \infty)\end{aligned}$$

(f) *The expected concentration level at the second jump time conditioned on that the first jump time is finite is given by*

$$\begin{aligned}&\mathbb{E}\left(\xi_{\tau_2} | X_0 = (0, z_0), \tau_1 < \infty\right) \\ &= \frac{\alpha}{\gamma} - \frac{\kappa_{-1}(\gamma^2 + \alpha\kappa_1)}{\kappa_1\gamma(\gamma + \kappa_{-1})} + \frac{\kappa_{-1}\gamma z_0}{\gamma(\gamma + \kappa_{-1})}\frac{1}{1 - \mathrm{e}^{-\kappa_1 z_0/\gamma}}\end{aligned}$$

The proof of the proposition above can be found in the appendix.
As one would expect, the expected jump time conditioned on that the process is in the on-branch depends only on the turning off rate κ_{-1}. In an expected period of $1/\kappa_{-1}$ time units a fraction of $\gamma/(\gamma+\kappa_{-1})$ of the possible amount of $\alpha/\gamma - z_0$ protein concentration is produced. The produced amount is larger for smaller turning off rates. For the parameter values of Figure 2.29 the expected holding time is 50 time units, which is in good agreement with the displayed expression curves. During the expected time in the on state, the gene produces about 94% of the maximal possible concentration, see Figure 2.29. Therefore, the process almost always comes close to its maximal concentration level.
If the process is in the off branch, both the expected holding time as well as the expected change in concentration depend on the turning on rate, the degradation rate, and the initial concentration value. Observe that for a further jump the expected jump time and the expected change in concentration also depends on the synthesis rate α, indirectly given by the respective starting point z_n. In the following we consider only the cases where the process has a jump in finite time. Note that the integral $I(\kappa_1, \gamma, z_0)$ in statement *(2c)* is finite but only numerically evaluable. Taking the parameter values from Figure 2.29 and a starting concentration value of 23 we find for the expected holding time in the off branch a time length of about 1.85 time units, and for the change in protein concentration -8.67 levels, conditioned on the event that the process has another jump in finite time. Again this is in good agreement with the behavior of the two expression curves from Figure 2.29. Furthermore, for the two extreme scenarios where the probability of dying out and of no extinction is very high, the change in concentration conditioned on that the process does not become extinct is similar to the unconditional event. To this end we write the conditional expectation in statement *(2d)* of above proposition in the form

$$\begin{aligned}
&\mathbb{E}\big(\xi_{\tau_1} - \xi_0 \big| X_0 = (0, z_0), \tau_1 < \infty\big) \\
&\quad = \frac{\gamma}{\kappa_1}\big(\mathrm{e}^{-\frac{\kappa_1 z_0}{\gamma}} - 1\big)\frac{1}{1-\mathrm{e}^{-\frac{\kappa_1 z_0}{\gamma}}} + z_0 \frac{\mathrm{e}^{-\frac{\kappa_1 z_0}{\gamma}}}{1-\mathrm{e}^{-\frac{\kappa_1 z_0}{\gamma}}} \\
&\quad = \mathbb{E}\big(\xi_{\tau_1} - \xi_0 \big| X_0 = (0, z_0)\big)\frac{1}{\mathbb{P}(\text{no extinction})} \\
&\qquad + z_0 \frac{\mathbb{P}(\text{extinction})}{\mathbb{P}(\text{no extinction})}.
\end{aligned}$$

If the probability of extinction is very small we get

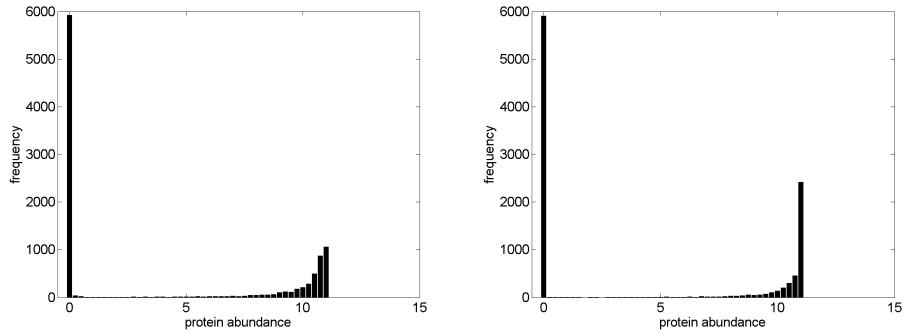
$$\mathbb{E}\big(\xi_{\tau_1} - \xi_0 \big| X_0 = (0, z_0), \tau_1 < \infty\big) = \mathbb{E}\big(\xi_{\tau_1} - \xi_0 \big| X_0 = (0, z_0)\big).$$

On the other hand, if the probability of extinction is very high, such that most of the paths become extinct before the first jump occurs, we may assume that the

expected change in concentration is nearly $-z_0$. Then, the conditional expectation reads

$$\begin{aligned}&\mathbb{E}\big(\xi_{\tau_1} - \xi_0 \big| X_0 = (0, z_0), \tau_1 < \infty\big) \\ &\qquad \approx z_0 \left(\frac{\mathbb{P}(\text{extinction})}{\mathbb{P}(\text{no extinction})} - \frac{1}{\mathbb{P}(\text{no extinction})} \right) = -z_0.\end{aligned}$$

A better understanding of the expression profiles of Figure 2.30 and Figure 2.31 can be derived from the statements *(2e)* and *(2f)*. Let us assume that the process is in state $(0, z_0)$ at time $t = 0$ and that it does not vanish at 0 during the first holding time, i.e., $\tau_1 < \infty$. Hence, starting at the initial concentration z_0, the concentration decreases until the first jump occurs at time τ_1. Then, concentration increases again until the second jump time τ_2, at which the process transits to the off branch and the gene product decays again. The expected time of the second jump is the typical time-scale for the process, i.e. until this time a fraction $\mathrm{e}^{-\kappa_1 z_0/\gamma}$ will be absorbed in 0 and the remaining $1 - \mathrm{e}^{-\kappa_1 z_0/\gamma}$ will come back with an expected concentration given by assertion *(2f)*. More precisely, a subpopulation in the order of $\mathrm{e}^{-\kappa_1 z_0/\gamma}$ will remain in the off branch and will get extinct until the time $\mathbb{E}\big(\tau_1 \big| X_0 = (0, z_0), \tau_1 < \infty\big)$. The remaining part will transit to the on branch and will reach an expected concentration of about $\mathbb{E}\left(\xi_{\tau_2} | X_0 = (0, z_0), \tau_1 < \infty\right)$ levels during a period of $1/\kappa_{-1}$ time units until it switches back to the off branch. Then, a similar procedure will be observed again. However, since both the size of the subpopulation which becomes extinct, and the expected time depend on the concentration at which the process starts in the off branch, the magnitudes may differ quite strongly after such an excursion is completed.
Such a behavior should be observable by simulating the process during a period of the above-mentioned time-scale. We have used the parameter values from Figure 2.30, but for better illustration we have taken a greater degradation rate, see Figure 2.32. Then, the expected time of the second jump and the expected concentration at the second jump time, conditioned on that the first jump time is finite, are $\mathbb{E}\left(\tau_2 | X_0 = (0, z_0), \tau_1 < \infty\right) = 49.62$ time units and $\mathbb{E}\left(\xi_{\tau_2} | X_0 = (0, z_0), \tau_1 < \infty\right) = 8.81$ concentration levels. For the extinction probability we find $R(\infty) = 0.57$. The corresponding empirical distribution is displayed in Figure 2.32(a) and is in good agreement with these theoretical values. For a simulation length of 50 time units about 5868 of the simulation runs ended at a concentration level lower than 0.02. The mean values of the concentration levels of the runs which ended in a concentration level higher than 0.02 is about 9.46. After the second jump time the gene product is degraded again, and concentration decreases. We can roughly estimate the further behavior of the process by taking the expected value of the concentration after the first two jumps as initial value. Now the extinction probability is drastically decreased. We find a



(a) (b)

Figure 2.32: Extinction behavior of the pure autocatalytic process during an excursion running (a) 50 and (b) 100 time units. The simulations start at $x_0 = (i, z_0) = (0, 1)$ and are repeated 10.000 times. The parameters are $\kappa_1 = 0.05,\ \kappa_{-1} = 0.025,\ \alpha = 1,\ \gamma = 0.09$.

value of $R(\infty) = 0.0075$. On the other hand, the expected time of the next two jumps and the expected concentration, conditioned on the event that the process does not remain in the off branch changes only moderately. For the expected time of the second jump time and the corresponding concentration we find the values $\mathbb{E}\left(\tau_2 | X_0 = (0, z_0), \tau_1 < \infty\right) = 42.93$ and $\mathbb{E}\left(\xi_{\tau_2} | X_0 = (0, z_0), \tau_1 < \infty\right) = 10.23$, respectively. Figure 2.32(b) displays the empirical distribution of the process for a simulation period of 100 time units. We have executed the simulations with the same parameter values and the same initial concentration. Again, the empirical moments are in good agreement with the estimated values above. We find that 5950 simulation runs ended at concentration levels smaller than 0.02, which is approximately equal to the sum of the extinction probabilities during the runs of the first two and the third and fourth jump time. The mean concentration of the simulation runs which ended at concentration levels higher than 0.02 is 10.43.
For the parameter values of Figure 2.30 we find $\mathbb{E}\big(\tau_1 \big| X_0 = (0, z_0), \tau_1 < \infty\big) = 25.78$, $\mathbb{E}\left(\tau_2 | X_0 = (0, z_0), \tau_1 < \infty\right) = 65.78$, $\mathbb{E}\left(\xi_{\tau_2} | X_0 = (0, z_0), \tau_1 < \infty\right) = 29.15$, and $R(\infty) = 0.0067$. Hence, in a simulation period of 10 time units most of the cells are still in their deactivated state, Figure 2.30(a). In a simulation period of 50 time units a fraction is still in its off state, and the remaining have not finished their first excursion, Figure 2.30(b). The empirical distribution is in good accordance with the expected concentration of about 29 levels. If we assume that the cells start their second excursion at this expected concentration level, we find for the expected times and concentration values, and for the extinction probability the values $\mathbb{E}\big(\tau_1 \big| X_0 = (0, z_0), \tau_1 < \infty\big) = 0.69$, $\mathbb{E}\left(\tau_2 | X_0 = (0, z_0), \tau_1 < \infty\right) = 40.69$, $\mathbb{E}\left(\xi_{\tau_2} | X_0 = (0, z_0), \tau_1 < \infty\right) = 49.25$, and

$R(\infty) = 5 \times 10^{-64}$. Hence, the expected time the process remains in its off state becomes quite short. Furthermore, the extinction probability is drastically decreased. A simulation period of 100 time units is approximately the time the process takes for two excursions. The expected concentration after two excursions is in accordance with the expression profile, Figure 2.30(c). If we run the simulation over 1000 time units, we have seen that more or less all cells are in their maximal expression state, Figure 2.30(d). This is in line with the results of Proposition 2.3.1. If we assume that in the third excursion the cells start at an expected initial concentration of about 49 levels, the extinction probability is around 10^{-107}, and the expected concentration at the end of this excursion is around 63. Hence the expected concentration increases gradually for increasing simulation periods, and the extinction probability becomes smaller and smaller. Furthermore, if we assume an initial concentration value of 100, the extinction probability is around 10^{-218} and the expected concentration after such an excursion is around 99. Hence, if the cells have reached their maximal expression level, more or less all of them will come back to their maximal concentration level after one excursion. Moreover, the expressions of most cells vanish after their first excursion. After that, the expressions of more or less no cells become extinct for a very long time. More precisely, if most of the cells have achieved their maximal expression level, the expected time until the next 67 cells will become extinct is in the order of 10^{221} time units which is far beyond any range of a cycle of any living organism. Hence we can call such a stage a quasi steady state.
For the parameter values of Figure 2.31(a) we find an extinction probability of about 0.98 during the first excursion. Hence, nearly all of the cells remain in their deactivated state. Only a very small fraction reaches a maximal expression state, in which they remain for a very long time. If the cells start at an initial value equal to 0.05, about 75% of the population will disappear during the first excursion, Figure 2.31(b). Again, the remainder will reach their maximal expression level in a time period of 1000 time units. If the initial concentration is increased to 0.5 only 8.2% of the population will disappear, Figure 2.31(a). For an initial value equal to 5, the probability of extinction is about 10^{-11}. Hence, in the given simulation length more or less all cells have reached their maximal expression level and remain there for a very long time, Figure 2.31(d).

Model III: Autocatalysis with positive basal transcription rate

The temporal evolution of the concentration of the gene product is given by

$$z(t) = \begin{cases} \frac{\alpha_0}{\gamma} + (z_n - \frac{\alpha_0}{\gamma})\mathrm{e}^{-\gamma(t-\tau_n)} & \text{if} \quad \theta_t = 0, \\ \frac{\alpha_1}{\gamma} + (z_n - \frac{\alpha_1}{\gamma})\mathrm{e}^{-\gamma(t-\tau_n)} & \text{if} \quad \theta_t = 1. \end{cases} \tag{2.56}$$

where τ_n denotes the most recent jump time and $z_n = \xi_{\tau_n}$. The survivor function of the inactive state reads

$$R(t) = \exp\left(-\kappa_1\big(\frac{\alpha_0}{\gamma}t + \frac{1}{\gamma}(z_n - \frac{\alpha_0}{\gamma})(1 - \mathrm{e}^{-\gamma t})\big)\right). \tag{2.57}$$

Letting t tend to infinity, we see that the probability that the process remains in the off-branch tends to zero. In this case we can use the results of Theorem 2.3.1 to obtain the density of the stationary distribution. Recall that ${}_1F_1$ denotes the Confluent Hypergeometric function, [106].

Theorem 2.3.3. *Let X_t be the PDMP for the autocatalytic network with positive basal transcription rate. The stationary distribution of the gene product reads*

$$\rho(z) = K(\gamma z - \alpha_0)^{a-1}|\gamma z - \alpha_1|^{b-1}\mathrm{e}^{\frac{\kappa_1}{\gamma}z},$$

with

$$K = \frac{\gamma}{\alpha_1}\frac{\Gamma(a+b)}{\Gamma(a)\Gamma(b)}\mathrm{e}^{-cu}\left(\frac{1}{1-u}\right)^a(1-u)^{1-b}\frac{1}{{}_1F_1\left(a, a+b, c(1-u)\right)},$$

where $a = \alpha_0\kappa_1/\gamma^2,\ b = \kappa_{-1}/\gamma,\ c = \alpha_1\kappa_1/\gamma^2$ and $u = \alpha_0/\alpha_1$. The expectation $\mathbb{E}(\xi_t)$ and the variance $\mathbb{V}(\xi_t)$ of the stationary distribution are given by

$$\mathbb{E}(\xi_t) = \frac{\alpha_1}{\gamma}\left(u - (u-1)\frac{a}{a+b}\frac{{}_1F_1(a+1, a+b+1, c(1-u))}{{}_1F_1(a, a+b, c(1-u))}\right)$$

and

$$\begin{aligned}\mathbb{V}(\xi_t) \;=\; &\left(\frac{\alpha_1}{\gamma}\right)^2(u-1)^2\frac{a}{a+b}\left(\frac{a+1}{a+b+1}\frac{{}_1F_1(a+2, a+b+2, c(1-u))}{{}_1F_1(a, a+b, c(1-u))}\right.\\ &\left.-\frac{a}{a+b}\frac{{}_1F_1^2(a+1, a+b+1, c(1-u))}{{}_1F_1^2(a, a+b, c(1-u))}\right).\end{aligned}$$

Again, the proof is postponed to the appendix section.

Time dependency

The empirical distributions for different simulation periods are displayed in Figure 2.33. The respective distribution parameters are listed in Table 2.11. In contrast to the pure autocatalytic process, a comparison of the distribution parameters and the histograms shows that both exhibit a gradual dependency on the time length of simulation. Except for a small time length of 10 time units the system always shows a unimodal distribution with a small distribution width. For a simulation

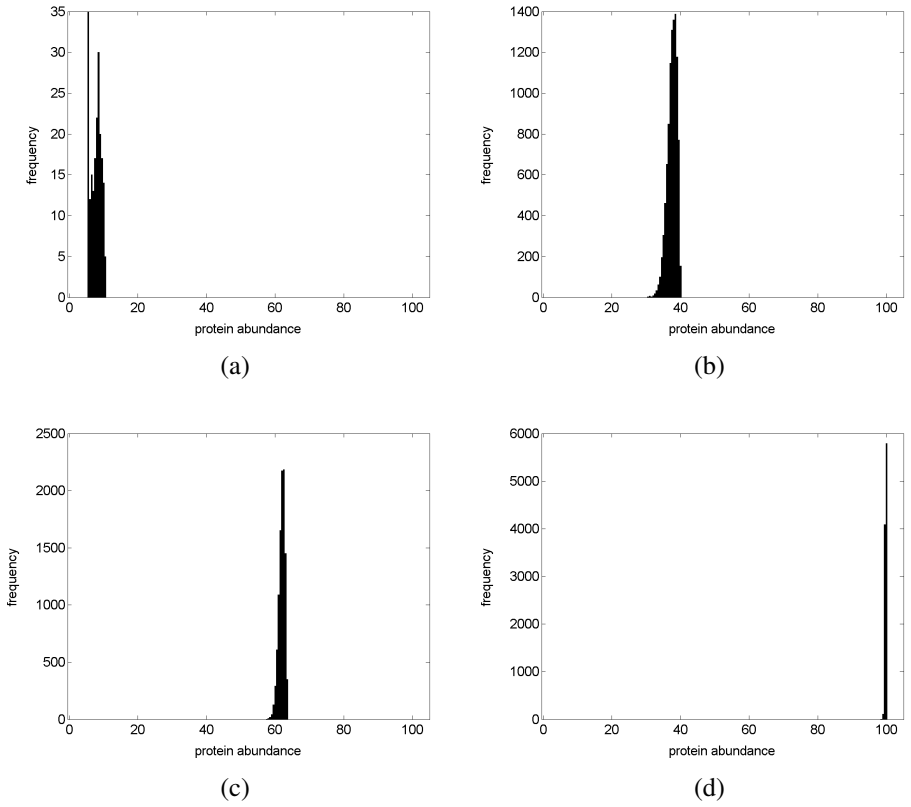


Figure 2.33: Empirical distributions of the protein concentrations of Model III for four different lengths of simulations. Each simulation starts at $x_0 = (i, z_0) = (0, 1)$ and runs for (a) 10, (b) 50, (c) 100, and (d) 1000 time units. The synthesis rates are $\alpha_0 = 0.5$ and $\alpha_1 = 1$. The remaining parameters are the same as for Figure 2.30.

time length	10	50	100	1000
$< X >$	7.61	37.51	61.91	99.75
$\sigma^2(X)$	2.13	2.0311	0.81	0.03

Table 2.11: Empirical distribution parameters for four different simulation lengths of the autocatalytic process with positive basal transcription rate.

length of 10 time units the distribution is bimodal with one peak around five and with a second peak around ten expression levels, Figure 2.33(a). Hence, as one would expect, compared to the pure autocatalytic system, even during a short period all cells exhibit expression. An increase of the simulation period to 50 time units makes the distribution unimodal and shifts the distribution peak to a value

between 35 and 40 expression levels, see Figure 2.33(b). A further increase of the time length to 100 leads to a further shift of the distribution mode to a value around 60, Figure 2.33(c). If the simulations run 1000 time units all cells express the gene product at maximal expression levels around 100, which is reflected by a small variance, see Figure 2.33(d) and Table 2.11. Hence, since transcription is always turned on, the present gene product causes the genes to be in their active state most of the time, which leads to a small distribution peak at expression levels which depend on the simulation period. Furthermore, a comparison of the empirical with the theoretical central moments shows that the system has indeed reached its stationary distribution in a period of 1000 time units. For the given parameter values we find $\mathbb{E}(X) = 99.75$ and $\mathbb{V}(X) = 0.025$.

Initial concentration dependency

If the simulation runs for different initial concentration values, the situation changes. Neither a binary nor a graded behavior is observed. Since expression always takes place independently of the initial concentration, during a time length of 500 time units more or less all cells have reached their maximal expression level of 100, see Figure 2.36. This is reflected in a very small variance lying between 0.02 and 0.03 for all initial values, see Table 2.12.

initial concentration	0.005	0.05	0.5	5
$< X >$	99.04	99.04	99.04	99.09
$\sigma^2(X)$	0.02	0.03	0.03	0.02

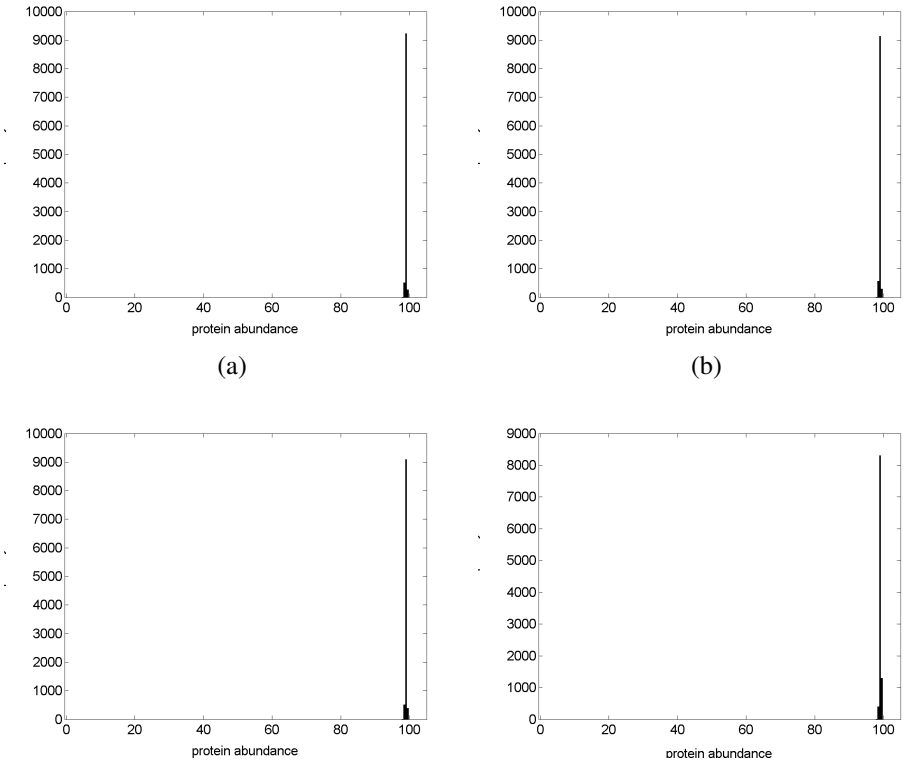
Table 2.12: Empirical distribution parameters for four different initial concentrations of the autocatalytic process with positive basal transcription rate.

Model IV: Autocatalysis with positive basal activation rate

In the two branches, the autocatalytic process with positive basal activation rates evolves like the pure autocatalytic process given by equations (2.53). The survival function of the off-branch reads

$$R(t) = \exp\left(-(\kappa_0 t + \frac{\kappa_1 z_n}{\gamma}(1 - \mathrm{e}^{-\gamma t}))\right).$$

Hence, the process will jump back to the on-branch almost surely, and we can apply the results of Theorem 2.3.1 to find its stationary distribution.



(a) (b) (c) (d)

Figure 2.34: Empirical distributions of the protein concentrations of Model III for four different initial protein concentrations. The simulations start in the off-branch with initial concentration equal to (a) 0.005, (b) 0.05, (c) 0.5, and (d) 5. The parameters are the same as the one used in Figure 2.33.

Theorem 2.3.4. *Let X_t be the PDMP for the autocatalytic network with positive basal activation rate. The stationary distribution of the gene product ξ_t is given by*

$$\rho(z) = K(\gamma z)^{a-1}(\alpha - \gamma z)^{b-1}\mathrm{e}^{\frac{\kappa_1}{\gamma}z}, \tag{2.58}$$

with

$$K = \frac{\gamma}{\alpha}\frac{\Gamma(a+b)}{\Gamma(a)\Gamma(b)}\frac{1}{{}_1F_1\left(a, a+b, c\right)}, \tag{2.59}$$

where $a = \kappa_0/\gamma,\ b = \kappa_{-1}/\gamma,\ c = \kappa_1\alpha/\gamma^2$. The expectation $\mathbb{E}(\xi_t)$ and the variance $\mathbb{V}(\xi_t)$ of the stationary distribution read

$$\mathbb{E}(\xi_t) = \frac{\alpha}{\gamma}\frac{a}{a+b}\frac{{}_1F_1(a+1, a+b+1, c)}{{}_1F_1(a, a+b, c)}, \tag{2.60}$$

and

$$\mathbb{V}(\xi_t) = \frac{\alpha^2}{\gamma^2}\frac{a}{a+b}\left(\frac{a+1}{a+b+1}\frac{{}_1F_1(a+2,a+b+2,c)}{{}_1F_1(a,a+b,c)}\right. \tag{2.61}$$

$$\left.-\frac{a}{a+b}\frac{{}_1F_1^2(a+1,a+b+1,c)}{{}_1F_1^2(a,a+b,c)}\right). \tag{2.62}$$

The proof of above theorem is similar to the one of Theorem 2.3.3 and therefore omitted.

Time dependency

Simulations of the autocatalytic process with positive activation rate for different simulation periods yield a distribution very similar to the one of a pure autocatalytic process. The basal activation rate leads only to a marginal decrease of the holding time in the deactivated state. Thus, below a critical time length the distribution is bimodal with one mode at zero and the other at the maximal possible expression level, see Figure 2.35(a) - (c). The minimal and the maximal expression levels are the most frequent. The remaining cells show intermediate expression levels. As for the pure autocatalytic network, a longer simulation period leads to higher maximal expression levels and to a greater number of cells showing expression. This can also be seen in an increase of the mean value of the protein concentration, see Table 2.13. If the simulation period is equal to 1000 time units, all cells are in their maximal expression state. Again, a comparison with the theoretical values shows that the system has almost reached its stationary distribution. The central moments read $\mathbb{E}(X) = 99.5$ and $\mathbb{V}(X) = 0.1$. As for the pure autocatalytic process, such a binary behavior cannot be seen by looking at the expression of the whole population. The empirical mean of the distribution increases gradually for increasing time lengths, see Table 2.13. Hence, due to an increased chance of being activated, the only difference to the pure autocatalytic network is that, in the given simulation periods, a little more cells have turned their expression on.

time length	10	50	100	1000
$< X >$	3.18	26.99	53.54	99.50
$\sigma^2(X)$	9.83	138.22	144.98	0.11

Table 2.13: Empirical distribution parameters for four different simulation lengths of the autocatalytic process with positive basal transcription rate.

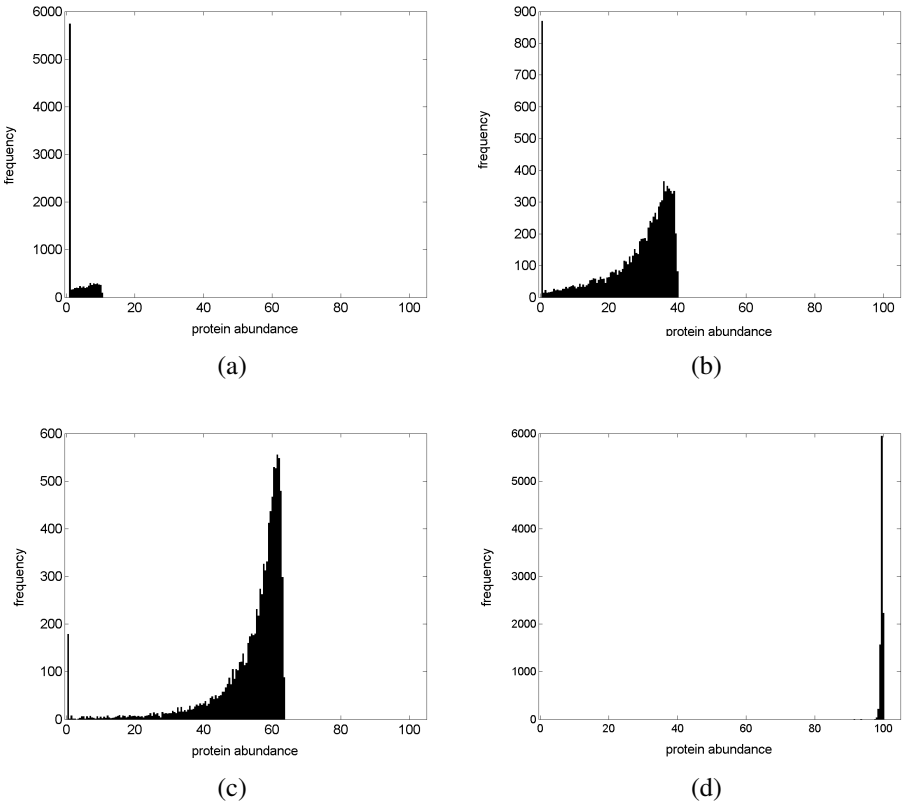


Figure 2.35: (a)-(d) Empirical distributions of the protein concentrations of Model IV for four different lengths of simulations. The simulations start at $x_0 = (i, z_0) = (0, 1)$ and run for (a) 10, (b) 50, (c) 100, and (d) 1000 time units. The turning on rates are $\kappa_0 = 0.01$ and $\kappa_1 = 0.05$. The remaining parameters are the same as for Figure 2.30.

Initial concentration dependency

On the other hand, simulation with different initial concentrations results in distributions similar to the ones obtained for an autocatalytic process with basal transcription rate. More or less all cells have approached their maximal expression levels in the given time length. However, if the process starts at small initial protein concentrations equal to 0.005 and 0.05, a very small subpopulation is still in the off state, Figure 2.36(a) and (b). This is reflected in a high variance of the two populations, see Table 2.14. When the initial concentration is increased to a value equal to 0.5 or higher, the variance decreases drastically. Now all cells exhibit expression levels around the maximal expression value, Figure 2.36(c) and (d). Hence, for small inducer amounts the system needs more time to reach its

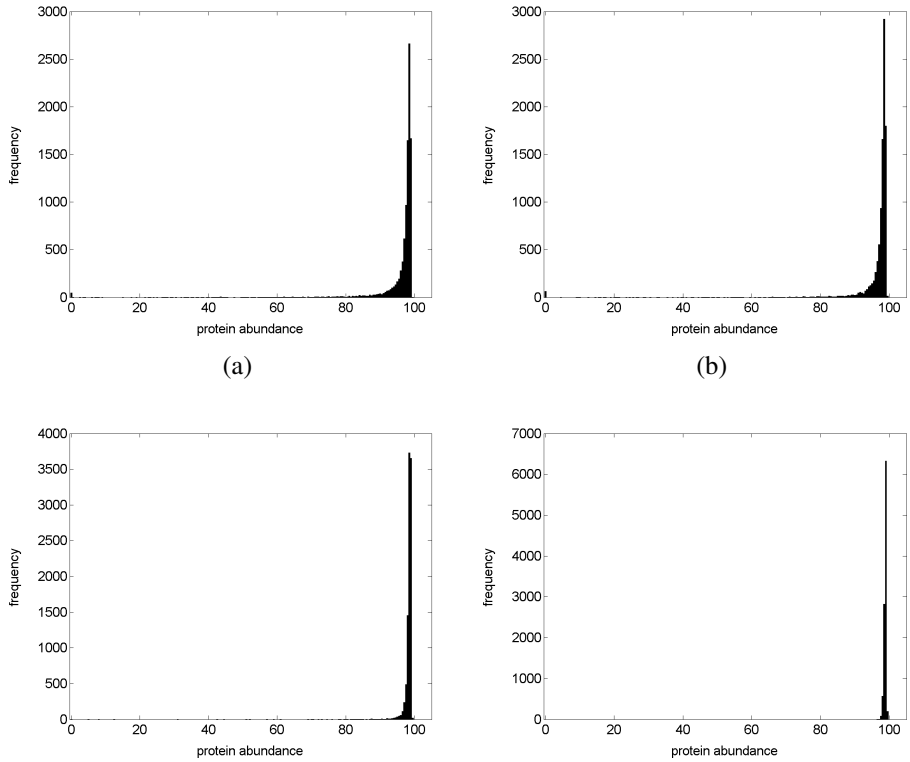


Figure 2.36: (a)-(d) Empirical distributions of protein concentrations of Model IV for four different initial protein concentrations. The simulations start in the off-branch with initial concentration equal to (a) 0.005, (b) 0.05, (c) 0.5, and (d) 5. The parameters are the same as the one used in Figure 2.35.

stationary distribution.

initial concentration	0.005	0.05	0.5	5
$< X >$	95.65	96	98.24	98.81
$\sigma^2(X)$	97.62	101.26	8.5	0.11

Table 2.14: Empirical distribution parameters for four different initial concentrations of the autocatalytic process with positive basal transcription rate.

2.3.5 Discussions and Conclusions

We propose PDMPs as an alternative approach to modeling gene regulatory networks. Such a model is an appropriate approach when some of the reactants occur in small numbers whereas the others are present in high numbers. In particular this is the case for many genetic regulatory networks where genes are typically present only in one or two copies. In such an approach, species occurring in small numbers are modeled as discrete entities while species occurring in high numbers are described by concentrations. Transitions between discrete entities are modeled in a random fashion whereas the kinetics of the continuous variables are modeled in a deterministic manner. In the present section we focussed on small autocatalytic genetic networks consisting of a positive feedback loop, in which a gene is activated by its own gene product.

We considered three types of autocatalytic networks: A pure autocatalytic network, a network with positive basal transcription rate, and a network with positive basal activation rate. For all three networks we determined the dual operators of the corresponding infinitesimal generators. It turns out that the equations of a one-dimensional correlated random walk arise from the stationary conditions on the dual operators. Hence, using a PDMP links modeling of genetic networks with a subfield of the theory of population dynamics in a quite natural way. Furthermore, for each system of equations we determined its unique solution. If this solution can be normalized, it is the stationary solution of the corresponding autocatalytic network. We have shown that this is the case for the autocatalytic network with positive basal transcription rate as well as for the system with positive basal activation rate. Furthermore we analyzed the empirical distribution for each network for four different simulation lengths and for four different initial product concentrations.

We showed that the solution of the correlated random walk for the pure autocatalytic network cannot be normalized, implying that the stationary distribution cannot have a density. The reason for this is that the sojourn time in the deactivated state can reach infinity. This suggests that the stationary distribution is concentrated at zero. We proved that the point measure at zero is indeed the only stationary distribution of the process. A numerical analysis of the empirical distribution revealed that the process may in general be far away from being in its stationary distribution. Simulation for four different time lengths results in a bimodal distribution with one mode at very low expression levels, and one at high expression levels. As long as the distribution is bimodal, all intermediate expression levels are also adopted. The bimodal distribution turns into a unimodal distribution, located at the maximal expression level, if the simulation period reaches a certain threshold. A similar behavior was obtained for different initial concentration values. Below a certain threshold of the initial values, the system shows a

binary response. Again, the distributions are bimodal with one peak at very low expression levels, and the other is located at the maximal expression level. In contrast to the case of different simulation lengths, now there are no intermediate expression levels. There are only two subpopulations present. Either all cells have turned their expression on or off. Both situations cannot be observed by looking only at the total population. The mean value of the protein concentration increases gradually for increasing time lengths and increasing initial protein concentrations. This finding was confirmed by an analysis of the extinction behavior of the process. We determined closed expressions for the expected first jump time and the corresponding expected change in concentration for the cases when the process starts in the on and off state. If the process starts in the off state, it is more reasonable to condition on the event that the first jump time is finite. In this case it will have at least two jumps. This period is quite a good candidate for the time scale of the process which we called an excursion. We have shown that the probability of extinction is mainly governed by the first excursion. After the first excursion the probability rapidly becomes very small, and nearly all of the sample paths will reach their maximal values. Then the time of extinction is beyond the lifespan of any living organism, and hence it is justified to call such a stadium a quasi steady state.

For the autocatalytic process with positive basal transcription rate, the solution of the correlated random walk can be normalized. The density and the first two central moments can be given in a closed analytic form. A numerical analysis of the empirical distribution exhibits a different behavior, compared to the one of the pure autocatalytic process. For different simulation lengths the distribution is, except for short time lengths, unimodal with a small width and exhibits a graded response, i.e., for longer simulation periods the modes are located at higher expression levels. If the simulation period reaches a certain length, the process has reached its stationary distribution, and more or less all cells exhibit maximal expression levels. Hence, for such a system the individual cells show a similar behavior as the total population does. This is also true for different initial protein concentrations. Independent of the initial concentrations, all cells have arrived at their maximal expression level in the given simulation period. Thus, if a gene is regulated by a positive feedback loop with positive basal transcription rate, a population of cells reflects, in good approximation, the average behavior of an individual cell. This is true for different expression periods as well as for different initial inducer amounts.

Furthermore, we determined the density of the stationary distribution of the autocatalytic process with positive basal activation rate. This density is also the solution of the equations of the corresponding correlated random walk. The density as well as the first two central moments could be given in a closed analytic form. An analysis of the empirical distribution showed a compounded behavior. For

different time lengths, the system behaves very similar as the pure autocatalytic system. If the simulation lengths are below a certain time length, the distribution is bimodal with one mode at low and the other at high expression levels. The only difference to the pure autocatalytic network is that now more cells have turned their expression on in a given simulation period. On the other hand, for different initial concentration values, the system behaves quite similarly to the autocatalytic process with positive basal transcription rates. Most of the cells exhibit expression at high expression levels resulting in a distribution which is nearly unimodal.

To summarize, by modeling only the promoter transitions as discrete stochastic events we could determine the stationary distribution of three different autocatalytic networks. Despite the simplified nature of the model we could show that different promoter actions will lead to different expression profiles. A pure autocatalytic network shows a binary response in relation to different time lengths and different initial inducer amounts. An autocatalytic network with positive basal transcription rate exhibits a totally different expression profile. If the gene possesses a basal and an excited state there is always enough gene product present which leads to the situation that the gene is mostly in its excited state. This leads to a sharp unimodal expression profile. For increasing time lengths, the mode is shifted gradually to higher expression levels. For increasing initial inducer amounts, the cells are always in their maximal expression state provided that the time period is long enough. If the gene product does not enhance the transcription rate but the chance of being activated, the network behaves like a pure autocatalytic system for increasing time periods, and like a system with positive basal transcription rate for different initial concentrations. Hence, our findings suggest that if a cell population should respond in a binary fashion, its promoter should be of the form of an autocatalytic system or of a network with positive basal activation rate. On the other hand, a regulatory system with positive basal transcription rates is advantageous if the whole cell population should respond precisely in time and independently of the initial inducer amount.

Since we have considered genes with one binding site in their regulatory region and gene products which are present as monomers, our findings cannot be observed by modeling such networks in a purely deterministic manner. In such a case one would always observe a gradual behavior. On the other hand, a bimodal expression pattern is seen only for a pure autocatalytic network in its quasi steady state. One reason for this might be the fact that the gene products are present only as monomers. If they would form multimers, we might find further bimodal expression patterns. This would be in accordance with the deterministic theory, where multimodal expression profiles can only be observed for systems with positive cooperativity.

Expressions similar to those we have found in our simulations for the time dependency of the pure autocatalytic network and the system with positive basal

activation rate were also be found in experiments in the literature, [74], [104]. Similar expression profiles as we have seen in our simulations for initial concentration dependency were also found in [8] and [74]. Unfortunately, we have not found expression profiles similar to the ones for the initial concentration dependency of the system with positive basal activation rate, and for the time and initial concentration dependency of the system with positive basal transcription rate.
For the biological network studied in [74] our simulations suggest that the underlying promoter is of the type of the pure autocatalytic network, since the experimental expression profiles for different inducer amounts differ strongly from the one we have found for the autocatalytic network with basal activation rate for different initial concentration values. Since there are only time dependent expression profiles for the promoter studied in [104] available, we cannot decide if it is more probable that the underlying promoter is of the type as in the pure autocatalytic network, or as in the the system with positive basal activation rate. For the biological network studied in [8] our simulations suggest that its promoter is probably of the type as in the pure autocatalytic network, since this is the only system which exhibits a bimodal expression profile for increasing inducer amounts. However, we cannot give a final answer, since we do not know which type of promoter underlies the positive feedbacks in above mentioned biological networks. There might be also further mechanisms which influence the expression. For instance, the comK proteins of *Bacillus subtilis* form tetramers which bind to their respective binding sites, whereas in our models transcription is activated by monomers. Nevertheless, by our results it should be possible to classify different promoters on the basis of their behavior. Moreover, since the parameters in our models are directly interpretable, such models are appropriate to make predictions on the behavior of such autocatalytic systems when one of the parameter is changed by mutations.

2.3.6 Appendix: Proofs of the Theorems

In the following we will present the missing proofs of the theorems and propositions from the previous sections.

Appendix A: Stationary Distributions

We start with the proof that the equation system of the correlated random walk is given by the dual operator of the corresponding infinitesimal generators and with the proof of the respective solutions.

Proof of Theorem 2.3.1. *(1)* According to equation (2.36) the generator is given

by

$$\begin{aligned} Gf\,(0,z) &= v^{(0)}(z)f_z(0,z) + \lambda(0,z)\big(f(1,z) - f(0,z)\big), \\ Gf\,(1,z) &= v^{(1)}(z)f_z(1,z) + \lambda(1,z)\big(f(0,z) - f(1,z)\big). \end{aligned}$$

Let ρ denote the sum of $\rho(z) = \rho(0,z)$ and $\rho(1,z)$. A stationary solution is characterized by the condition $G^*\rho_t(z) = 0$. From

$$\begin{aligned} < Gf, \rho > &= \int_0^\infty f(0,z)\big(\lambda(1,z)\rho(1,z) - \lambda(0,z)\rho(0,z)\big)\mathrm{d}z \\ &\quad + \int_0^\infty f(1,z)\big(\lambda(0,z)\rho(0,z) - \lambda(1,z)\rho(1,z)\big)\mathrm{d}z \\ &\quad + \int_0^\infty f_z(0,z)v^{(0)}(z)\rho(0,z)\mathrm{d}z + \int f_z(1,z)v^{(1)}(z)\rho(1,z)\mathrm{d}z \end{aligned}$$

we reason that $\rho(0,z)$ and $\rho(1,z)$ have to be weak differentiable. Furthermore, if $v^{(0)}(z) = \alpha_0 - \gamma z$ and $v^{(1)}(z) = \alpha_1 - \gamma z$, both $\rho(0,z)$ and $\rho(1,z)$ have to vanish at $z = 0$. If $v^{(0)}(z) = -\gamma z$ and $v^{(1)}(z) = \alpha - \gamma z$, $\rho(1,z)$ has to be equal to zero at $z = 0$. Then we obtain for G^* the formula

$$\begin{aligned} G^*\rho(0,z) &= -\partial_z\big(v^{(0)}(z)\rho(0,z)\big) + \lambda(1,z)\rho(1,z) - \lambda(0,z)\rho(0,z), \\ G^*\rho(1,z) &= -\partial_z\big(v^{(1)}(z)\rho(1,z)\big) + \lambda(0,z)\rho(0,z) - \lambda(1,z)\rho(1,z). \end{aligned}$$

From the stationary condition we find by adding the first and the second equation, and by integration that

$$v^{(0)}(z)\rho(0,z) + v^{(1)}(z)\rho(1,z) = C \tag{2.63}$$

for a constant C. Since either $\rho(0,0) = \rho(1,0) = 0$ or $\rho(1,0) = v^{(0)}(0) = 0$ we obtain $C = 0$. Thus

$$v^{(0)}(z)\rho(0,z) = -v^{(1)}(z)\rho(1,z). \tag{2.64}$$

From the last equation we obtain for $v^{(0)}(z) = \alpha_0 - \gamma z,\ v^{(1)}(z) = \alpha_1 - \gamma z$ that

$$\rho(0,z) = -\frac{\alpha_1 - \gamma z}{\alpha_0 - \gamma z}\rho(1,z) \tag{2.65}$$

which is valid for all $z \neq \frac{\alpha_0}{\gamma}$. Since $\rho(0,z), \rho(1,z) \geq 0$, we conclude that $\frac{\alpha_0}{\gamma} < z \leq \frac{\alpha_1}{\gamma}$. From equation (2.64) we obtain the boundary conditions

$$\rho(1, \frac{\alpha_0}{\gamma}) = \rho(0, \frac{\alpha_1}{\gamma}) = 0. \tag{2.66}$$

If $v^{(0)}(z) = -\gamma z$ and $v^{(1)}(z) = \alpha - \gamma z$ we receive

$$\rho(0,z) = \frac{\alpha - \gamma}{\gamma z}\rho(1,z) \tag{2.67}$$

which is valid for all $z \neq 0$. Again, since $\rho(0,z), \rho(1,z) \geq 0$ we obtain $z \leq \frac{\alpha}{\gamma}$ and from (2.64) we conclude

$$\rho(0, \frac{\alpha}{\gamma}) = 0. \tag{2.68}$$

(2) 1. The proof of this assertion works in the same way as the proof for the autocatalytic system with positive basal transcription rate by setting $\alpha_0 = 0$ and $\alpha_1 = \alpha$ which is why we skip it.
2. Let $\lambda(0,z) = \kappa_1 z,\ \lambda(1,z) = \kappa_{-1}$ and $v^{(0)}(z) = \alpha_0 - \gamma z,\ v^{(1)}(z) = \alpha_1 - \gamma z$. Replacing $\rho(0,z)$ in $G^*\rho(0,z) = 0$ by (2.65) we obtain

$$\rho_z(1,z) = \left(\frac{\gamma - \kappa_{-1}}{\alpha_1 - \gamma z} - \frac{\kappa_1 z}{\alpha_0 - \gamma z}\right)\rho(1,z)$$

which is valid for all $\frac{\alpha_0}{\gamma} < z < \frac{\alpha_1}{\gamma}$. Solving this equation for an initial value $\rho(1,z_0)$ we obtain equation system (2.50).
3. In the same way we conclude for $\lambda(0,z) = \kappa_0 + \kappa_1 z,\ \lambda(1,z) = \kappa_{-1}$ and $v^{(0)}(z) = -\gamma z,\ v^{(1)}(z) = \alpha - \gamma z$ that $\rho(1,z)$ is given as a solution of

$$\rho_z(1,z) = \left(\frac{\kappa_0 + \kappa_1 z}{\gamma z} + \frac{\gamma - \kappa_{-1}}{\alpha - \gamma z}\right)\rho(1,z)$$

for all $0 < z < \frac{\alpha}{\gamma}$. Thus, for $z_0 \in (0, \frac{\alpha}{\gamma})$ we find the desired equations (2.51).

□

Appendix B: Pure Autocatalytic Networks

To show that $\delta_{(0,0)}$ is the only stationary probability measure we need the following lemma. Therefore we introduce the functions

$$\begin{aligned} p(b,h) &= \exp\left(-\frac{\kappa b}{\gamma}\left(1 - e^{-\gamma h}\right)\right), \\ q(a,b) &= \exp\left(-\frac{\kappa}{\gamma}(b-a)\right) \end{aligned}$$

for $0 < a < b$ and $h > 0$. Then, the probability that the pure autocatalytic process is in a certain interval of the off-branch can be estimated as follows.

Lemma 2.3.2. *Let $0 \leq a \leq b$, and $(X_t)_{t\geq 0}$ be the pure autocatalytic PDMP. Then it holds that*

$$\mathbb{P}\big(X_{t+h} \in \{0\} \times (ae^{-\gamma h}, be^{-\gamma h}]\big) \geq p(b,h)\mathbb{P}\big(X_t \in \{0\} \times (a,b]\big),$$

for all $h > 0$.

Proof. If the process is at $(0,z)$ at time t_0 and does not jump during the time interval $[t, t+h]$, then it is at $ze^{-\gamma h}$ at time $t+h$. From (2.54) we know that the probability that no jumps will occur in this time interval is given by

$$\mathbb{P}\big(\text{no jump}|X_t = (0,z)\big) = \exp\left(-\frac{\kappa z}{\gamma}\left(1 - e^{-\gamma h}\right)\right).$$

With this we obtain the following estimate for all $a \leq x \leq b$:

$$\mathbb{P}\big(\text{no jump}|X_{t_0} \in \{0\} \times [a,b]\big) \geq \exp\left(-\frac{\kappa b}{\gamma}\left(1 - e^{-\gamma h}\right)\right) = p(b,h).$$

□

With this result we can show now that each half-open interval of the off-branch has measure zero with respect to the stationary distribution from which the statement of Theorem 2.3.2 follows immediately.

Proof of Theorem 2.3.2. Let $\mu = (\mu_0, \mu_1)$ be an invariant probability on $\{0,1\} \times [0,\infty)$ and $0 < a < b$. Let

$$\varepsilon = \mu_0\big((a,b]\big) = \mathbb{P}\big(X_t \in \{0\} \times (a,b]\big),$$

where $(X_t)_{t\geq 0}$ denotes the PDMP started from this invariant distribution μ. Let $h = \frac{1}{\gamma}(\log b - \log a)$, $b_1 = e^{-\gamma h}b = a$, $a_1 = e^{-\gamma h}a$. By the Lemma, we have

$$\mu_0\big((a_1,b_1]\big) = \mathbb{P}(X_{t+h} \in \{0\} \times (a_1,b_1]) \geq \mu_0((a,b])p(b,h) = \varepsilon q(a,b).$$

Define $b_n = e^{-n\gamma h}b$ and $a_n = e^{-n\gamma h}a$ for $n \geq 1$ and note $b_n = a_{n-1}$. By induction, we have

$$\begin{aligned}\mu_0(]a_n,b_n]) &\geq \varepsilon q(a,b)q(a_1,b_1)\cdots q(a_{n-1},b_{n-1}) \\ &= \varepsilon \exp\left(-\frac{\kappa}{\gamma}(b - a_{n-1})\right) = \varepsilon \exp\left(-\frac{\kappa b}{\gamma}(1 - e^{-n\gamma h})\right)\end{aligned}$$

for all $n \geq 1$. Since the intervals are disjoint, we get

$$\mu_0\big((0,a]\big) = \sum_{n=1}^{\infty} \mu_0\big((a_n,b_n]\big) \geq \varepsilon \sum_{n=1}^{\infty} \exp\left(-\frac{\kappa b}{\gamma}(1 - e^{-n\gamma h})\right).$$

But since the sum diverges, this is only possible if $\varepsilon = 0$. We have shown that

$$\mu_0\big((a,b]\big) = 0$$

for all $0 < a < b$. From this we immediately get $\mu_1((a,b]) = 0$ for all $0 \leq a < b$, and finally $\mu = (\delta_0, 0)$, i.e. the measure μ is concentrated in $(0,0)$. □
Next we prove the relations for the conditional expectations of the first and second jump times and the corresponding changes for the concentrations.

Proof of Proposition 2.3.1. *1. (a)* This follows immediately from the density of the distribution of the first jump time which is given by

$$f^{(1)}_{\tau_1}(t) = \kappa_{-1} e^{-\kappa_{-1} t} \mathbb{1}_{[0,\infty)}(t). \tag{2.69}$$

(b) The flow of the pure autocatalytic system reads $z(t) = \frac{\alpha}{\gamma} + (z_0 - \frac{\alpha}{\gamma})\mathrm{e}^{-\gamma t}$. Together with (2.69) we find for the expected change in concentration taken place until the first jump occurs that

$$\begin{aligned}
\mathbb{E}(\xi_{\tau_1} - \xi_0 | X_0 = (1, z_0)) &= \int_0^\infty (z(t) - z_0)\kappa_{-1} e^{-\kappa_{-1} t} \mathrm{d}t \\
&= \int_0^\infty \left(\frac{\alpha}{\gamma} + (z_0 - \frac{\alpha}{\gamma}) e^{-\gamma t} - z_0 \right) \kappa_{-1} e^{-\kappa_{-1} t} \mathrm{d}t \\
&= (\frac{\alpha}{\gamma} - z_0) \frac{\gamma}{\gamma + \kappa_{-1}}.
\end{aligned}$$

2. (a) By equation (2.55) we already know that with positive probability no further jump occurs. Hence, the expected time until the first jump occurs achieves infinity.
(b) The absolutely continuous part of the distribution of τ_1 given that $X_0 = (0, z_0)$ has density

$$f^{(0)}_{\tau_1}(t) = \kappa_1 z_0 e^{-\gamma t} \exp\left(-\frac{\kappa_1 z_0}{\gamma} (1 - e^{-\gamma t}) \right). \tag{2.70}$$

With this we find for the expected change in concentration

$$\begin{aligned}
&\mathbb{E}(\xi_{\tau_1} - \xi_0 | X_0 = (0, z)) \\
&= -z_0 e^{-\kappa_1 z_0/\gamma} + \frac{\kappa_1 z_0^2}{\gamma} e^{-\kappa_1 z_0/\gamma} \int_0^1 (u-1) \exp\left(\frac{\kappa_1 z_0}{\gamma} u \right) \mathrm{d}u \\
&= -z_0 e^{-\kappa_1 z_0/\gamma} + \frac{\kappa_1 z_0^2}{\gamma} e^{-\kappa_1 z_0/\gamma} \left(\frac{\gamma}{\kappa_1 z_0} - \frac{\gamma^2}{(\kappa_1 z_0)^2} e^{\kappa_1 z_0/\gamma} + \frac{\gamma^2}{(\kappa_1 z_0)^2} \right) \\
&= \frac{\gamma}{\kappa_1} \left(e^{-\kappa_1 z_0/\gamma} - 1 \right).
\end{aligned}$$

(c) The expectation of the first jump time conditioned on that the process has another jump in finite time is given by

$$\begin{aligned}
&\mathbb{E}\big(\tau_1\big|X_0=(0,z_0),\tau_1<\infty\big)\\
&\quad= \kappa_1 z_0\frac{\exp(-\kappa_1 z_0/\gamma)}{1-\exp(-\kappa_1 z_0/\gamma)}\int_0^\infty t\mathrm{e}^{-\gamma t}\exp\left(\frac{\kappa_1 z_0}{\gamma}\mathrm{e}^{-\gamma t}\right)\mathrm{d}t\\
&\quad= \frac{\kappa_1 z_0}{\gamma^2}\frac{\exp(-\kappa_1 z_0/\gamma)}{1-\exp(-\kappa_1 z_0/\gamma)}\int_0^1 \ln(u)\exp\left(\frac{\kappa_1 z_0}{\gamma}u\right)\mathrm{d}u.
\end{aligned}$$

The integral $I(\kappa_1,\gamma,z_0) := -\int_0^1 \ln(t)\exp(\frac{\kappa_1 z_0}{\gamma}t)\mathrm{d}t$ in the last equation is not analytical solvable but converges and thus can be computed numerically.
(d) For the expected change in concentration at the first jump given that the first jump time is finite we find

$$\begin{aligned}
&\mathbb{E}(\xi_{\tau_1}-\xi_0|X_0=(0,z),\tau_1<\infty)\\
&\quad= \int_0^\infty (z_0e^{-\gamma t}-z_0)\kappa_1 z_0\frac{\exp(-\kappa_1 z_0/\gamma)}{1-\exp(-\kappa_1 z_0/\gamma)}e^{-\gamma t}\exp\left(\frac{\kappa_1 z_0}{\gamma}\mathrm{e}^{-\gamma t}\right)\mathrm{d}t\\
&\quad= \kappa_1 z_0^2\frac{\exp(-\kappa_1 z_0/\gamma)}{1-\exp(-\kappa_1 z_0/\gamma)}\left(\frac{1}{\kappa_1 z_0}-\frac{\gamma}{(\kappa_1 z_0)^2}e^{\kappa_1 z_0/\gamma}+\frac{\gamma}{(\kappa_1 z_0)^2}\right).
\end{aligned}$$

(e) The relation for the expected time of the second jump is received by

$$\begin{aligned}
&\mathbb{E}\left(\tau_2|X_0=(0,z_0),\tau_1<\infty\right)\\
&\quad= \int_0^\infty\int_0^\infty (t_2+t_1)\mathrm{d}\mathbb{P}_{\tau_2|X_0=(1,z_0\mathrm{e}^{-\gamma t_1})}(t_2)\mathrm{d}\mathbb{P}_{\tau_1|X_0=(0,z_0),\tau_1<\infty}(t_1)\\
&\quad= \mathbb{E}\left(\tau_1|X_0=(1,z_0\mathrm{e}^{-\gamma t_1})\right)+\mathbb{E}(\tau_1|X_0=(0,z_0),\tau_1<\infty).
\end{aligned}$$

(f) The expected concentration at the second jump time conditioned on that the first jump time is given by

$$\begin{aligned}
&\mathbb{E}\left(\xi_{\tau_2}|X_0=(0,z_0),\tau_1<\infty\right)\\
&\quad= \int_0^\infty\int_0^\infty\left(\frac{\alpha}{\gamma}+(\mathrm{e}^{-\gamma t}z_0-\frac{\alpha}{\gamma})\mathrm{e}^{-\gamma t'}\right)\kappa_{-1}\mathrm{e}^{-\kappa_{-1}t'}\frac{\kappa_1 z_0}{1-\mathrm{e}^{-\kappa_1 z_0/\gamma}}\mathrm{e}^{-\gamma t}\\
&\qquad\times\exp\left(-\frac{\kappa_1 z_0}{\gamma}(1-\mathrm{e}^{-\gamma t})\right)\mathrm{d}t'\mathrm{d}t\\
&\quad= \frac{\kappa_1 z_0}{\gamma(1-\mathrm{e}^{-\kappa_1 z_0/\gamma})}\left(\frac{\alpha}{\gamma\kappa_1 z_0}(1-\mathrm{e}^{-\kappa_1 z_0/\gamma})+\frac{\kappa_{-1}}{\gamma(\gamma+\kappa_{-1})\kappa_1^2 z_0}\right)\\
&\qquad\times\left(z_0\gamma\kappa_1-\gamma^2-\alpha\kappa_1+(\gamma^2+\alpha\kappa_1)\mathrm{e}^{-\kappa_1 z_0/\gamma}\right).
\end{aligned}$$

□

Appendix C: Autocatalytic Network with Positive Basal Transcription Rate

We come to the proof of the formula of the density of the stationary distribution, and their first two central moments of an autocatalytic system with positive basal transcription rate.

Proof of Theorem 2.3.3. According to Theorem 2.3.1 the solution of the corresponding random walk is given by

$$\rho(z) = \rho(1,z_0)\mathrm{e}^{\frac{\kappa_1}{\gamma}(z-z_0)}(\alpha_1-\alpha_0)\frac{(\gamma z-\alpha_0)^{\frac{\alpha_0\kappa_1}{\gamma^2}-1}}{(\gamma z_0-\alpha_0)^{\frac{\alpha_0\kappa_1}{\gamma^2}}}\left(\frac{\gamma z-\alpha_1}{\gamma z_0-\alpha_1}\right)^{\frac{\kappa_{-1}}{\gamma}-1}$$

for some $z_0 \in (\alpha_0/\gamma, \alpha_1/\gamma)$. Let a, b, c and u be defined as above and $K = \rho(1,z_0)\exp(-\kappa_1 z_0/\gamma)(\alpha_1-\alpha_0)(\gamma z_0-\alpha_0)^{-a}(\gamma z_0-\alpha_1)^{1-b}$. To obtain a probability distribution K must fulfill

$$\begin{aligned} & K\int_{\alpha_0/\gamma}^{\alpha_1/\gamma}(\frac{\gamma z}{\alpha_1}-u)^{a-1}(1-\frac{\gamma z}{\alpha_1})^{b-1}\mathrm{e}^{c\frac{\gamma z}{\alpha_1}}\mathrm{d}z \\ &= K\frac{\alpha_1}{\gamma}\frac{\Gamma(a)\Gamma(b)}{\Gamma(a+b)}\mathrm{e}^{cu}\left(\frac{1}{1-u}\right)^a(1-u)^{b-1}{}_1F_1(a,a+b,c(1-u)) = 1. \end{aligned}$$

Set

$$H = \frac{\Gamma(a)\Gamma(b)}{\Gamma(a+b)}\left(\frac{1}{1-u}\right)^a(1-u)^{b-1}\mathrm{e}^{cu}.$$

Then, for the expectation we find

$$\begin{aligned} \mathbb{E}(\xi_t) &= K\int_{\alpha_0/\gamma}^{\alpha_1/\gamma} z(\frac{\gamma z}{\alpha_1}-u)^{a-1}(1-\frac{\gamma z}{\alpha_1})^{b-1}\mathrm{e}^{c\frac{\gamma z}{\alpha_1}}\mathrm{d}z \\ &= K\left(\frac{\alpha_1}{\gamma}\right)^2 H\Big(u\,{}_1F_1(a,a+b,c(1-u)) \\ &\quad -(u-1)\frac{a}{a+b}{}_1F_1(a+1,a+b+1,c(1-u))\Big). \end{aligned}$$

The second moment is given by

$$\begin{aligned} \mathbb{E}(\xi_t^2) &= K\int_{\alpha_0/\gamma}^{\alpha_1/\gamma} z^2(\frac{\gamma z}{\alpha_1}-u)^{a-1}(1-\frac{\gamma z}{\alpha_1})^{b-1}\mathrm{e}^{c\frac{\gamma z}{\alpha_1}}\mathrm{d}z \\ &= K\left(\frac{\alpha_1}{\gamma}\right)^3 H\Big(u^2\,{}_1F_1(a,a+b,c(1-u)) \\ &\quad -(u-1)\frac{a}{a+b}\Big(2u\,{}_1F_1(a+1,a+b+1,c(1-u)) \\ &\quad -(u-1)\frac{a+1}{a+b+1}{}_1F_1(a+2,a+b+2,c(1-u))\Big)\Big). \end{aligned}$$

□

Conclusions

In the first part we investigated the dynamical behavior of the two genetic oscillators Hes1 and Hes7 which play a crucial role during somitogenesis in vertebrates. For the two genes it is commonly assumed that the binding activity in the respective promoters should be given by a Hill coefficient equal to two. This is based on the fact that both genes form dimers. However, for Hes1 this assumption leads to damped oscillations. One possible explanation would be that there is additional nonlinearity in the promoter. To address this issue, we modeled the promoter activity by response functions including the number of binding sites in the promoter. Then the Hill coefficient was estimated through approximation of the response functions by Hill functions. For the estimated Hill coefficient we found a value greater than the one commonly assumed in literature. For the underlying negative feedback loop of the Hes1 oscillator we used a Goodwin system. In contrast to delay differential equations (DDE), which are commonly used in literature, this allows a more explicit description of the intermediate processes during transcription and translation. Using our estimated value for the Hill coefficient we found that this increased value is not sufficient to explain the oscillatory behavior, which is in accordance to the DDE approach. Thus, our findings suggest that there must be some additional nonlinearity processes outside of the regulatory region.

Since the half lives of the Hes7 mRNA and protein differ from the one of Hes1, a Hill coefficient equal to two in a DDE system is sufficient to explain the oscillation of Hes7 with a period of two hours. However, using a similar approach to the Hes1 for estimating the promoter activity of Hes7 results again in an elevated value of the Hill coefficient. Applying this value to a DDE system from literature leads to a different oscillatory behavior. Our findings can no longer explain the experimental results that an elongation of the half life of the Hes7 protein leads to damped oscillations. Using our estimated value the DDE system still shows sustained oscillation with a period of two hours. Hence, as for the Hes1 oscillator, a more sophisticated model is required for the Hes7 oscillator. Since both genes are degraded via the ubiquitin pathway we proposed an ODE system including a Michaelis-Menten term describing the degradation of Hes7. Assuming that the mutation done in the experiments, which results in a decrease of the affinity of

Hes7 to ubiquitin, affects mainly the binding rate constants, we showed that this leads to an increase in the Michaelis-Menten constant. Thus we increased the Michaelis-Menten constant while keeping all other parameters fixed. In this case the system showed damped oscillations as observed in the experiment described in literature. Also not done so far, it should be not difficult to apply the same system with slight modifications to the Hes1 oscillator. Then it should be possible to achieve sustained oscillations for the value of the Hill coefficient estimated in the first section.

In the second part we proposed a novel approach to modeling gene regulatory networks. This approach is based on PDMPs introduced by Davis in 1984. It is a hybrid approach in the sense that the state variable of the process can be split in a discrete and a continuous variable. In the present setting we used the discrete variable to describe the random transitions between different states of the gene. The gene products were described deterministically by continuous variables.

In the first section of the second part, a simulation algorithm for PDMPs was presented and discussed. We applied this approach to an inducible gene where the inducers are present in constant amounts, to an autocatalytic network, once where the gene products are present as monomers and once where they are present as dimers, and to a toggle switch. Simulation of the stationary distribution of an inducible gene modeled once by a Markov jump process and once by a PDMP revealed a similar behavior of the two models. The profiles have always the same shape. However, whereas the range of the distribution of a PDMP is bounded the range of the Markov jump process is unbounded and consequently has a more diffuse profile. This is in accordance with the theoretical results that the expectation for these two models coincides, whereas the variance of the PDMP model is smaller by the amount of the expectation than the variance of a Markov jump process.

For a positive feedback loop consisting of a gene with one binding site in its regulatory region to which its gene product binds as a monomer, we showed that there is a positive probability that gene expression expires even for positive protein concentrations. This could also be seen by simulations of the process. Simulations of the discrete process have shown a similar behavior. Furthermore, simulation of the PDMP exhibit an unimodal as well as a bimodal expression profile for a fixed simulation period. Additionally, we investigated the role of dimerization in a positive feedback loop. Now, taking the same parameter set and simulation periods the protein levels do not vanish on either, a PDMP or a Markov jump process. This suggests that dimerization can stabilize gene expression in a positive feedback loop.

For a model of a toggle switch where both genes have one binding site and where the proteins are present as monomers, the system switches between a state in which one of the genes is present at maximal expression level while the other is

present at lowest expression level, and a state in which both genes are suppressed. Such a behavior cannot be understood from a deterministic model which possesses only one steady state. However, the system remains only for a relatively short period in one of these states, and one would expect that the system switches between only the two states where one of the gene exhibit high and the other exhibit low expression levels. The behavior changes if one includes dimerization of the two gene products. In this case the system shows a more switch-like behavior. Now, the system stays for long time periods in one of the states where one gene exhibits high and the other gene exhibits low expression values, interrupted by very short periods where both genes are turned on or off.
Furthermore, we compared the computing time of Gillespie's algorithm with the simulation algorithm for a PDMP. We measured the cpu time of both algorithms for the inducible promoter system, and the positive feedback loop with and without dimerization of the transcription factors. Independently whether the holding times are given by an analytical formula or not, the hybrid algorithm needs only less than 5% of the computing time of the SSA.
In the second section we analyzed noise reduction by a negative feedback loop modeled by a PDMP. We showed that the stationary distribution is given as the solution of a one-dimensional correlated random walk. Besides the stationary distribution, the first two central moments could be given in a closed analytical formula as well. Then, attenuation of noise was measured by means of the coefficient of variation. In contrast to classical modeling of attenuation of noise, where a negative feedback loop always reduces noise, we found that for a PDMP reduction is rather the exception than the rule. This suggests that, when noise is caused by transitions of the promoter is bigger than noise caused by fluctuations in transcription or translation, a negative feedback loop is in general not able to reduce the noise in the system. At least this is the case for systems where the promoter contains only one binding site and the proteins are present as monomers.
In the third section of the second chapter we applied PDMP to autocatalytic networks. We considered three types of networks which we called a pure autocatalytic network, an autocatalytic network with positive basal transcription rate, and an autocatalytic network with positive basal activation rate. Again, we could determine the stationary distributions for all three networks in a closed analytical formula. For the pure autocatalytic network we proved the conjecture from the first section of the second chapter that the only stationary distribution is indeed the point mass concentrated at zero. However, by extinction analysis we showed that there is a quasi steady state in which the mode is located around the maximal expression level. We showed that in many situations the process reaches this distribution quite fast and remains in it for large time spans, which are far beyond any range of cycles of any living organism. For the other two networks we found, as in the case of a negative feedback loop, that the stationary distributions are given

as the solutions of one-dimensional correlated random walks. We found that the distribution is unimodal with mode located around the maximal expression levels. Furthermore we analyzed the dependence of all three networks on different initial inducer amounts and on different expression periods by numerical means. In contrast to a classical approach we found that such systems can show a graded as well a binary response. A pure autocatalytic network and an autocatalytic network with positive basal activation rate exhibit a binary response during increasing simulation lengths, whereas an autocatalytic network with positive transcription rate exhibit a graded response. For different inducer amounts a pure autocatalytic network responds in a binary fashion, whereas the distribution of the other two networks is always unimodal. Hence, an autocatalytic network with positive basal transcription rate is advantageous when the whole cell population should respond precisely in time and independently of initial inducer amounts. On the other hand, if it is advantageous that not all cells respond in the same manner, a pure autocatalytic would be the right choice. For a mixed behavior, binary response in time but unimodal response for different inducer amounts, an autocatalytic network with basal activation rates would be the better choice.

The results of the first chapter have shown that the understanding of the promoter activity is crucial to explain the oscillatory behavior of the molecular clocks Hes1 and Hes7. In the deterministic setting, this requires a profound knowledge of the value of the Hill coefficient. As it was shown, both a value too low or too high can lead to behavior different from the one observed in experiments. For the Hes1 oscillator, the estimated Hill coefficient is too small to achieve sustained oscillations with a period of about 2 hours. On the other hand, for the Hes7 oscillator the estimated Hill coefficient is too high to explain the damped oscillations caused by mutation of the Hes7 protein. However, we have to concede that our estimates for the Hill coefficient are quite rough. For a model-based approach, as we have proposed, the data is very sparse. On the other hand, for a direct estimate, by fitting a Hill function to dose-response data, data is lacking entirely.
The results of the first two sections showed that the standard models for the Hes1 and Hes7 oscillators are too simplistic to explain the experimental results described in literature. Hence, a more sophisticated modeling is required. One possibility is to include protein modification steps into the models like phosphorylation or ubiquitination, which often take place in a nonlinear fashion. By a more sophisticated model for the Hes7 oscillator, an elevated Hill coefficient could be successfully brought into accordance with damped oscillations caused by increased half-lives of the Hes7 protein.
As it was shown in the first chapter, promoter activity can have great influence on the dynamical behavior of a genetic network. To address this issue, an alternative approach to model genetic networks was proposed in the second chapter of this

thesis. This approach allows to model promoter activity in an explicit form and thereby allows to investigate variability of gene expression caused by the inherent stochastic turning on and off processes. In particular, it allows to investigate variability of gene expression originating from the promoter activity as the only source of randomness.
As it was shown in the first section of the second chapter, an inducible gene and an autocatalytic network show similar dynamical behavior if they are modeled by a time-continuous Markov jump process or by a PDMP. This suggests that there is not too much loss of information if a genetic network is modeled by a PDMP instead of a time-continuous Markov jump process. As shown in the second and third section of the second chapter, in contrast to the time-continuous Markov jump processes, it is possible to find analytical solutions of the stationary distributions for genetic networks modeled by PDMPs. A further advantage of PDMPs compared to time-continuous Markov jump processes is the very short computing time. Hence, if there is no need for a complete stochastic description of the regulatory network, simulation can be strongly speeded up by using a PDMP instead of a time-continuous Markov jump process.
Furthermore, we showed that a PDMP reveals properties of genetic networks which could not be observed by a deterministic approach. For instance, expression of a pure autocatalytic network modeled by a PDMP expires whereas it would reach its steady state level if the network would be modeled by an ODE. As far as we know, even for a time-continuous Markov jump process this property was not observed beforehand. Furthermore, a binary response for increasing time periods or different inducer amounts, and the flipping of a toggle switch between three states could not be observed in a deterministic approach. Here, the system would have one stable steady state. A further issue which could not be observed by a deterministic approach is attenuation of noise by a negative feedback. Whereas in a deterministic approach a negative feedback is always superior in respect of noise attenuation to an unregulated system, this is not the case for a PDMP. Moreover, it appears that this would be rather the exception than the rule, at least for an autoregulative network where the gene possesses only one binding site in its promoter and the gene product is present as monomers.

Bibliography

[1] C.M. Ajo-Franklin, D.A. Drubin, J.A. Eskin, E.P. Gee, D. Landgraf, I. Phillips, and P.A. Silver. Rational design of memory in eukaryotic cells. *Genes Dev.*, 21:2271–2276, 2007.

[2] D. Allwright. A global stability criterion for simple control loops. *J. Math. Biol.*, 4:363–373, 1977.

[3] M. Andrecut and S.A. Kauffman. Noise in genetic toggle switch models. *J.Int.Bioinform.*, 3(1), 2006. 0023.

[4] A. Arkin, J. Ross, and H. H. McAdams. Stochastic kinetic analysis of developmental pathway bifurcation in phage-lambda infected *Escherichia coli* cells. *Genetics*, 149:1633–1648, 1998.

[5] S. Artavanis-Tsakonas, M.D. Rand, and R.J. Lake. Notch signaling: Cell fate control and signal integration in development. *Science*, 284:770–776, 1999.

[6] M. R. Atkinson, M. A. Savageau, J. T. Myers, and A. J. Ninfa. Development of genetic circuitry exhibiting toggle switch or oscillatory behavior in Escherichia coli. *Cell*, 113:597–607, 2003.

[7] A. Audibert, D. Weil, and F. Dautry. In vivo kinetics of mRNA splicing and transport in mammalian cells. *Mol. Cell. Biol.*, 22:6706–6718, 2002.

[8] A. Becskei, B. Séraphin, and L. Serrano. Positive feedback in eukaryotic gene networks: cell differentiation by graded to binary response conversion. *EMBO J.*, 20:2528–35, 2001.

[9] A. Becskei and L. Serrano. Engineering stability in gene networks by autoregulation. *Nature*, 405:590–593, 2000.

[10] A. Belle, A. Tanay, L. Bitincka, R. Shamir, and E.K. O'Shea. Quantification of protein half-lives in the budding yeast proteome. *Proc. Natl. Acad. Sci. USA*, 103:13004–13009, 2006.

[11] Y. Bessho, H. Hirata, Y. Masamizu, and R. Kageyama. Periodic repression by the bHLH factor Hes7 is an essential mechanism for the somite segmentation clock. *Genes Dev.*, 17:1451–1456, 2003.

[12] Y. Bessho, G. Miyoshi, R. Sakata, and R. Kageyama. Hes7: a bHLH-type repressor gene regulated by notch and expressed in the presomitic mesoderm. *Genes Cells*, 6:175–185, 2001.

[13] Y. Bessho, R. Sakata, S. Komatsu, K. Shiota, S. Yamada, and R. Kageyama. Dynamic expression and essential functions of Hes7 in somite segmentation. *Genes Dev.*, 15:2642–2647, 2001.

[14] S. R. Biggar and G. R. Crabtree. Cell signaling can direct either binary or graded transcriptional responses. *EMBO J.*, 20:3167–3176, 2001.

[15] W.J. Blake, G.Balázsi, M.A. Kohanski, F.J. Isaacs, K.F. Murphy, Y. Kuang, C.R. Cantor, D.R. Walt, and J.J. Collins. Phenotypic consequences of promoter-mediated transcriptional noise. *Molecular Cell*, 24:853–865, 2006.

[16] W.J. Blake, M. Kærn, C.R. Cantor, and J.J. Collins. Noise in eukaryotic gene expression. *Nature*, 422:633637, 2003.

[17] H. Bolouri and E. H. Davidson. Transcriptional regulatory cascades in development: Initial rates, not steady state, determine network kinetics. *Proc. Natl. Acad. Sci. USA*, 100:9371–9376, 2003.

[18] H. S. Booth, C. J. Burden, M. Hegland, and L. Santoso. A stochastic model of gene regulation using the chemical master equation. In A. Deutsch, L. Brusch, H. Byrne, G. de Vries, and H. Herzel, editors, *Mathematical Modeling of Biological Systems*, pages 71–81. Birkhäuser Boston, 2007.

[19] R. Bundschuh, F. Hayot, and C. Jayaprakash. Fluctuations and slow variables in genetic networks. *Biophys. J.*, 84:1606–1615, 2003.

[20] C.M. Crews. Feeding the machine: Mechanisms of proteasome-catalyzed degradation of ubiquinated proteins. *Curr Opin in Chemical Biology*, 7:534–539, 2003.

[21] F. H. C. Crick. On protein synthesis. *Symp Soc Exp Biol.*, 12:138–63, 1958.

[22] F. H. C. Crick. Central dogma of molecular biology. *Nature*, 227:561–563, 1970.

[23] M. H. A. Davis. Piecewise-deterministic Markov processes: A general class of non-diffusion stochastic models. *J. R. Statist. Soc.* B, 46:353–388, 1984.

[24] M. Delbrück. Statistical fluctuations in autocatalytic reactions. *J. Chem. Phys.*, 9:120–124, 1940.

[25] P.P. Dennis and A. Omer. Small non-coding RNAs in *Archaea*. *Curr. Opin. Microbiol.*, 8:685–694, 2005.

[26] I. Edery, L. J. Zwiebel, M. E. Dembinska, and M. Rosbash. Temporal phosphorylation of the drosophila period protein. *Proc. Natl. Acad. Sci. USA*, 91:2260–2264, 1994.

[27] R. Edwards, R. Gibson, R. Illner, and V. Paetkau. A stochastic model for circadian rhythms from coupled ultradian oscillators. *Theor. Biol. Med. Model*, 4:1(1), 2007.

[28] M. B. Elowitz, A. J. Levine, E. D. Siggia, and P. S. Swain. Stochastic gene expression in a single cell. *Science*, 297:1183 – 1186, 2002.

[29] M.B. Elowitz and S. Leibler. A synthetic oscillatory network of transcriptional regulators. *Nature*, 403:335–338, 2000.

[30] T.S. Gardner, C.R. Cantor, and J.J. Collins. Construction of a genetic toggle switch in *Escherichia coli*. *Nature*, 403:339–42, 2000.

[31] M. A. Gibson and J. Bruck. Efficient exact stochastic simulation of chemical systems with many species and many channels. *J. Phys. Chem. A*, 104:1876–1889, 2000.

[32] D. T. Gillespie and L. R. Petzold. Improved leap-size selection for accelerated stochastic simulation. *J. of Chem. Physics*, 119:8229–8234, 2003.

[33] D.T. Gillespie. A general method for numerically simulating the stochastic time evolution of coupled chemical reactions. *J. Comput. Phys.*, 22:403–434, 1976.

[34] D.T. Gillespie. Exact stochastic simulation of coupled chemical reactions. *J. Phys. Chem.*, 81:2340–2361, 1977.

[35] D.T. Gillespie. Approximate accelerated stochastic simulation of chemically reacting systems. *J. Chem. Phys.*, 115:1716–1733, 2001.

[36] S. Godstein. On diffusion by discontinuous movements and on the telegraph equation. *Quart. J. Mech. Appl. Math.*, 4:129–156, 1951.

[37] A. Goldbeter. A model for circadian oscillations in the drosophila period protein (per). *Proc. Royal Soc. Lond. B.*, 261:319–324, 1995.

[38] B. C. Goodwin. *Temporal organization in cells*. Academic Press London/New York, 1963.

[39] B. C. Goodwin. Oscillatory behavior in enzymatic control processes. *Adv. Enzyme Regul.*, 3:425–438, 1965.

[40] Y. Gotoh, N. Masuyama, K. Dell, K. Shirakabe, and E. Nishida. Initiation of Xenopus oocyte maturation by activation of the mitogen-activated protein kinase cascade. *J. Biol. Chem.*, 270:25898–25904, 1995.

[41] I. Greenwald. Lin-12/notch signaling: Lessons from worms and flies. *Genes Dev*, 12:1751–1762, 1998.

[42] I. Greenwald and G.M. Rubin. Making a difference: the role of cell-cell interactions in establishing separate identities for equivalent cells. *Cell*, 68:271–281, 1992.

[43] J. S. Griffith. Mathematics of cellular control processes I. Negative feedback to one gene. *J. Theor. Biol.*, 20:202–208, 1968.

[44] J. Guckenheimer and P. Holmes. *Nonlinear Oscillations, Dynamical Systems, and Bifurcations of Vector Fields*. Springer-Verlag, New York, 1993.

[45] K. P. Hadeler. Reaction transport equations in biological modeling. *Math. Comp. Model.*, 31:75–81, 1998.

[46] P.E. Hardin, J.C. Hall, and . M. Rosbash. Feedback of the drosophila period gene product on circadian cycling of its messenger RNA levels. *Nature*, 343:536–540, 1990.

[47] E.L. Haseltine and J.B. Rawlings. Approximate simulation of coupled fast and slow reactions for stochastic chemical kinetics. *J. Chem. Phys.*, 117:6959–6969, 2002.

[48] P. Heitzler, M. Bourouis, L. Ruel, C. Carteret, and P. Simpson. Genes of the enhancer of split and achaete-scute complexes are required for a regulatory loop between notch and delta during lateral signalling in drosophila. *Development*, 122:161–171, 1996.

[49] T. Hillen. A turing model with correlated random walk. *J. of Math. Biology*, 35:49–72, 1996.

[50] H. Hirata, Y. Bessho, H. Kokubu, Y. Masamizu, S. Yamada, J. Lewis, and R. Kageyama. Instability of Hes7 protein is crucial for the somite segementation clock. *Nature Genetics*, 36:750–754, 2004.

[51] H. Hirata, S. Yoshiura, T. Ohtsuka, Y. Bessho, T. Harada, K. Yoshikawa, and R. Kageyama. Oscillatory expression of the bHLH factor Hes1 regulated by a negative feedback loop. *Science*, 298:840–843, 2002.

[52] D.A. Hume. Probability in transcriptional regulation and its implications for leukocyte differentiation and inducible gene expression. *Blood*, 96:2323–2328, 2000.

[53] A.N. Imbalzano, K.S. Zaret, and R.E. Kingston. Transcription factor (TF) IIB and TFIIA can independently increase the affinity of the TATA-binding protein for DNA. *J. Biol. Chem.*, 269:8280–8286, 1994.

[54] F. J. Isaacs, J. Hasty, C. R. Cantor, and J. J. Collins. Prediction and measurement of an autoregulatory genetic module. *Proc. Natl. Acad. Sci. USA*, 100:7714–7719, 2003.

[55] Chen J., Kang L., and Zhang N. Negative feedback loop formed by lunatic fringe and Hes7 controls their oscillatory expression during somitogenesis. *Genesis*, 43:196–204, 2005.

[56] A. Jõers, V. Jaks, J. Kase, and T. Maimets. p53-dependent transcription can exhibit both on/off and graded response after genotoxic stress. *Oncogene*, 23:6175–6185, 2004.

[57] C. Jouve, I. Palmeirim, D. Henrique, J. Beckers, A. Gossler, D. Ish-Horowicz, and O. Pourquié. Notch signalling is required for cyclic expression of the hairy-like gene Hes1 in the presomitic mesoderm. *Development*, 127:1421–1429, 2000.

[58] J.E. Ferrell Jr. and E.M. Machleder. The biochemical basis of an all-or-none cell fate switch in xenopus oocytes. *Science*, 280:895–898, 1998.

[59] J. Puchałka and A. M. Kierzek. Bridging the gap between stochastic and deterministic regimes in the kinetic simulations of the biochemical reaction networks. *Biophys. J.*, 86:1357–1372, 2004.

[60] M. Kac. A stochastic model related to the telegrapher's equation. reprinted in *Rocky Mtn. J. Math.*, 4:497–509, 1974.

[61] T.B. Kepler and T.C. Elstondagger. Stochasticity in transcriptional regulation: Origins, consequences, and mathematical representations. *Biophys J*, 81:3116–3136, 2001.

[62] T.R. Kiehl, R.M. Mattheyses, and M.K. Simmons. Hybrid simulation of cellular behavior. *Bioinformatics*, 20:316–322, 2004.

[63] A. M. Kierzek. Stocks: Stochastic kinetic simulations of biochemical systems with gillespie algorithm. *Bioinformatics*, 18:470–481, 2002.

[64] J. Kimble and P. Simpson. The LIN-12/Notch1 signaling pathway and its regulation. *Ann. Rev. Cell Dev. Biol.*, 13:333–361, 1997.

[65] M.S. Ko, H. Nakauchi, and N. Takahashi. The dose dependence of glucocorticoid-inducible gene expression results from changes in the number of transcriptionally active templates. *EMBO J.*, 9:2835–2842, 1990.

[66] B.P. Kramer, A.U. Viretta, M. Daoud-El-Baba, D. Aubel, W. Weber, and M. Fussenegger. An engineered epigenetic transgene switch in mammalian cells. *Nat. Biotechnol.*, 22:867–870, 2004.

[67] H. A. Kramers. Brownian motion in a field of force and the diffusion model of chemical reactions. *Physica*, 7:284–304, 1940.

[68] A. M. Kringstein, F. M. V. Rossi, A. Hofmanndagger, and H. M. Blau. Graded transcriptional response to different concentrations of a single transactivator. *Proc. Natl. Acad. Sci. USA*, 95:13670–13675, 1998.

[69] Y.A. Kuznetsov. *Elements of Applied Bifurcation Theory*. Springer, New York, 1995.

[70] H. Kwon, S. Park, S. Lee, D.-K. Lee, and C.-H. Yang. Determination of binding constant of transcription factor AP-1 and DNA. *Eur. J. Biochem.*, 268:565–572, 2001.

[71] N. Le Novere and T.S. Shimizu. Stochsim: modelling of stochastic biomolecular processes. *Bioinformatics*, 17:575–576, 2001.

[72] J. Lewis. Autoinhibition with transcriptional delay: A simple mechanism for the zebrafish somitogenesis oscillator. *Curr. Biol.*, 13:1398–1408, 2003.

[73] T. Lipniacki, P. Paszek, A. Marciniak-Czochra, A.R. Brasier, and M. Kimmel. Transcriptional stochasticity in gene expression. *J. Theor. Biol.*, 238:348–367, 2006.

[74] H. Maamar and D. Dubnau. Bistability in the *Bacillus subtilis* K-state (competence) system requires a positive feedback loop. *Mol. Microbiol.*, 56:615–624, 2005.

[75] N. MacDonald. Time lag in a model of a biochemical reaction sequence with end product inhibition. *J. Theor. Biol.*, 67:549–556, 1977.

[76] N. MacDonald. *Biological Delay Systems: Linear Stability Theory*. Cambridge University Press, Cambridge, UK, 1989.

[77] J.S. Mattick and I.V. Makunin. Small regulatory RNAs in mammals. *Hum. Mol. Genet.*, 14:R121–R132, 2005.

[78] H. H. McAdams and A. Arkin. Stochastic mechanisms in gene expression. *Proc. Natl. Acad. Sci. USA*, 94:814–819, 1997.

[79] M.Griffith, T.Courtney, J. Peccoud, and W.H. Sanders. Dynamic partitioning for hybrid simulation of the bistable HIV-1 transactivation network. *Bioinformatics*, 22:2782–2789, 2006.

[80] N. A. M. Monk. Oscillatory expression of Hes1, p53, and NF-κB driven by transcriptional time delays. *Curr. Biol.*, 13:1409–1413, 2003.

[81] J. Müller, C. Kuttler, B.A. Hense, S. Zeiser, and V. Liebscher. Transcription, intercellular variability and correlated random walk. *Math. Biosci.*, 216:30–39, 2008.

[82] J. D. Murray. *Mathematical Biology I.* Springer, 3 edition, 2002.

[83] N. Ohki and M. Hagiwara. Bio-object, a stochastic simulator for post-transcriptional regulation. *Bioinformatics*, 21:2478–2487, 2005.

[84] I. Palmeirim, D. Henrique, D. Ish-Horowicz, and O. Pourquié. Avian hairy gene expression identifies a molecular clock linked to vertebrate segmentation and somitogenesis. *Cell*, 91:639–648, 1997.

[85] J. Peccoud and B. Ycart. Markovian modelling of gene products synthesis. *Theor. Pop. Biol.*, 48:222–234, 1995.

[86] C.M. Pickart. Mechanisms underlying ubiquitination. *Annu Rev Biochem*, (70):503–533, 2001.

[87] O. Pourquié. The segmentation clock: Converting embryonic time into spatial pattern. *Science*, 301:328–330, 2003.

[88] A. Raj, C.S. Peskin, D. Tranchina, D.Y. Vargas, and S. Tyagi. Stochastic mRNA synthesis in mammalian cells. *PLoS Biology*, 4:1707–1719, 2006.

[89] C. Rao and A. Arkin. Stochastic chemical kinetics and the quasi-steadystate assumption: Applications to the Gillespie algorithm. *J. Chem. Phys.*, 118:4999–5010, 2003.

[90] C. V. Rao, D. M. Wolf, and A. P. Arkin. Control, exploitation and tolerance of intracellular noise. *Nature*, 14:231–237, 2002.

[91] J. M. Raser and E. K. O'Shea. Control of stochasticity in eukaryotic gene expression. *Science*, 304:1811 – 1814, 2004.

[92] K. Rateitschak and O. Wolkenhauer. Intracellular delay limits cyclic changes in gene expression. *Math. Biosci.*, 205:163–179, 2007.

[93] B. Reddy and J. Yin. Quantitative intracellular kinetics of HIV type 1. *AIDS Res Hum Retroviruses*, 15:273–283, 1999.

[94] E. Robey. Notch1 in vertebrates. *Curr. Opin. Genet. Dev.*, 7:551–557, 1997.

[95] Vallabhajosyula R.R. and Sauro H.M. Stochastic simulation gui for biochemical networks. *Bioinformatics*, 23:1859–1861, 2007.

[96] S.I. Rubinow. *Equilibrium binding of macromolecules with ligands*. Biological Kinetics. Cambridge University Press, 1991.

[97] S.I. Rubinow and L.A. Segel. *Positive and negative cooperativity*. Biological Kinetics. Cambridge University Press, 1991.

[98] H. Salis and Y. Kaznessis. Accurate hybrid stochastic simulation of a system of coupled chemical or biochemical reactions. *J. Chem. Phys.*, 122(054103), 2005.

[99] M.S. Samoilov and A.P. Arkin. Deviant effects in molecular reaction pathways. *Nat. Biotechnol.*, 24:1235–1240, 2006.

[100] M.A. Savageau. Comparison of classical and autogenous systems of regulation in inducible operons. *Nature*, 252:546–549, 1974.

[101] D.B. Schulman and D.R. Setzera. Identification and characterization of transcription factor IIIA from *Schizosaccharomyces* pombe. *Nucleic Acids Res.*, 30:2772–2781, 2002.

[102] L. A. Segel, editor. *Biological Kinetics*. Cambridge University Press, 1991.

[103] Y. Setty, A. E. Mayo, M. G. Surette, and U. Alon. Detailed map of a cis-regulatory input function. *Proc. Natl. Acad. Sci. USA*, 100:7702–7707, 2003.

[104] D.A. Siegele and J.C. Hu. Gene expression from plasmids containing the araBAD promoter at subsaturating inducer concentrations represents mixed populations. *Proc. Natl. Acad. Sci. USA*, 94:8168–8172, 1997.

[105] P. Simpson. Lateral inhibition and the development of the sensory bristles of the adult peripheral nervous system of Drosophila. *Development*, 109:509–519, 1990.

[106] L.J. Slater. *Generalized Hypergeometric Functions*. Cambridge University Press, 1966.

[107] W.K. Smits, C.C. Eschevins, K.A. Susanna S. Bron, and O.P. Kuipers L.W. Hamoen. Stripping *Bacillus*: ComK auto-stimulation is responsible for the bistable response in competence development. *Mol Microbiol.*, 56:604–14, 2005.

[108] M.A. Sørensen and S. Pedersen. Absolute *in vivo* translation rates of individual codons in *Escherichia coli*. The two glutamic acid codons gaa and gag are translated with a threefold difference in rate. *J. Mol. Biol.*, 222:265–280, 1991.

[109] A. Ström, P. Castella, J. Rockwood, J. Wagner, and M. Caudy. Mediation of NGF signaling by post-translational inhibition of Hes-1, a basic helix-loop-helix repressor of neuronal differentiation. *Genes Dev.*, 11:3168–3181, 1997.

[110] K. Takebayashi, Y. Sasai, Y. Sakai, T. Watanabe, S. Nakanishi, and R. Kageyama. Structure, chromosomal locus, and promoter analysis of the gene encoding the mouse helix-loop-helix factor Hes-1. *J. Biol. Chem.*, 269:5150–5156, 1994.

[111] M. Thattai and A. van Oudenaarden. Intrinsic noise in gene regulatory networks. *Proc.Natl.Acad.Sci.USA*, 98:8614–8619, 2001.

[112] T. Tian and K. Burrage. Stochastic models for regulatory networks of the genetic toggle switch. *Proc.Natl.Acad.Sci.USA*, 103:8372–8377, 2006.

[113] J.J. Tyson and H.G. Othmer. The dynamics of feedback control circuits in biochemical pathways. *Prog. Theor. Biol.*, 5:1–62, 1978.

[114] N.G. van Kampen. *Stochastic Processes in Physics and Chemistry*. North-Holland-Elsevier, 1992.

[115] J.M. Vilar, C. C. Guet, and S. Leibler. Modeling network dynamics: the lac operon, a case study. *J. Cell Biol.*, 161:471–476, 2003.

[116] J.M. Vilar and S. Leibler. DNA looping and physical constraints on transcription regulation. *J. Mol. Biol.*, 331:981–989, 2003.

[117] M.C. Walters, S. Fiering, J. Eidemiller, W. Magis, M. Groudine, and D.I.K. Martin. Enhancers increase the probability but not the level of gene expression. *Proc. Natl. Acad. Sci. USA*, 92:7125–7129, 1995.

[118] J.D. Watson and F.H. C. Crick. Molecular structure of nucleic acids. a structure for deoxyribose nucleic acid. *Nature*, 171:737–738, 1953.

[119] L.S. Weinberger, J.C. Burnett, J.E. Toettcher, A.P. Arkin, and D.V. Schaffer. Stochastic gene expression in a lentiviral positive-feedback loop: HIV Tat fluctuations drive phenotypic diversity. *Cell*, 122:169–182, 2005.

[120] P.J. Wilderman, N.A. Sowa, D.J. FitzGerald, P.C. FitzGerald, S. Gottesman, U.A. Ochsner, and M.L. Vasil. Identification of tandem duplicate regulatory small RNAs in pseudomonas aeruginosa involved in iron homeostasis. *Proc. Natl. Acad. Sci. USA*, 101:9792–9797, 2004.

[121] D.M. Wolf and F.H. Eeckman. On the relationship between genomic regulatory element organization and gene regulatory dynamics. *J. Theor. Biol.*, 195:167–186, 1998.

[122] B.S. Wolner and J.D. Gralla. TATA-flanking sequences influence the rate and stability of TATA-binding protein and TFIIB binding. *Biol. Chem.*, 276:6260–6266, 2001.

[123] N. Yildirim and M. C. Mackey. Feedback regulation in the lactose operon: a mathematical modeling study and comparison with experimental data. *Biophys J.*, 84:2841–2851, 2003.

[124] M. Zeeb and J. Balbach. Single-stranded DNA binding of the cold-shock protein CspB from *Bacillus subtilis*: NMR mapping and mutational characterization. *Protein Sci.*, 12:112–123, 2003.

[125] S. Zeiser, U. Franz, and V. Liebscher. Autocatalytic genetic networks modeled by piecewise-deterministic Markov processes. *J. Math. Biol.*, 2009. DOI 10.1007/s00285-009-0264-9.

[126] S. Zeiser, U. Franz, J. Müller, and V. Liebscher. Hybrid modeling of noise reduction by a negatively autoregulated system. *Bull. Math. Biol.*, 71:1006–24, 2007.

[127] S. Zeiser, U. Franz, O. Wittich, and V. Liebscher. Simulation of genetic networks modelled by piecewise deterministic Markov processes. *IET Syst. Biol.*, 2:113–35, 2008.

[128] S. Zeiser, H.V. Liebscher, H. Tiedemann, I. Rubio-Aliaga, G.K. Przemeck, M.H. de Angelis, and G. Winkler. Number of active transcription factor binding sites is essential for the Hes7 oscillator. *Theor. Biol. Med. Model*, 3(11), 2006.

[129] S. Zeiser, J. Müller, and V. Liebscher. Modeling the Hes1 oscillator. *J. Comput. Biol.*, 14:984–1000, 2007.

[130] S. Zeiser, O. Rivera, C. Kuttler, B. Hense, R. Lasser, and G. Winkler G. Oscillations of Hes7 caused by negative autoregulation and ubiquitination. *Comput. Biol. Chem.*, 32:47–51, 2008.

Acknowledgements

Most parts of this thesis were done while I was employed at the Helmholtz Zentrum München, Institute of Biomathematics and Biometry, Munich, Germany.
I am deeply grateful to Volkmar Liebscher for the friendly and helpful supervision during this work. For his constant interest in the project and plenty of constructive and interesting discussions. He consistently allowed this thesis to be my own work, but steered me in the right direction whenever he thought I needed it. Furthermore I would like to thank for many warm hospitalities in Greifswald.
I am obliged to Prof. G. Winkler for his interest in my work and financial support.
I am very grateful to my former colleagues Uwe Franz, Johannes Müller, and Olaf Wittich for their interest in the project, help, and valuable and stimulating discussions during and in particular after their time at the institute.
Beside those mentioned, I would like to thank all my other former colleagues at the institute for the enjoyable cooperation, support, and the nice time spent both in- and outside the institute.

Selbständigkeitserklärung

Hiermit erkläre ich, dass diese Arbeit bisher von mir weder an der Mathematisch-Naturwissenschaftlichen Fakultät der Ernst-Moritz-Arndt-Universität Greifswald noch einer anderen wissenschaftlichen Einrichtung zum Zwecke der Promotion eingereicht wurde. Ferner erkläre ich, dass ich diese Arbeit selbständig verfasst und keine anderen als die darin angegebenen Hilfsmittel benutzt habe.

(Stefan Zeiser)

List of Publications

The thesis is based on the following scientific research papers.

- Zeiser S, Liebscher HV, Tiedemann H, Rubio-Aliaga I, Przemeck GK, de Angelis MH, Winkler G. Number of active transcription factor binding sites is essential for the Hes7 oscillator. Theor. Biol. Med. Model. 2006; 3:11.
- Zeiser S, Müller J, Liebscher V. Modeling the Hes1 oscillator. J. Comput. Biol. 2007;14(7):984-1000.
- Zeiser S, Rivera O, Kuttler C, Hense B, Lasser R, Winkler G. Oscillations of Hes7 caused by negative autoregulation and ubiquitination. Comput. Biol. Chem. 2008;32(1):47-51.
- Zeiser S, Franz U, Wittich O, Liebscher V. Simulation of genetic networks modelled by piecewise deterministic Markov processes. IET Syst. Biol. 2008; 2(3):113-35.
- Zeiser S, Franz U, Müller J, Liebscher V. Hybrid modeling of noise reduction by a negatively autoregulated system. Bull. Math. Biol. 2009; 71(4): 1006-24.
- Zeiser S, Franz U, Liebscher V. Autocatalytic genetic networks modeled by piecewise-deterministic Markov processes. J. Math. Biol. 2009; Mar 27. DOI 10.1007/s00285-009-0264-9.

The following publications prepared during the PhD study are not addressed in this thesis.

- Rubio-Aliaga I, Soewarto D, Wagner S, Klaften M, Fuchs H, Kalaydjiev S, Busch DH, Klempt M, Rathkolb B, Wolf E, Abe K, Zeiser S, Przemeck GK, Beckers J, de Angelis MH. A genetic screen for modifiers of the delta1-dependent notch signaling function in the mouse. Genetics. 2007;175(3): 1451-63.
- Tiedemann HB, Schneltzer E, Zeiser S, Rubio-Aliaga I, Wurst W, Beckers J, Przemeck GK, de Angelis MH. Cell-based simulation of dynamic expression patterns in the presomitic mesoderm. J. Theor. Biol. 2007;248(1):120-9
- Müller J, Kuttler C, Hense BA, Zeiser S, Liebscher V. Transcription, intercellular variability and correlated random walk. Math. Biosci. 2008;216(1): 30-9.